SSD 83-0075-1

LOW CONCENTRATION RATIO SOLAR ARRAY FOR LOW EARTH ORBIT MULTI-100 kW APPLICATION

VOLUME 1—DESIGN, ANALYSIS AND DEVELOPMENTAL TESTS

FINAL REPORT
JULY 1983

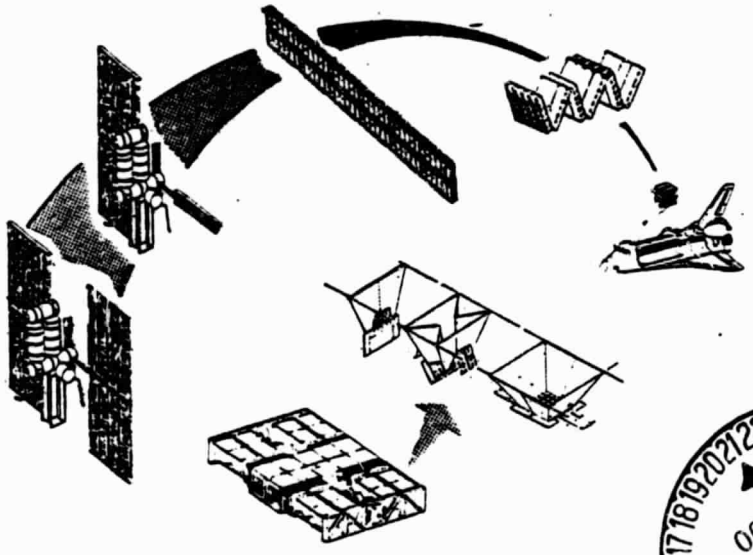

Prepared for:

National Aeronautics and Space Administration
George C. Marshall Space Flight Center
Marshall Space Flight Center, AL 35812

Contract NAS8-34214

Shuttle Integration & Satellite Systems Division

Rockwell International

SSD83-0075-1

LOW CONCENTRATION RATIO SOLAR ARRAY FOR LOW EARTH ORBIT MULTI-100 kW APPLICATION FINAL REPORT

VOLUME I - DESIGN, ANALYSIS AND DEVELOPMENTAL TESTS

JULY 1983

PREPARED FOR:

NATIONAL AERONAUTICS AND SPACE ADMINISTRATION
GEORGE C. MARSHALL SPACE FLIGHT CENTER,
AL 35812

Rockwell International
Shuttle Integration &
Satellite Systems Division
12214 Lakewood Boulevard
Downey, California 90241

TECHNICAL REPORT INDEX/ABSTRACT

ACCESSION NUMBER							DOCUMENT SECURITY CLASSIFICATION	
							UNCLASSIFIED	

TITLE OF DOCUMENT

Low Concentration Ratio Solar Array for Low Earth Orbit Multi-100 kW Application, Final Report, Vol. 1 - Design, Analysis and Developmental Tests

LIBRARY USE ONLY

AUTHOR(S)

Nalbandian, S. J., French, E. P., et al

CODE	ORIGINATING AGENCY AND OTHER SOURCES	DOCUMENT NUMBER
	Rockwell International Corporation Shuttle Integration and Satellite Systems Division	SSD83-0075-1

PUBLICATION DATE	CONTRACT NUMBER
July 1983	NAS8-34214

DESCRIPTIVE TERMS

Concentrators, Solar Arrays, Concentrator Arrays, Concentrating Silicon Solar Cells, Concentrating Gallium Arsenide Cells, Low Earth Orbit Multi-100 kW Solar Array Design

ABSTRACT

This report describes a preliminary design effort directed toward a low-concentration-ratio photovoltaic array system based on 1984 technology and capable of delivering multi-hundred kilowatts (300 kW to 1000 kW range) in low earth orbit. The array system consists of two or more array modules each capable of delivering between 113 kW to 175 kW using silicon solar cells or gallium arsenide solar cells, respectively.

The array module deployed area is 1320 square meters and consists of 4356 pyramidal concentrator elements. The module, when stowed in the Space Shuttle's payload bay, has a stowage volume of a cube with 3.24 meters on a side. The concentrator elements are sized for a geometric concentration ratio (GCR) of six with an aperture area of 0.5 meters x 0.5 meters.

Volume 1 discusses the structural analysis and design trades leading to the baseline design. It describes the configuration, as well as optical, thermal and electrical performance analyses that support the design and overall performance estimates for the array. Experimental results are also presented for a concentrator element using both silicon and gallium arsenide solar panels. They confirm the preliminary design analysis and performance estimates. Recommendations are provided for future development effort for low earth orbit application. Volume 2 provides drawings for the preliminary design configuration and for the test hardware that was fabricated for design evaluation and test.

FOREWORD

This report describes the effort performed for the preliminary design of low-cost concentrator multi-hundred kilowatt solar arrays. The Volume 1 report summarizes activities performed between June 18, 1981 and July 1983, as required by Contract NAS8-34214 Statement of Work. Volume 2 contains drawings prepared describing the preliminary design configuration, test hardware and manufacturing flow concept. The report was prepared by the Shuttle Integration and Satellite Systems Division of Rockwell International Corporation for the NASA George C. Marshall Space Flight Center (MSFC), Huntsville, Alabama. The NASA technical Contractor Officer Representative for the activity is Mr. W. L. Crabtree. The contents of this document are not necessarily endorsed by the NASA-MSFC.

Mr. S. J. Nalbandian is the project supervisor. Dr. E. P. French is the assistant project supervisor. Principal contributors to the project were:

J. B. Adkins	Mechanism Design
H. C. Ayers	Reflector Design
Z. Backovsky	Testing and Thermal Analysis
R. A. Bellgardt	Electrical Test Equipment
M. S. Biss	Overall Preliminary Design
J. L. Edwards	Structural Analysis
J. D. Eliot	Mechanical Test Equipment
Dr. E. P. French	Optical and Thermal Analysis
G. C. Frey	Materials
R. V. Frost	Reflector Panel Fabrication
H. S. Greenberg	Initial Structural Design and Analysis
K. M. Hicks	Manufacturing Planning
Dr. L. Hsu	Solar Cell Technology
R. L. Long	Materials
M. W. Mills	Electrical Testing and Analysis
Dr. T. S. Nishimoto	Structural Analysis
F. A. Perry	Structural Analysis
A. M. Pope	Development Plans
D. A. Reed	Initial Preliminary Design
A. A. Sileski	Test Planning
L. Vega	Test Hardware

CONTENTS

CONTENTS (contd)

ILLUSTRATIONS

ILLUSTRATIONS (cont'd)

ILLUSTRATIONS (contd)

TABLES

TABLES (contd)

NOMENCLATURE

Symbol	Explanation	Typical Units
A	Area	m^2
B	Radiosity	W/m^2
C	Cost	$
CR	Concentration ratio	—
D	Mast diameter	m
EI_b/EI_ℓ	Batten stiffness ratio	—
f	Efficiency factor; current-voltage function	—; —
FF	Fill factor	—
F	Radiation exchange factor; Newton-Raphson function "script F"	—; —
GRC	Geometric concentration ratio	—
h	Convective heat transfer coefficient	$W/m^2\ K$
H	Concentrator height; irradiance	m; W/m^2
i	Cell current	A
$\overline{I}$	Incident ray vector	
I	Radiation intensity; short-circuit current	W/m^2; A
J	Current density	A/cm^2
ℓ	Average harness length	m
L	Illumination level; mast deployed length	suns; m
m	Number of groups of cells in series	—
N	Number; stacking parameter; load factor	—; —; —
$\overline{N}$	Vector normal to reflecting surface	—
n	Number of parallel cells in a group	—
P	Power	W
P_{kj}	Geometric matrix	W
Q	Heat flow	—
$\overline{R}$	Reflected ray vector	—
s	Projected width of reflector	m
S	Solar constant	W/m^2

NOMENCLATURE (contd)

Symbol	Explanation	Typical Units
t	Thickness	m
T	Absolute temperature	K
v	Cell voltage	volts
V	Open-circuit voltage	volts
W	Width	m; m
X	Coordinate in concentrator geometry; deployed length	m; m
Y	Coordinate in concentrator geometry; extended length	m
Z	Coordinate in concentrator geometry	m
α	Absorptance; X-axis direction angle; current temperature coefficient	—; deg; A/K
β	Y-axis direction angle; voltage temperature coefficient	deg; volts/K
γ	Z-axis direction angle; log illumination coefficient	deg; volts
ε	Hemispherical emittance	—
η	Efficiency (fractional)	—
θ	Reflector slope; pointing angle	deg; deg
ρ	Reflectance; (mass) density	—; kg/m^3
σ	Stefan-Boltzmann constant	$W/m^2\ K^4$
ψ	Efficiency temperature coefficient	K^{-1}

Subscript

A	Area
a	Albedo
beam	beam (intensity)
B	Base
corr	Corrected value
c	Solar cell (solar); concentrator; capability
e	Earth emission

Subscript	Explanation
H	Harness (electrical)
ℓ	Losses (miscellaneous)
ns	non-specular (diffuse)
o	Reference or standard value
max	maximum
opt	Optical
meas	Measured value
p	Solar panel; packing fraction; parallel (solar panel)
R	Radiator
t, T	Total
X	Referring to X-coordinate
Y	Referring to Y-coordinate
S	Specular; series (solar panel)
D	Diffuse
Abs	Absorbed

1.0 INTRODUCTION

Space Transportation System (Shuttle) operational usage in the 1980's will allow routine access to earth-orbiting space systems (e.g., space base scientific and public service platform missions). These low earth orbit (~ 500 km) space systems are expected to required power system capabilities of multi-100-kW power levels to perform a variety of missions. The ability to provide the required power levels is limited by the cost of solar arrays within use of existing technology.

1.1 RESULTS OF PRIOR STUDIES

NASA Marshall Space Flight Center has funded studies[1][2][3]* which show that a concentrator solar array concept can reduce the recurring array and operational costs by a factor of three or more over that attainable with current planar arrays.

For the recurring solar array costs goals to be met and the desired performance characteristics to be maintained, technology advancements are needed in three major areas for solar array configurations. These are:

1. Lower cost, large area, lightweight deployable structures that lead to a compact stowage volume compatible for launch to orbit by the Shuttle vehicle.
2. Lower cost, larger-area, higher-efficiency solar cells suitable for low-concentration ratio (CR) applications.
3. Lightweight concentrator configurations designed to provide the desired concentration ratio and compatible with the solar array deployment scheme selected and the severe temperature cycling incurred in low earth orbit.

1.2 PROGRAM OBJECTIVES

A large-area array, with a geometric CR of about six suns, has been selected as a relatively low risk development to demonstrate technology

*Superscript numbers in parenthesis indicate references.

readiness by the end of 1984. This program has as its prime objective the preliminary design of a concentrator solar array system capable of providing in excess of 300 kW power, deliverable to the user system in orbit by a single Shuttle launch. Up to four solar array modules (each having a power output greater than 100 kW) would comprise the array. The preliminary design effort, including critical technology demonstrations, was completed in June 1983. The concentrator array design provides for utilization of either silicon (Si) or gallium arsenide (GaAs) solar cells for conversion of solar energy to electrical power.

Rockwell's recent experience with concentrating solar arrays has confirmed the choice of a low-CR system for the high-power, low-cost objectives of this program. During 1977-78 a study of high (500X) cassegrainian concentrators using gallium arsenide GaAs solar cells was carried out for the Air Force.[4] Emphasis was on laser and nuclear hardness. Solar cells and a brassboard concentrator were evaluated experimentally. The study showed the advantages of the GaAs cells (high temperature capability and radiation resistance) and the cassegrainian geometry from the standpoint of threat survival. However the sophisticated optics and the heat pipe required for cell cooling did not lend themselves to low-cost or light weight array design.

The solar array study[3] for NASA/MSFC which immediately preceeded the present contract confirmed the judgement that low-CR designs would be the most cost-effective. The essence of the argument is that, beyond a concentration of six or so, little further reduction in cell cost is achieved. On the other hand increased concentration makes the design optics, cell cooling methods and structure more difficult and expensive so that the overall cost of power increases rather than decreases.

Figure 1-1 illustrates these points. Economics of scale and substantial reduction in solar cell costs result in big cost gains in going from a state-of-the-art planar array of the Solar Electric Propulsion (SEP) stage type to a multi-100 kW low-CR array. Complexity and increased component sophistication erode the cost advantage for higher CR designs (e.g., 20X or more).

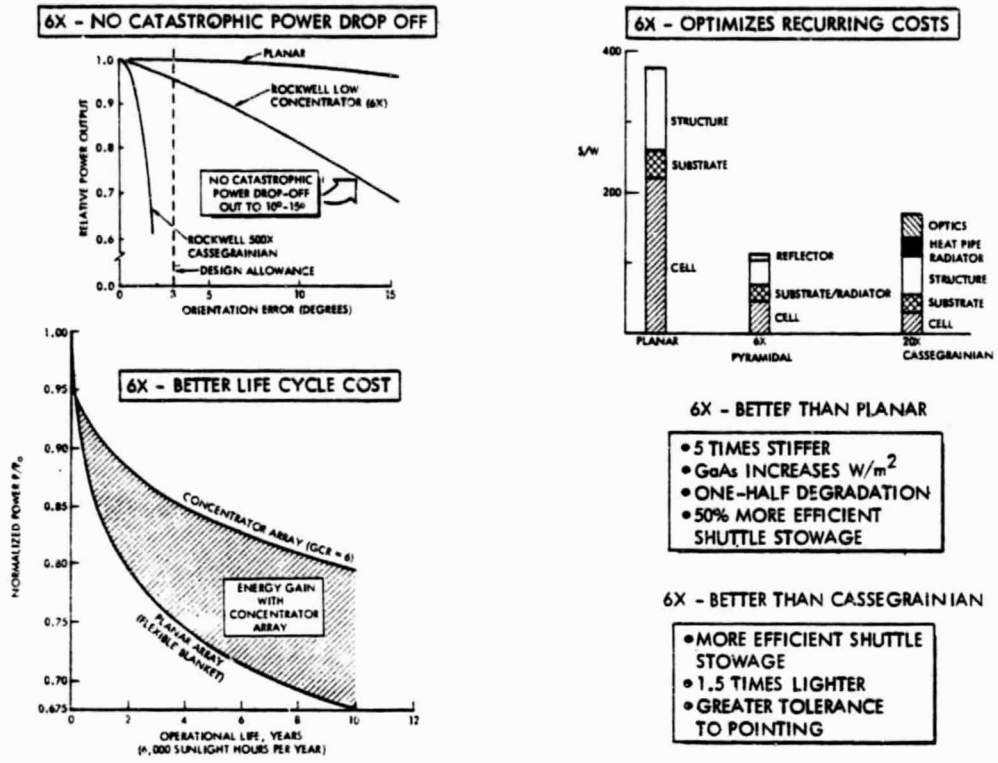

Figure 1-1. The Advantages of a Low CR Design

The issue of pointing accuracy requirements also favors low CR designs. As Figure 1-1 shows, a 6X concentrator is not sensitive and can accommodate several degrees of off-pointing with small loss in output. This greatly relaxes design tolerances and reduces the impact of structural distortions (both transient and steady state) associated with stationkeeping and thermal gradients.

1.3 PROGRAM APPROACH

The approach builds upon results of Rockwell's previous study to provide a preliminary design consistent with the goals of the project, namely technology readiness in the mid-1980's, compatibility with a Shuttle launch, and low recurring and life cycle costs. The overall program objectives are:

- To perform a preliminary design of a low concentration ratio (CR = 2-6) solar array for multi-100 kW (300 kW-1000 kW) low earth orbit application having a low recurring cost with a 1984 technology readiness date.

- Design, fab, test subelements/components to support the preliminary design.
- Identify technology deficient area and scope tasks for resolution.
- Generate cost and schedule for ground test module.

No specific application has been identified for the array design. Rather a generic design has been developed, consistent with the following ground rules:

- Concentration ratio (CR) = 2 to 6.
- Four-sided concentrator module approach.
- Targeted for $30/watt recurring (1978 dollars).
- Use 1984 technology readiness date.
- Design for low earth orbit (LEO) application.
- Design should be consistent with both silicon and GaAs cells.
- Stowage method should be fold-up.
- Design should provide maximum kW per Shuttle launch consistent with other guidelines.
- Watts/kg goal not specified but to be governed by transportation cost penalties and reasonable extension of state-of-the-art.
- Practical configurations compatible with Orbiter cargo compartment and on-orbit maintenance operations.
- Rating of 300 kW to 1000 kW.

The work has been carried out under four technical tasks. These tasks are interrelated logically as shown in Figure 1-2. A brief description of the tasks is included here. They are more completely discussed in later sections of the report.

Task 1 is a preliminary design effort using the pyramidal concentrator element concept defined in Reference (1) as a point of departure. A selected array configuration has been derived through an orderly series of trade studies. These, together with the mission and orbital considerations typical of operation in low earth orbit, have been used to establish a baseline solar array configuration. Each major subsystem (primary structure, integration hardware, reflector/concentrator structure, and solar cell stack/radiator) has been studied separately in order to optimize the array system and to

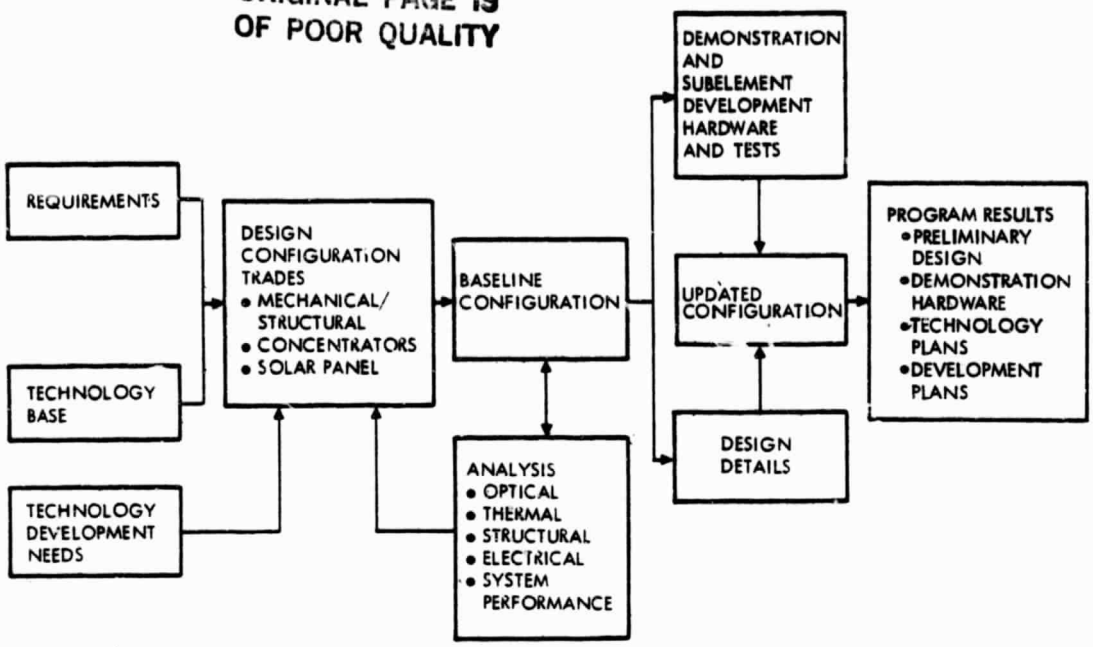

Figure 1-2. Program Logic

assess technology deficiencies. Near the end of the contract effort the results of design analysis, technology reassessment, and subelement demonstration tests (Task 2) was used to update and verify the preliminary design of the array system.

Task 2 deals with the demonstration testing of certain subelements and components. It was designed to provide early insight into component performance and to show confidence that the design concept will work. This task is a major activity of the contract (over one-third of the overall effort). The subelements tested included solar cells (both GaAs and Si) mounted on passive substrate/radiators and a full size reflector/concentrator element. Solar cells, radiator and concentrators were integrated for functional testing. Models demonstrating the stowed and deployment method were also made.

Task 3 addresses development planning for multi-hundred kilowatt arrays. Areas of technology for which there is now insufficient engineering knowledge to support a sound preliminary design were identified. A supporting research technology (SRT) plan for two items identified (welded interconnects, reflector optical stability) are discussed in Section 8. Technologies which will require experimental demonstration in order to establish near-term

feasibility are also provided. Test requirements, tooling, equipment, and facilities were defined and a plan is provided covering the design and fabrication of a ground test/flight test demonstration model for the array as a whole.

Task 4 considered the integration requirements of the array. Mission and orbital constraints typical in low earth orbit were used in an analysis of system interfaces pertaining to the Shuttle orbiter (STS) and those pertaining to large user space vehicle systems. A generic approach was used for the latter since specific missions have not been identified in this procurement. Task 4 results can be used to define specific interface compatibility of the array system for potential low earth orbit mission applications (e.g., Space Station).

The technical effort has been carried out over a two-year period according to the schedule shown in Figure 1-3. Periodic reporting of technical results has been made through monthly letter reports (not shown on the schedule), a mid-term report,[5] and in oral presentations at NASA Marshall Space Flight Center.

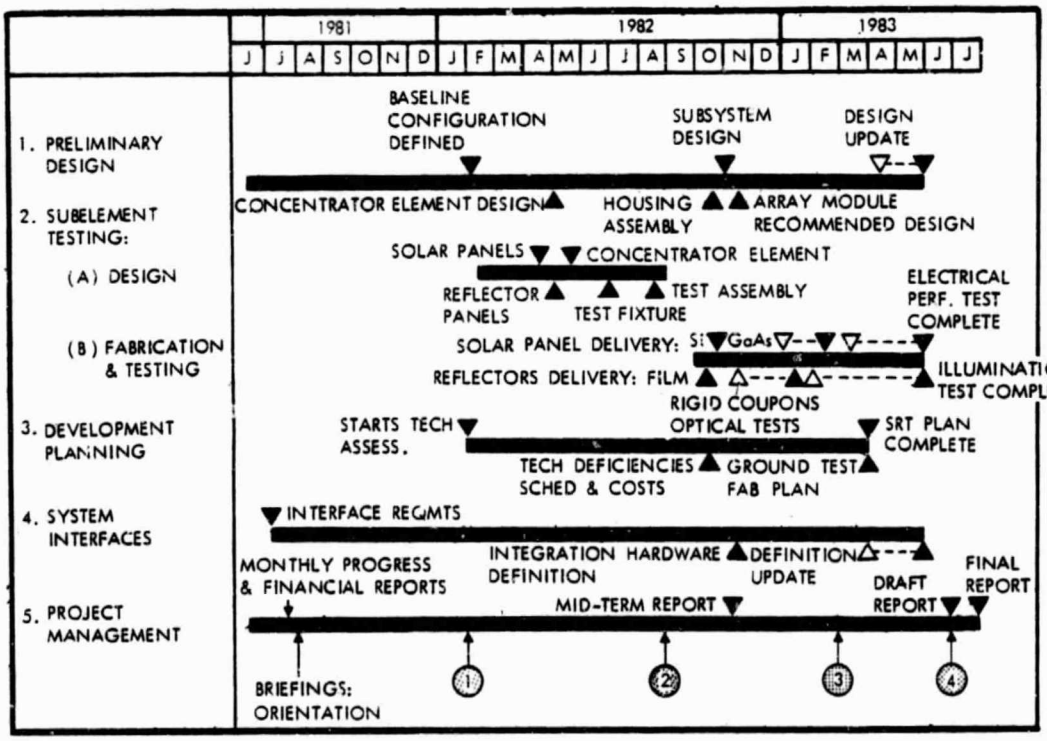

Figure 1-3. Project Schedule

1.4 PROGRAM SUMMARY

1.4.1 Description of the Array Design

The program has developed a preliminary design, described by a total of 30 drawings (see Figure 3-1 and Volume 2). The final design is derived from the baseline design described in the mid-term report[5] with some updates resulting from the test results obtained under the program. The fundamental unit of the array is the module. In the stowed condition it occupies a cube 3.24 m on a side. As many as four of these modules can be cradle-supported in the payload bay of the Shuttle. In the deployed configuration each module extends to a rectangle 19.4 m by 68 m in size. Individual concentrators are hung on cables extending between a housing (in which the folded concentrators are contained during launch) and an end cap. Three pairs of extendable lattice masts are mounted in canisters back-to-back within the housings. They serve to extend the two end caps (and with them the cable-supported rows of concentrators) and to hold them in place when fully extended. The housings and end caps are open truss structures. The masts are hybrid structures consisting of a double-laced section at the canister end and a single-laced section extending to the end caps.

The individual concentrator element takes the form of a truncated pyramid with an aperture of 0.5 m by 0.5 m and truncated base (where the solar panel is located) sized to give a geometric concentration ratio of six. The reflectors are made from aluminized Kapton film 50 μm (2 mil) thick bonded to graphite composite frames. Two of the four sides are hinged and fold inward for stowing. The truncated opening formed at the base of the reflectors is closed out by a solar panel, containing either 50 mm by 50 mm silicon cells or 20 mm by 20 mm gallium arsenide cells laid down on two aluminum sheets hinged for folding. The aluminum half-panels serve as substrates for the cells. The aluminum extends outward beyond the cell area to serve as a radiator with an area twice the solar cell area. Electrical output from individual half-panels is collected and transmitted from one element to another by Kapton-insulated copper flat conductors, 0.14 mm thick.

Each array module consists of 4356 concentrator elements and weighs 4242 kg (for silicon) or 4264 kg (for GaAs). Projected area of the deployed array is 1320 m^2. Other design characteristics are given in Figure 1-4. The beginning of life (BOL) power output in space is 113 kW (for silicon) and 175 kW (for GaAs).

1.4.2 Trades and Analysis

Structural and volumetric requirements determined the size and shape of the module as a whole and its components. The cross sectional area available in the Shuttle payload bay and a variety of other considerations led to the choice of six layers or stacks into which the stowed module could be packaged for launch. The stacking parameter affected the size of the concentrator elements, the effectiveness of the radiators for a given weight, and strength of the lattice masts which could be accommodated within the housing envelope.

Detailed analysis of mast performance by Astro Research Corp. under a subcontract to support this program, defined buckling loads that led to the choice of a hybrid design having high strength at the root and less strength and weight at the tip where loads were reduced. Computer models for the module structure were generated to verify that modal frequencies were separated by a decade or more from potential excitation frequencies. Deflection due to stationkeeping thrust, thermal distortion and other sources was assessed to insure that optical pointing errors did not exceed the three degrees assumed as a design requirement.

Special-purpose thermal analyses were performed to assess the effects of thermal cycling and to optimize radiator size and weight. A detailed thermal model of the concentrators was prepared which took into account illumination distributions, radiation exchange between adjacent concentrators and electrical-thermal coupling of the solar panel. Results showed that no component reached excessive temperatures. The reflector film reached a maximum temperature of 130°C. Solar cell maximum temperatures were also 130°C. Average cell temperature was 116°C for GaAs and 120°C for silicon. During eclipse transients thermal stresses in the reflectors were limited to 1/4 of that for the high-temperature yield stress.

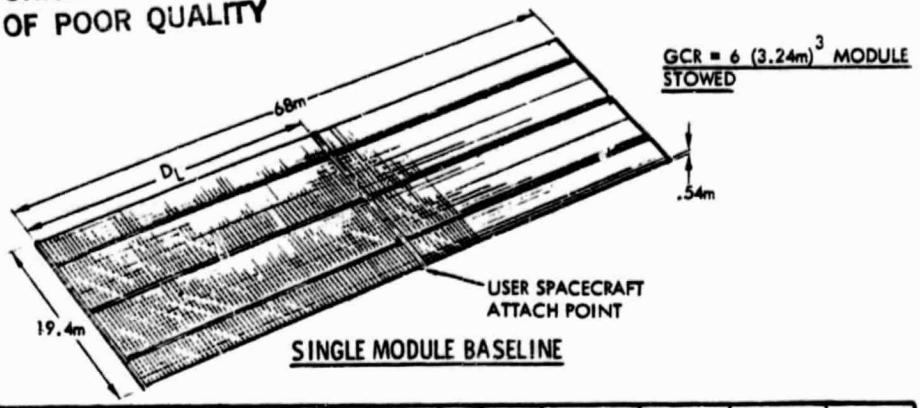

AREA:

NUMBER OF CONTAINERS	NUMBER OF MASTS	NUMBER OF CONC STACKS	NUMBER OF CONC PER STACK	MODULE WIDTH (m)	MAST DIAMETER (m)	D_L (m)	DEPLOYED ARRAY AREA (m^2)	NUMBER OF CONC	TOTAL CONC APERTURE (m^2)	OVERALL PACKING FACTOR (%)
6	6	66	66	19.4	.64	32.4	1320	4356	1089	82.5

WEIGHT:

N	NUMBER OF MASTS	NUMBER OF CONC	CONCENTRATOR ELEMENT (kg)				CONTAINER AND CANNISTERS (kg)		TOTAL (kg)
			REFLECTORS (FILM FRAME)	SOLAR PANEL	HARNESS	TOTAL	CONTAINERS/ MECHANISMS & HARNESS	CANISTER/ MAST	
6	6	4356	.253	.305	.11 (Si) .09 (GaAs)	.67 (Si) .65 (GaAs)	712 (Si) 799 (GaAs)	630	4264 (Si) 4242 (GaAs)

Figure 1-4. Array Module Design Characteristics

Extensive ray-tracing analyses of the concentrator were carried out to determine optical performance for cases of normal incidence and varying amounts of off-pointing. Average concentration over the solar panel was found to be 4.64 (77% optical efficiency) at 0° pointing angle. Efficiency falls off very gradually, with no catastrophic drop out to angles as high as 15 degrees off normal. Light reflected from the upper corners of the concentrator was found to be ineffective in illuminating the solar panel cell area but did contribute significantly to heating the reflectors.

The laboratory electrical tests performed on cells and panels supplied by Applied Solar Energy Corporation (ASEC) and Spectrolab, the two solar cell subcontractors, resulted in refinement in the solar cell models used for performance estimates in the mid-term report.[5] These cell models were incorporated into a combined electrical-thermal model of the concentrator. Sample calculations showed that by connecting each row of cells across a half-panel in parallel, mismatch effects due to temperature and illumination non-uniformities could be greatly reduced, compared with a design in which each cell was connected in series.

Peak power outputs per concentrator element were calculated to be 26.4 watts for silicon and 40.5 watts for GaAs during space operation.

1.4.3 Cost and Performance Analysis

Three different approaches were used to develop cost estimates for components of the array. Lattice mast assembly and solar panel costs were based upon subcontractor projections for the 1984 time period. Reflector panel costs were based on materials and processes analysis for semi-automatic production. Structural components were estimated by means of a mass algorithm derived from historical costs for space hardware. Transportation costs to orbit, costs of drag make-up propulsion and the effect of cell degradation in orbit are additional factors which were taken into account to estimate life-cycle energy costs.

Electrical output at beginning of life was estimated from the detailed output per concentrator element described above. for the standard conditions of zero point angle and minimum earth radiation. These results were used to derive lumped parameter performance analysis with which to explore the effects of many variables. The lumped parameter method was also used to predict ground test performance. Table 1-1 summarizes the array module performance parameters.

Table 1-1. Solar Array Module Performance Parameters

Parameter	Cell Type	
	Silicon	GaAs
Watts/m^2 (BOL)	85	133
Watts/kg (BOL)	27	41
Recurring Cost (BOL) 1982 $/W	114	166
Life Cycle Energy Cost (10 years) 1982 $/kWh	4.0	4.4

1.4.4 Demonstration Tests and Experimental Operations

Early in the program three structural-kinematics models were fabricated to aid in visualizing the structural and kinematic properties of the array. These included a 1/15 scale deployment simulator, a four-element dynamic simulator and a full-scale engineering aid model.

Fabrication experiments were carried out on many candidates for both film-frame and rigid panel reflectors. Satisfactory panels were fabricated using Kapton film on molded graphite composite frames. Laboratory optical tests on these panels gave reflectance values of 89%. Stretched film panels have remained taut and unwrinkled for over a year.

Laboratory electrical tests were performed on both single solar cells and solar cell panels. Both ASEC and Spectrolab, the subcontractors, provided individual cell air mass zero (AMO) outputs referenced to primary balloon flight standards. They also measured representative spectral response curves and panel output at one sun AMO. Panel outputs were confirmed by Rockwell after delivery. All panels exceeded specified requirements by a substantial margin.

Current-voltage characteristics for both silicon and GaAs cells were determined in Rockwell's Large Area Pulsed Solar Simulator (LAPSS) facility at elevated temperatures and in concentrated light of AMO spectral quality. The data was used to update cell models for performance predictions.

Full scale illumination and performance tests were performed on a demonstration concentrator in natural sunlight at Seal Beach and at Table Mountain Solar Observatory. Distribution of concentrated sunlight in the plane of the solar panel was measured by photographing a diffuse reflecting plate. Panel and solar cell temperatures were measured by thermocouple and infrared camera. Electrical performance was measured for both silicon and GaAs panels as a function of pointing angle and during controlled distortion of the concentrator geometry.

Test results on the demonstration concentrator matched predicted performance very well in general. Illumination distributions and average value agreed with ray trace calculations in the sense that local CR variations were similar and average optical efficiency fell off gradually with pointing angle as predicted. Apparent concentrations were approximately 0.6 suns higher than predicted, however. This is believed to be attributable to the presence of diffuse light coming from directions near the sun rather than being spread uniformly as assumed in the theoretical calculations.

Measured power outputs of 24 watts for the silicon panel and 15 watts for the GaAs half-panel (30 watts per panel) agree closely with predictions for Table Mountain conditions. The gradual fall off of output with pointing angle also followed the predicted trend. Distortions in which one or both hinged reflector panels were moved inward produced a rapid drop in output. Measured solar cell temperatures varied from 44° to 71° C, agreeing reasonably well with pretest predictions of 55° to 79° C. Cell temperature distributions measured with infrared camera agreed qualitatively with analytical predictions.

The following sections of this volume provide detail description of the design, trade studies, analysis, experimental results and other activities performed during the contract effort.

2.0 CONCENTRATOR ARRAY DESIGN CRITERIA

The design requirements for the array encompass three mission phases: launch, deployment, and orbital operations. No specific missions have been identified. Rather, the design is a generic one for high-power space systems Shuttle-launched into low earth orbit.

2.1 LAUNCH

In its stowed configuration the solar concentrator array module must be of a size that fits within the Shuttle bay dynamic envelope, allows air lock ingress/egress, and installation of payload ground handling mechanisms. The module must stay within the Shuttle cargo bay longitudinal center of gravity envelope.[6] Module attachments to the Shuttle orbiter should be compatible with the location and load capability of the orbiter attachments and/or cradle installation. The attachments should provide access for removal of the array module by means of the remote maneuvering system (RMS) in orbit.

2.1.1 Static Loads

The critical load factors listed in Table 2-1 were used to determine the Shuttle launch-induced loads. The landing load factors are included to provide for the possibility of mission abort-induced return and landing. The structure will withstand a differential pressure of 3450 Nm^{-2} (0.50 psi).

Table 2-1. System Requirements for Structural Design (Launch Phase)

- STS (Orbiter) compatibility
- Orbiter cargo bay dynamic envelope
- Quasi-steady state flight loads — acceleration in g's

	N_x* (axial)	N_y* (yaw)	N_z* (pitch)
• Boost environment	+2 -5	± 3	± 5
• Landing	+1.8 -2.0	± 1.5	+ 4.2 - 1.0

* Load factors in Orbiter coordinates.

2.1.2 Dynamic Loads

The solar array module must survive the Shuttle cargo bay acoustic environment (decibels versus frequency) given by the dotted line of Figure 2-1 (taken from Ref. 6). This curve represents the recommended environment based on STS-1 through STS-4 flight data. The stowed solar array module will have a minimum modal frequency of 9.0 Hz.

2.1.3 Thermal Environment

It is assumed that the module will be electrically inert during the launch phase, with negligible heat dissipation. The thermal behavior is determined by the closed-door environment of the Shuttle bay, as modeled by the Simplified Payload/Orbiter Thermal Simulator (SPORTS model)[8]. This model provides thermal characteristics (temperatures, capacitances and conductances) for exposed payload bay surfaces and boundary temperatures for the underlying structure.

2.1.4 Electrical Environment

It is assumed that the module will be electrically inert during launch.

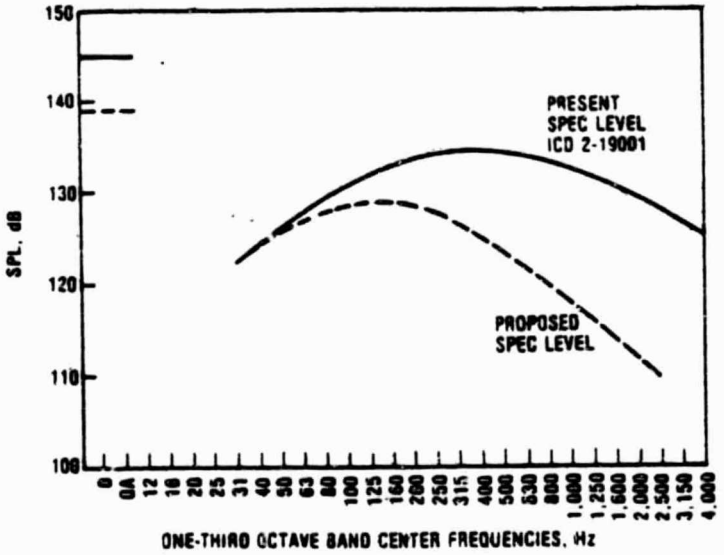

Figure 2-1. Revised Empty Payload Bay Acoustic Criteria for Lift-off

2.2 DEPLOYMENT

This phase includes (1) the detachment and removal of the solar array modules from the orbiter's cargo bay and attachment to the user satellite, (2) articulation and deployment of the folded array module containers, and (3) extension of the deployable masts and individual concentrator elements.

The attachment interface will have provisions for soft docking of the array to the user spacecraft. The attachment interface will also have provisions for structural attachment, transmission of power to the spacecraft, and two-axis articulation of the array to maintain pointing toward the sun to within $\pm$ 0.5 degrees. Electrical power for deployment and extension of the solar array module will be provided by either Shuttle or user spacecraft.

2.2.1 Static Loads

Static loads during this phase are assumed to be no greater than static loads during orbital operation.

2.2.2 Dynamic Loads

The structural attachments to the payload bay must provide for controlled release and removal of the solar array module. The rate of extension of the masts and release rates for concentrator structural components shall not impose loads in excess of the launch and orbital operations capability.

2.2.3 Thermal Environment

The open-door environment of the Shuttle bay will be simulated by the SPORTS model during the early portion of the deployment phase.

2.2.4 Electrical Environment

The array will be protected from electrical transients associated with partial illumination of elements during the deployment phase.

2.3 ORBITAL OPERATION

The array modules are designed to keep life-cycle energy costs low for low-earth-orbit satellites. Performance factors such as array module power per unit weight and power per unit deployed area are considered important to the extent of their influence on cost effectiveness in orbit. Modularity is

a major consideration in developing an acceptable design concept that can be used for a wide range of power needs of future satellites. General system requirements are tabulated in Table 2-2 and discussed below.

2.3.1 Static Load

The solar array masts, housing and concentrator element subsystems shall sustain the loads associated with atmospheric drag, gravity gradient and solar pressure within acceptable deformation tolerances. The altitude range for orbital operation is assumed to be 500 to 600 km. Acceptable deformation is defined as that which maintains all concentrators optical axis within three degrees of the solar direction under the combined influence of mechanical loads, thermal stresses and pointing errors for the array as a whole.

2.3.2 Dynamic Loads

The attachment of the array to the user spacecraft will result in the transfer of dynamic perturbations of two types, namely spacecraft pointing and stationkeeping and Shuttle docking maneuvers. To provide adequate frequency separation between the array and the spacecraft control system, a minimum modal frequency (cantilevered from the user spacecraft interface) of 0.037 Hz is required.

2.3.3 Thermal Environment

In addition to direct solar load, the array is exposed to Earth emission and albedo. Global annual average values of 237 watts m^{-2} and 0.3, respectively, were used to evaluate Earth radiation effects on the design. Orbit inclination values between 28.5 and 57 degrees were assumed to evaluate eclipse duration, irradiation fluence levels and array-Earth configuration factors. Thermal interaction between array and spacecraft is assumed to be second order and will be ignored due to lack of specific knowledge about spacecraft geometry and thermal characteristics.

2.3.4 Electrical Environment

It is assumed that the solar array delivers power to a spacecraft bus at a voltage between 150 and 300 volts.

Table 2-2. System Requirements for Orbital Operations

- Orbit of 500-600 km (introduces launch site and inclination restrictions)
- Attitude control
  - Stationkeeping acceleration ranges from 0.001 g to 0.01 g
  - Control system frequency separation of at least one decade
- Thermal loading (not to exceed $\pm$ 1° average in pointing error)
- Array orientation (not to exceed $\pm$ 0.5° in pointing error)
- Atmospheric drag (4.3×10^{-4} N/m^2)
- Solar pressure (4.5×10^{-6} N/m^2 in GEO)
- Gravity gradient (7.3×10^{-5} N/m^2)

2.4 REQUIREMENTS

In addition to the detailed criteria established by the three operational phases of any mission, the array design is governed by the ground rules previously enumerated in Section 1.3. Of greatest influence on the design are:

- Very near term technology readiness (1984)
- Silicon and gallium arsenide compatibility
- Shuttle compatibility
- Very large power capability (multi-100 kW)

The solar array described in this report satisfies these and other constraints which were considered for this program. However, in a particular future application, some or all of the constraints may be modified or removed, permitting a better specific design in that case. For example, a later technology readiness date, say 1990, would be able to take advantage of improved solar cells and developmental advances in reflector fabrication. Although GCR=6 is a good compromise for a concentrator compatible with both cell types, a silicon design is optimized at lower values and a GaAs design at higher. In the latter case it should be possible to reduce cell costs and radiator weight by designing for GaAs cells only. For lower power, a smaller concentrator element size can be used to lower cell operating temperature.

Shuttle transport to orbit is the likely mode for all large solar arrays in the foreseeable future. The present design makes effective use of cubical stowed modules (see Figure 2-2) to use the available payload bay capability

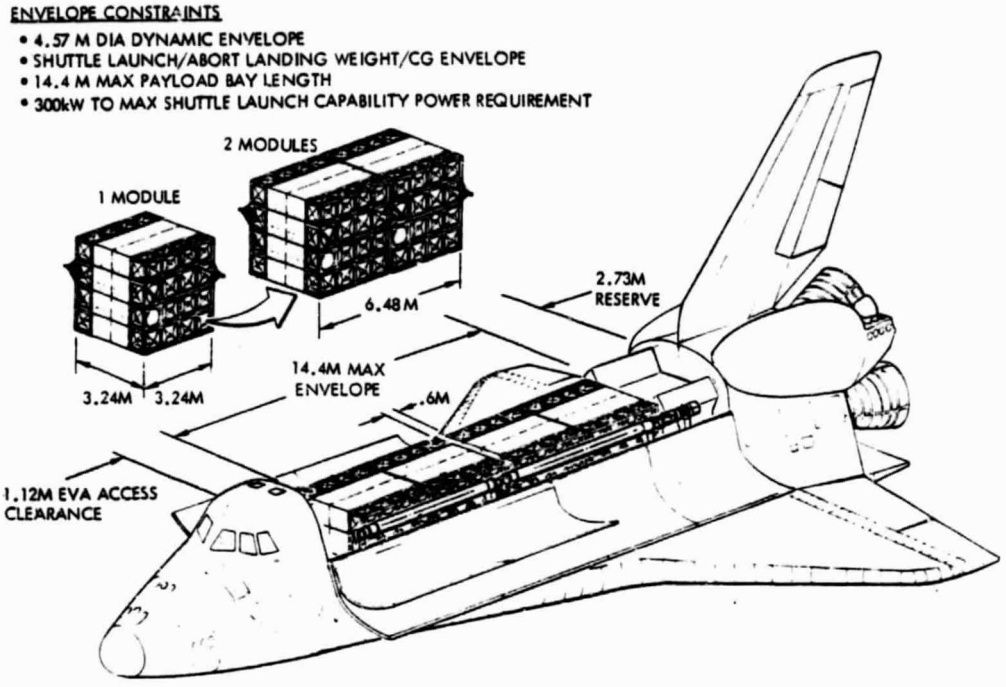

Figure 2-2. Modularity for Shuttle Compatibility

to launch from 452 to 700 kW per flight. When intermediate power levels are required, more flexibility is possible in the design of modules and in sizing concentrators.

3.0 DESIGN DESCRIPTION

3.1 DRAWING TREES AND TOP LEVEL DRAWINGS

The solar array preliminary design is embodied in a set of drawings which, together with associated callouts and specifications, provides a physical description of the system as a whole and its associated subsystems. Figures 3-1 and 3-2 are drawing trees showing the relationship between individual subassembly drawings making up the total preliminary design and test hardware. Those drawings illustrating major assemblies are included in Volume 2.

The array module design has been broken down into three major subsystems: the container structure, module integration hardware and the power-generating or concentrator element. Figure 3-3 illustrates the nomenclature adopted for the solar array. The fundamental building block is the container which, when assembled into a single module and deployed, forms a large rectangular area of 19.4 m x 68 m. Modules attach to the user spacecraft along the longitudinal centerline of the container housing. The module structure consists of a set of six container housings attached end-to-end containing the folded concentrator stacks, deployable masts and their canisters, and end caps which are extended by the masts. The power-generating components of the array are the concentrator elements containing reflector panels which concentrate light onto the solar panels and a flat wire harness to combine and collect the power output of individual elements of the module.

3.2 BASELINE AND UPDATES (OVERVIEW)

The performance of the demonstration concentrator element conformed in all respects with design predictions. There have been few updates, therefore, on the baseline design defined in the mid-term report.[5]

Two approaches to reflector manufacture were retained in the baseline, namely the film-frame and the rigid panel. Difficulties in the fabrication of a successful reflector panel (i.e., one having acceptable flatness) using rigid-panel technology led to the conclusion that this approach should not

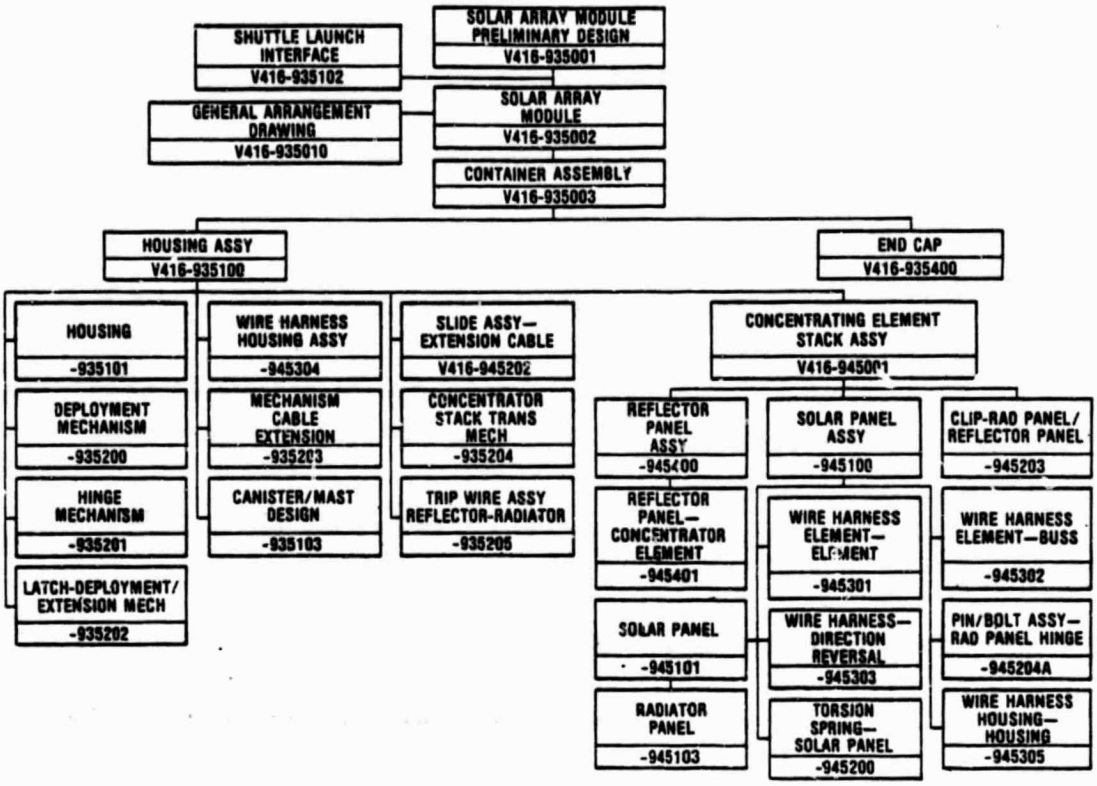

Figure 3-1. Preliminary Design Drawing Tree

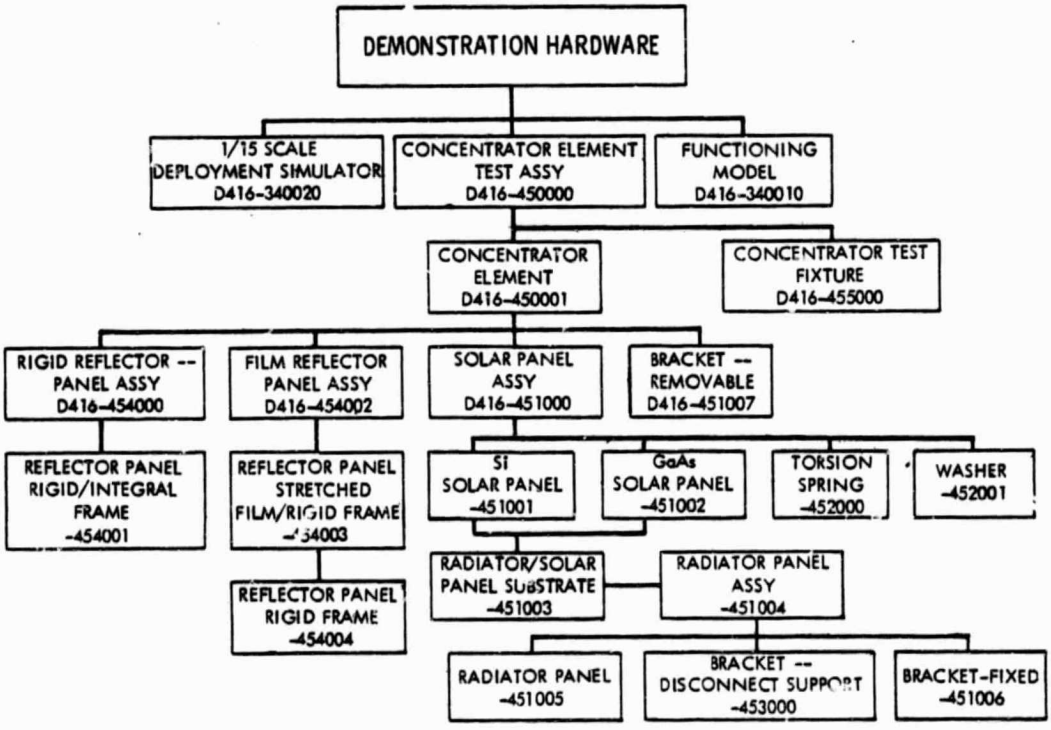

Figure 3-2. Test Hardware Drawing Tree

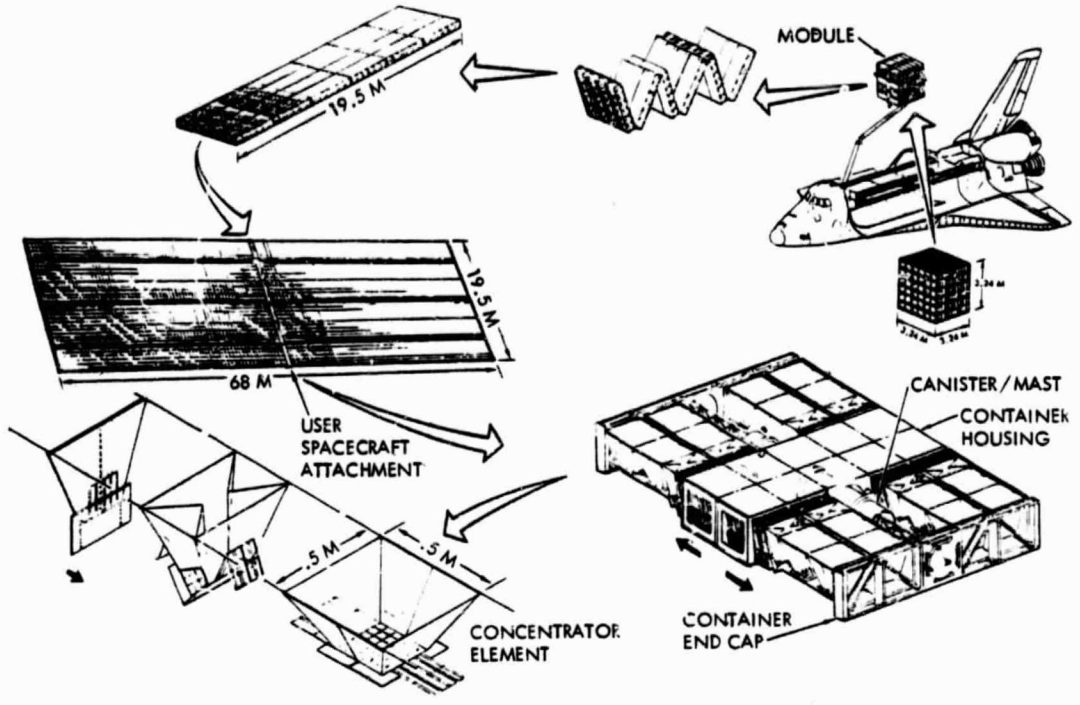

Figure 3-3. Concentrator Array Module Nomenclature

be used in a near-term (1984) design and the film-frame approach was selected for the final design. However, the rigid-panel approach still appears to have potential cost advantages and is discussed in Section 8 as a design improvement.

The baseline design took a conservative approach to the use of protective diodes at the panel level. Electrical experiments on the delivered solar panels has given more information on cell reverse bias characteristics and made possible the reduction of protective diodes for gallium arsenide panels in the final design.

Structural design of the array proceeded on the assumption that in the stowed configuration the modules could be attached to the Orbiter payload bay either by a cradle or by an integral supporting structure held together by an interior latch system. In the final design the cradle concept has been chosen.

3.3 MODULE CONFIGURATION

The solar array is designed to be transported in the form of modules within the 4.6-m-diameter, 14.4-m-long dynamic envelope of the Shuttle payload bay. The cubical designs illustrated in Figure 3-4 provide the compact stowage of up to four single or two dual modules per Shuttle flight (see Figure 3-5). Compactly folded concentrator elements contained within the modules are protected from damage due to vibration and acoustic loads during launch by means of separation buttons on vulnerable surfaces. Structural integrity of the containers is maintained by means of a cradle system which maintains the module structure under compression during launch. Acceleration loads are carried out through attach points and transmitted to the Shuttle structure through a cradle or support structure.

The single module, packaged in the form of a cube 3.24 m long per side, will be removed from the bay and deployed using the remote maneuvering system (RMS) arm grappling the cradle attached to the module. The six folded container sections of the array module will deploy in accordian fashion, driven by rotary incremental actuators. Five such actuators, each redundant in itself, and each producing a 6.8 N-m of torque will execute the 180° rotation at each joint to produce the 19.4-m-long deployed container sections (see Figure 3-6). The total time required for this maneuver is 29 minutes. Each actuator provides 17.0 N-m holding torque while the linear incremental actuators drive the latching mechanism closed, taking 10 seconds. Extension of the contractor elements are then accomplished by the two sets of three canister-deployed continuous longeron double/single-laced (hybrid) masts which extend the end cap, carrying out the concentrator extension mechanism cables and the first concentrator element in each stack. Each mast extends a total of 32.4 m from the end of its canister.

3.4 CONTAINER STRUCTURE

Figure 3-7 illustrates the baseline design of a single container. Listed below is the description of each subelement or subsystem housing in the container. The module consists of six containers with two masts/canisters in three of the containers. The other three containers have concentrator elements stowed in lieu of the masts/canisters shown in Figure 3-7. Thus a sub-module can be formed using pairs of containers consisting of one with masts/canisters and another without.

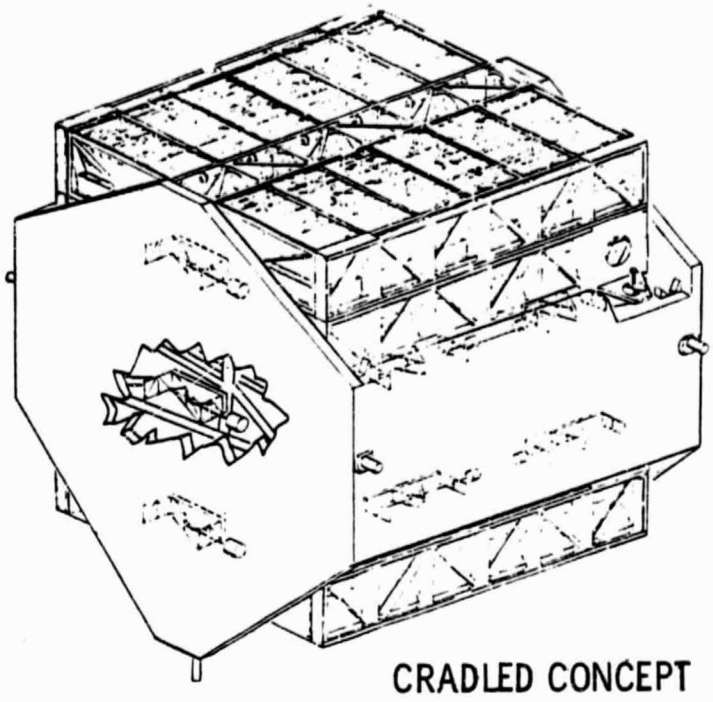

Figure 3-4. Solar Array/Shuttle Interface

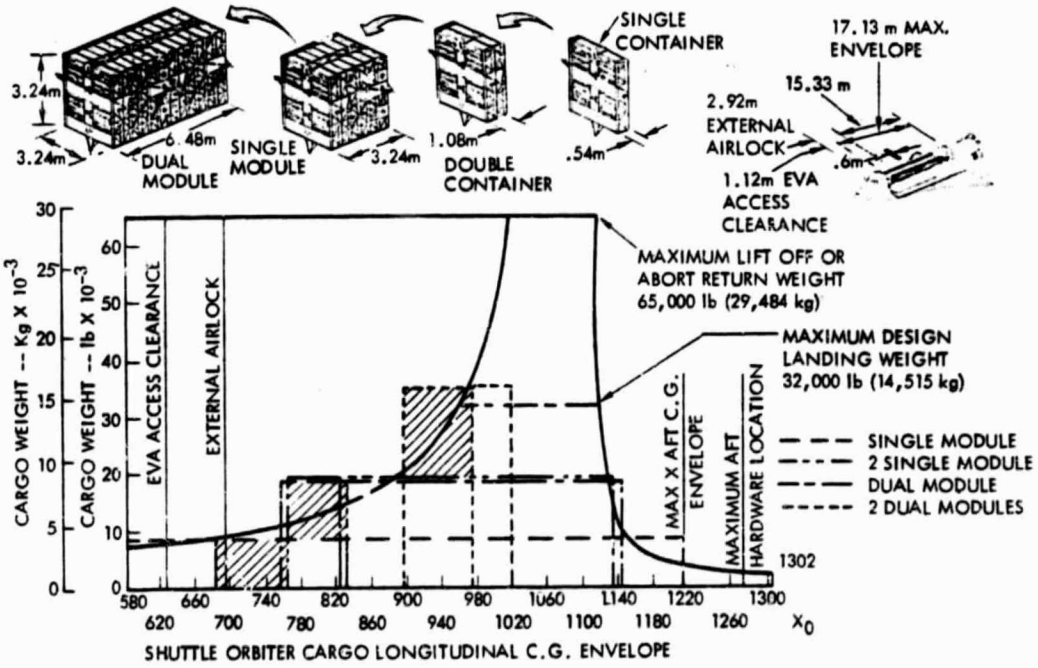

Figure 3-5. Array Module Stowage in Shuttle

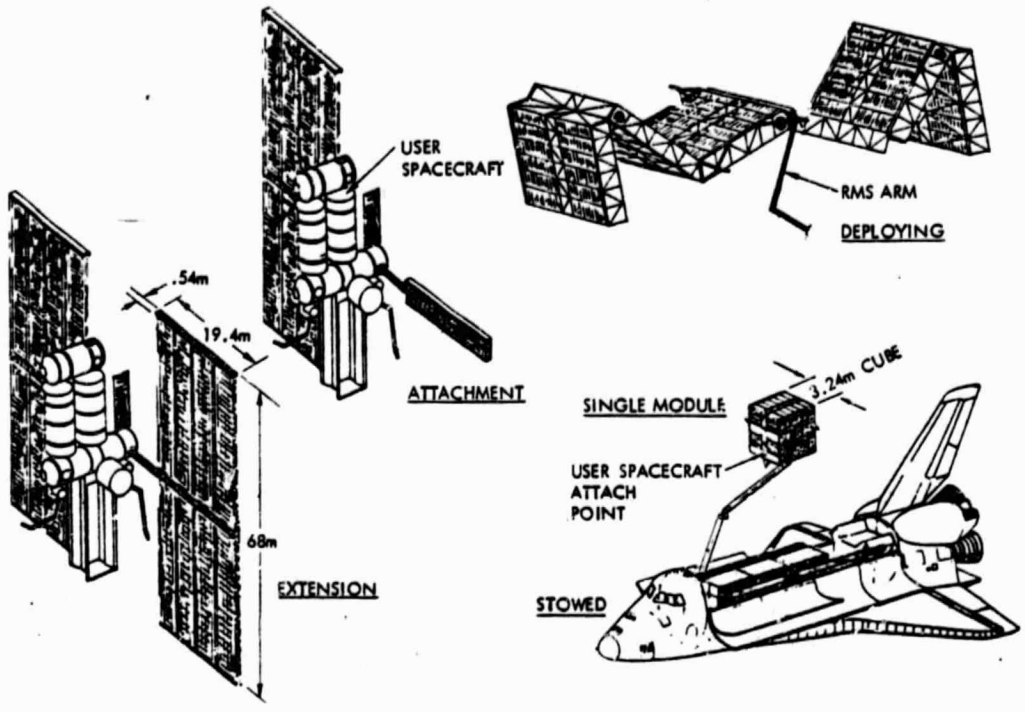

Figure 3-6. Concentrator Array Module Design Configuration

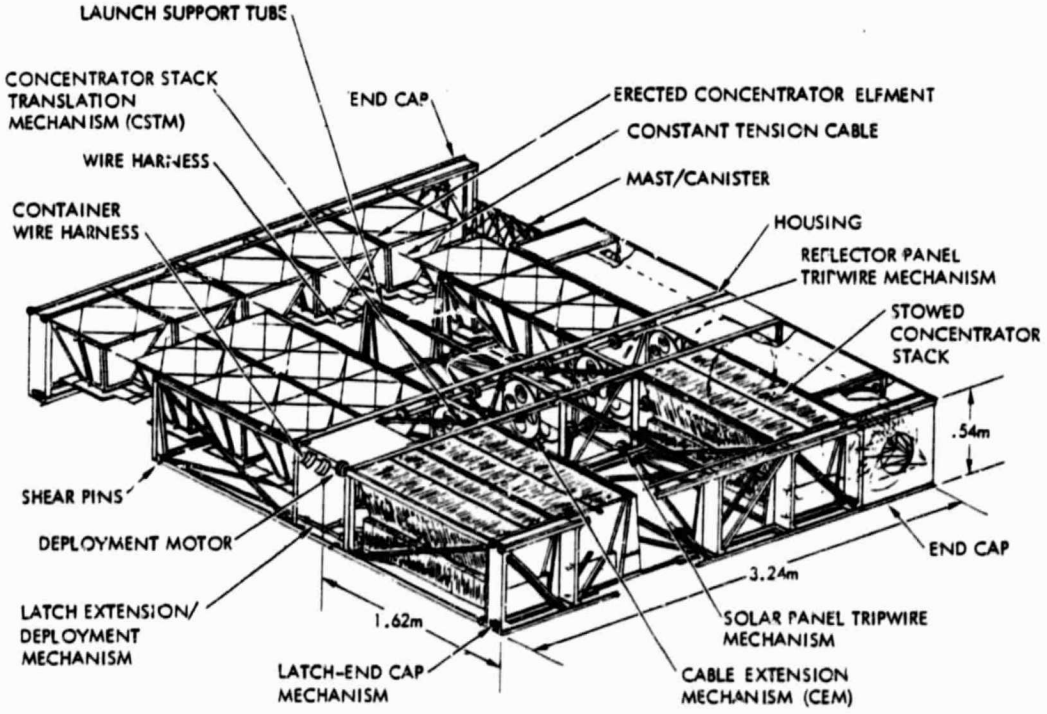

Figure 3-7. Container Structures/Mechanisms/Subsystems

3.4.1 Housing

The housing is the focal point of the structural system with all subsystems being attached to the housing. The prime drivers in the sizing of the housings were the concentrator element size, Shuttle compatibility, and static and dynamic loads. Also due to the large number of parts involved, a common, simple, mass-producible concept was required. The design that was selected was a design symmetrical about the longitudinal centerline. Each housing is 0.54 m high x 3.24 m wide x 3.24 m long. There are two types of housings, one with five concentrator stack bays and a mast bay per side, and one with six concentrator stack bays per side.

The housing is a truss-type structure made from two machined parts, four types of extrusions, one type of bent sheet metal, flat sheet metal shear webs and gussets. These parts are of 2024-T6 aluminum except for the launch support tubes which are stainless steel. Down the center of the housing is a truss-type boss 0.54 m high x 0.05 m wide with the longerons being T-extrusions running the full length of thehousing on both outer corners, top and bottom. All parts begin or end at these longerons. The latch mechanisms, hinge mechanism, deployment motor, wire harnesses, CEM's, CSTM's, solar panel tripwire mechanism, reflector panel tripwire mechanism and the other mechanical subsystems are mounted inside this box section. On the outboard sides of this central box are the concentrator stack bays. Each bay is 0.54 m long (having six equal bays per side). On the housings with mast bays, a concentrator stack bay is modified by closing out the top and bottom of the structure with shear panels, and adding structures to which the extension motors and structural tie-downs are mounted. The bays are divided by a truss structure having the launch support tubes at the top to carry the launch loads of the concentrator element stacks. On the end cap/housing interface there is an L-extrusion with shear pins at the base and vertical bent sheet metal stiffeners to support the launch support tubes. The launch support tubes also attach to the end cap to dump longitudinal launch loads into the end cap. Inside the launch support tubes exists a thin bonded silicon rubber sheet with a slightly smaller inside diameter than the slide mechanism outside diameter. This allows the extension of the concentrator elements to be semi-controlled. The cable extension mechanism (CEM) cable runs down the center of the launch support tubes and attaches to the end cap.

3.4.2 End Cap

The end cap is extended by the masts and is used to extend the concentrator elements from the housing, extend the constant tension cables from their mechanisms, and to carry the loads during stationkeeping from the concentrator elements to the masts. The end caps are held in place during launch by a combination of shear pins, latches, and if one is required, the cradle system. The structure was designed to use very few parts to produce the structure. In the structural design, all the end caps can be built from one type of machined part, two types of extrusion, and one type of bent sheet metal along with flat sheet metal gussets and shear panels. The end cap design uses for 2024-T6 aluminum.

3.4.3 Canister/Mast Design

The concept calls for a deployable structure (Figure 3-8) to extend the end caps from the housing, drawing the CTM cables and the first concentrator in each stack out of the housing. The mast also carries the on-orbit stationkeeping loads from the end caps and concentrator elements to the housing. The mast chosen is a hybrid-type single/double-laced continuous longeron, canister-deployed mast using S-glass/epoxy for the longerons, battens and diagonals (see Figure 3-8). The canister envelope is to be 1.62 m long with maximum outside diameter of 0.50 m. The mast itself will be 0.44 m diameter and 32.4 m long, fully extended. The longerons are a square cross section 6.6 mm x 6.6 mm, the battens are a rectangle cross section (W/T = 2.75) of 3.74 mm x 10.11 mm, and the diagonals are a round cross section 3.3 mm diameter; all are of pultruded S-glass epoxy. The hybrid mast design is capable of sustaining acceleration forces greater than 0.012 g before longeron buckling occurs. The masts are spaced to carry approximately 12 concentrator element stacks each. The drive motors are each controlled through a central servo control unit to allow for uniform extension. Each motor drives a bull gear with a pinion, requires 260 watts of power, and takes 27 minutes to fully extend one side of the array. The prime drivers in sizing the mast were the maximum outside diameter of the canister, the g loading during on-orbit stationkeeping, and the maximum stowed length of the canister.

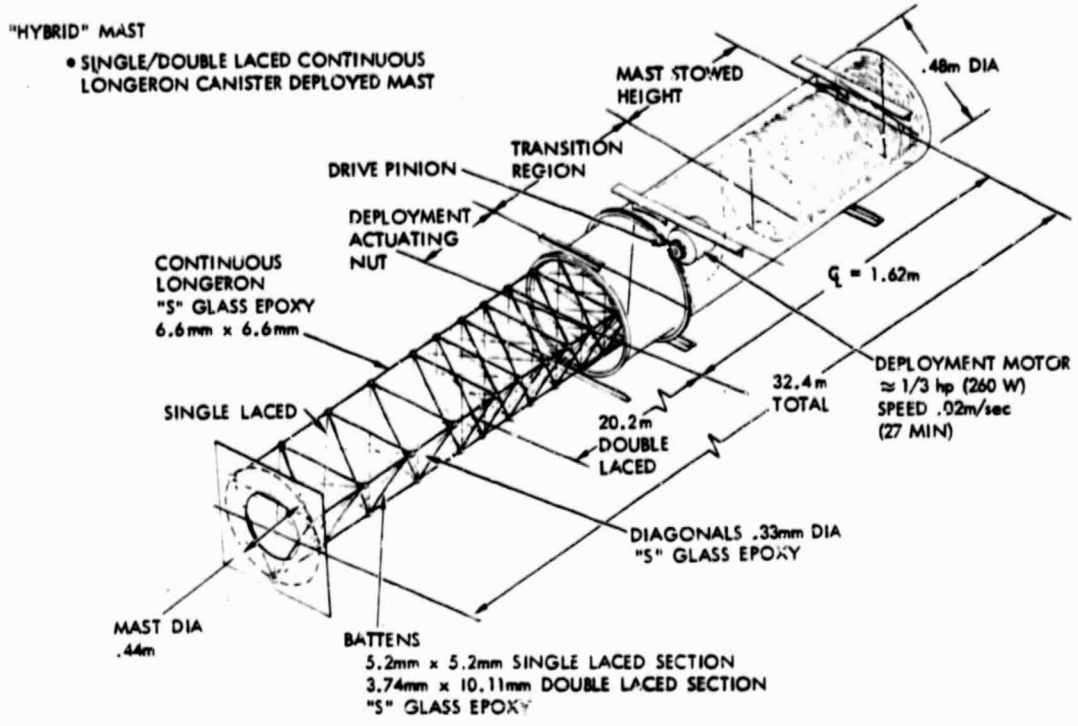

Figure 3-8. Mast Mechanism and Structure
(Astro Research Data)

3.4.4 Concentrator Stack Translation Mechanism (CSTM)

The CSTM assembly consists of a pair of CFS's mounted to a small pulley. Each assembly is mounted to the backside of a CEM and attached by a 0.51 mm stainless steel cable to the last slide assembly in each set of concentrator element stacks (see Figure 3-9). At the end of the mast extension, during thermal growth, or on-orbit stationkeeping, the CSTM maintains the extended stacks under 7.2 N of pre-tension, allowing the last two and one-half concentrators to remain erected in the housing and translate within the launch support tubes. The maximum extension of the CSTM cable is 1.0 m. The pulley is manufactured from a thermoplastic, and the CFS's are stainless steel wound on the pulley. There are 78 identical CSTM's required in the single module concept.

3.4.5 Cable Extension Mechanism (CEM)

The mechanism consists of a pulley assembly 0.31 m diameter that plays out braided stainless steel cable 0.51 mm diameter, 35 m long at constant tension using two constant force springs (see Figure 3-9). At full extension, the cable is under 20 N tension providing planar stability for the concentrator elements. There is one CEM between each concentrator element stack per direction and one per direction on each end of the stacks. The mechanism is a simple design calling for seven different kinds of parts. The pulley and spring housings are thermoplastic, the constant force springs are stainless steel, and the structure is aluminum sheet metal. There are seventy-eight CEM assemblies in the single module concept.

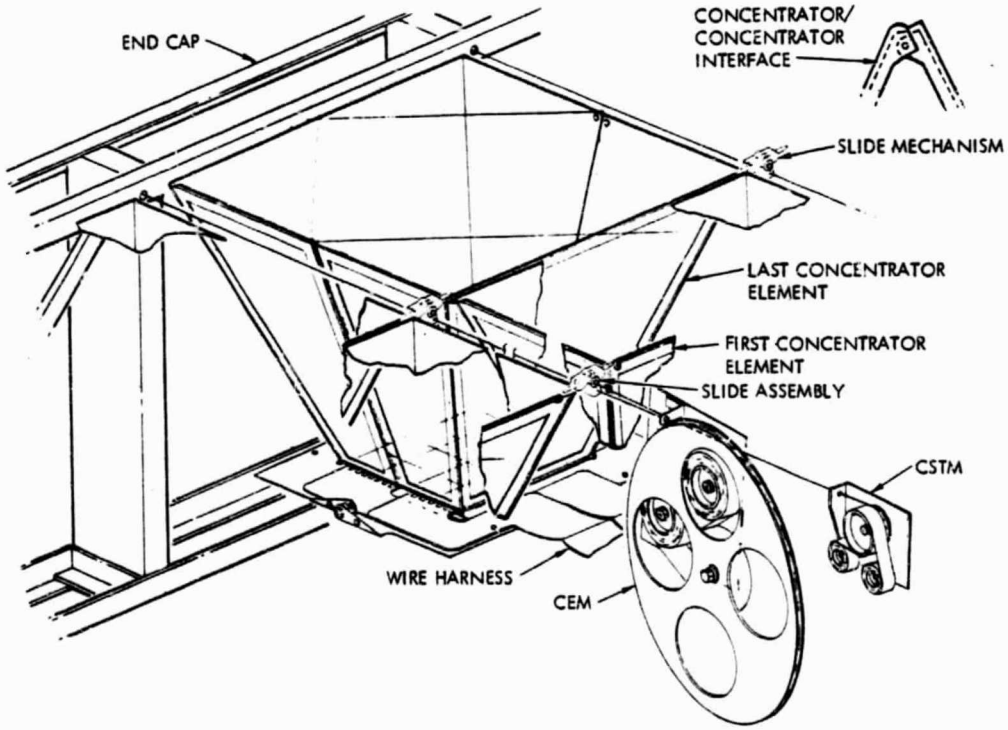

Figure 3-9. Concentrator Element Interfaces

3.4.6 Slide Assembly

The slide assembly functions as the tie point for the concentrator stack/stack interface, the concentrator stack/launch support tube interface, the concentrator stack/CEM cable interface, and the concentrator element stack spacer (see Figure 3-9). The slide mechanism is a two-part molded thermoplastic part that is assembled on the CEM cable with adjacent concentrator element stacks. When the assembly process is finished, it allows the concentrator elements to act as a continuous sheet, as opposed to individual rows. There are approximately 5000 slide assemblies in a single array module.

3.4.7 Latch-End Cap Extension Mechanism

At the interface between the end cap and the housing on the end of the housing with the container/container latching mechanism is a device called the latch-end cap extension mechanism (see Figure 3-10). The assembly allows activation of the latching mechanism in the end cap while the end cap is adjacent to the housing but does not interfere with the end cap extension. The mechanism is attached by a control rod to the latch deployment/extension mechanism bell crank. When the bell crank is actuated, the control rod activates a slider linkage mechanism across the housing/end cap interface closing and locking the latch using a spring retained over-center hinge. The latch-end cap extension mechanism is made from 2024-T6 aluminum and requires ten assemblies for either single- or double-module concepts.

3.4.8 Reflector Panel Tripwire Mechanism

The reflector panel tripwire mechanism works in conjunction with, and in much the same manner as the solar panel tripwire mechanism. The cables run from the end cap to the housing on the top of the concentrator elements. There are two 0.51 mm stainless steel cables per concentrator element stack (see Figure 3-11). The cables run from the top center of the end cap in an alternate zigzag fashion from one reflector half panel eyelet to the next concentrator element reflector half panel on the opposite side of the bay. This pattern continues all the way back to the housing. Upon leaving the last concentrator element, the cables enter the center of the housing box structure longeron cap in each concentrator stack bay, through the wire tension sensor, and to the torque tube pulley system. The pulley/torque tube system is made from graphite/epoxy tube and attached by bearing/flange to the housing. The

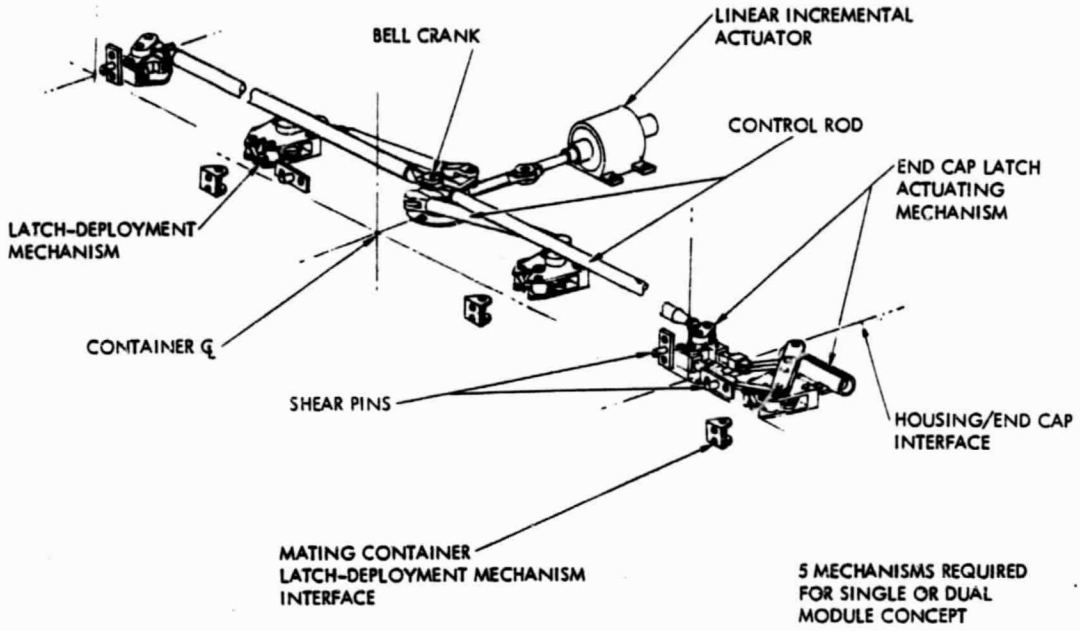

Figure 3-10. Deployment Latch Mechanism

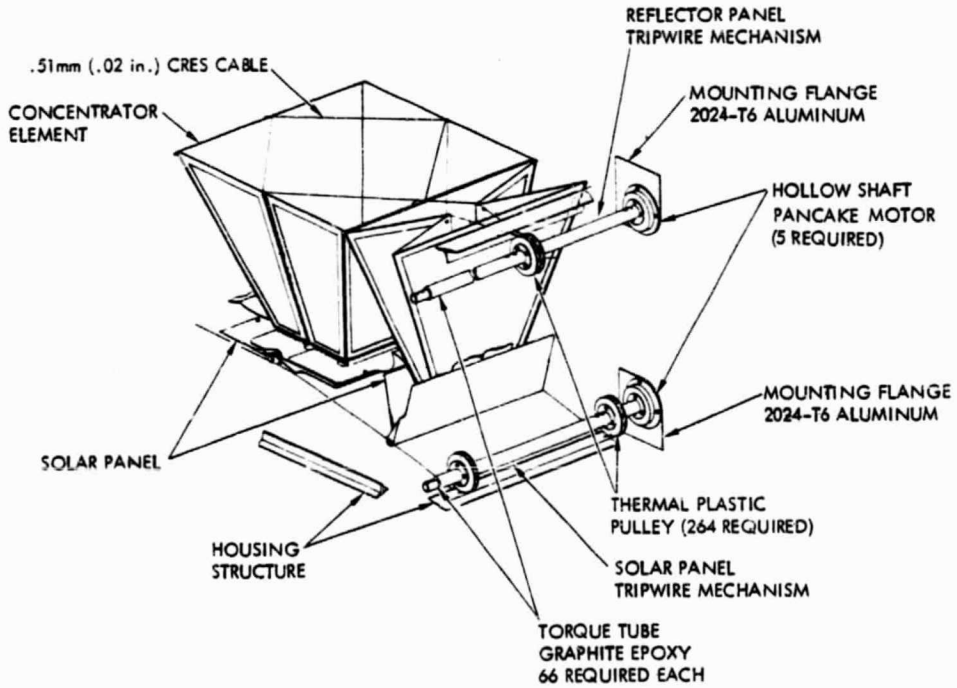

Figure 3-11. Reflector/Solar Panel
Tripwire Mechanism

tube runs the length of the housing. The torque tube/pulley assembly is driven by a hollow shaft motor mounted to the housing. The pulleys are made from a thermoplastic and mounted to the torque tube. When the cable is drawn in, the panel hinges are over-centered, similar t. the solar panels, and the panels stow. There are two total assemblies in each housing, twelve per single module, all using redundant parts.

3.4.9 Solar Panel Tripwire Mechanism

Incorporated into the design of the system is the ability to stow the module after it has been extended, either for orbit transfer or at end of life for retur" to earth for refurbishmen:. The solar panels have torsionally loaded springs at their hinge line, and need an external force applied to trip the over-center hinge/spring mecha.ism to assure proper stowage (see Figure 3-11). When the concentrator ele.ents are in the stowed configuration, the solar panels are perpendicular to the housing base with the panel hinge line being at the bottom. In the erected configuration, the solar panels are parallel with the base but translated up. The radiator panel tripwire mechanism consists of one set of 0.51 mm stainless steel cables per concentrator stack bay and a torque tube/ pulley system inside the housing. The cables start at the lower outboard corners of each stack bay and run from solar panel hinge to solar panel hinge on the same side of the stack bay. After running through all 66 concentrator elements, the cable runs through the lower housing box longeron, the cable tension sensor, and to the torque tube/pulley system. The pulley system is allowed to play out cable as the concentrator elements are deployed, allowing no restriction of the elements. During stowage, the mechanism is engaged taking up the cable, over-centering the hinges on the solar panel thus allowing stowage sequence to take place. The design and materials are the same as the reflector panel tripwire mechanism.

3.5 MODULE INTEGRATION HARDWARE

The housings are assembled as containers (fully assembled with all subsystems) and joined to the other containers to form a module; they are alternately hinged top and bottom so that they fold like a carpenter's rule. The design calls for staggering the mast/element and all element housings so that there are never more than 12 concentrator element stacks between each

mast. When fully assembled with end caps, the stowed single module configuration is a cube 3.24 m on a side, and when deployed, it is 0.54 m high x 3.24 m wide x 19.4 m long. For the dual module concept, they are assembled in much the same manner with only five hinge lines (6.48 m apart instead of 3.24 m), the five additional points being fixed on the ground by replacing the deployment motors with a machined fitting, and the latching mechanisms by bolts. Due to the minimum gauge extrusion chosen, the structure is already close to minimum practical manufacturing capability for this type of design, so there is no structural weight penalty for the dual module concept. The dual module envelope is 6.48 m long x 3.24 m wide x 3.24 m high stowed and deploys to an envelope of 0.54 m high x 3.24 m wide x 38.9 m long.

3.5.1 Hinge Mechanism

The containers are hinged together along common centerlines. In both the single- and dual-module concepts, there are five hinge lines. On the hinge lines, along the top of the container/container interfaces, there are six hinge points: two hinge points on each end cap, two in the central area of the housing, one at the end of one longeron, and the other hinge being the deployment motor at the end of the other longeron. On the hinge lines along the bottom of the container/container interface, there are eight hinge points: six the same as the top and two additional on the outboard edge of each housing adjacent to the end caps. The hinge structure is designed such that the parts are interchangeable The central housing structure also requires machined parts. The parts are left- and right-handed, but can be used as a pair at all container/container interfaces. With the addition of one machined part to replace the deployment motor and the insertion of bolts to replace the latch mechanism, the single module concept can be converted to a dual module. The hinge mechanism is made from off-the-shelf ball bearings and machined 2024-T6 aluminum plate.

3.5.2 Deployment Mechanism

Each container interfaces with the next via a set of ball bearing hinges and a deployment motor. The motor chosen is a rotary incremental actuator. The baseline actuator is a small angle permanent magnet stepper attached to a harmonic drive speed reducer. The motor has a built-in redundant motor to maintain a minimum envelope. The harmonic drive ratio is 100:1 with an output

capability of 0.432 kg-sec^2 m (10 slug-ft^2), a holding torque of 17 N-m (150 in.-lb) powered, 5.7 N-m (50 in.-lb) unpowered, and a power requirement of 8 watts (24 VDC). The total weight of each motor is 0.91 kg (2 lb). Due to the compact size of the actuators, the motors can be used on either the single- or dual-module concepts without paying an additional weight or power penalty. There are a total of five motors required whether it is the single- or dual-module concept.

3.5.3 Latch-Deployment/Extension Mechanism

The housing to housing and end cap to end cap latch mechanisms share a common design, allowing for mass production of the latches. By installing different clevis inserts in the latch mechanism, they all become interchangeable. There are four latch mechanisms per container, two located in the housing box structure at the end of the longerons, opposite the deployment motor and hinge mechanism, and two in each end cap. The latches are driven by control rods from a bell crank assembly, which in turn is driven by a linear incremental actuator. The actuator is a small angle permanent magnet stepper with an output force of 44.5 N (10 lb) and a holding force of 13.3 N (3.0 lb). The latches on the end caps are actuated by control rods from the bell crank to the latch-end cap extension mechanism, which in turn actuates the latch mechanism locking the containers together. The latch mechanism is an over-center hinge design so all loads are transferred through the latch housing to the structure and not back to the bell crank or motor.

The latch housing is made from 2024-T6 aluminum and the linkage is made from stainless steel. There are a total of 20 latch mechanisms for the single module concept.

3.5.4 Shear Pins

The module structure makes extensive use of shear pins. By using a common design, the shear pins become a mass producible item. During the launch configuration, the container/container interfaces are retained in the transverse axis using shear pins. The end caps are also held in their respective transverse axis using them. As the module is deployed, the containers hinge about their deployment axis and latch with the adjacent container. During on-orbit maneuvering the shear pin design translates the shear and torsional loads

across the container/container interface, and the latch and deployment mechanism takes the tension loads. The shear pins are made from stainless steel, with the single module concept requiring approximately 175 shear pin assemblies.

3.5.5 Wire Harness (Container/Container)

The wire harness in the housing runs from one end of the housing box structure to the other. The wire harness acts as the bus for the individual concentrator stacks, and has disconnects on either end for the housing/housing interface. The wire harness is made from a Kapton insulator with a copper bus. The bus will be two conductors wide, 0.125 m wide each, and 0.30 mm thick. There are up to ten of these layers deep (where housing ends in a user attach fitting). The total number of these harnesses required for the single module concept is six.

3.6 CONCENTRATOR ELEMENTS

The fundamental premise behind the design of a concentrating array is the substitution of optical surfaces (the concentrator) for much of the area normally occupied by solar cells. In order for this approach to be effective, the concentrator must be light in weight, much cheaper than the cells it replaces, and must have reasonably high optical efficiency. These requirements impose severe limitations on concentrator design. A variety of approaches have been considered. The film-frame reflector configuration shown in Figure 3-12 has been selected for the concentrator element design.

The selected concept of a concentrator element has an aperture of 0.5 m x 0.5 m x 0.37 m high, and a solar cell area at the base of the reflector panels of 0.2 m x 0.2 m. The concentrator elements fold along the corners of the reflector panels and down the center of the side reflector panels. The solar panels attach to the bottom of the reflector panels and hinge along the same concentrator element centerline. They also hinge along the base of the full reflector panels. The concentrator element design is compatible with either the GaAs or the Si solar panels. With the present design, the assembled, stowed, single concentrator element total thickness is 20 mm.

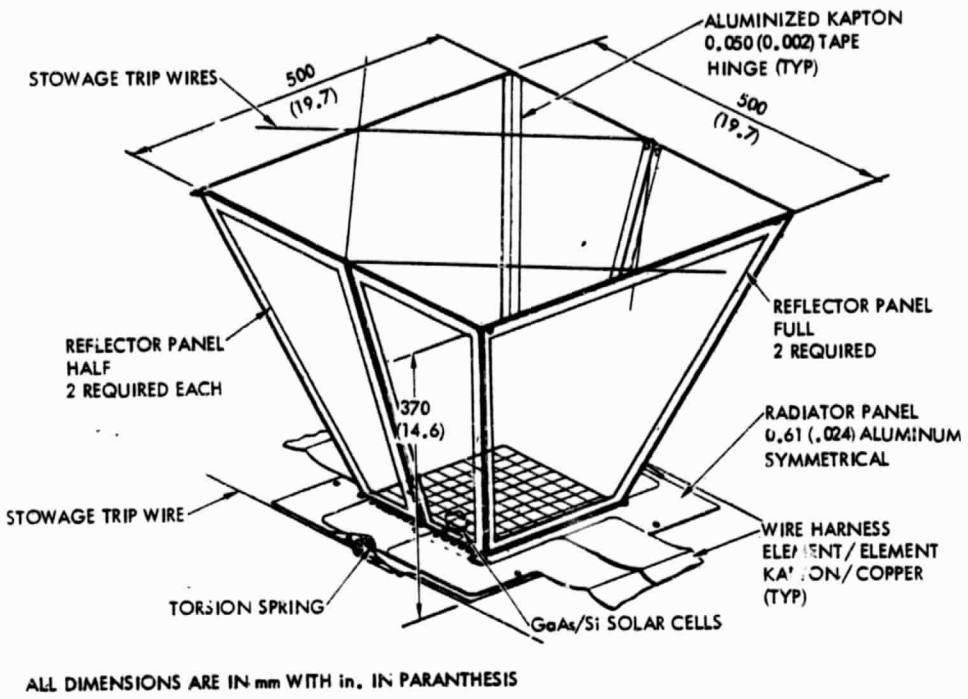

Figure 3-12. Concentrator Element Details

3.6.1 Reflector Panels

Figure 3-13 illustrates the major approaches considered. They break down into two categories, rigid panels and stretched films. Under the rigid panel category, the honeycomb panels are the strongest and most rigid; and they can be constructed with simple tooling well within familiar fabrication technology. They tend to be heavy, however, and there is concern that the optical quality will be compromised by dimpling of facesheets. A molded polysulfone graphite frame with a 0.05 mm aluminized Kapton film is the selected design to produce a set of single lightweight, thin panels that are taped together at the hinge lines using 0.05 mm aluminized Kapton tape. An alternate concept (rigid panels) of molding the panels as one single unit with the hinge molded in with only one taped hinge could be a development item that would reduce both weight and cost (see Figure 3-13).

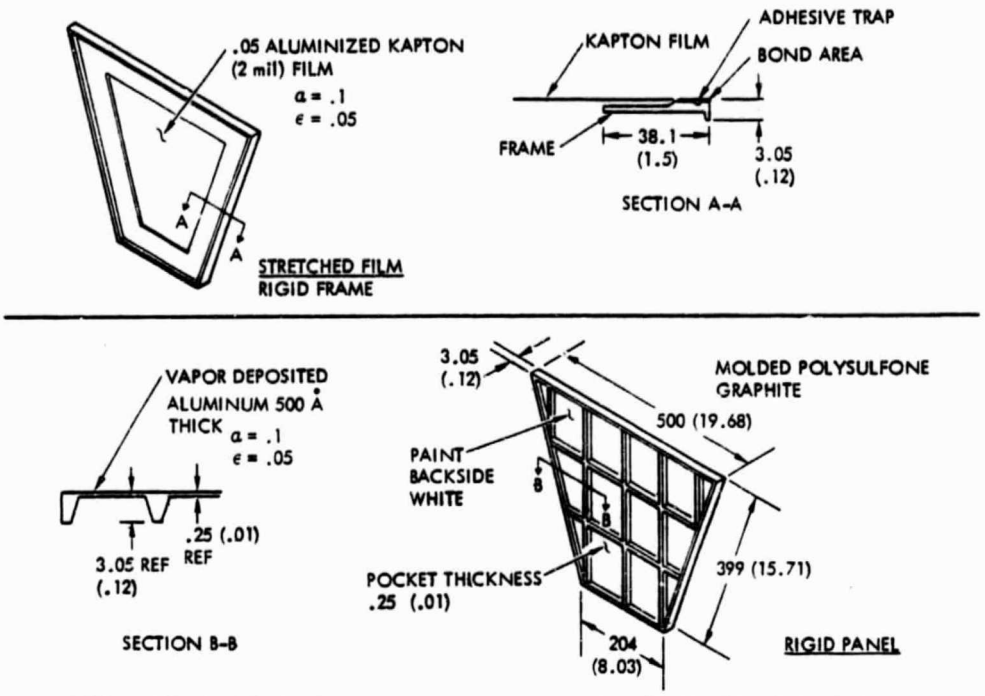

NOTE: ALL DIMENSIONS ARE IN MILLIMETERS (INCHES IN PARENTHESES) EXCEPT AS NOTED

Figure 3-13. Reflector Panels

The lightest concept considered for reflector panel construction was a stretched film supported by catenary wires. This concept was eliminated from further consideration because of difficulties in achieving a credible design for the mechanisms which erect and tension the support wires. The favored approach is the use of rigid-frame support for stretched aluminized Kapton film panels. This concept and the solid, rigid panel concept referred to above can be used interchangeably in the construction of the four-panel pyramidal concentrator configuration.

The frame on the stretched film concept is made in much the same manner as the rigid panel. The selected concept calls for a chopped fiber impregnated thermal plastic (polysulfone graphite) frame molded as a single panel. The frames are then secondary-bonded to 0.05 mm double-aluminized Kapton film. The film has a specular surface on the reflector side and a diffuse surface on the frame side.

Figure 3-14 illustrates the use of either the stretched film or the rigid panel version to make up a complete concentrator element consisting of two whole panels and two sets of hinged half-panels. The corners of the whole panels are suspended from the CEM cables by means of a slide wire mechanism, leaving the hinged panels and the hinged radiator free to fold compactly for stowage. Table 3-1 lists the thicknesses of the concentrator parts in stowed conditions.

3.6.2 Solar Panel and Harness

It is a design requirement that the solar array be compatible with both silicon (Si) and gallium arsenide (GaAs) solar cells. Because of detailed differences in available cell sizes and in cell characteristics, solar panel designs for the two-cell types will be different in some respects. Every effort has been made to minimize these differences without seriously compromising the capabilities of either. Table 3-2 lists the characteristics of the two panels. Differences in the areal density between the two cell types is compensated for by reducing the thickness of the radiator/substrate for the GaAs panel.

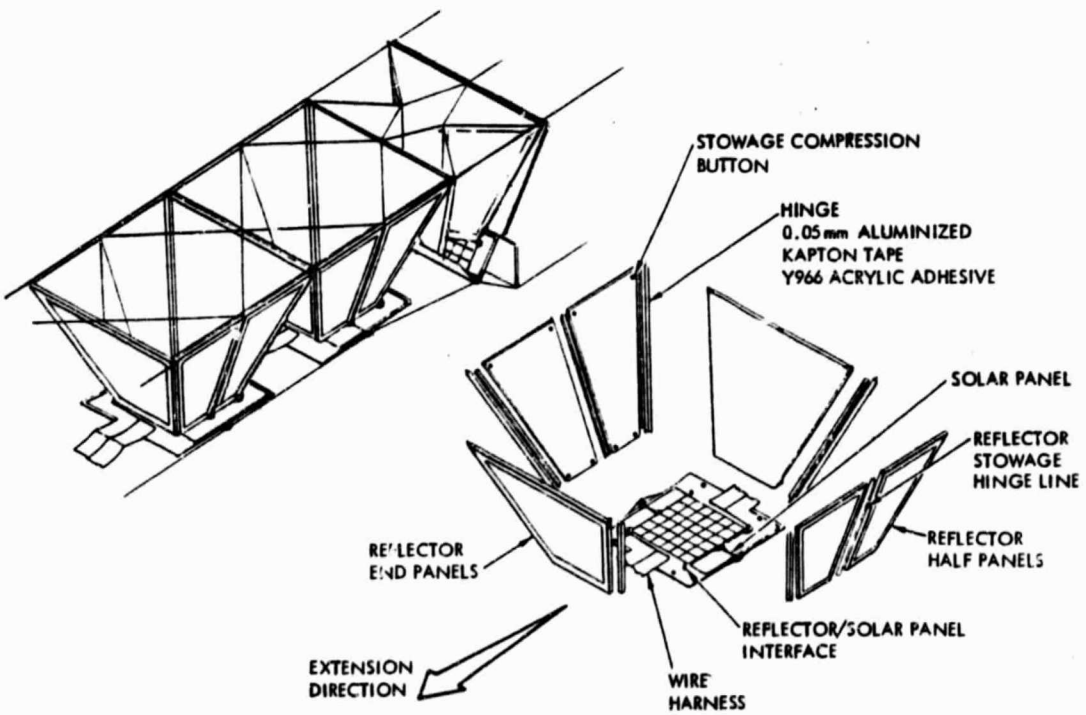

Figure 3-14. Concentrator Element
(Stretched Film or Rigid Frame)

Table 3-1. Stack Breakdown

Part	Thickness	Quantity	Total
Reflector end panels	3.25	2	6.5
Reflector half panels	3.25	2	6.5
Solar half panels	1.0	2	2.0
Miscellaneous	0.83	6	5.0
Total			20 mm
Note: All dimensions are in mm			

Table 3-2. Solar Panel Characteristics

Solar Cell Characteristics	Si	GaAs
Conversion efficiency at 28°C (%)	14	18
Solar absorptance	0.70	0.75
Low CR optimized	Yes	Yes
BSR	Yes	N/A
BSF	No	N/A
Thickness (mm)	0.25	0.30
Surface dimensions (mm)	50x50	20x20
Cover type/thickness (mm)	Fused silica/0.2	Fused silica/0.2
Substrate/Radiator Characteristics		
Thickness (mm)	0.6	0.5
A_R/A_p	2.0	2.0
Solar absorptance	0.22	0.22
Emissivity	0.85	0.85

Figure 3-15 illustrates the mechanical design of the radiator/substrate which is common to both cell types. The radiator is the area extending beyond the solar panel and has twice the area of the substrate. It folds using over-center hinges so that the cell covered surfaces do not touch in the stowed condition (15 mm gap). The half-panels are identical parts having turned up flanges on the sides and thermoplastic shoulder bolts holding the panels together. Around both shoulder bolts are torsion springs that cause the panels to open. Stamped into the radiator panel is a small flange that fits over the lug on the base of reflector panel. A spring clip then fits over the assembly to lock the flange over the lug. On the other end of the solar panel/reflector panel hinge line, a small right angle bracket fits on the panel over the reflector panel lug and is riveted to the solar panel. The lug is retained in the bracket by a cotter pin.

The silicon design radiator panels are made from 6061-T6 aluminum 0.64 mm (0.5 mm for GaAs) thick. A white thermal control coating is then applied. A layer of insulation is then bonded to the panel. The insulator is 0.025 mm Kapton film bonded with a low viscosity high temperature epoxy. The solar cells are then installed and the wire harness attached to the cells and fully bonded to the radiator panels.

CELL TYPE	PANEL SIZE			CELL SIZE
	A	B	C	
Si	353	353	.6	50 X 50 X 0.25
GaAs	353	353	.5	20 X 20 X 0.3

RADIATOR DESIGN DRIVERS

- THERMAL CONDUCTIVITY
- INTERCHANGEABLE PANELS
- HINGED INTERFACE
- COMPACT PACKAGING
- CELL PROTECTION
- SIMPLE HARNESS INTERFACE
- CONSISTENT MASS FOR Si OR GaAs

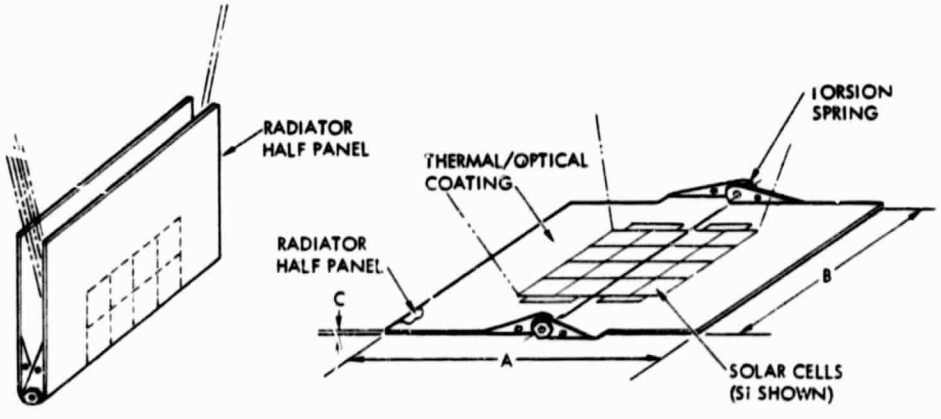

ALL DIMENSIONS ARE IN MILLIMETERS, WIRE HARNESS OMITTED FOR CLARITY

Figure 3-15. Solar Panel Design

3.6.3 Electrical Design for Silicon Cells

The electrical design of the silicon solar panel is comprised of two aspects, the design of the concentrator element and the design of the solar array module and the electrical strings of which it is comprised. This distinction is made because of the vastly different and largely independent set of design requirements which affect the two levels of the array design.

The solar panel design is driven by the available cell sizes, the inherent physical properties of the devices, and the environment in which the device must operate.

For silicon solar cells there are two basic limitations on device size. The first limit is the Czochralski crystal growth technique which presently limits boule diameter to approximately 102 mm (4 in.). As a result, cell size is restricted to approximately a 59 mm x 59 mm maximum. This large cell fabrication technology for planar array application is being pursued under the auspices of the NASA JSC by Applied Solar Energy Corporation (ASEC). ASEC was the silicon solar cell panel subcontractor for this project. The cell size selected for the silicon solar cells was based upon the following rationale.

The baseline concentrator design requires the cell area for the solar panel to be approximately 200 mm x 200 mm when deployed. Each half-panel is then 100 mm x 200 mm. As each half-panel within the element is isolated from its mate, the array of solar cells must fit within this area. Obviously, a 59 mm x 59 mm cell would not be appropriate for this panel size due to a poor packing factor. If the boules were grown in a nominal 70 mm (3 in.) diameter, the cells could be made 50 mm x 50 mm. This device would fit the available envelope and still embody the large-area/low-cost production concept.

The second limitation is the effective series resistance of a device which is to be used for concentrator application. Assessments of the applicability of large-area devices to concentrators do not appear favorable. The high-current density and long transmission distances in the n-contact grids of a concentrating solar cell appear to result in prohibitively high series resistance losses. This is usually overcome by changing the grid pattern and using more than one n-bar contact. The revised grid pattern is not a problem. However, the use of more than one n-bar contact results in a packing factor penalty which would negate the benefit of the multiple n-bars.

The use of multiple wraparound n-bar contacts would eliminate the series resistance and packing factor losses in a large-area device. This solution, however, is not without limitations. These devices have not economically been made in production quantities (estimated increase of 15-20% per cell over front/back contact cells). The solar cell electrical interconnects in a wraparound panel design become a constraining factor. The wraparound contacts dictate the use of in-plane stress relief within the interconnect. The in-plane stress relief interconnect design is impeded by having to be immersed in a material which could reduce the effective stress-relieving ability of the interconnect design. The thermal conduction requirements in a concentrating solar array are such that the rear cell surface must be totally immersed in the void-free adhesive which holds the cells to the radiators. Due to the requirement to keep the cell-substrate bond line thin, the interconnect is trapped in a narrow region. The in-plane interconnect material is prevented from deforming out of plane to any degree, and material fatigue is enhanced. The interconnect design for a ten-year LEO mission must survive a difficult environment (typically, 55,000 temperature cycles from -100°C to +125°C). Many planar solar arrays have been designed for similar missions, including e high expansion aluminum substrate characteristics. The stringent requirements seem to favor an out-of-plane stress relief interconnect design.

The selected baseline design is a conventional front/back contact cell, a silver mesh interconnect with an out-of-plane stress relief loop bonded to an insulated aluminum radiator with a silicone elastometer adhesive. These aspects or the design embody no new technologies. The low-CR optimized cell and interconnect have to be more fully developed and qualified for space application.

The technology needed to use a welding process for solar array manufacturing is new. A welding process was selected for interconnecting the cells within the array and for attaching the wire harness to the array. This selection was based upon two criteria, the relatively high operating temperature of the solar panel and the long, low earth on-orbit life for the array. These two factors, when applied to the relatively well known fatigue life characteristics of soldered interconnections, raise serious questions about

the ability of a soldered system to survive the mission environment. The welding interconnection process is not well understood, and represents a technology development item. The proponents of this process claim it can meet both the high operating temperature and long cycle life over wide temperature extremes required for this solar array application. The potential capabilities of this process have yet to be realized in a U.S. solar array manufacturing environment.

Concentrator half-panels must be series interconnected in order to develop a reasonable voltage for transmission of the large amounts of electrical power which the array produces. The selection of a transmission voltage should be based upon a user spacecraft system study and not on the solar array characteristics alone. In this case, where no user spacecraft was defined, engineering judgement dictated a bus voltage to be in the range of 150 to 300 V. In the absence of any more specific design criteria, a further judgement was made. All concentrator elements within a deployed row are interconnected in series (i.e., one deployed row of 66 concentrators equals one electrical string).

The design of an electrical string is driven by two considerations: (1) minimize the length of the conduction path, and (2) minimize the generated magnetic fields caused by "current loops" in the electrical network. Figure 3-16 illustrates the harness design for both the silicon and GaAs versions of an array module.

Every half-panel is protected from reverse bias damage by the use of peripheral current bypass (shunt) diodes. These are bonded to the top surface of the radiator outside the confines of the reflectors. The need for bypass diodes is established by the relatively high bus voltage dictated by any high-power solar array and the electrical power subsystem in general. The effects of shadowing, associated with deployable solar arrays when coupled with these relatively high voltages, could pose a serious threat to the solar array. An analysis has been performed to determine the approximate reverse bias potentials which could occur in the baseline design. In the absence of a specific mission scenario, several assumptions as to operation of the solar array within an electrical power subsystem and a given orbital environment must be made.

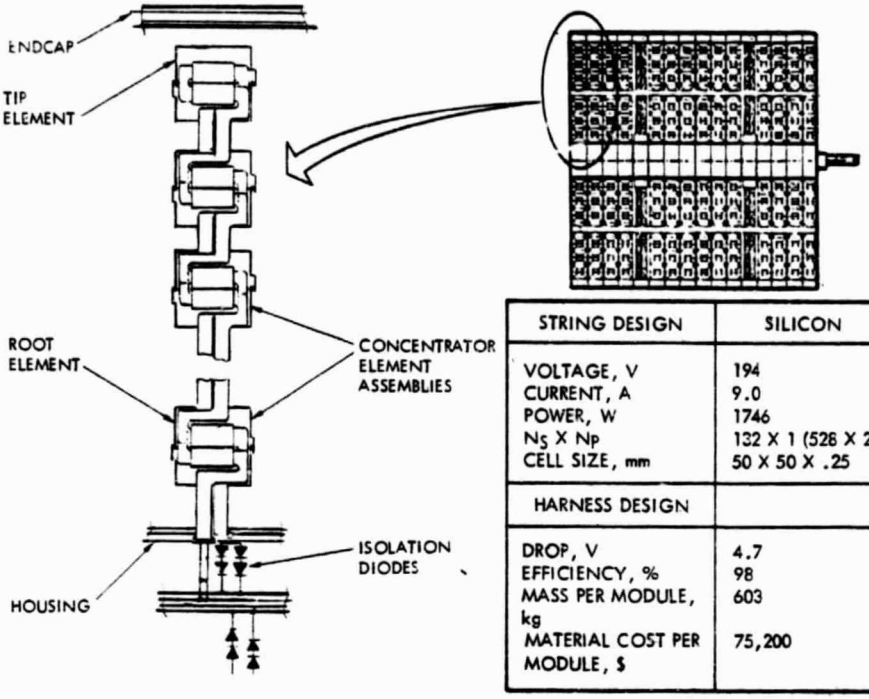

STRING DESIGN	SILICON	GaAs
VOLTAGE, V	194	257
CURRENT, A	9.0	2.6
POWER, W	1746	669
N_S X N_P	132 X 1 (526 X 2)	33 X 1 (330 X 5)
CELL SIZE, mm	50 X 50 X .25	20 X 20 X .30
HARNESS DESIGN		
DROP, V	4.7	1.6
EFFICIENCY, %	98	99
MASS PER MODULE, kg	603	581
MATERIAL COST PER MODULE, $	75,200	72,500

Figure 3-16. Electrical String Layout and Harness Design

Typical of these is whether the array is series or shunt regulated, and what the operational temprature of the partially deployed array would be. The results of this analysis show reverse bias potentials on the order of -20 V can be expected across a non-illuminated half-panel. (Four series cells translate into -5 V per cell.) This potential is not considered particularly dangerous with respect to known space-type solar cells. There are uncertainties in the preliminary analysis which, when coupled with relatively unknown reverse bias characteristics of the baseline large-area, low-CR optimized silicon solar cells, could reverse this assessment. Data collected as to the reverse bias characteristics during the concentrator testing indicated that only one diode was required (see Section 7.3.6). An assessment of this situation determined that bypass diode protection is a viable approach to eliminating a possible problem with the baseline design. This is supported by the ease with which this design feature can be incorporated into the baseline design.

The individual electrical strings are isolated from the main power bus by isolation diodes. These diodes perform two functions:

- They prevent an electrical string whose open-circuit voltage is less than the bus voltage from becoming a net electrical power consumer.
- They can prevent certain short-circuit failure modes of the wire harness from being a catastrophic failure.

A series/parallel redundant configuration was chosen for the baseline design. This configuration is required to meet the "no single-point failure" criterion which has been adopted in this array design. Again, any specific failure mode analysis to demonstrate the performance of the isolation diodes requires certain assumptions as to solar array operation within the user spacecraft electrical power subsystem to be made. It can be shown that under certain circumstances anything less than series/parallel redundant diodes will not allow the solar array to pass the "no single-point failure" criterion. This assessment is not unique to this solar array design; it has validity in a large number of, if not all, applications. The physical location of the diodes with respect to the overall layout is a detail design that can be determined for a specific array design based upon application requirements.

As is the case with most protective devices, certain design penalties are incurred. The penalties which are imposed on the design are small when compared to the benefits of the diode configuration. There is a distribution system efficiency penalty with the efficiency of the diode package at approximately 98 for a 194V bus. Another penalty to the design is cost. The total cost of the diodes (both isolation and bypass) is small when compared to the total solar array module cost. Diode unit costs are relatively low when compared to solar cell unit costs, and there are relatively few diodes.

3.6.4 Electrical Design for Gallium Arsenide (GaAs) Cells

The general design drivers for the GaAs half-panels are identical to those for the silicon half-panels. It is the detailed implementation which differs. The cell size, bypass diode placement, panel output characteristics, solar cell interconnect selection, etc., are all likely to be different from the silicon half-panel design. The contractual requirement for a design which is

consistent with both silicon and GaAs solar cells has, however, been achieved. The consistency lies in the concentrator element physical characteristics and in compatibility of either design with a single structural/mechanical design. The electrical design is comprised of two basis tasks — that of concentrator element design, and design of the solar array module.

The GaAs solar panel design, like the silicon design, is driven by available cell sizes. For GaAs solar cells there are presently only two cell sizes from which to choose: 20 mm x 20 mm, and 20 mm x 40 mm. This may change as GaAs cell manufacturing technology is developed. The inherent brittleness of the GaAs cell substrate will present a considerable challenge, and may prove to be a limiting factor, in the maximum area per device which is economically feasible. It is not clear, at this time, that large-area devices are the best approach to lowest cost per watt with this substrate/device type. Ultimately, the selection of a cell size will be driven by the cost factor, and the concentrator configuration will be designed to utilize the lowest-cost device.

The selection between the two available cell sizes was driven by the dimensions of the concentrator element which require the cells to be located within an approximate 100 mm x 200 mm envelope on the half-panel. This requires an integral number of cells to fit within the 100 mm envelope dimension. This simple consideration, plus restraints on cell/interconnect orientation due to the concentrator configuration, tends to favor the 20 mm x 20 mm over the 20 mm x 40 mm cell size. A development contract currently under way to produce GaAs devices (USAF low cost GaAs solar cell development, Reference 9) has adopted this 20 mm x 20 mm cell size as a program goal. The results of this development will not be available until mid-1984. The development of a larger area device would likely proceed, but could not be cost-competitive until development was complete. This program's contractual requirement is for end of 1984 technology readiness. This is consistent with existing development contracts for a 20 mm x 20 mm cell. No such contracts exist for a larger cell, and including this cell in a baseline design would require technology development at a rate beyond existing planning.

There are fifty 20 mm x 20 mm x 0.3 mm solar cells on each half-panel. The illumination distribution (see Section 5.4) suggested a high degree of electrical paralleling within the half-panel to minimize output mismatch losses. The selected configuration consists of groups of five cells connected in parallel (N_p = 5). Ten of these cell assemblies are connected in series (N_S = 10). This design should perform as though it were comprised of ten extremely large area (2000 mm^2) GaAs devices in series.

To protect the devices from the space radiation environment, a fused silica coverslide (0.2 mm thick) is applied to the cell top surface. The selection of fused silica was based upon several considerations; among these are availability, cost, and resistance to radiation degradation. The adhesive used to bond these covers could be either DC93-500 or (if proven to be less expensive) fluorinated ethylene-propylene (FEP). The FEP option would also eliminate the relatively expensive ultra violet filter which must be applied to the fused silica to protect the DC93-300. It may also be possible to use a matte front surface coverglass to eliminate the magnesium fluride (MgF_2) anti-reflection coating. An additional array fabrication step is included to further protect the cells from particulate radiation. The area surrounding the ohmic contact will be coated, after array assembly, to increase the effective shielding density over this surface.

The array on each half-panel must be protected from reverse-bias effects. The technique adopted in the baseline GaAs design is the same as that used in the silicon design — peripheral bypass diodes. The reverse-bias characteristics of the GaAs devices and the response of the baseline design in the operational scenario determine the placement of the diode shunts within the electrical string. In the absence of comprehensive, statistically based test data on mass-produced GaAs solar cells, the selection of this tap point is somewhat arbitrary. This is complicated by lack of in-depth operational scenario for the solar array. To help alleviate the former problem, Rockwell performed some reverse-bias testing on GaAs devices in conjunction with hardware testing (see Section 7.6). These test data established a performance benchmark which was used in updating the baseline design. The assumptions, with regard to cell and operational performance, have driven the design to an electrical tap with

a shunt diode at every two series cells. This is a conservative approach which may be modified as necessary for a specific array design and application. Isolation diode protection is identical to the silicon string design, i.e., series/parallel redundant.

The interconnection of these half-panels into an electrical string is handled in the same way as in the silicon design. The difference lies in the number of concentrator elements needed to develop bus voltage. The higher per cell output voltage and the greater number of series cells per half-panel dictate fewer series concentrators per electrical string. Each deployed row will contain four strings. In this configuration (see Figure 3-16), the output characteristics of an electrical string would then be:

- Max. output power = 669 watts
- Current at P_M = 2.6 amperes
- Voltage at P_M = 257 volts

The assembly of the cells into an array will utilize a welding process. This assembly technique is subject to all the restrictions and reservations described in the discussion of the silicon design.

The interconnect design will be the out-of-plane stress relief type. This was selected because of the front/back contact configuration which will most likely be used on the early production GaAs cells. The cell will be bonded to the substrate/radiator using a silicone elastomer adhesive. A relatively low-cost system could be a mixture of RTV-566 and RTV-567. Bondline thickness control is critical to regulate mass properties, to ensure adequate curing of the adhesive, and to maintain good thermal conduction between the cell and the radiator.

Wire harness design is similar to the silicon array. The current density is determined per the technique discussed in Section 5.5. Because there are four strings per deployed row of concentrators, there are additional conductors necessary to deliver power from the electrical strings which terminate away from the root of the extended row. This is unlike the silicon design which has only one string per deployed row.

The coverglass material selected for the GaAs devices is fused silica. The adhesive is DC93-500. The FEP/frosted, fused silica covering system may not be applicable to GaAs devices due to the extreme temperature and pressure

cycle needed to reflow the adhesive. This process may, especially if a curved platen technique were to be needed, cause excessive breakage of the brittle GaAs cell. The developmental emphasis should remain upon low-cost production of cells and substrates, not on a potentially lower-cost covering process. The GaAs upper ohmic contact will — like the silicon design — be coated to protect against low energy protons and other particulate radiation.

3.6.5 Harness Design

The interconnection of the individual concentrator element assemblies into an electrical string is accomplished through the use of flat, flexible printed-circuit wire harnesses. This type of wire harness offers several distinct advantages over a conventional round wire-bundle harness. Production of this type of harness is highly automated, resulting in relatively low unit cost. The harness is flat and thin, offering unparalleled packaging options when space is at a premium, as in the fully stowed configuration. The thinness results in an extremely flexible harness which is necessary for the complete unfolding of the harness during deployment of the concentrators from the densely stowed condition with a minimum of stress. Wire routing can be as complex as necessary without the production problems associated with round wire conductors because the wiring layout is fixed by artwork. This same artwork, when coupled with a photo resist/etching process, accounts for the ease and consistency with which even complicated routings are reproduced.

Multi-layer printed circuitry is common, but at the expense of thinness and flexibility. Two laminated harness layers are used within the deployed rows. This is used in an area such that no storage (thinness) or bending (flexibility) penalties are incurred. The main power bus, which runs centrally through the housing, builds up to twelve separate layers as additional container housing are picked up before entering the user attach fittings on the last housing. This harness is ten separate layers thick where it passes over the last rotating hinge line. The layers are not laminated together so as to maintain as flexible a harness as possible. The baseline array module voltages are about 194 volts for Si and 257 volts for GaAs.

The harness is sized so as to maintain an optimum current density in all sections under nominal conditions. This optimization is described in Section 5.5. The optimum current density is maintained by varying the cross-sectional area of the conductor to accommodate the current in the circuit branch. For printed circuitry, this is achieved by varying the width of the conductors which are uniform in thickness, or by using multiple parallel layers of conductors, or both.

The selected materials are copper conductors, laminated between layers of Kapton by a modified acrylic adhesive. The copper used within the electrical strings is 0.14 mm thick, with 0.025 mm adhesive and insulator layers. The copper used within the housing is 0.28 mm thick with similar adhesives and insulators. Localized plating of the copper may be needed to enhance weldability. The width of the copper varies depending upon the current from either the silicon or GaAs cell designs.

4.0 MANUFACTURING SEQUENCES

The array module design described in Section 3.0 lends itself to a logical fabrication plan by which parts and materials are constructed and assembled into the finished system. This section provides a step-by-step description of the manufacturing sequences required.

Figure 4-1 illustrates fabrication of individuals sets of reflectors panels. Each concentrator element requires two full panels and four half-panels. Each panel consists of a molded frame so configured that only the extreme outer edge of the Kapton reflecting film is adhesively bonded to the frame. Panel frames are molded, cleaned of flashing and inspected. Adhesive is then added to the bonding area and the aluminized film is applied under tension.

Individual panels are taped to form the corners of the pyramidal concentrator elements (Figure 4-2). Reverse-taping is applied at the fold lines joining half-panels. Individual concentrator elements are joined to adjacent elements by means of pinned joints. The reflector panel subassemblies are stored in folded condition, ready for later assembly operations.

Figure 4-3 shows the procedures for fabrication of the solar panel subassembly. Substrate-radiators are formed as half-panels of sheet aluminum; configuration details include hinge brackets. The central area where solar cells will be applied is masked off and the remaining (radiator) surface is painted with optically selective paint. An electrically insulating layer of Kapton film is bonded over the aluminum substrate; solar cells are bonded to the Kapton and interconnected. (Note: Solar cells will be supplied by subcontractor; the entire lay-down procedure may also be performed by subcontractor.) Completed solar panel halves are joined into subassemblies by means of springs, bolts, washers and nuts. Individual solar panel subassemblies are connected by wire harness assemblies; a special harness terminates each row and provides connections with a central module harness. Protective diodes are installed on the panels.

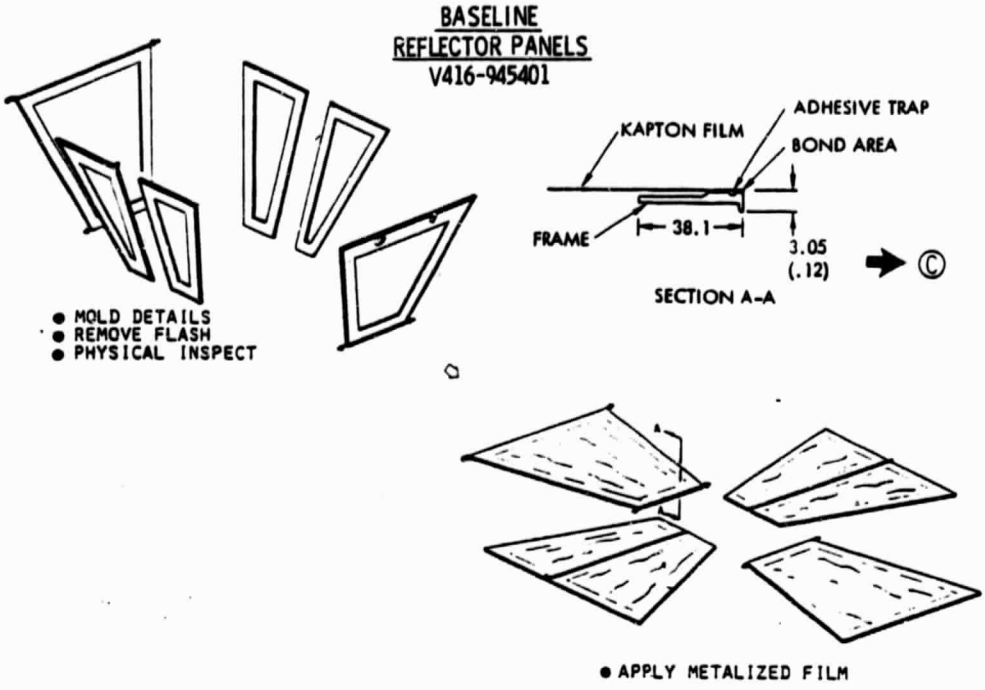

Figure 4-1. Reflector Panel Assembly

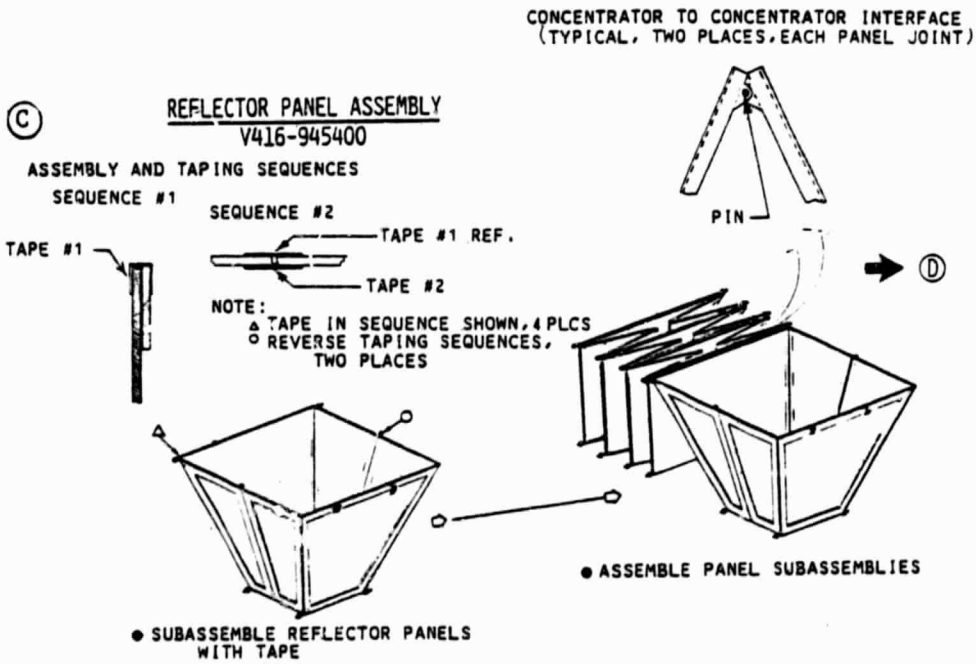

Figure 4-2. Concentrator Element Subassembly and Stack Assembly

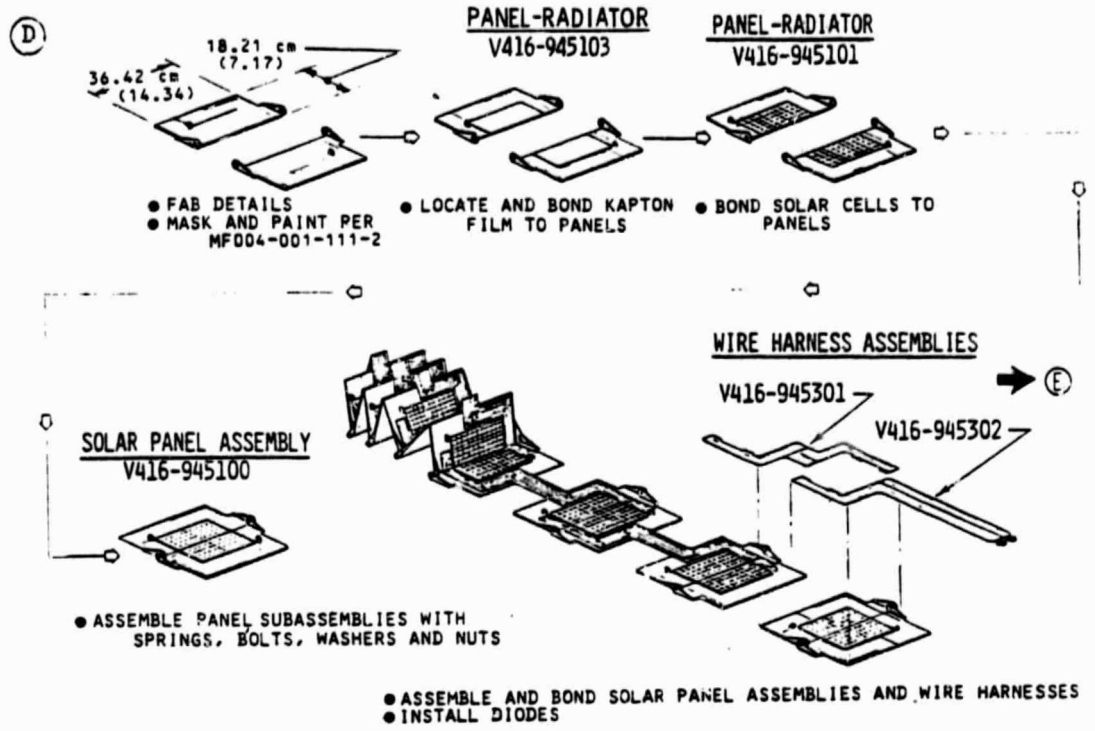

Figure 4-3. Solar Panel Subassembly

The concentrator element stack assembly is formed by joining the reflector panel subassembly with the solar panel subassembly (Figure 4-4). Individual concentrators are joined at the perimeter of the solar cell panel by means of bond clips. Concentrator elements are folded after assembly and stored ready for later steps in the sequence.

The housing assembly (Figure 4-5) is constructed from elementary structural members by means of riveted joints. The launch support tubes, which support the folded concentrator elements, are installed on the complete structure. Two end caps are assembled separately. The configuration shown accommodates two canister/mast assemblies and 8 rows of concentrator elements for a single container array module design.

Figure 4-6 illustrates the steps taken to add mechanisms to the housing. These include the solar panel tripwire mechanisms, the reflector tripwire mechanisms, the concentrator stack translation mechanization and the cable extension mechanism. Required brackets are fabricated, assembled and installed on the housing. Similarly, the mechanisms are fabricated, assembled and installed.

CONCENTRATING ELEMENT STACK ASSEMBLY
V416-945001

(E)

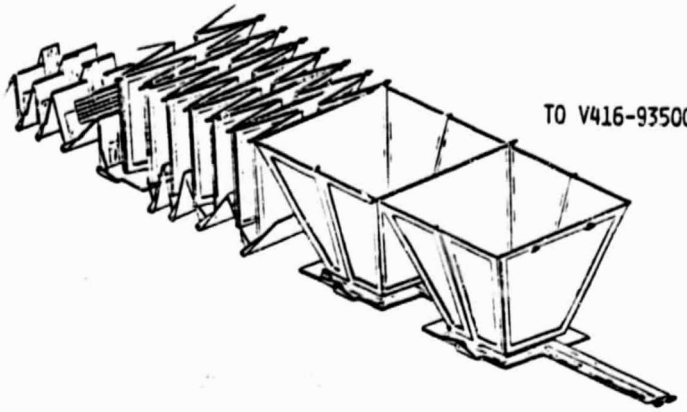

TO V416-935002 ASSEMBLY

TO CONTAINER ASSEMBLY

(Figure 4-8)

• ASSEMBLE REFLECTOR PANEL ASSEMBLY AND SOLAR PANEL ASSEMBLY. INSTALL AND BOND CLIPS

Figure 4-4. Stack Assembly

HOUSING ASSEMBLY
V416-935101

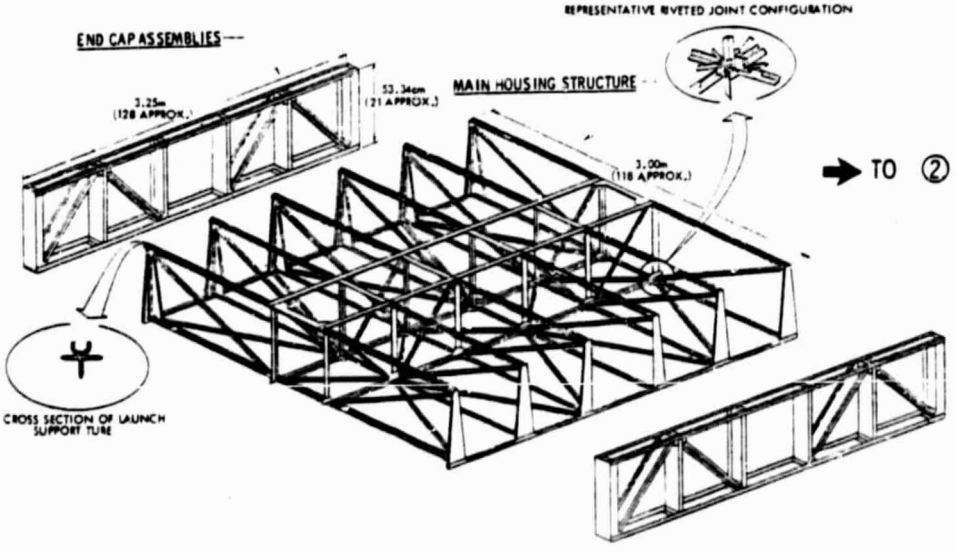

• FABRICATE DETAILS
• ASSEMBLE STRUCTURE AND INSTALL LAUNCH SUPPORT TUBES

Figure 4-5. Housing Assembly

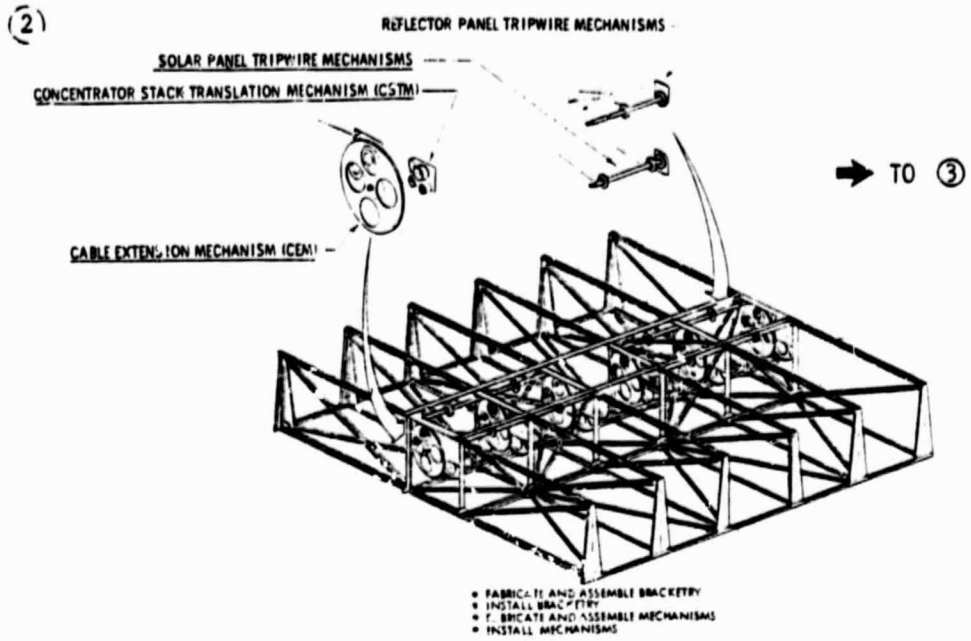

Figure 4-6. Installation of Array Mechanisms

The central wire harness which collects power from the harnesses servicing individual rows of concentrators is installed below the mechanisms along the central axis of the housing (Figure 4-7). Mast/canister assemblies are installed in pairs, back-to-back within one row of the container housing which would normally contain concentrators. The baseline module is made up of three containers with mast pairs and 10 rows of concentrator elements and three without masts (12 rows of concentrator elements) as shown in Figure 3-7, Section 3.4. The mast/canister units are assembled and delivered as a unit by the subcontractor. Other configurations are possible as indicated by Figures 4-5 through 4-9, which show 8 rows of concentrator elements and a pair of masts.

The concentrator stack assemblies are installed in the container rows as shown in Figure 4-8. Individual concentrator elements are supported by means of slide assemblies which ride on the launch support tubes. Stack harness terminals are hooked up to the central collection harness running through the center of the housing. Electrical checkout is performed after assembly.

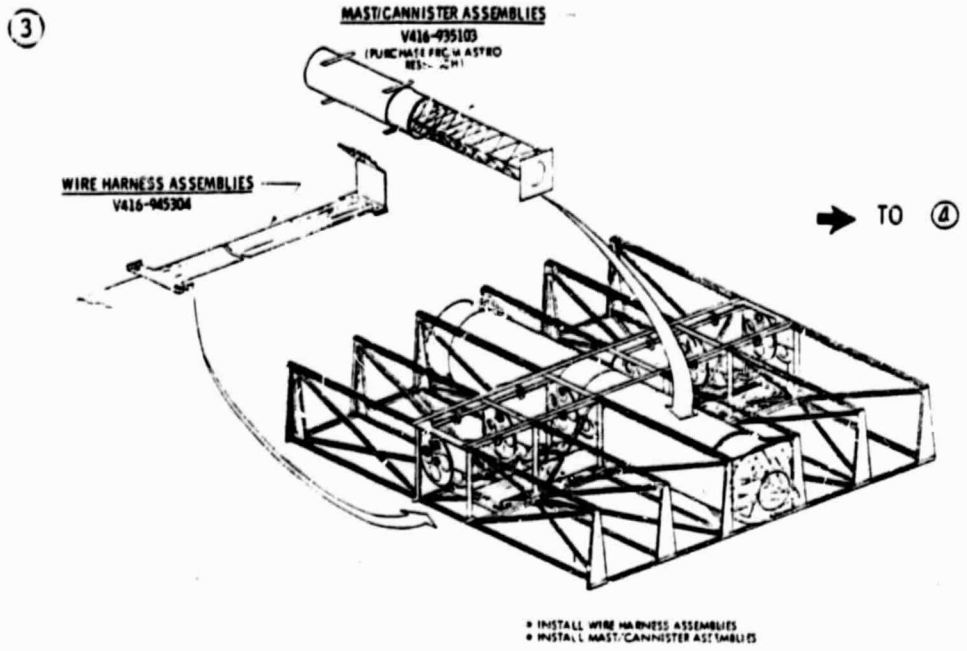

Figure 4-7. Mast and Wire Harness Assemblies

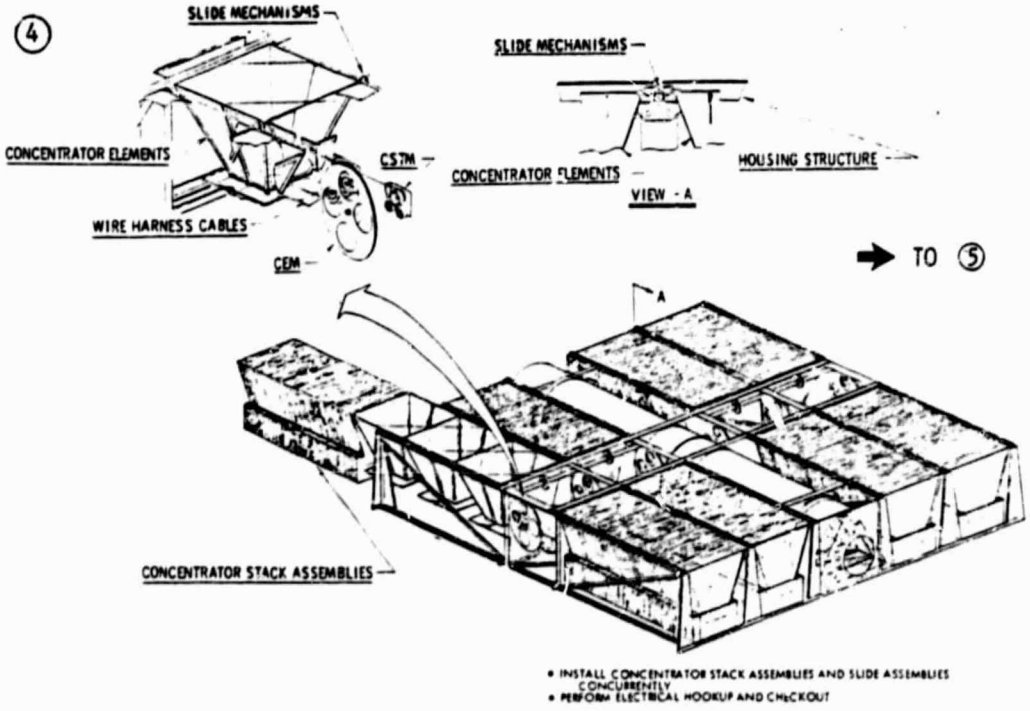

Figure 4-8. Concentrator Stack Installation

The last procedure in container assembly is the installation of end caps and access panels (see Figure 4-9). The end caps are attached to the ends of the masts, the last concentrator element in each row and the cables which maintain tension upon which the concentrator elements ride. Access panels are installed which close out the top, bottom and ends of the central housing space. A final inspection completes the container assembly. The module assembly utilizing more than one container assembly can be interconnected as discussed in Section 3.5.

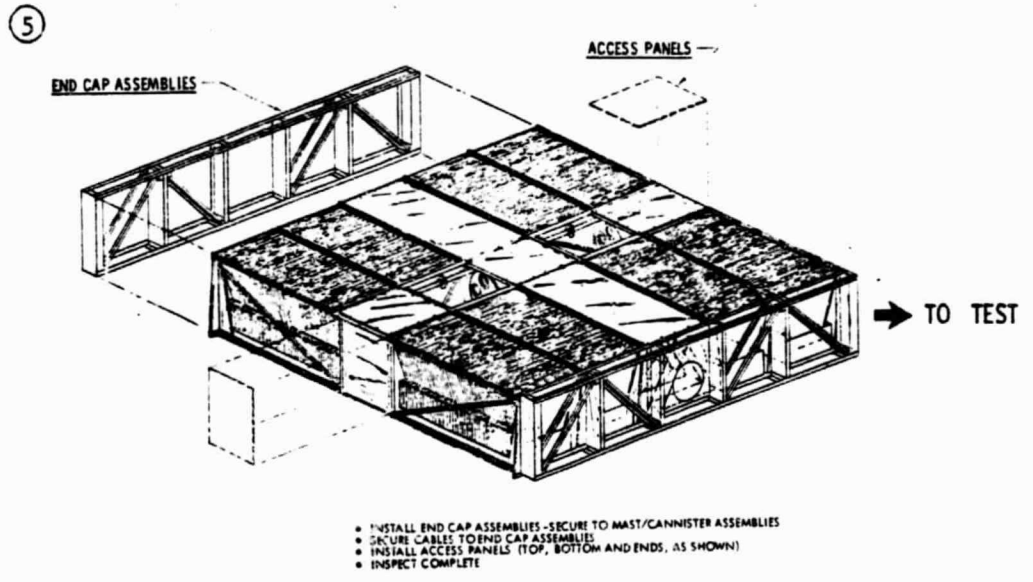

Figure 4-9. End Cap and Access Panel Assembly

5.0 ARRAY TRADE STUDIES AND PERFORMANCE ANALYSIS

This section describes in detail the features of the GaAs and silicon versions of the concentrator array design. An account of the trade studies and parametric analyses from which the design was derived is included.

The overall credibility of the final array design which results from this program will rest upon design judgement, analytical predictions and test results. Table 5-1 lists the important design issues which have been identified and categorizes them in terms of method of verification. Some issues, such as those relating to mechanisms, mechanical supports and connectors, are not readily solved by analysis alone, yet embody familiar principles and techniques. For these issues design judgement is appropriate. There are a number of issues, particularly those relating to structural, optical, thermal and electrical performance, where good quantitative prediction methods exist. Here, parametric analysis is most effective in establishing component design features. Finally there are other issues, some critical to the design, which are either new or embody features not conducive to analysis. These require experimental demonstration of their feasibility.

5.1 TRADE STUDIES

The design depends upon the results of a large number of trade studies involving structural, electrical, optical and thermal considerations. The chief structural trades are summarized in Table 5-2. They deal with geometrical constraints as well as with the stresses and deformations associated with thermal gradients and static and dynamic loads.

A major driver throughout the design has been the stacking parameter, N. Not only does it affect structural and volumetric properties of the module as a whole; it also influences thermal performance, solar cell sizing, electrical design and possibly cost and weight. The implications of other choices for N are discussed later in Section 9.

Table 5-1. Concept Verification Major Design Issues

ITEM NO.	DESIGN ISSUES	DESIGN JUDGMENT	ANALYSIS	TESTING
1	CONCENTRATOR PACKAGES WITHIN PRESCRIBED ENVELOPE		X	X
2	SOLAR CELL, RADIATOR SUITABILITY FOR LAUNCH		X	
3	CONTAINERS AND TIE SYSTEM SUITABILITY FOR LAUNCH	X	X	
4	RELEASE OF SUPPORT FITTINGS (IF NECESSARY)	X		
5	REMOVAL FROM SHUTTLE/POSITION FOR DEPLOYMENT	X		
6	DEPLOYMENT OF CONTAINERS AND LOCKING OF JOINTS	X		
7	RELEASE OF END CAPS FROM MODULAR TIES	X		
8	MAST EXTENSION	EXISTING DESIGN		
9	EXTENSION OF CONCENTRATORS AND SOLAR PANELS	X		X
10	EXTENSION OF CABLES AND POWER TRANSMISSION LINES	X		X
11	FINAL LOCKING OF ARRAY	X		
12	DEVELOPMENT/MAINTENANCE OF REQUIRED CABLE TENSION	X	X	
13	REFLECTOR SPECULAR QUALITY TO REQUIREMENT			X
14	REFLECTOR FLATNESS QUALITY TO REQUIREMENT		X	X
15	REFLECTOR ARRAY DIMENSIONAL QUALITY	X		X
16	REFLECTOR POINTING ACCURACY TO REQUIREMENT		X	
17	SOLAR ARRAY MODULE CONFIGURATION GENERAL STABILITY		X	
18	SOLAR ARRAY MODULE CONFIGURATION USER SPACECRAFT LOAD SUITABILITY		X	
19	SOLAR CELL/RADIATOR PERFORMANCE		X	X
20	TOTAL CONCEPT WEIGHT VERIFICATION		X	X

Table 5-2. Summary of Structural Trade Studies

Trade Issue	Design Choice	Rationale
Module stowed dimensions	Cube, 3.24 m per side	Orientation-insensitive, less than one-quarter bay length
Stacking parameter, N	N = 6	Efficient, low mass radiator; adequate mast diameter
Single-axis vs. dual-axis deployment	Single axis	Efficient use of canister stowage, less complex, simpler user vehicle interface
Shear-panel vs. drag truss Housing design	Drag truss	Lighter weight, low cost
Mast design	Canister deployed hybrid (single- and double-laced) continuous longeron	Adequate bending strength; stowage room for canister envelope.

The electrical trades are summarized in Table 5-3. Component availability, design judgement and quantitative analysis all played a part in the selection process. Electrical trades were carried out at the cell, panel and module level in order to optimize output with respect to cost and weight.

Optical trades are summarized in Table 5-4. Two of the most significant, namely the selection of geometric concentration ratio (GCR) and the rejection of selective ("cold mirror") reflecting surfaces were decided during the proposal phase for this program. Much of the optical analysis performed has been directed toward predicting sensitivity to pointing errors. However, it also served to select optimum thermo-optical reflector characteristics.

Thermal analysis has been used primarily to assess output performance of the design but also served to optimize radiator size and thickness and to select reflector back-surface coatings (see Table 5-5). More exotic candidates were considered as substrate-radiator materials before aluminum sheet was selected. Alternatives such as pyrolytic graphite may be further considered as design improvements.

In the following sections, the individual trades and analyses are presented in more detail.

Table 5-3. Summary of Electrical Trade Studies

Trade Issue	Design Choice	Rationale
Coverslide	0.2 mm thick fused silica	Common for Si and GaAs.
Silicon cell size	50 mm x 50 mm x 0.25 mm	Largest available size fitting panel area with good packing density.
Gallium arsenide cell size	20 mm x 20 mm x 0.30 mm	Same as above.
Interconnect design	Silver mesh welded, out-of-plane stress relief loop	Large number of thermal cycles.
String design	Parallel cells in each half-panel. GaAs -- four electrical strings per row; Si -- one electrical string per row.	Minimizes illumination mismatch losses. Moderate module voltage.
Harness design	Flat flexible cable, counter current harness	Excellent packaging, necessary flexibility, minimizes EMI

Table 5-4. Summary of Optical Trade Studies

Trade Issue	Design Choice	Rationale
Concentration ratio	GCR = 6	Best compromise for both Si and GaAs
Reflector wavelength selectivity	Non-selective (aluminum)	Selective coatings are angle-sensitive.
Treatment of reflector corners	Full specular reflectivity for corners	Highest electrical output; acceptable reflector temperatures.

Table 5-5. Summary of Thermal Trade Studies

Trade Issues	Design Choice	Rationale
Radiator-substrate material	Aluminum sheet	Cheap, familiar, workable material with adequate conductivity.
Radiator size and thickness	Radiator area twice solar panel; 0.5/0.6 mm (GaAs/Si) Al sheet	Minimizes radiator specific weight; maintains acceptable Si cell temperature.
Reflector back surface treatment	High diffuse reflectivity	Improved radiator heat rejection (top side).

5.2 STRUCTURAL ANALYSIS

The studies described in this section cover a wide range of topics from the dynamic behavior of entire arrays to local stresses developed within individual members. The design constraints arise both from launch/landing in the Shuttle payload bay and from operation attached to a space vehicle in low earth orbit. Structural trades played a major role in establishing the size and shape of the final array module design and its component parts.

The prime structural elements in the design are the six lattice masts which actuate deployment of the array and provide structural support when deployment is complete. A number of trades and analyses dealing with the masts themselves have been performed by the subcontractor, Astro Research Corporation. These are described in references 10 and 11 and summarized here.

5.2.1 Structural Requirements and Constraints

Certain constraints have been imposed on the design by the terms of the contract itself. The requirement that all components chosen be consistent with 1984 technology rules out materials and devices which are not well along in development. Operation in low earth orbit introduces considerations of atmospheric drag and gravity gradient force. It also increases the frequency and decreases the range of the thermal cycling due to earth eclipse. The requirement for a Shuttle launch of multi-100 kW arrays influences the geometry of both the stowed and deployed structures.

The generic application mission of the array module had an influence on the structural design. The acceleration associated with stationkeeping could not be narrowly defined thus requiring that a broader range of values be considered.

The requirement for compatibility with the Shuttle payload bay has resulted in the stowed configuration shown in Figure 3-4, Section 3. The cradled concept provides internal support members designed to withstand the quasi-static launch loads given in Table 2-1 and to transfer these loads to the exterior of the module, to be picked up by the external support mechanism. Experience with several Shuttle flights has generated new launch and landing load data[12] which suggests that the design loads may be reduced in the future.

The stowed modules must also withstand the vibrational and acoustic loads described in Figures 3-4, Section 3, 5-1 and 5-2. There is also an indication that these requirements may be reduced as presented in Reference 7.

Operation of the deployed array in low earth orbit introduces a different set of structural requirements. The array is acted on by a number of forces. Some, like solar pressure, are negligible. Others such as atmospheric drag can introduce small structural deflections; a more significant effect of atmospheric drag, however, is the need for periodic thruster operation to counteract orbital changes (stationkeeping). Gravity-gradient force is too small to produce significant steady-state deflections; however the force is periodic (twice orbital frequency) and is thus capable of resonating with low-frequency modes in a large structure.

The largest loads encountered in orbit result from stationkeeping acceleration. Since no specific space vehicle has been prescribed for this program, the probable range of accelerations has been approached parametrically. From recent studies of large space structures and their on-orbit thrust requirements, a range of from 450 N (100 lb.) to 1800 N (400 lb.) was estimated. Figure 5-3

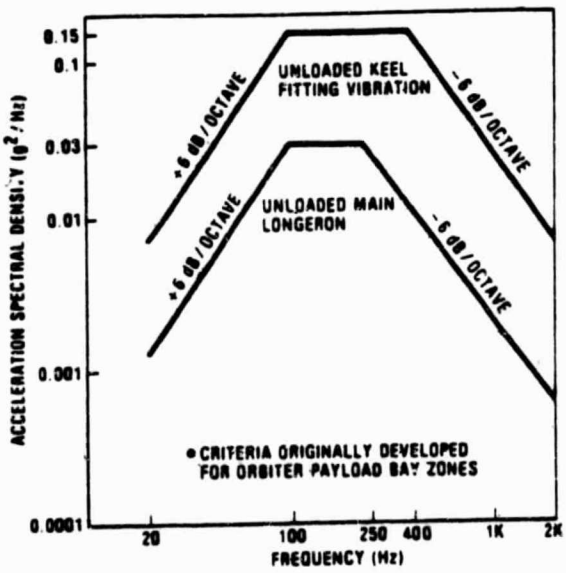

Figure 5-1. Unloaded Main Longeron and Keel Vibration Estimates

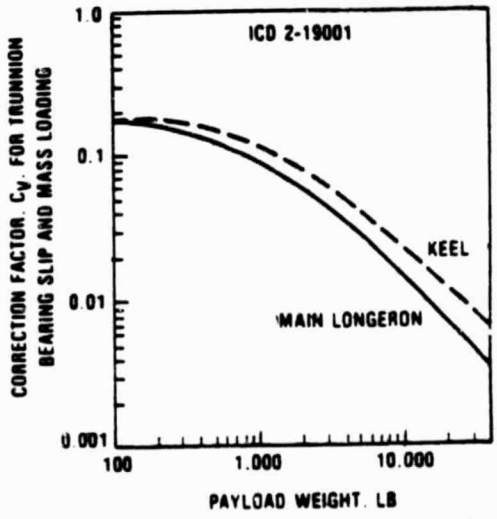

Figure 5-2. Vibration Attenuation Factors

DYNAMIC RESPONSE

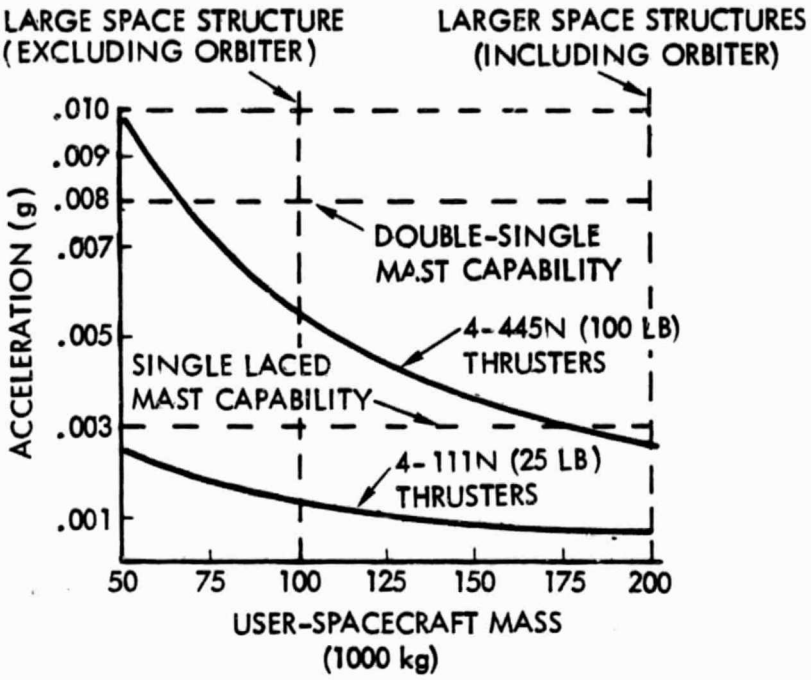

Figure 5-3. Stationkeeping Accelerations

presents acceleration levels for both thrusts as applied to space vehicle masses (including arrays) from 50,000 to 200,000 kg. The resulting accelerations range from 0.001 to 0.01 g. Superimposed on the plot are the capabilities of two lattice mast designs, to be discussed later.

5.2.2 Structural Trades and Analysis

Module Geometry

The stowage volume for sizing the array module was based upon trade studies performed to determine the size of concentrator elements that could be efficiently packaged in a cube with side dimensions that would fit within the Shuttle orbiter cargo bay. Figure 5-4 presents the issues and the interrelationship of the number of containers and concentrator element size that could be stacked within the 3.24 m per side array module stowed volume. The N = 6 configuration was selected on basis of number of concentrator elements required for providing high power (∿100 kW), structural compatibility between mast diameter and deployed length, and upon thermal consideration for passive radiator sizing.

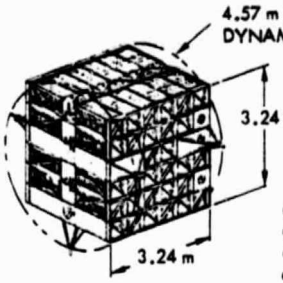

ISSUES/DRIVERS

- DEPLOYMENT COMPLEXITY
- ARRAY MODULE ASPECT RATIO
- CANISTER LENGTH
- CONCENTRATOR STACK LENGTH
- MAST DIAMETER
- PACKAGING EFFICIENCY
- ELEMENT SIZE (CONCENTRATOR)

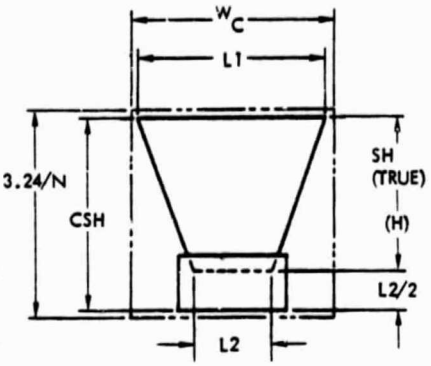

*N = NUMBER OF CONTAINER STACKS

NOTE: ALL DIMENSIONS IN METERS

N*	3.24/N	L1	L2	H	CSH	W_C	SH	MAST DIAMETER	
1	3.240	3.15	1.286	2.333	3.155	3.24	2.512	3.14	NEW MAST DEVELOPMENT REQUIRED HEAVY RADIATOR
2	1.620	1.55	0.633	1.148	1.552	1.62	1.236	1.52	
3	1.080	1.00	0.408	0.740	1.001	1.080	0.797	0.98	
4	0.810	0.75	0.306	0.555	0.751	0.81	0.598	0.70	
5	0.648	0.60	0.245	0.444	0.602	0.648	0.478	0.57	
6	0.540	0.50	0.204	0.370	0.501	0.540	0.399	0.44	
7	0.463	0.42	0.171	0.317	0.426	0.463	0.341	0.40	NOT ENOUGH STRUCTURAL DEPTH, TOO MANY PARTS REQUIRED FOR MULTI-100 kW APPLICATION
8	0.405	0.36	0.147	0.277	0.371	0.405	0.298	0.34	
** 12	0.270	0.25	0.102	0.185	0.250	0.270	0.199	0.21	

**COULD BE APPLICABLE TO SPACE STATION APPLICATION POWER LEVEL

Figure 5-4. Shuttle Moldlines Versus Concentrator Element Envelope

The overall dimensions of the deployed and extended module represent the simultaneous satisfaction of several extension length criteria:

- Mast Stowage Limit — The maximum extended length of continuous longeron canister deployed single/double-laced mast 0.44 m in diameter which can be stowed in the 1.62 m canisters.
- Concentrator Stowage Limit — The maximum extended length (0.5 m per concentrator) which can be spanned by the number of folded concentrators (20 mm per concentrator) stowable in the container housings.
- Mast Stress Limit — The mast length capable of carrying the 0.008 g stationkeeping load with 1.5 safety factor.

Table 5-6 illustrates these limit lengths and the corresponding number of extended concentrators which could be accommodated.

Table 5-6. Comparison of Module Extension Limits

Limit Criteria	Extension Length	Equivalent No. of Concentrators
Mast stowage	35	70
Concentrator stowage	40	80
Mast stress	32.4	66

Mast Dimensions

The dimensions of the stowed module and of the individual concentrator elements require each canister-deployed mast to be confined in the stowed condition in a space of 0.54 m by 0.54 m by 1.62 m. In addition, the structural design of the housing incorporates girders which restrict the available stowage area to an inside diameter of 0.476 m and, thus, the nominal mast diameter to 0.443 m.

As in many large space structures presently under study, the strength of the Astromast structure becomes the most important design criterion, although stiffness must also be considered.

Astro Research, the subcontractor, has analyzed both a single-laced and a double-laced mast that incorporates twice as many battens and lacing as normal which increases the local buckling strength of the longerons.

As sizing criterion, two ultimate levels of uniform lateral acceleration were provided for a load case in which the mast would act like a fixed-end cantilever: 0.004 g for the standard single-laced mast and 0.008 g for the double-laced mast. In addition, the double lacing in the tip portion of the Supermast can be eliminated where bending forces remain below the strength level of a single-laced configuration.

The masses contributing to bending forces during lateral accelerations were specified as

- End cap, 13.1 kg per mast at tip
- Concentrators, 254 kg per mast acting at the tip
- Astromast, as determined by design variables, distributed

In addition, a concentric axial compression load of 330 N per mast, resulting from the tensioning mechanism of the array, was specified.

Figure 5-5 shows single-laced mast capabilities as a function of mast radii and stationkeeping accelerations. The figure also shows the required canister lengths associated with the radius and deployed lengths. The maximum canister envelope is approximately 0.49 m which limits the maximum mast radius to 0.44 m.

The structural capability of a 0.44 m diameter mast extended 32.6 (root length) is 0.004 g acceleration. Increasing the stationkeeping acceleration above 0.004 g requires a stronger single/double laced mast combination. Figure 5-6 represents the structural capabilities of a single/double laced mast (hybrid mast) as a function of mast radius, accelerations and batten stiffness (EI_b/EI_ℓ). Double lacing requires more stowage area, thus to maintain a 1.62 canister height envelope requires rectangular battens to increase packing efficiency. Utilizing a 0.44 m hybrid mast with batten width to thickness ratio (W/t) of 2.5 allows 0.008 g stationkeeping maneuver.

Dynamic analyses were performed on both dual direction extension (Case 1) and single direction extension (Case 2) configurations as shown in Figure 5-7. The appendage-clamped frequencies were developed to assess user spacecraft controls compatibility. A decade separation of controls bandwidth with appendage frequencies generally assures no interaction. Systems being designed with less separation, including intersection of structural frequencies with controls frequency range, would require precise knowledge of the structural frequency and the associated damping. An indication of loads and pointing sensitivity to transient loading to the user spacecraft is shown for two typical configurations. Case 1 represents the baseline array module configuration and Case 2 configuration assumes an array module deploying concentrator elements from the container housing in one direction only. The response frequencies, end cap (tip) accelerations and the mast root moment (M) are provided for both cases (R is the rigid body mode in the disturbance direction).

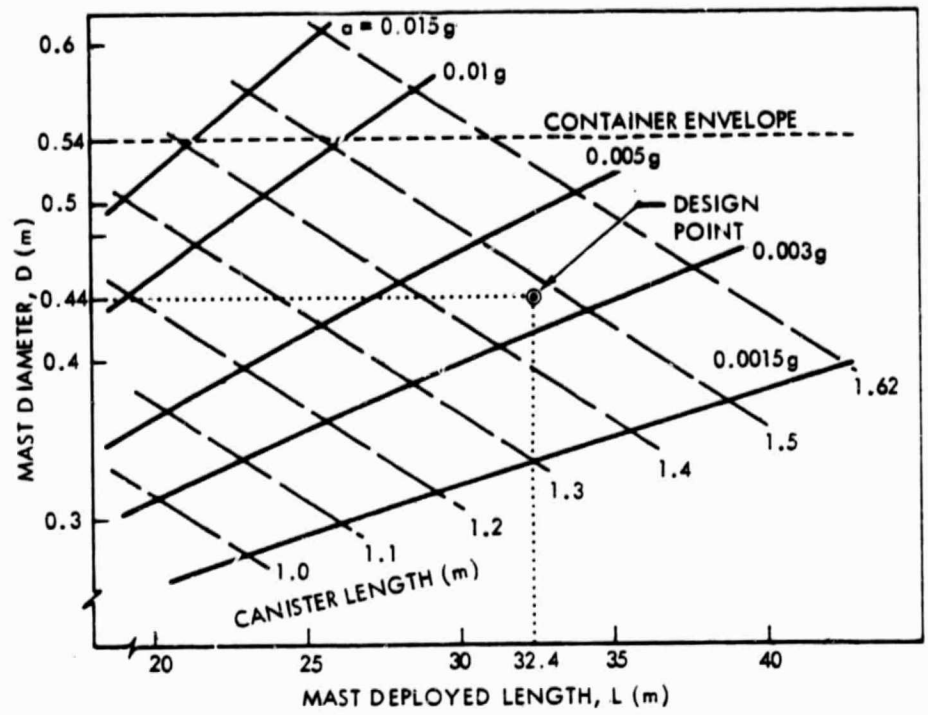

Figure 5-5. Mast Structural Capability (Single Laced)

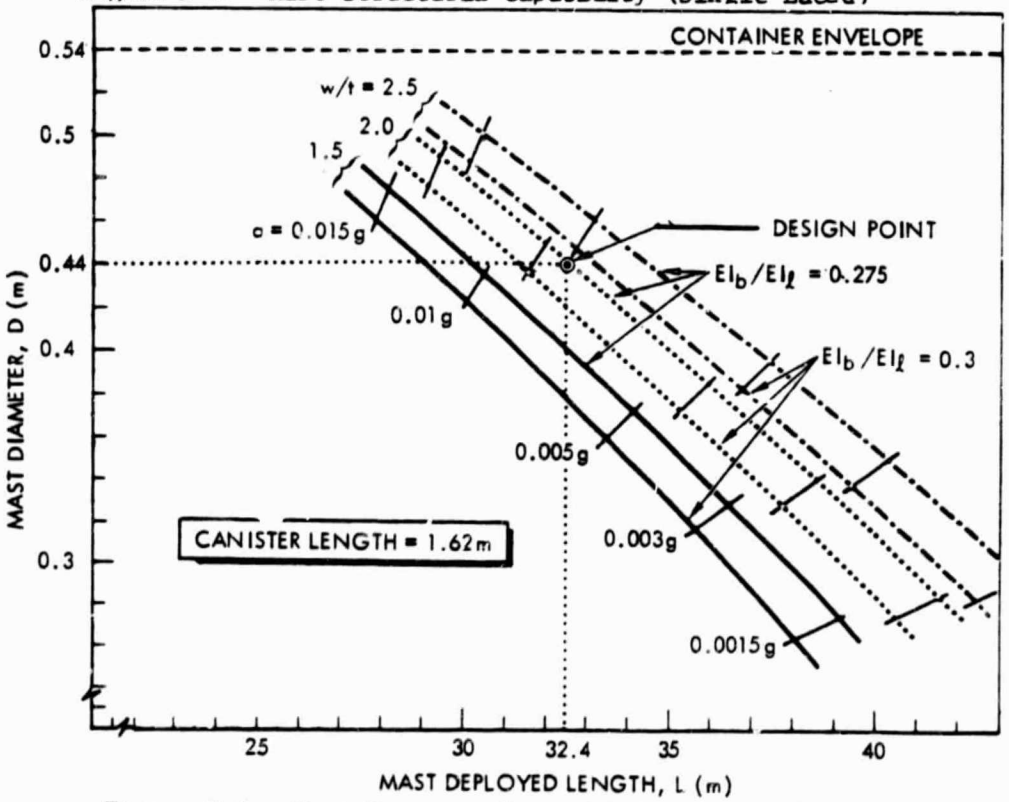

Figure 5-6. Mast Structural Capability (Hybrid)

MODAL ANALYSIS

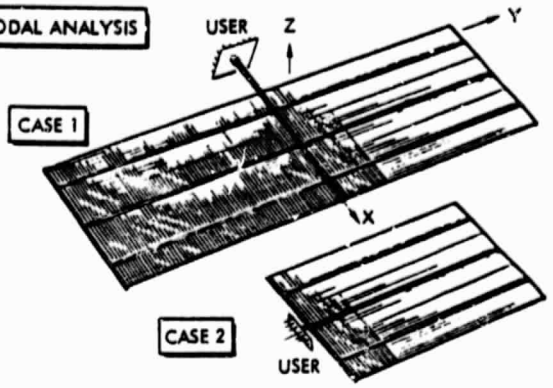

NO.	MODAL FREQ (Hz)	CHARACTERISTICS
1	0.037	HOUSING TENSION
2	0.049	HOUSING BENDINC
3	0.064	MAST BENDING OUT-OF-PLANE
1	0.048	MAST BEND OUT-OF-PLANE
2	0.074	MAST IN-PLANE BENDING & PLANE TORSION
3	0.076	OUT-OF-PLANE TORSION

RESPONSE CHARACTERISTICS

	CASE 1			CASE 2		
NO.	FREQ (Hz)	TIP ACC (g)	MAST ROOT M (N-m)	FREQ (Hz)	TIP ACC (g)	MAST ROOT M (N-m)
R	0.	0.001	0	0.	0.001	0
1	0.037	0.00003	0.169	0.048	0.0028	27.0
2	0.049	0.0029	22.76	0.074	0.00001	0.07
3	0.064	0.	0.001	0.076	0.00005	0.88
4	0.074	0.00002	0.24	0.547	0.00036	9.36
		0.0039	23.17		0.0042	36.9

Figure 5-7. Array Module (Baseline) Dynamic Analysis

Support Cable Tension Requirements

The primary structural system is composed of the housing, mast, end cap, and the tensioning cables carrying the concentrators. This closed force system must be able to carry the additional loads associated with station-keeping. Table 5-7 summarizes the results of NASTRAN[13] modeling of a single module supported by single-laced masts. The design cable tension of 20 N is well below the buckling limit.

Table 5-7. General Module Stability

Load Condition Tension per Cable	Eigen Value (Load Level Factor)
18 N	7.7
30 N	4.4
135 N	Buckling of closed force system

Load Capability of Housing and End-Cap Members

Structural strength in the direction normal to the mast axes is provided by the interconnected container housings (at the canister end) and by interconnected end caps to which the extending ends of the mast are attached. Early designs used shear panels of solid aluminum sheet for both housing and end caps. However, minimum gauge requirements imposed by reasonable-cost manufacturing procedures resulted in high weights for these components. Considerably lighter structures were achieved by the use of diagonally braced trusses .

Simplified load distribution models were used to determine stresses in each structural element of housing and end cap due to launch on stationkeeping accelerations. Figures 5-8 and 5-9 list the structural capability and the ultimate applied loads for each member. The ultimate load assumes a 1.5 factor of safety.

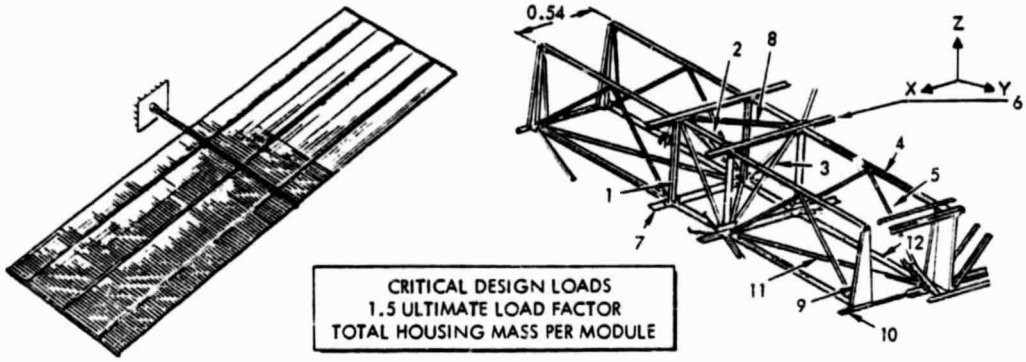

CRITICAL DESIGN LOADS
1.5 ULTIMATE LOAD FACTOR
TOTAL HOUSING MASS PER MODULE

MEMBER	AREA (mm^2)	CAPABILITY	CRITICAL LOAD CONDITION	APPLIED LOAD (ULT)	TOTAL MASS PER MODULE (kg)
1	75	10,500 N	LAUNCH ($N_Z = \pm 5$)	10,200 N (AXIAL)	9.4
2	40	5,500 N	LAUNCH ($N_Y = \pm 3$)	1,700 N (AXIAL)	4.6
3	75	10,500 N	STA KP (.01 g) (TORSIONAL)	6,400 N (AXIAL)	10.4
4*	220	950 N/mm^2	LAUNCH ($N_Z = \pm 5$) (BENDING)	700 N/mm^2	107.0
5	40	1,500 N	STATIONKEEPING	NEGLIGIBLE	12.3
6	100	22,400 N	STATIONKEEPING (.01 g)	22,400 N (AXIAL)	21.5
7	40	5,000 N	LAUNCH STABILITY	—	3.4
8	75	10,500 N	STA KPG (.01 g) (TORSIONAL)	6,400 N (AXIAL)	11.4
9	40	9,400 N	LAUNCH STABILITY	—	5.0
10	40	9,400 N	LAUNCH STABILITY	—	4.3
11	40	1,500 N	LAUNCH STABILITY	—	9.8
12	75	2,040 N	LAUNCH STABILITY	—	22.9
				TOTAL	222.0

*STAINLESS STEEL LAUNCH SUPPORT TUBE

Figure 5-8. Container/Housing

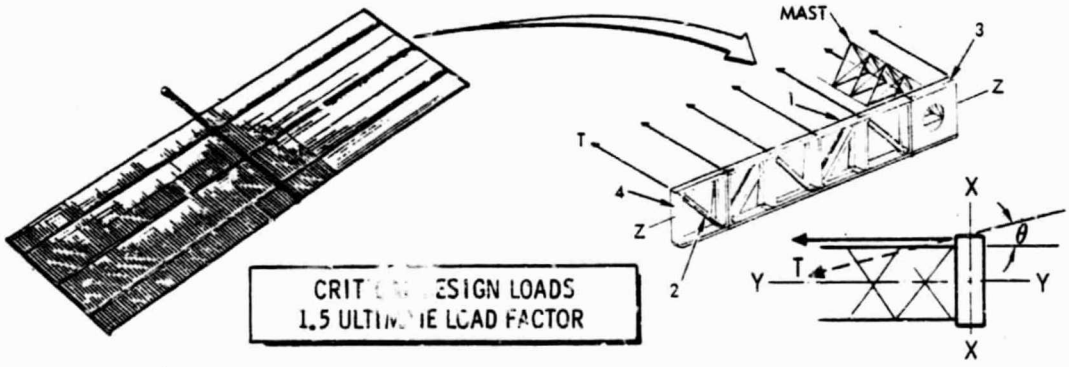

CRIT[illegible]ESIGN LOADS
1.5 ULTIM[illegible]E LOAD FACTOR

MEMBER	AREA	CAPABILITY	CRITICAL LOAD CONDITION T = 27N	APPLIED LOAD (ULT)	NUMBER REQUIRED PER SIDE	TOTAL MASS (kg)
1	40 mm^2	4700N	BENDING X-X	4500N	4	8.6
2	40 mm^2	4600N	TORSION Z-Z	2000N	66	5.6
	THICKNESS					
3	.75 mm	250 N/mm^2	SHEAR (HINGES)		24	3.3
4	.75 mm	250 N/mm^2	SHEAR (TORSION)		42	5.9
TOTAL (PER SIDE)						23.4

Figure 5-9. Container/End-Cap

5.2.3 Structural Performance of the Design

Modal Analysis

In order to provide the user spacecraft minimal controls design interaction with the appendage, the array structure must maintain at least an order of magnitude frequency separation from possible excitation frequencies, and sustain dynamic loads induced by spacecraft maneuvers. A NASTRAN mathematical model was developed to evaluate the module characteristics and the parameters that would indicate coupling with the user spacecraft. The model was utilized to determine the overall fundamental frequency for both single and dual modules. The first mode of a single module is 0.027 Hz which is 71 times the LEO gravity gradient disturbance frequency (Figure 5-10). The first mode frequency of a dual module is 0.01 Hz which is 26 times the LEO gravity gradient disturbance frequency (Figure 5-11).

Module Deflections

Solar heating of the sun-facing side of masts, housing and end-caps can result in thermal distortion of the module when concentrators are extended. Absorption of solar energy by the top surfaces and shadowing of the lower ones results in a thermal gradient estimated to be 25°C. The resulting differential expansion produces bending of the structure and a corresponding rotation of the concentrator optical axes. However, as shown in Table 5-8 the pointing errors introduced by this effect are not large and will not result in serious thermal distortions. Thermal distortion of the masts is negligible. Atmospheric drag will produce 0.01 degree pointing errors, also negligible.

The most critical deflections are created by stationkeeping maneuvers. The range used for preliminary design calculations, 0.01 to 0.001 g has been used to estimate deflections. Deflections in mast, housing and cables are all small at the lower limit, but 0.01 g stationkeeping acceleration and other sources of deflection produce transients exceeding 3 degrees (see Table 5-8).

Thermal Stresses in Reflector Panels

The thermal gradients generated during the eclipse cycle, as discussed in Section 5.3.3, produce stresses in the Kapton reflector film due to the differential expansion of film and frame. A NASTRAN model was used to compute the biaxial stresses produced in such film-frame structures. Figure 5-12 shows stress levels parametrically and for the design values of frame cross-

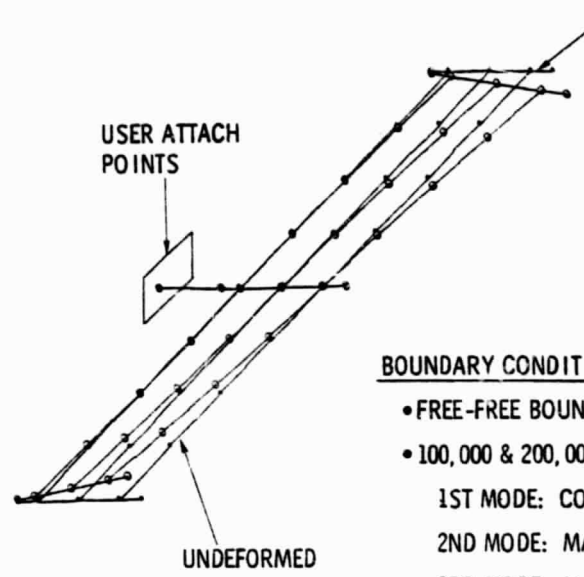

NOTE: CABLES NOT SHOWN.

BOUNDARY CONDITIONS	MODAL FREQ. (Hz)
• FREE-FREE BOUNDARY	
• 100,000 & 200,000 kg USER-SPACECRAFT	
1ST MODE: CONTAINER/HOUSING (TORSIONAL)	0.027
2ND MODE: MAST BENDING (OUT-OF-PLANE)	0.031
3RD MODE: MAST BENDING (IN-PLANE)	0.036

FIRST MODE FREQUENCY SEPARATION OF 71 TIMES LEO GRAVITY GRADIENT DISTURBANCE FREQUENCY

Figure 5-10. Modal Analysis - Single Module

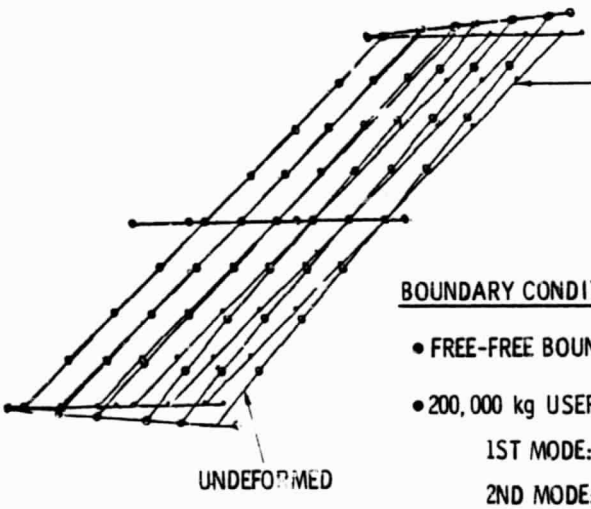

NOTE: CABLES NOT SHOWN

BOUNDARY CONDITIONS	MODAL FREQ (Hz)
• FREE-FREE BOUNDARY	
• 200,000 kg USER-SPACECRAFT	
1ST MODE: CONTAINER/HOUSING (TORSIONAL)	0.01
2ND MODE: CONTAINER/HOUSING (BENDING)	0.02
3RD MODE: MAST BENDING (OUT-OF-PLANE)	0.02

FIRST MODE FREQUENCY SEPARATION OF 26 TIMES LEO GRAVITY GRADIENT DISTURBANCE FREQUENCY

Figure 5-11. Modal Analysis - Dual Module

Table 5-8. Dimensional Stability and Deflections (Single Module)

STRUCTURAL ELEMENT	NORMAL OPERATIONS (OUT-OF-PLANE CURVATURE) (DEGREE)	.01g STATIONKEEPING MANUEVER (OUT-OF-PLANE TRANSLATION) (m)
MAST	0.001 (THERMAL)	3.0
CONTAINER/HOUSING	0.57 (THERMAL)	0.3
CONTAINER/END-CAP	0.57 (THERMAL)	NEGLIGIBLE
CONCENTRATOR SUPPORT CABLE	0.01 (ATM. DRAG)	0.7
SUB TOTAL	0.81	-
MANUFACTURING TOLERANCES	±0.25	-
ARRAY POINTING	±0.5	-
TOTAL SUN POINTING ERROR	1.4	
REMARKS	3.0 DEGREES USED IN PERFORMANCE ESTIMATES	STATIONKEEPING TRANSLATIONS (DISPLACEMENTS) ARE STRUCTURALLY ACCEPTABLE

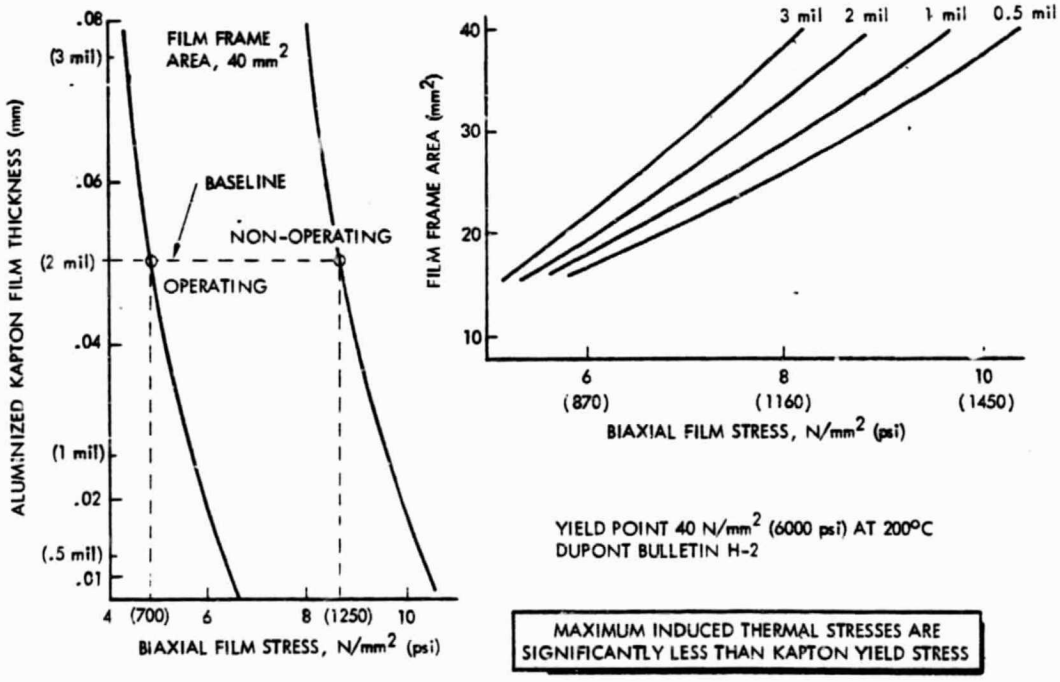

Figure 5-12. Thermal Stresses in Film-Frame Reflector Panels

section and film thickness. Maximum stresses fall a factor of five below the yield stress for Kapton at 200°C. Since these maximum stress a develop at much lower temperatures, plastic failure seems very unlikely.

5.2.4 Dynamic Analysis

Container/Housing Latching Mechanism

Active latching is required at deployment hinge joints to ensure longeron stiffness and continuity of tensile strength. During orbit make-up maneuvers, the maximum longeron bending moments are produced at the user spacecraft interface. The mast critical latch load is the first joint closest to the user spacecraft (excluding the user attach point). Applying a 0.01 g orbit make-up to a dual module array creates a 16,000 Nm (Figure 5-13) bending moment at the first deployment joint. Two active latches attached to the container longerons opposite the joint hinges and capable of 16,000 N plus 300 N (4,400 lb.) preload, will ensure longeron structural integrity and acceptable stiffness.

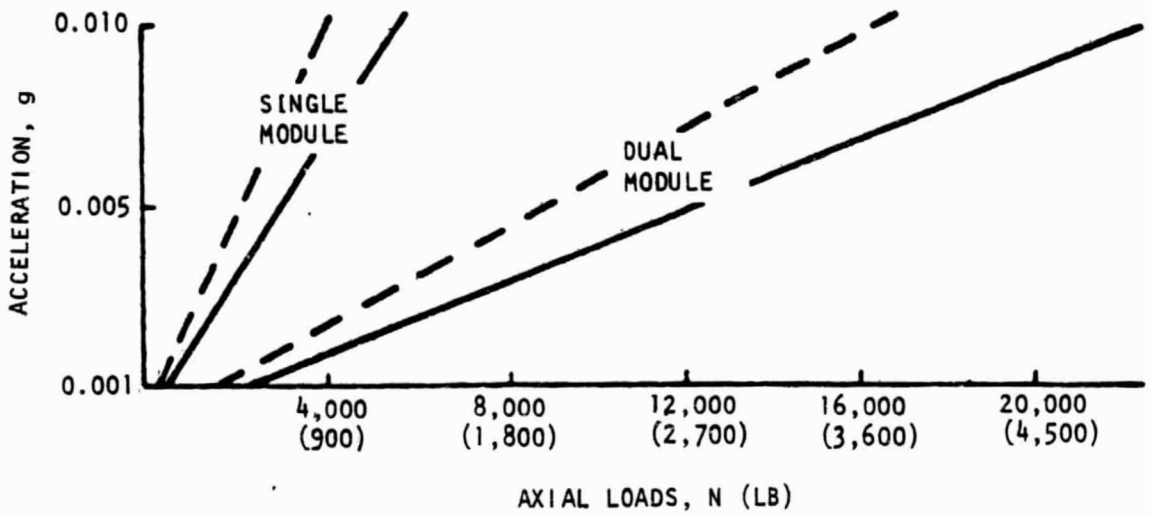

Figure 5-13. Latching Mechanism Loads

Deployment Actuators

The deploying array will be maneuvered at mid-span, allowing translation and rotations in both directions so as to minimize inertial loads being transferred to the RMS (Figure 5-14). The deployment actuators were sized based on Schaeffer Magnetics specifications for a Type 2 actuator which produces 7.0 Nm output torque and when activated will create 0.0009 rad/sec^2 radial acceleration of the two container sections in opposite directions. Full rotation (180°) of the actuator (Type 2) at a 7.0 Nm constant torque requires approximately 29 minutes (Figure 5-14). Installing a Type 3 actuator which produces 45 Nm torque will rotate through 180° in approximately 5 minutes.

Concentrator Support Cables and Tensioners

The individual concentrator elements, each approximately 0.70 kg are supported on cables suspended between the end-caps and the negator mechanisms located in the container/housing. A second tensioning mechanism is applied to the concentrator elements themselves to prevent translations during an in-phase stationkeeping maneuver. The concentrator tensioners will also ensure reflector hinge flatness. The present design value of 20 N tension per cable plus 7 N per concentrator row is more than sufficient to maintain planar integrity during normal operation. During a stationkeeping maneuver, however, there is a translation and rotation of the concentrator elements.

The concentrator oscillations initiated by the maneuver will "settle" as a function of cable tension (frequency) and system damping. Figure 5-15 represents the settling time and approximate power output as a function of cable tension. The 1.5% damping value utilized in this analysis is based on vibrational tests conducted by Astro Research. Multi-jointed structures similar in nature to a continuous longeron mast has damping values ranging from 1.1 to 2.0%. This value does not include energy loss due to the concentrators on the cables and therefore is conservative.

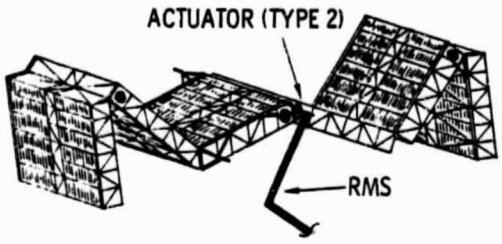

- SCHAEFFER MAGNETICS ACUTATOR
  - TYPE 2, 1 kg PER ACTUATOR
    - OUTPUT TORQUE -- 7 N-m
    - 180 deg ROTATION -- 29 min
  - TYPE 3, 1.5 kg PER ACTUATOR
    - OUTPUT TORQUE -- 45 N-m
    - 180 deg ROTATION -- 5min

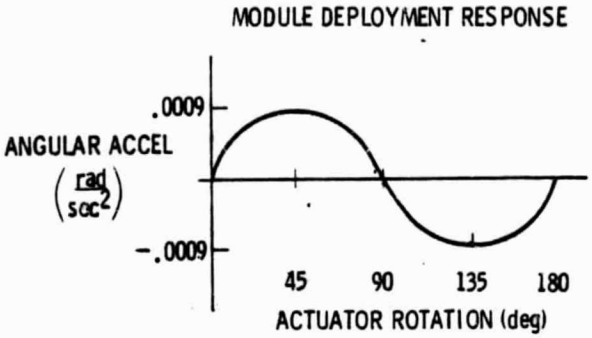

DEPLOYMENT DYNAMICS
(TYPE 2 ACTUATOR)
DOES NOT DRIVE PRIMARY
STRUCTURE SIZING

Figure 5-14. Module Deployment

- .008g STATIONKEEPING ACCELERATION (HYBRID MAST)
- 1.5% DAMPING

20N SUPPORT CABLE (WITHIN PRESENT TECHNOLOGY)
7N CONCENTRATOR TENSIONER
98% POWER OUTPUT .9 min
99+% POWER OUTPUT 4.2 min

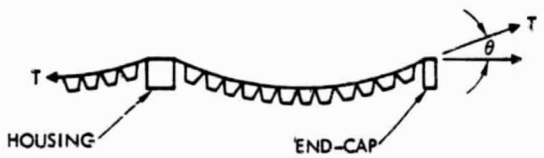

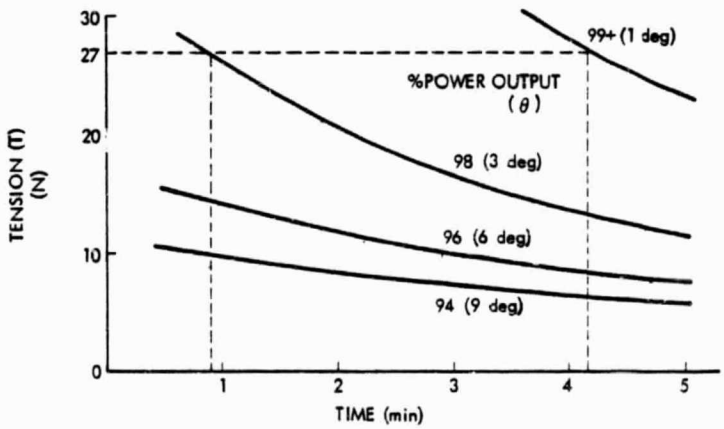

Figure 5-15. Power Output as a Function of Cable Tension

5.3 THERMAL ANALYSIS

Thermal analysis of the array as a whole and of its components supports the design process in several ways. Component temperature predictions are needed throughout in order to guide the selection of appropriate materials and surface treatments. Temperature distributions and temperature transients are required to assess thermal stress levels and thermal distortion effects. Finally, the electrical output of the solar panel is strongly temperature-dependent. Early in the program simplified thermal analyses were carried out in support of the design effort. These studies served to establish temperature distributions and to evaluate thermal stresses and thermal distortion effects as well as to optimize radiator size and thickness. In general the results did not uncover any serious design problems.

More accurate evaluation of concentrator temperatures has now been completed. It takes into account the coupled thermal and electrical behavior of the solar cell panel. This includes the (non-uniform) absorption of solar energy, heat loss by radiation and conduction and the conversion of light to electrical power. This was accomplished by the simultaneous solution of thermal and electrical networks using a Rockwell-developed thermal analyzer code. The thermal behavior of the concentrator was solved by the built-in logic of the analyzer code while the electrical behavior of the solar cell network was solved by a special Newton-Raphson procedure.[14]

The thermal analyzer code accounts for thermal radiation exchange between nodes by assigning "script FA" values which depend on internode configuration factors (functions of geometry only) and the surface emittances of the nodes. Script FA's were evaluated for both inner and outer surfaces of the concentrator nodes from the local irradiance and radiosity by solving radiosity networks defined by

$$H_i = \sum_{j=1}^{N} F_{ij} B_j \qquad (5\text{-}1)$$

$$B_j = \sigma \varepsilon_j T_j^4 + (1 - \varepsilon_j) H_j \qquad (5\text{-}2)$$

Surface emittances were assumed to be independent of temperature and equations 5-1 and 5-2 were solved for the hypothetical temperature distribution

$\sigma T_i^4 = 1$; $\sigma T_j^4 = 0$. Under these circumstances

$$\mathcal{F}_{ji} = H_j - B_j \qquad (5\text{-}3)$$

Three separate networks are involved. Node surfaces on the bottom of the substrate-radiator "see" only the environment and thus are simply evaluated ($\mathcal{F}A_j = \varepsilon_j A_j$). The network within the concentrator can be represented by a limited number of reflector zones exchanging radiation amongst themselves and with individual solar cells. The gridwork of perpendicular V-shaped channels formed by the top surfaces of the radiators and the under surfaces of the reflectors presents a more difficult problem. In principle each node in this third network exchanges radiation directly, or by multiple reflections, with every other inner node throughout the entire array. However, by treating all concentrators as identical elements in an infinite array, the network can be represented adequately by six distinct radiator nodes, three reflector nodes, and one each for the inter-element electrical harness and the gap between radiators.

Separate mathematical models were generated for the gallium and silicon baseline concentrators. Each incorporated individual models of cell electrical performance, the distribution of direct and reflected sunlight, heat conduction through the substrate-radiator and a thermal radiation model which considered the hindered view from reflectors and radiator due to the presence of adjacent concentrators.

5.3.1 Reflector Panel Temperatures

The temperature distribution over the reflector panels is determined by the distribution of incident and reflected sunlight (evaluated by the ray-tracing methods described in Section 5.4) and by the presence of adjacent concentrators which hinder reradiation.

Typical concentrator temperature distributions are illustrated in Figures 5-16 and 5-17 which show the effects of fully reflecting corners and low (0.15) rear-surface emissivity on reflector panel temperature distribution. Multiple reflections from rays originating in the corners tends to heat the lower portion of the reflector panels. Low emissivity on both front ($\sim$ 0.05) and back surfaces of the panels results in fairly high temperatures.

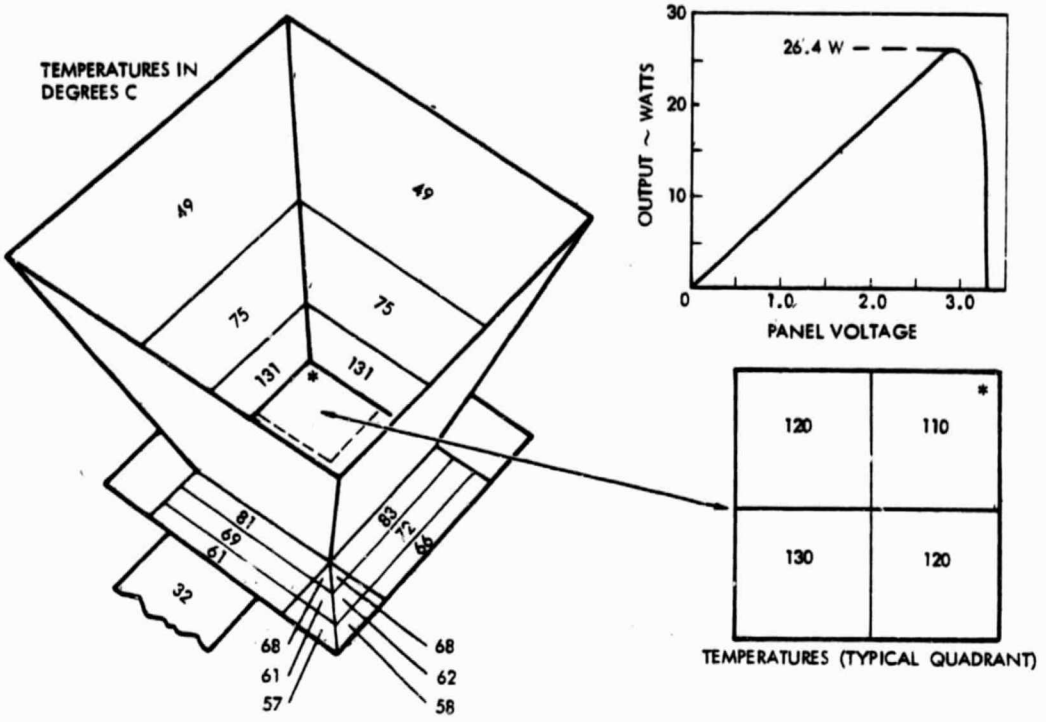

Figure 5-16. Coupled Thermal-Electric Model Results
(Updated Silicon Baseline)

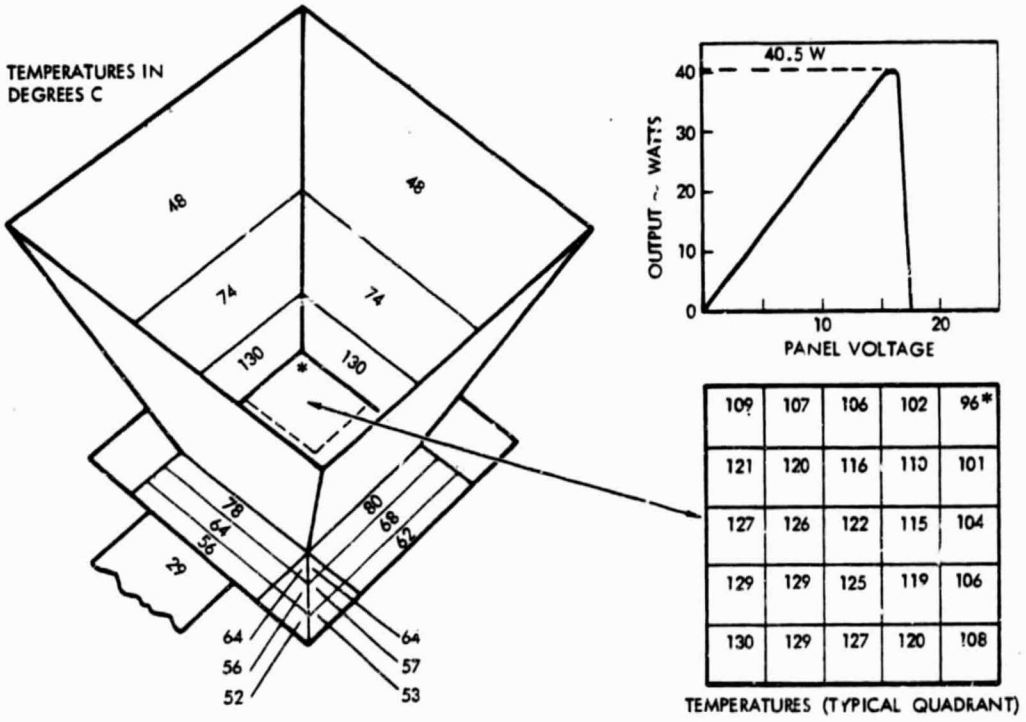

Figure 5-17. Coupled Thermal-Electrical Model Results
(Updated GaAs Baseline)

Although these temperatures are not expected to be design limiting, they can be reduced by one of several methods. The outer (non-reflecting) surfaces of the reflector panels can be coated with high-emissivity material to improve heat rejection. However, a portion of that rejected heat must go to the radiators, thus impairing their performance in keeping the solar cells cool. Another approach is to make the reflector corners non-specular (diffuse), thus reducing the amount of multiple reflection which contributes to the overheating. This method, however, results in large overall light losses with consequent reduction in electrical output. A third alternative is to make only the upper corners of the reflectors diffuse. That region contributes most to the heating and very little to the illumination of the cells.

5.3.2 Radiator/Substrate Mass Optimization

Heat is carried away from the solar cells by conduction in an aluminum sheet which serves as both substrate and radiator. Its effectiveness in distributing heat depends on its size and thickness. These factors, in turn, determine the mass of the sheet per unit of aperture[15] area. For a particular aperture size and relative radiator area, sheet mass can be reduced by decreasing its thickness. However, this results in an increase in cell temperature with consequent loss in electrical conversion efficiency. By reducing the scale of the concentrator, on the other hand, the same performance can be achieved with a thinner sheet, reducing the mass per unit aperture by almost 50%. Figure 5-18 illustrates this point. This scale effect on radiator performance is one of the reasons for choosing the N = 6 baseline configuration instead of the N = 4 configuration.

Pyrolitic graphite has lower density, higher thermal conductivity and lower thermal expansion than aluminum. These properties would confer weight and performance advantages. However, uncertainties about cost of fabrication in very thin sections and vibration sensitivity make it a high-risk choice for the near term.

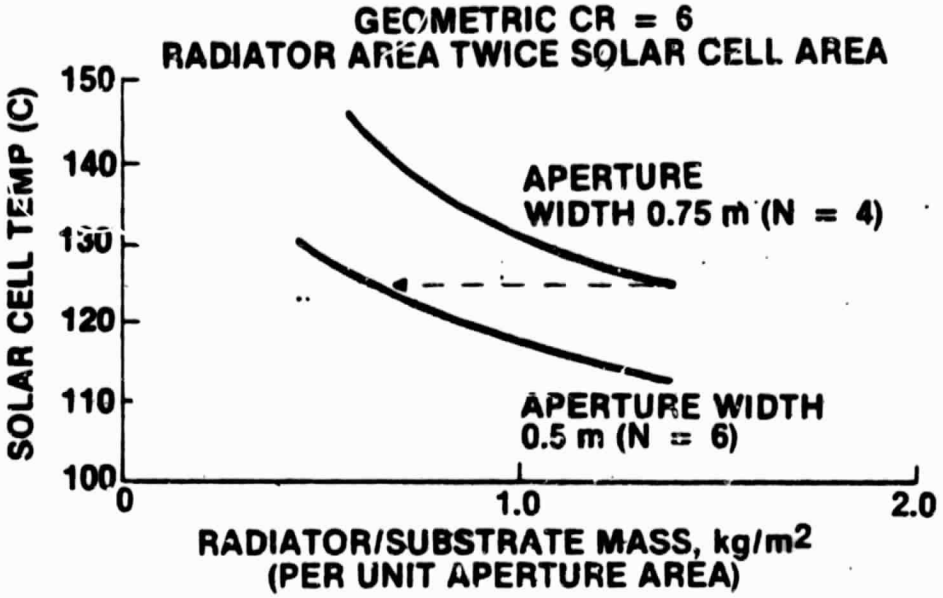

Figure 5-18. Scale Effect on Radiator/Substrate

5.3.3 Thermal Cycling of Film Reflectors

Two options were considered for reflector panel design, namely rigid and stretched film. In the stretched film option which has been chosen for the final design, aluminized Kapton is bonded to a rigid frame made of molded chopped fiber. In operation the reflector film must be under moderate tension in order to maintain a flat, wrinkle-free mirror surface.

During the orbital cycle, the reflector panels will alternately heat up and cool down. However, due to the substantial differences between the thermal capacities of the two, frame temperature will lag film temperature. This will result in reduced stress at the beginning of the sunlit period and increased stress at the beginning of eclipse. Figure 5-19 illustrates this transient behavior. It is clear however that the temperature gradients between film and frame are much less than the steady-state temperature difference assumed in early structural analysis.

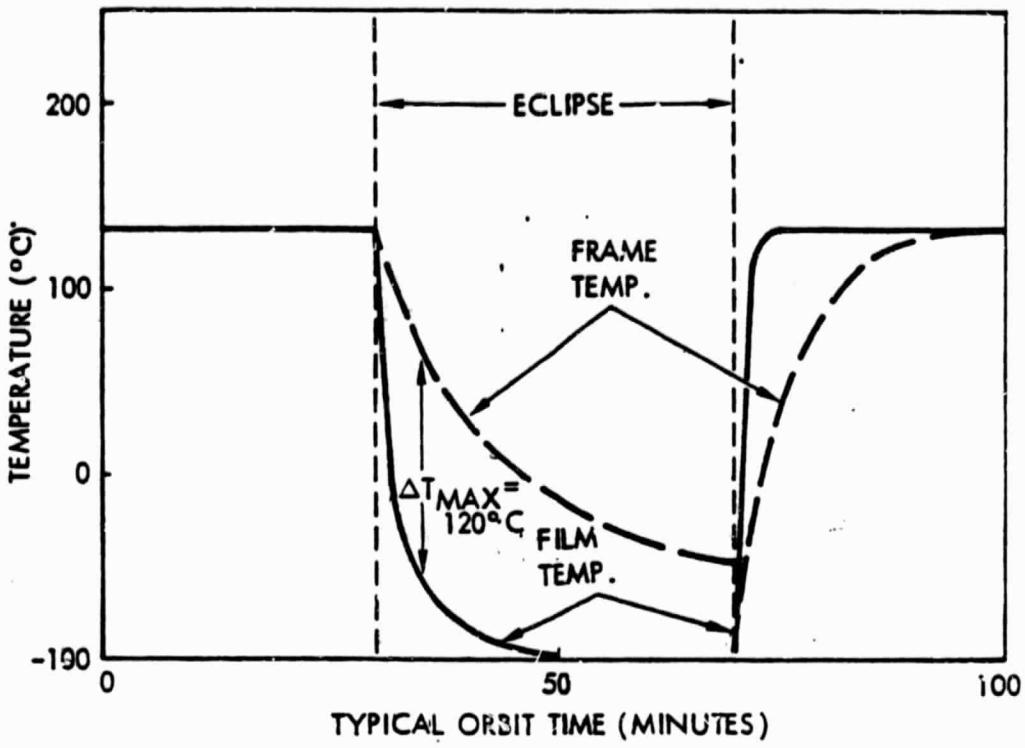

Figure 5-19. Transient Temperatures for Frame-Film Reflectors

5.3.4 Module Thermal Distortion

Solar heating of the sun-facing side of caps and containers can result in thermal distortion of the module when concentrators are extended. Absorption of solar energy by the top surfaces and shadowing of the lower ones results in a thermal gradient estimated to be 25°C. The resulting differential expansion produces bending of the structure and a corresponding rotation of the concentrator optical axis (Figure 5-20). However, as shown in Table 5-9 the pointing errors introduced by this effect are not large and will not result in significant light loss.

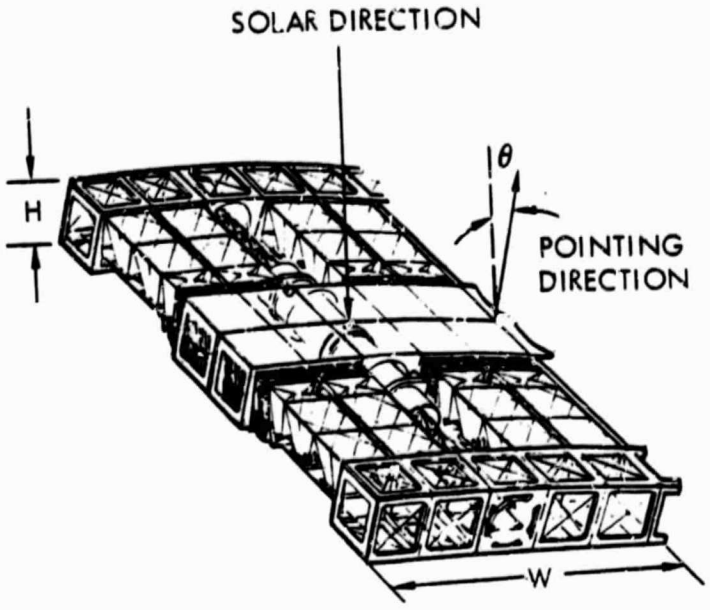

Figure 5-20. Differential Expansion Results

Table 5-9. Container Thermal Distortion

Configuration	Container Depth, H (m)	Module Width, W (m)	Pointing Error, (deg)
N = 4	0.81	13.0	0.25
N = 6	0.54	19.5	0.57

5.4 OPTICAL PERFORMANCE

The distribution of illumination produced by the reflecting panels of the concentrator is important for two reasons: first, differential illumination of the solar cells may have an adverse effect on output; second, the non-uniform illumination can result in large temperature gradients. These effects have been investigated by means of a Rockwell-developed ray-tracing program RAYPYR. Incoming light is represented by a large number of equally spaced, parallel rays emanating from the solar direction. Off-axis pointing is characterized by the direction angles with respect to the coordinate axes. The program follows each ray individually, through multiple reflections if necessary, until it either reaches the truncated bottom (representing the solar panel) or is reflected back out the entrance aperture.

5.4.1 Geometry of the Optical System

The concentrators treated by RAYPYR have the shape of a right, four-sided pyramid, truncated to form a base which corresponds to the solar cell panel (see Figure 5-21). The larger, upper square is the aperture, the smaller bottom square is the base and the trapezoidal sides are the reflectors.

The coordinate system is a right-hand cartesian one, with the Z-axis parallel to the optical axis and the X- and Y-axes aligned with the sides of the base. Ray directions are characterized by direction angles with respect to the three coordinate directions.

The shape of the concentrator is determined by three parameters: base width (W); concentrator height (H); and reflector slant angle (θ). In a conventionally designed concentrator, these parameters are chosen so that an incoming ray parallel to the optical axis, which strikes an edge of the aperture, produces a reflected ray which strikes the opposite edge of the base. This condition is satisfied (see Figure 5-22) when

$$\frac{W}{H} = -(\tan 2\theta + \cot \theta) \qquad (5\text{-}4)$$

Each reflector is divided into sections and the amount of energy absorbed in each is calculated. The truncated bottom surface is divided into a square

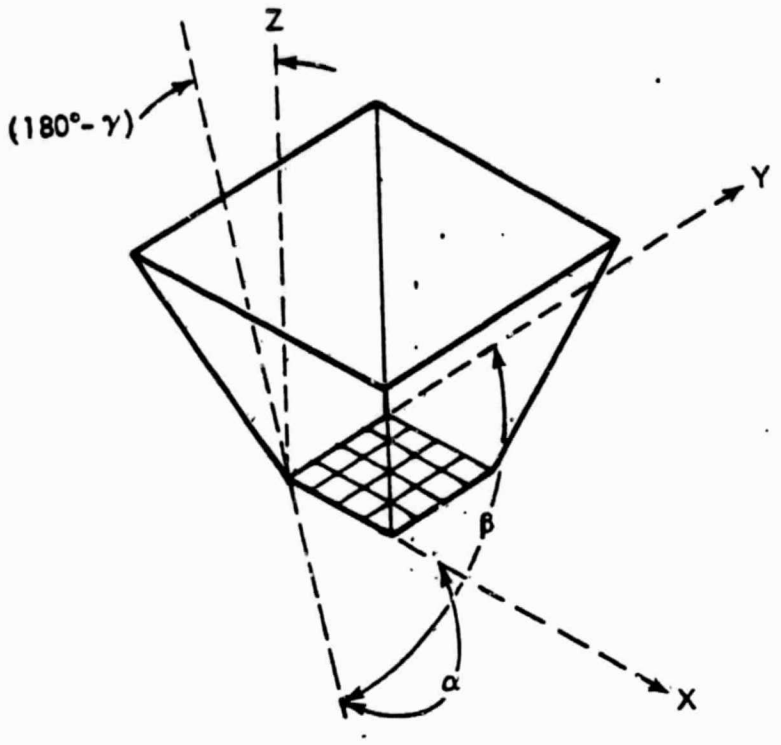

Figure 5-21. Coordinate System for Pyramidal Concentrators

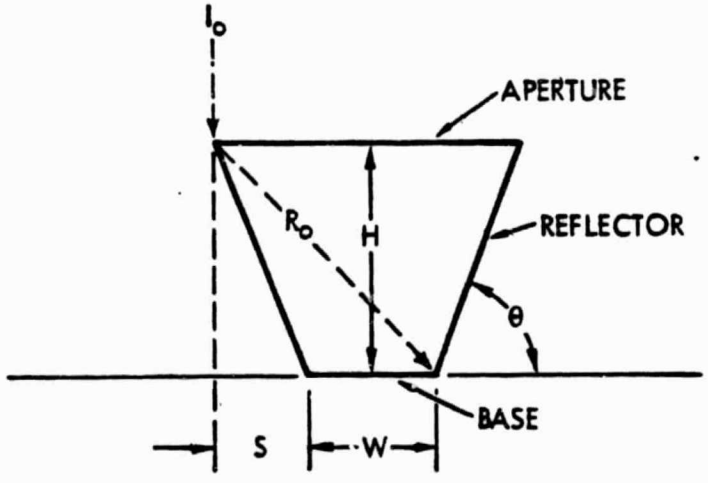

Figure 5-22. Geometry of Limiting Ray (Conventional Design)

grid representing the cells making up the solar panel. The energy reaching each cell is calculated by summing the contribution of all rays which reach it. Even though a large number of incoming rays are used (typically 90,000), uneven distributions can result due to the fortuitous pileup of equally spaced incident rays in certain grid squares. This problem is alleviated by introducing random spacing for the incident rays.

5.4.2 Ray Reflection

The basic relationship governing specular reflection is Snell's law: The angle of incidence equals the angle of reflection. In vector form (16)

$$\overline{R} = \overline{I} - 2(N \cdot I)\,\overline{N} \tag{5-5}$$

The incident ray is expressed in terms of its direction cosines.

$$\overline{I} = \cos \alpha_1\,\overline{X} + \cos \beta_1\,\overline{Y} + \cos \gamma_1\,\overline{Z} \tag{5-6}$$

The normal to the reflector is given in general terms as

$$\overline{N} = -\sin \theta\,(P_{k_1}\,\overline{X} + P_{k_2}\,\overline{Y}) + \overline{Z} \cos \theta \tag{5-7}$$

The coefficients P_{kj} take on the values -1, 0, +1 depending on which of the four reflectors is involved.

The dot product in Equation 5-5 becomes

$$N \cdot I = -\sin \theta\,(P_{k_1} \cos \alpha_1 + P_{k_2} \cos \beta_1) + \cos \theta \cos \gamma_1 \tag{5-8}$$

The components of the reflected ray (the direction cosines) are obtained by substituting Equations 5-6, 5-7 and 5-8 into Equation 5-5:

$$\cos \alpha_2 = \cos \alpha_1 + 2\,(N \cdot I)\,P_{k_1} \sin \theta$$

$$\cos \beta_2 = \cos \beta_1 + 2\,(N \cdot I)\,P_{k_2} \sin \theta$$

$$\cos \gamma_2 = \cos \gamma_1 - 2\,(N \cdot I) \cos \theta$$

The ray tracing process follows individual rays from their initial positions in the aperture plane through one or more intersections with reflector, base or aperture planes. In general, a given ray may intersect more than one reflector plane. The intersection of interest is the one having the smallest Z change, after eliminating backward intersections and the trivial

case of intersection with the plane containing the initial point. If there are no reflector intersections between the aperture and the base, the ray is terminated and its contribution is added to the base (if downward directed) or considered lost through the aperture.

5.4.3 Verification of Ray Trace Analysis

The analysis described above predicts illumination distributions with good accuracy and resolution, as determined by comparative results for cases where accurate analytical results are possible. Figure 5-23 shows the distribution in illumination over one quadrant of a solar panel for an ideal pyramidal concentrator with a GCR of six and a specular reflectance of 0.9, aligned directly toward a point sun. For this case, the boundaries between differently illuminated regions (the diagonal lines in Figure 5-23) and the local CR values can be accurately calculated and are indicated by underlined numbers. The circled numbers are the average CR's for each square cell, as calculated by ray-tracing, using a sample of 90,000 rays equally distributed at the aperture. The differences in local CR values are within a few tenths of a sun and the overall energy balance is within a few tenths of a percent.

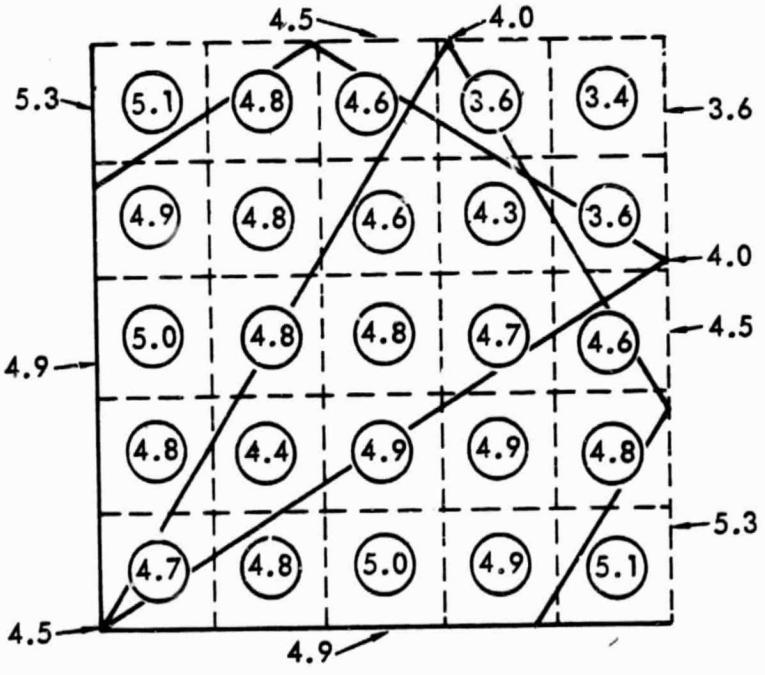

Figure 5-23. Comparison of CR Distributions Obtained Analytically with RAYPYR Results (ρ_s = 0.9, GCR = 6, Zero Pointing Angle)

Certain cases involving diffuse radiation can be solved analytically, using the radiosity network approach described in Section 5.3. Three such cases have been chosen to compare with the results of the RAYPYR Monte Carlo methods:

Case 1. Radiation entering the aperture is isotropic. The reflector panels are perfectly diffuse with a reflectance $\rho_D = 0.9$.

Case 2. The entering radiation is isotropic and the reflectors are ideally specular ($\rho_S = 1.0$).

Case 3. The entering radiation is collimated and the reflectors are perfectly diffuse as in Case 1.

The average irradiation of the base plane, as calculated by both methods, is compared in Table 5-10. The agreement is satisfactory and confirms the validity of diffuse radiation calculation by RAYPYR. Table 5-10 also illustrates the ineffectiveness of isotropic diffuse reflectance as far as base plane (solar panel) illumination is concerned.

Table 5-10. Comparison of Concentrator Base Irradiation Calculations

Case No.	Incident Radiation	Panel Reflectance		Base Irradiation (suns)	
		ρ_D	ρ_S	RAYPYR	Radiosity Analysis
1	Diffuse	0.9	0.0	0.74	0.76
2	Diffuse	0.0	1.0	1.00	1.00
3	Collimated	0.9	0.0	1.45	1.45

5.4.4 Ray Trace Results for the Pyramidal Concentrator

Figure 5-24 illustrates typical ray trace histories. Shown in projection are the paths of rays which strike different regions of the concentrator. Those striking the base (region 1) directly undergo no reflections. Those striking the sides (region 2) have only one reflection, provided Equation 5-1 applies, as it does in the baseline concentrator design. Rays striking region 3 in the corner experience two reflections before reaching the base and rays striking region 4 undergo a several reflections before being reflected out the aperture without illuminating the base.

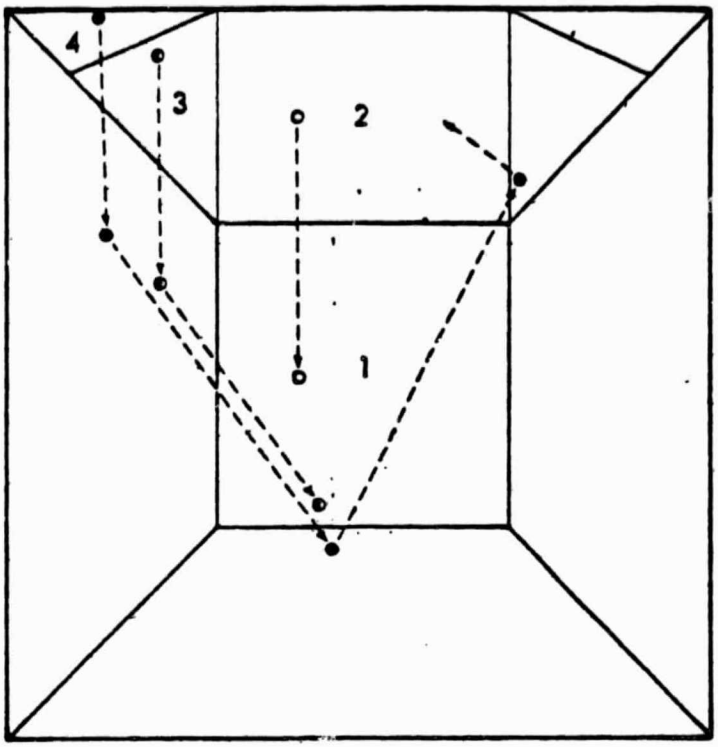

Figure 5-24. Typical Ray Trace Histories

Ray trace analysis of the GCR = 6 pyramidal concentrator gave optical efficiencies and detailed distributions of illumination for three reflector configurations for moderate pointing errors (0 to 5 degrees). The configurations include reflector designs with fully reflecting, non-reflecting and partially reflecting corners. Table 5-11 summarizes the results. They show that:

1. Penalties for off-axis pointing are rather small (3-4%) for angles up to 3 degeees.
2. Tilt orientation has only a slight effect on optical efficiency (see Figure 5-25).
3. Making the corner "gaps" transp. nt (that is, non-reflecting) reduces heat load on the reflector panels by a factor of three and makes panel illumination uniform (Figure 5-26), but at the cost of over 20% loss in optical efficiency.
4. Making the tips of the corners non-reflecting (Figure 5-27) substantially decreases reflector heat loads and increases the uniformity of illumination at only a modest cost (4%) in optical efficiency.

Table 5-11. Optical Performance of CR = 6 Concentrators

Configuration	Pointing Error (°)	Effective CR	Energy Distribution (percent)			
			Base	Reflectors	Gaps	Reflected out
Fully reflective corners	0	4.64	77.3	14.5	0.0	8.2
	1	4.62 4.63*	77.0 77.2	14.6 14.6	0.0 0.0	8.3 8.2
	3	4.49 4.47*	75.0 74.6	15.1 15.3	0.0 0.0	9.9 10.2
	5	4.37 4.29*	73.1 71.8	15.2 15.7	0.0 0.0	11.7 12.6
Nonreflective corners	0 1 3 5	3.61 3.59 3.47 3.36	60.2 59.9 57.9 56.2	4.8 5.0 5.5 5.8	35.0 35.0 35.0 35.0	0.0 0.1 1.6 2.9
Corner tips nonreflective	0 1 3 5	4.46 4.44 4.28 4.11	74.3 74.0 71.4 68.8	9.0 9.1 9.7 12.1	16.7 16.7 16.8 14.8	0.0 0.2 2.1 4.4

Note: *Values with asterisk represent tilt along diagonal. Others are for tilt parallel to sides.

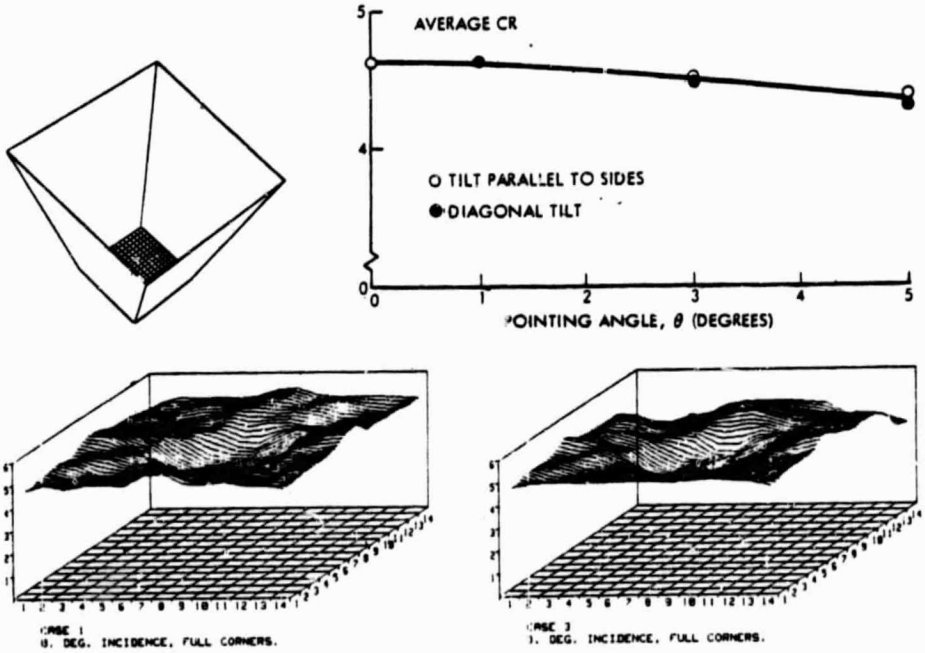

Figure 5-25. Optical Performance — Fully Reflecting Corners (Geometric CR = 6.0; Reflectivity 90%)

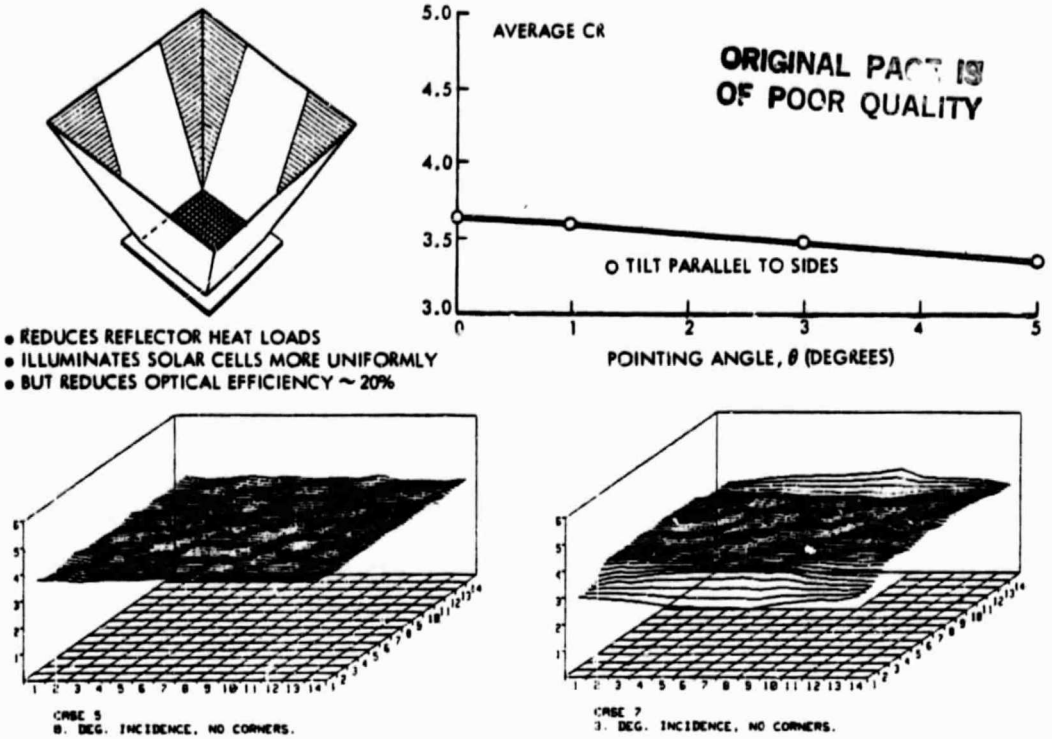

Figure 5-26. Optical Performance — Nonreflecting Corners
(Geometric CR = 6.0; Reflectivity 90%)

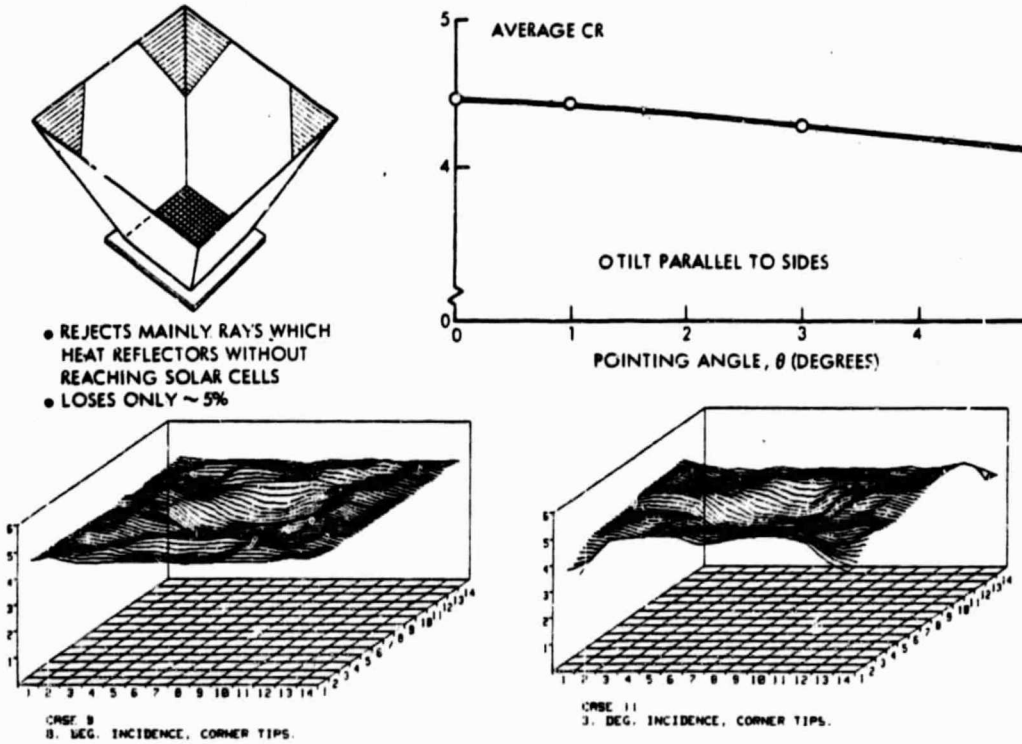

Figure 5-27. Optical Performance — Nonreflecting Corner Tips
(Geometric CR = 6.0; Reflectivity 90%)

It is interesting to note that optical performance of pyramidal concentrators falls slowly with pointing error, even up to 15 degrees (see Figure 5-28). Thus there is no catastrophic loss of power, even for large concentrator rotations.

5.5 ELECTRICAL ANALYSIS

The electrical design of the array requires consideration of the output characteristics of individual solar cells, their behavior in groups when interconnected into panels and electrical strings of panels, and the large-scale collection and distribution of power at the module and array level. Since compatibility with both silicon and gallium arsenide is a requirement, the final design embodies compromises brought about by the differing cell sizes and output characteristics of the two types.

5.5.1 Solar Cell Models

Analytical estimates of solar panel performance were needed well before final experimental data became available from the demonstration panels delivered by the subcontractors (ASEC and Spectrolab). Therefore mathematical models of silicon and GaAs cell characteristics were developed, based upon preliminary data from the subcontractors and the extensive JPL data on silicon cells given in Reference 17. In a later section, these cell models are compared with experimental data.

The models assume that over the range of interest the current-voltage characteristic of a cell is invariant with temperature and illumination when nondimensionalized with respect to short-circuit current and open-circuit voltage.

$$i/I = f(v/V) \tag{5-9}$$

The short-circuit current and open-circuit voltage are assumed to depend on temperature and illumination (over the range of conditions of interest) according to

$$I = [I_o + \alpha(T - T_o)] \cdot (L/L_o) \tag{5-10}$$

$$V = V_o - \beta(T - T_o) + \gamma \log_e (L/L_o) \tag{5-11}$$

Figure 5-29 summarizes the cell characteristics which have been used for detailed thermal electrical analysis of solar panel performance. The values have been updated from those used in the mid-term report [5] based upon the experimental results obtained in this program.

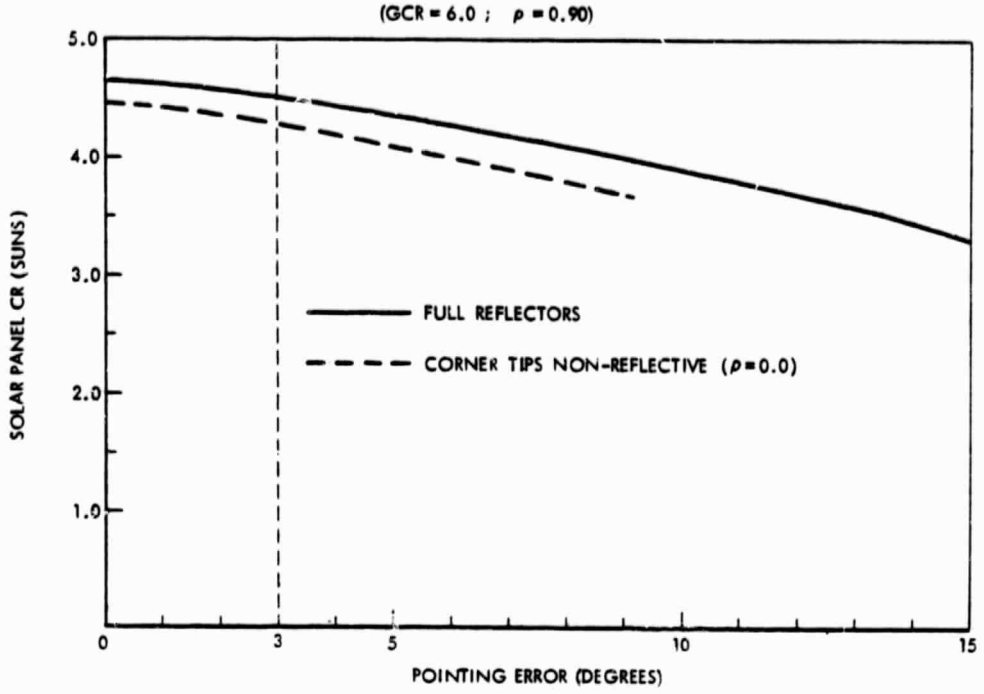

Figure 5-28. Ray-Tracing Results — Average Flux Incident on Solar Panel

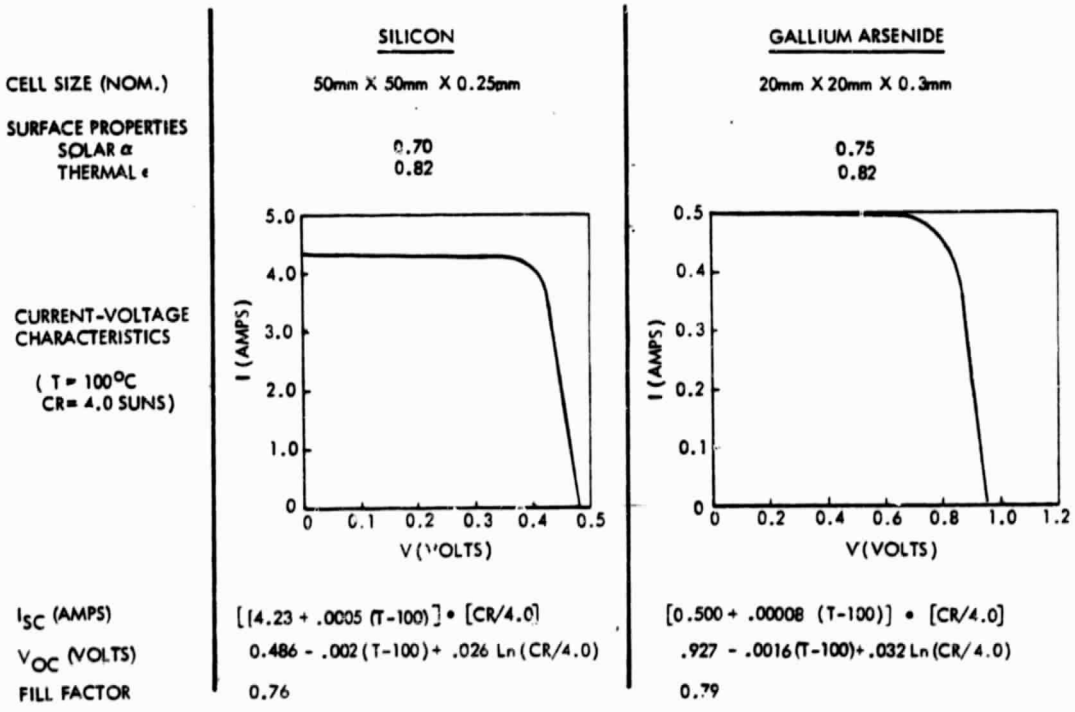

Figure 5-29. Solar Cell Characteristics and Performance Models (BOL)

5.5.2 Electrical Network Model

The cell performance equations apply to each cell in the panel but individual cell outputs and the output of the panel as a whole must conform to the constraints of the electrical network.

The individual solar cells in a panel are arranged in electrical configurations having m groups of n parallel cells connected in series. Typically, for a 10-cell by 10-cell panel, this might involve 20 groups of 5 parallel cells. Solar cell output current is a function of temperature, illumination and applied load. For the present work relatively simple analytical expressions have been selected but the approach is not dependent on a particular analytical approximation.

In the steady state the total current through each group of n parallel cells is the same and equal to the panel current, i_p. We define the function

$$F = \sum^{n} i - i_p \qquad (5\text{-}12)$$

which can be brought closer and closer to zero by successive applications of the Newton-Raphson process:

$$v_2 = v_1 - F(v_1)/F'(v_1) \qquad (5\text{-}13)$$

The function F and its derivative F' are evaluated from the local cell conditions by substitution from the performance equations above.

$$F(v) = \sum^{n} I\, f(v/V) - i_p \qquad (5\text{-}14)$$

$$F'(v) = \sum^{n} (I/V)\, f'(v/V) \qquad (5\text{-}15)$$

Panel voltage is obtained by summing the voltages across all groups of parallel cells.

5.5.3 Coupled Thermal-Electrical Analysis

Non-uniform illumination of the solar cell panel produces non-uniformity in the individual cell temperatures and in their electrical characteristics. Since the cells in a panel are interconnected electrically, it is not possible to operate each cell at its maximum power point and there is a consequent loss in output. This power loss is analogous to the "mismatch loss" found in a planar solar array made up of dissimilar cells.

The energy converted to electricity by the solar cells leaves the system in a form not considered by the thermal analyzer equations. In effect each cell has a heat sink equal to its power output. This output varies from cell to cell and depends upon the electrical load imposed on the panel as a whole, the panel electrical network, local illumination intensity and cell temperature. Thus thermal behavior of the solar cell panel is coupled to electrical behavior (Figure 5-30) and both must be evaluated simultaneously. This has been accomplished by means of logical instructions written into the variables block of the Rockwell thermal analyzer program.

Mismatch effects due to non-uniform illumination are very evident when all cells are connected in series. However, if groups of cells are connected in parallel across each half-panel, the losses are greatly reduced. Figure 5-31 illustrates this effect. The three curves show the ideal power output (uniform temperature and illumination) and actual output calculated for two electrical configurations. When all 36 cells (for this example) are connected in series the output curve shows a power loss of over ten percent. However, when groups of three adjacent cells are connected in parallel, the loss is reduced to about one percent.

Similar results have been obtained for other panel configurations consisting of 16 to 100 cells. In general, the use of parallel cell groups is quite effective in limiting performance losses due to non-uniform illumination. Figure 5-32 presents the distribution of illumination, cell temperature and cell power output for the 16-cell baseline silicon panel design at the peak-power operating point. Pairs of cells on each side of the hinge line are in parallel. The smoothing effect on cell output is evident.

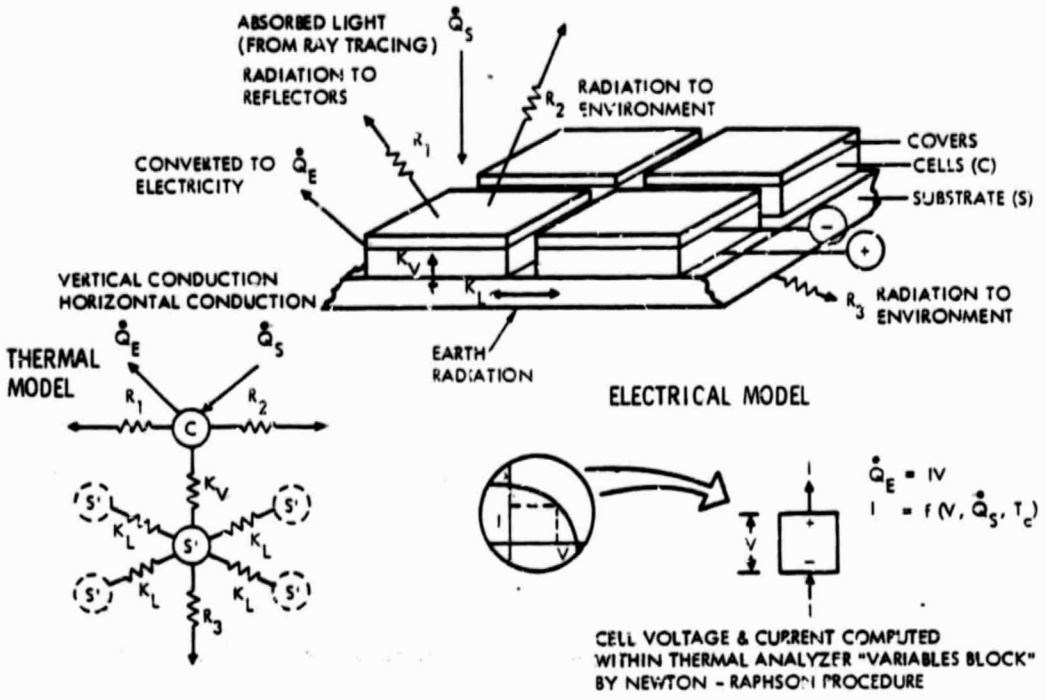

Figure 5-30. Coupled Thermal-Electric Math Model

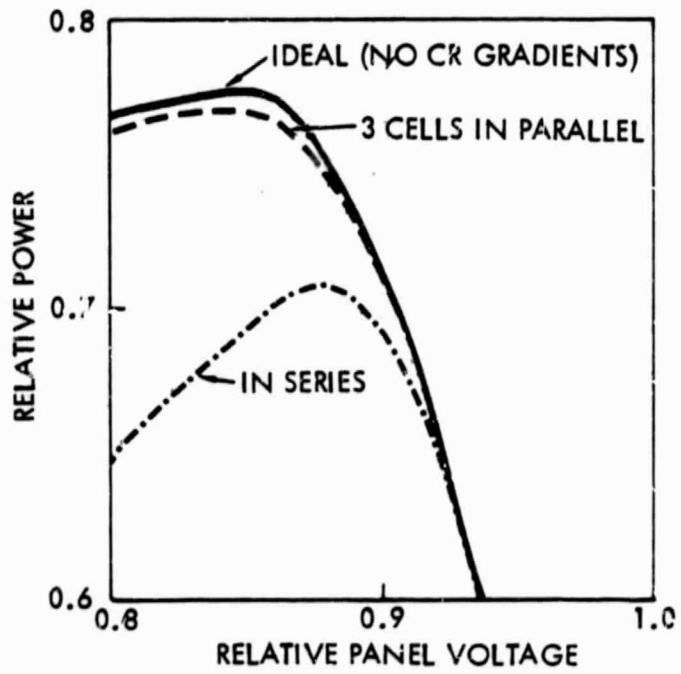

Figure 5-31. Effect of Panel Electrical Network on Output (36 Silicon Cells per Panel)

Cell Illumination
(Suns)

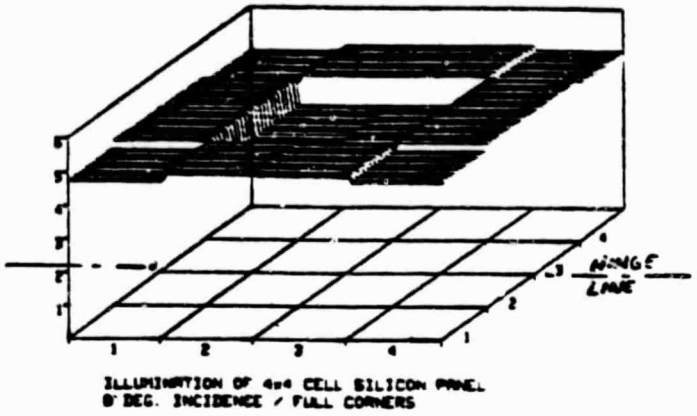

ILLUMINATION OF 4x4 CELL SILICON PANEL
0 DEG. INCIDENCE / FULL CORNERS

Cell Temperature
(C)

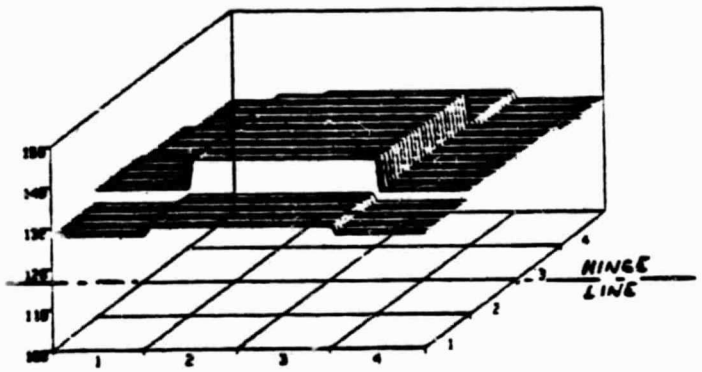

TEMPERATURE MAP (DEG. C) OF 4x4 CELL SILICON PANEL
0 DEG. INCIDENCE / FULL CORNERS

Cell Output
(watts)

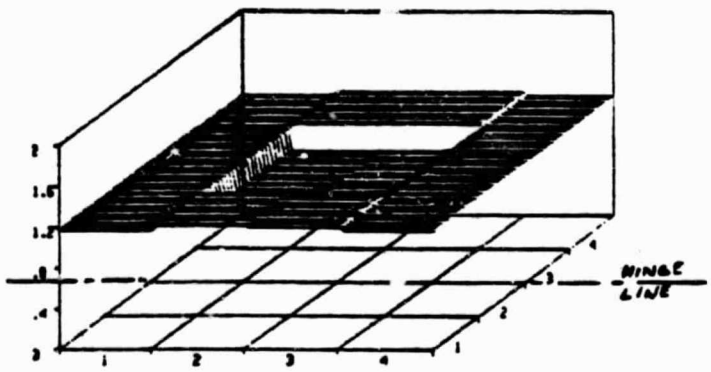

POWER DISTRIBUTION (WATTS) OF 4x4 CELL SILICON PANEL
0 DEG. INCIDENCE / FULL CORNERS

Figure 5-32. Cell Characteristics at Maximum Power
(Baseline Silicon Solar Panel)

5.5.4 Harness Optimization

A flat flexible cable was selected to interconnect individual concentrator elements within an electrical string. This type of cable also collects electrical power from all the strings and distributes it to the user attach fitting. The selection was based upon the need for flexibility and high packing density as well as the usual space design requirements such as low outgassing and environmental resistance. The variables which are important to the design of the cables are: physical configuration of the solar array, solar array system electrical characteristics, physical properties of the cable materials, and the cost estimating relationships (unit costs) of both the solar array and the harness. The contractual requirement which governs the design is to minimize the system recurring cost of power.

An optimum current density (J_H) in the electrical distribution system can be determined as a tradeoff of harness cost (C_H) and the cost of added concentrator capability (C_c) to compensate for harness losses while delivering constant power to a load. This statement embodies the cost optimization concept expressed in Equation 5-17, where C_T is total system cost, and A_H is the harness cross-sectional area:

$$\frac{dC_T}{dA_H} = \frac{dC_H}{dA_H} + \frac{dC_c}{dA_H} = 0 \qquad (5\text{-}17)$$

Two assumptions are made in deriving the expression in Equation 5-18, below. The first is that the harness material is available on a cost per square meter of surface area basis (not cross-sectional area) when purchased in the large quantities which would be needed to support this program. Not independent of this is the second assumption that the thickness of the metal laminate layer does not significantly affect the cost per square meter of harness surface area. This cost is assumed to be driven by the number of parts to be processed and the number of process steps per part and not the variation in time it takes to complete one of several steps involved (i.e., the etching of the metal circuitry). Hence, the cost optimized current density is given by:

$$J_H = \sqrt{\frac{1}{\rho t}\,\frac{C_H'}{C_c'}} \qquad (5\text{-}18)$$

where ρ is the bulk resistivity of the conductor, t is the selected thickness of the metal laminate layer, C_H' is cost per square meter of harness surface area, and C_c' is the cost per watt of electrical power.

Once a conductor current density is determined all other relevant harness characteristics are fixed. The previously mentioned variables such as configuration and electrical properties are known for the preliminary design. The parametric cost optimized characteristics are given below in Table 5-12. I_T is the total current to the load. V_c is the source output voltage before harness losses are incurred and m is the mass density of the conductors. The cost estimating relationships are discussed in Section 6.

The preceding optimization would differ if the system were to be optimized for minimum mass. The current density would then be given by:

$$J_H = \sqrt{\frac{m}{\rho}} P_c' \quad , \tag{5-19}$$

where P_c' is the specific power (watts/kg) of the array. All the other harness characteristics would follow.

The term $\bar{\ell}$ in the preceding expressions refers to the average length of harness over which power must be transmitted to reach the user attach fitting. For the Si design configuration shown in Figure 3-16 (Section 3.6), this is given by:

$$\bar{\ell} = 2.8(n-1)\left(\frac{Y}{n} + \frac{X}{N^2\sqrt{GCR}}\right) + 6.48\left(6 - \frac{6}{N} - \frac{42}{N^2}\right)\left(1 + \frac{1}{N}\right) \tag{5-20}$$

where X is the deployed length, Y is the extended length, n is the number of concentrators per string and p is the number of strings per array. For the Si harness layout chosen, $\bar{\ell}$ tends toward a value of approximately two times the minimum distance between the user attach fitting and the tip of the median concentrator element assembly.

The GaAs harness is slightly different due to the four electrical strings per row of deployed concentrator elements and is given by:

$$\bar{\ell} = 2.8(h-1)\left(\frac{Y}{n} + \frac{X}{N^2\sqrt{GCR}}\right) + 6.48\left(6 - \frac{6}{N} - \frac{42}{N^2}\right)\left(1 + \frac{1}{N}\right) + \frac{3Y}{4} \quad ,$$

where h is the number of concentrators per string.

Table 5-12. Harness Design Characteristics

Characteristic	Parametric Expression	Design		Units
		Si	GaAs	
Resistance	$R_H = \frac{\rho \bar{\ell}}{A_H} = \frac{\rho \bar{\ell} J_H}{I_T}$	0.016	0.005	ohm
Voltage drop	$V_H = I_T R_H = \rho \bar{\ell} J_H$	3.4	1.5	volt
Power loss	$P_H = I_T V_H = \rho \bar{\ell} J_H I_T$	1452	927	watt
Efficiency	$E_H = \frac{V_C - V_H}{V_C} = 1 - \frac{\rho \bar{\ell} J_H}{V_C}$	0.982	0.995	—
Mass per module	$M_H = (\text{volume})\ m = \bar{\ell} \frac{I_T}{J_H} m$	603	581	kilogram
Material cost per module	$C_H = (\text{surface})\ C_H' = \frac{\bar{\ell}}{t} \frac{I_T C_H'}{J_H}$	75.2K	72.5K	dollars
Effective length				
Si:	$\bar{\ell} = 2.8(n-1)\left(\frac{Y}{n} + \frac{X}{N^2\sqrt{GCR}}\right) + 6.48\left(6 - \frac{6}{N} - \frac{42}{N^2}\right)\left(1 + \frac{1}{N}\right)$	163	86.4	meter
GaAs:	$\bar{\ell} = 2.8(h-1)\left(\frac{Y}{n} + \frac{X}{N^2\sqrt{GCR}}\right) + \frac{3Y}{4} + 6.48\left(6 - \frac{6}{N} - \frac{42}{N^2}\right)\left(1 + \frac{1}{N}\right)$			

6.0 COST PROJECTIONS AND ARRAY PERFORMANCE

The design described in the preceding sections may be compared with other arrays on the basis of various figures of merit such as watts per square meter, watts per kilogram and dollars per watt. Evaluation of such parameters requires the estimation of size, weight, cost and net electrical output for a yet-to-be-built device. However, the present design has been developed in sufficient detail that good estimates of area (total and useful aperture) and mass are possible. The performance analysis methods developed have been shown to be capable of close estimates of electrical output. The greatest uncertainty lies in the prediction of cost.

Three kinds of costs are of interest: development costs; recurring costs; and life cycle costs. Because the present design is constrained to the use of near-term (1984) technology, the development costs are relatively low. Development costs and schedules are addressed in Section 8. Recurring costs and life cycle costs are treated in this section.

6.1 APPROACH TO RECURRING COST ESTIMATES

In a preceeding study of low-cost concentrating solar array concepts[1], Rockwell used a combination of two different approaches to arrive at recurring cost estimates for a variety of configurations. This same approach has been applied to the present design. For general structural components a mass algorithm was used to estimate cost from mass properties. For certain particular components, however, costs were estimated from supplier projections based on specific production details.

Parametric models based on mass have been applied to spacecraft as a whole, and to major subsystems separately. Many cost models in current use predict recurring costs for spacecraft and some subsystems reasonably well. They include cost factors usually neglected in conceptual studies and, therefore, reflect the "real world." In Reference 1, a mass algorithm was developed from a concensus of several such models.

$$C = 1{,}680{,}000\left(\frac{\text{Mass}}{454}\right)^{0.85} \qquad (6\text{-}1)$$

Cost (C) is in 1979 dollars; mass is in kilograms.

The array also contains major components for which better independent cost estimates can be made. The production costs for mast - canister assemblies are well-established and subcontractor estimates have been used. The reflector panels are required in large numbers of identical units, lending themselves to mass production. Thus reflector panel costs are based on large-volume production, considering the unit costs of material, molding process, and aluminization. Solar cell cost projections for both silicon and gallium arsenide are based upon projections made by the two solar cell subcontractors. Table 6-1 summarizes the projections for both types of solar panels.

6.2 COMPONENT WEIGHTS AND COSTS

The two approaches to recurring cost estimation have been combined to give an overall array module cost in the following way. Mass estimates are established for the various components and subsystems making up the module. They are obtained from the mass property evaluation in Section 5.2 and listed in the first two columns of Table 6-2. Cost estimates for canister-masts, reflector panels and solar panels (based on production methods and supplier projections) are entered in the cost columns of Table 6-2. The masses associated with these components are subtracted from the total module mass, leaving a residual mass (1204 kg) allocated to the remaining components not yet costed.

The mass algorithm is used to estimate costs for the remaining components. First, Equation 6-1 is applied to the residual mass to obtain a cost of $3,850,000 in 1979 dollars. An escalation factor of 25% is applied to arrive at a cost of $4,810,000 in 1982 dollars. Finally, the total cost is distributed among the individual components in Table 6-2 on a mass-proportional basis.

6.3 LIFE CYCLE COSTS (LCC)

Solar arrays are often compared on the basis of recurring cost of power, where the power is that at beginning of life (BOL) and the cost is simply the production cost of the array or module. In fact there are other factors, not related to hardware development, which influence the cost of power and the cost of energy over the lifetime of an array. These include: cost of transportation to orbit; cost of propulsion required to overcome drag; cost of on-orbit maintenance, if any; and performance (power) degradation over the array lifetime. All of these costs are mission-dependent.

Table 6-1. Solar Panel Cost Estimation — 1982 Dollars, 1984 Technology

	COST ESTIMATING RELATIONSHIP	SOLAR PANEL COST BREAKDOWN ($)
LOW CR SOLAR CELLS		
• SILICON		
• 50 mm BY 50 mm BY 0.25 mm CELL 0.20 mm TEXTURED QUARTZ / DC93-500 COVERING	$66 EACH[1.]	1056
• GALLIUM-ARSENIDE		
• 20 mm BY 20 mm BY 0.30 mm CELL 0.20 mm TEXTURED QUARTZ / DC93-500 COVERING	$48 EACH[2.]	4800
FABRICATION		
• ARRAY ASSEMBLY	$8000 / m^2	335
• RADIATOR	$1000 / m^2	125
SOLAR PANEL (TOTAL PER CONCENTRATOR ELEMENT)		
• SILICON (50 mm X 50 mm)		1056
• GALLIUM-ARSENIDE (20 mm X 20 mm)		4800

1. ASEC COST ESTIMATE FOR CELL & GLAZING PLUS OCLI COST ESTIMATE FOR COVER
2. SPECTROLAB, INC. COST ESTIMATE FOR CELLS & GLAZING PLUS OCLI COST ESTIMATE FOR COVER

Table 6-2. Weight and Cost Estimates for Si and GaAs Modules

Component or Subsystem	Mass (kg)		Cost (1982 $ M)	
	GaAs	Si	GaAs	Si
Cable extension mechanisms	156		0.62(a)	
Canisters and masts	630		1.15(b)	
Container end cap	50		0.20(a)	
Container housing and latches	227		0.91(a)	
Concentrator tensioners	55		0.22(a)	
Deployment actuators	5		0.02(a)	
Stowage tripwire mechanism	108		0.43(a)	
Electrical harness and insulation	581	603	2.32(a)	2.41(a)
Reflector panels (film-frame)	1102		0.31(c)	
Solar panels and radiators	1328		22.91(d)	6.60(e)
Totals	4242	4264	29.09	12.87

Notes: (a) Based on mass algorithm; costs apportioned by mass.
(b) Astro Research estimate.
(c) Materials and semi-automated processing.
(d) Spectrolab solar cell/glazing estimate.
(e) ASEC solar cell/glazing estimate.

6.3.1 Transportation Costs

Like the recurring cost, the cost of transporting an array into orbit must be born each time a new unit is put into service. Whether or not the array is the sole payload of a given flight, all or a portion of the flight costs are chargeable to the life cycle energy cost. Depending on the characteristics of the launch orbit, costs will be determined either by the stowed volume or stowed mass of the array.

Figures 6-1 and 6-2 present the payload capability of the Shuttle Orbiter as a function of orbital characteristics for both the Eastern and Western Test Ranges (ETR and WTR). The performance is based on high performance main engines (SSME's) and solid rockets (SRB's). Superimposed is the mass of four modules (17,000 kg), the maximum number which can be accommodated within the spatial limits of the payload bay. Two launch modes are displayed: standard ascent, in which orbital insertion is accomplished by the Orbital Maneuvering System (OMS) engines and direct insertion, in which orbital circularization is performed by the SSME's.

For launches in the standard ascent mode only low orbital altitudes can be achieved (300 km at WTR and 400 km at ETR). However, when the direct insertion mode is used, altitudes above 500 km can be reached at low inclinations. When orbital inclination is increased, the payload capacity becomes mass-limited rather than volume-limited. This is particularly true for ETR launches.

Transportation costs have been established as $30\overline{M}$ per launch in 1982 dollars. This represents an escalation to 1982 dollars, based upon a 1975 dollar cost of $18,000,000 for Civil U.S. Government usage[18]. Cost on a dollars/watt basis depends upon which type of solar cell is used and whether the mission orbit results in a volume- or mass-limited situation.

6.3.2 Cost of Aerodynamic Drag Makeup

Because of their large areas solar arrays contribute significantly to the drag of the spacecraft to which they are attached. At low altitudes this drag is significant and would produce a rapid decay of the spacecraft orbit if not compensated for by make-up thrust. In a prior study of low-earth-orbit operations[1] propellant requirements were calculated for 300 kW and 1000 kW

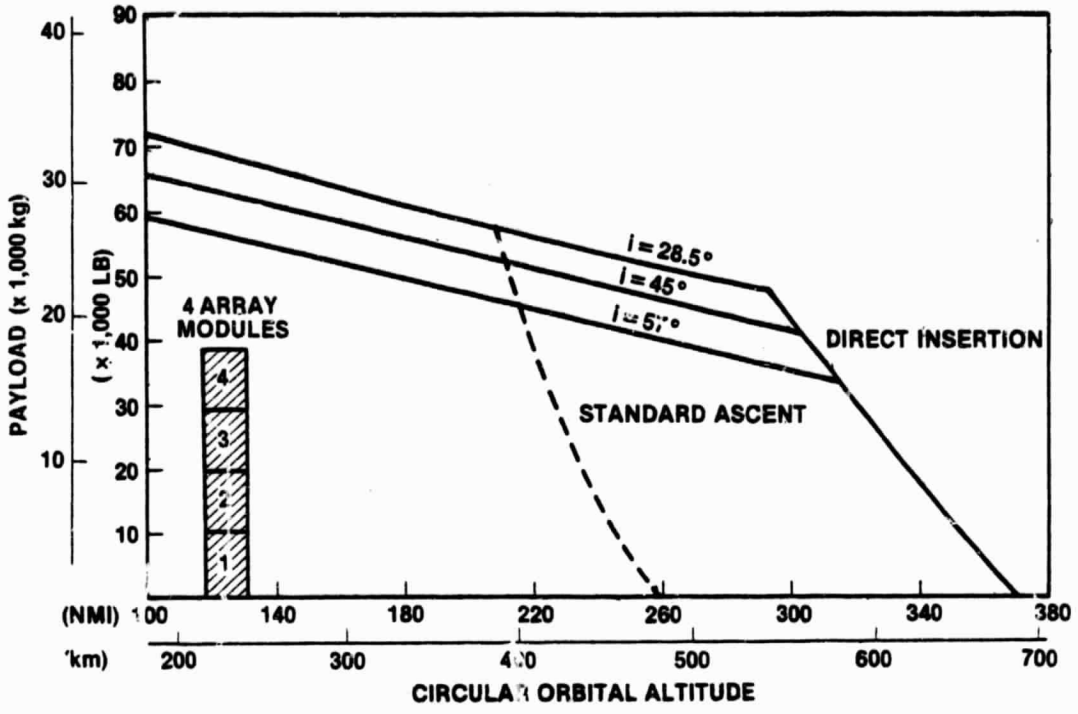

Figure 6-1. ETR Launch

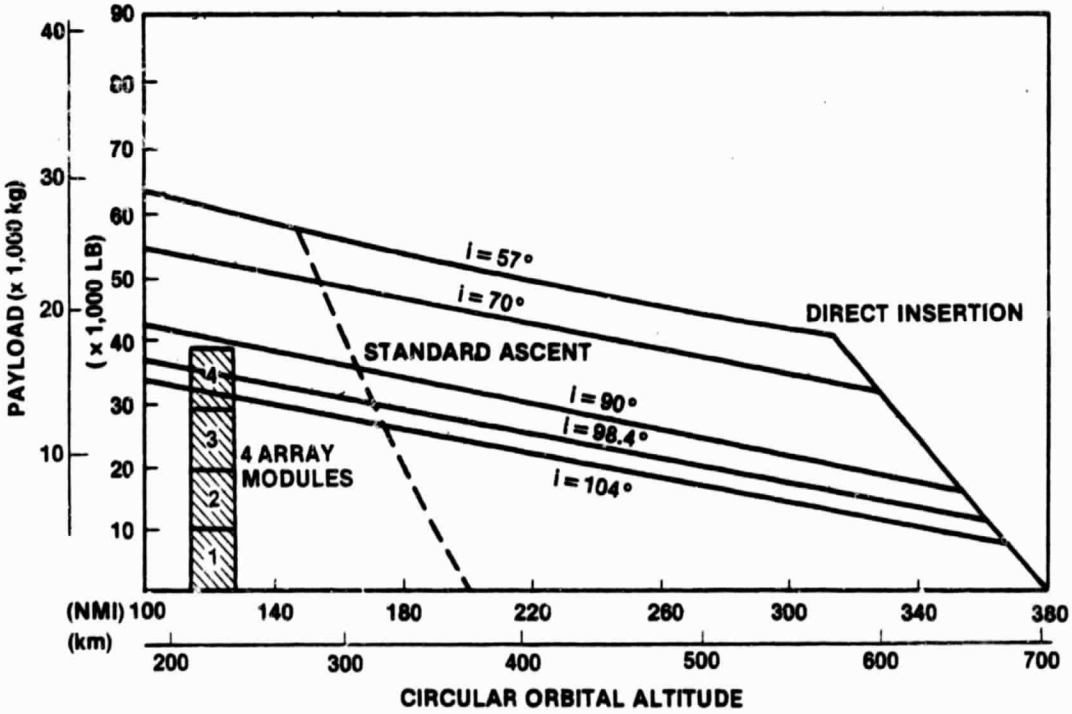

Figure 6-2. WTR Launch

solar arrays. These results have been scaled (drag proportional to area) for the present design and presented in Figure 6-3. The curves are based on the assumptions of nominal maximum solar activity (January 1990), constant solar pointing of the array and typical storable bi-propellant specific impulse.

From Figure 6-3 it can be seen that large amounts of propellant are required to maintain 300-km orbits (e.g., 10,000 kg per year). Thus, it appears best to operate such systems in LEO at about 500 to 600 km altitudes. At these altitudes, reasonable quantities of propellant can maintain the array in orbit for ten years or longer.

6.3.3 Other Cost Factors

In the previous contract[1] it was shown to be cost-ineffective to maintain a low cost solar array by modular replacement; that is, to replace individual modules when their output is reduced due to environmental radiation or the progressive failure of circuit components. It was found that the cost of an over-designed array, sized to deliver the required power at end of life (EOL) was much less than the costs of delivering and maintaining a smaller array sized on the basis of beginning of life (BOL) performance.

The present pyramidal concentrator array design has advantages over a planar SEP-type array in its resistance to output degradation due to radiation. Both the radiator-substrate and the reflector panels provide substantial radiation shielding. Table 6-3 summarizes the factors effecting radiation degradation for the two array types over a ten-year operating life. The SEP array has a thinner (0.15 mm versus 0.2 mm) coverslide and no reflector panels on the front surface. The relative shielding on the rear surface is even lighter due to the presence of a Kapton blanket rather than a 0.6 mm (Si) aluminum substrate. On the other hand the pyramidal array incurs a pointing error loss, which can occur throughout the array life, and a small reflector surface degradation which increases with time.

Figure 6-4 illustrates the relative total energy produced by the two array types when each is sized for the same BOL output. Over a ten year life, the pyramidal array will yield 13% more energy.

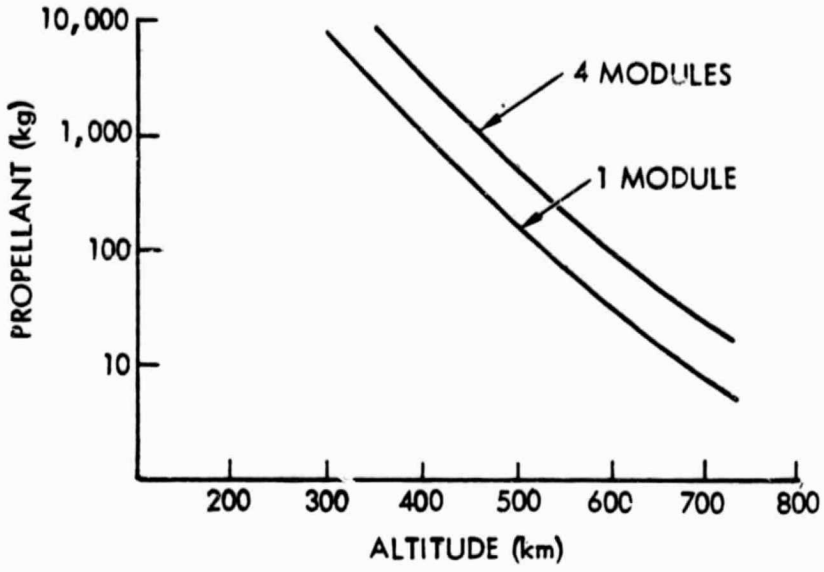

Figure 6-3. Annual Propellant Requirement

Table 6-3. Radiation Degradation Effects for Planar and Pyramidal Arrays (Silicon Designs)

	Planar Array (SEP Technology)	Pyramidal Array (Baseline Design)
Front Surface		
Shielding mass (g/cm^2)	0.039	0.160
10 year fluence (e/cm^2)	4.0×10^{14}	0.6×10^{14}
Rear Surface		
Shielding mass (g/cm^2)	0.021	0.203
10 year fluence (e/cm^2)	8.0×10^{14}	0.5×10^{14}
Power Losses (%)		
Optical degradation	—	3.0
Pointing error	—	5.0*
Solar cell	32.5	13.0
Total	32.5	21.0*

* May occur throughout array life.

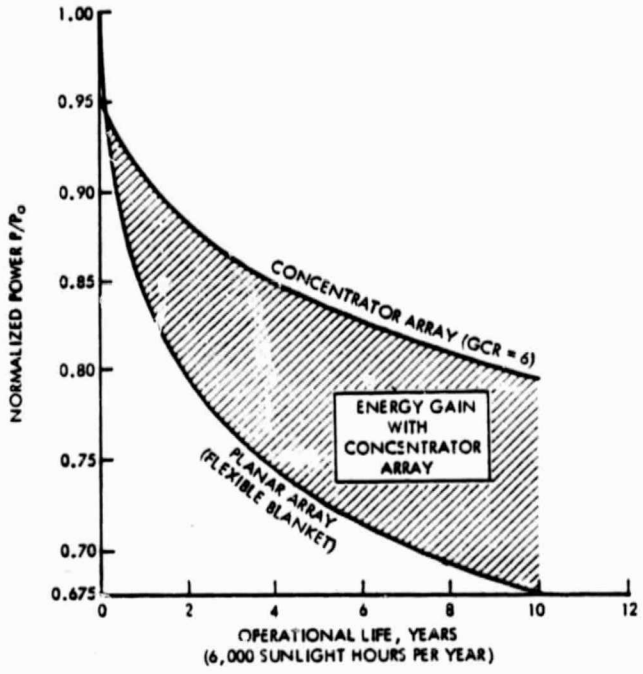

Figure 6-4. Life Cycle Energy Cost Analysis (Si Solar Cells)

6.3.4 LCC Comparisons

Life cycle costs will vary with array size, orbital inclination and altitude and mission duration. In order to illustrate the interplay of the various costs, a comparison has been made among three arrays: the planar SEP; the silicon concentrator and the gallium arsenide concentrator. Table 6-4 gives the appropriate characteristics of modules for all three.

Life cycle costs have been calculated for each of the above, according to the following assumptions:

1. Sufficient modules included to yield EOL output of comparable value for Si configuration (GaAs module provides 1.5 times Si modules).
2. 500 km circular orbit at 28.5° inclination.
3. 10 year (60,000 sunlight hours) mission life.

Table 6-5 summarizes the results. Due primarily to lower recurring costs, but also to smaller degradation losses, both concentrator arrays have life cycle energy costs much lower than state-of-the-art planar arrays.

Table 6-4. Module Characteristics

	Planar (SEP)	Pyramidal Concentrators	
		Si	GaAs
BOL Power (kW)	13	113	175
Mass (kg)	210	4264	4242
Stowed length (m)	1	3.24	3.24
Deployed areas (m^2)	135	1320	1320
Recurring cost ($\bar{M})	5.2	12.9	29.1

Table 6-5. Life Cycle Energy Cost Comparison

	Planar (SEP) Silicon (10 modules)	Pyramidal (Baseline)	
		Silicon (1 module)	GaAs (1 module)
BOL power (kW)	130	113	175
10 year EOL power (kW)	88	90	139
10 year energy (kWh)	5.6×10^6	5.74×10^6	8.89×10^6
Array mass (kg)	2100	4264	4242
Array stowed length (m)	10	3.24	3.24
Array area (m^2)	1350	1320	1320
Recurring cost ($\bar{M})	52	12.9	29.1
Transportation cost ($\bar{M})	23	7.5	7.5
Drag makeup cost ($\bar{M})	2.5	2.5	2.5
Total cost ($\bar{M})	77.5	22.9	39.1
Life cycle cost ($/kWh)	13.8	4.0	4.4

6.4 ARRAY MODULE PERFORMANCE

In Section 5 a detailed approach to concentrating array performance was described. The local distribution of concentrated sunlight over the solar panel was calculated by ray tracing. Local solar cell temperatures and their individual electrical contributions were calculated by a detailed mathematical model. Finally, individual concentrator power outputs were summed for a whole module, with allowances for the calculated power loss in the electrical harness.

Two versions of the detailed performance model were written, one for silicon solar panels and one for gallium arsenide. For each version, power output calculations were made for minimum and maximum earth radiation conditions. These correspond to array orientations at sunrise/sunset and at solar noon. The results indicate that the concentrating array output is quite insensitive to varying thermal radiation from the environment. Table 6-6 summarizes the results for the minimum earth radiation condition. They show that the higher conversion efficiency and lower temperature sensitivity of gallium arsenide cells results in a 55 percent performance advantage over silicon cells which helps to compensate for the higher cost of gallium arsenide.

Table 6-6. Performance Estimates for Si and GaAs Array Modules (4356 concentrator elements, 1320 m^2 deployed area)

Solar Cell Type	Mass (kg)	Cost ($M)	Power (kW BOL)	Watts/ m^2	Watts/ kg	$/ Watt
Gallium Arsenide (20 mm x 20 mm x 0.3 mm)	4242	29.1	175	133	41	166
Silicon (50 mm x 50 mm x 0.25 mm)	4264	12.9	113	85	27	114

The same detailed modeling could have been used to explore performance variations due to off-pointing and also to predict the performance during ground testing. This would have required substantial additional effort and is unnecessary to the objectives of the program. Instead the detailed results have been used to refine a simplified lumped-parameter performance model. This model, which was originally developed under the previous contract[1], has been extended to include factors which come into play during ground testing.

Solar cell operating temperature is obtained from the steady-state heat balance equation written for a unit area of the solar cell panel:

$$S(CR)\eta_{opt}(\alpha_c - f_\ell f_p \eta_c) + (I_e\varepsilon_2 + I_a\alpha_2)(1 + A_R/A_p) = h_a(T_c - T_a)[1 + 2\eta_R(A_R/A_p)]$$

$$+ [(F_c\varepsilon_c + \varepsilon_2) + (F_1\varepsilon_1 + \varepsilon_2)\ \eta_R(A_R/A_p)]\ \sigma T_c^4 \qquad (6\text{-}2)$$

The first term represents the product of the energy incident on the panel, $S(CR)\eta_{opt}$, and the fraction which must be dissipated as heat, $\alpha_c - f_\ell f_p \eta_c$. The second term represents the additional heat load from earth radiation absorbed on the rear surface of panel and radiator. As a simplifying approximation, the temperature gradient from front to rear surface of the panel is neglected.

Heat is dissipated by radiation from both front and rear surfaces of the panel and radiator. During ground testing, convection to the surrounding air is also an important heat loss mechanism. These processes are described by the second and first terms on the right hand side, respectively.

Solar cell conversion efficiency is assumed to have a linear dependence on cell temperatures

$$\eta_c = \eta_o - \psi(T-301) \qquad (6\text{-}3)$$

Simultaneous solution of Equations (6-2) and (6-3) yields an equilibrium value for the solar cell temperature and a corresponding value for the conversion efficiency. Array output per unit projected area becomes:

$$P/A = S\ \eta_{opt}\ f_\ell f_p f_A \eta_c \qquad (6\text{-}4)$$

where the three f-factors correct for miscellaneous array losses (cell mismatch, harness resistance, ultra-violet loss), cell packing factor, and concentrator effective area ratio, respectively.

Equations 6-2, 6-3 and 6-4 can be programmed on a hand calculator and will give rapid performance estimates for any desired range of parameters. The estimates are made realistic by using the detailed performance calculations previously described to obtain empirical values for the factors which may be uncertain. Table 6-7 lists these empirical factors.

Table 6-7. Lumped Parameters Derived from Detailed Solutions

Parameter	Nominal Value		Remarks
	Space	Ground Test	
η_{opt}	0.77	0.77	Varies with pointing
f_ℓ	0.92	0.96	No ultra-violet, harness losses for ground test
F_c	0.92	0.92	
F_1	0.36	0.80	No adjacent concentrators for ground test
η_R	0.59	0.71	Varies with $T_c^{3/2}$
h_a (W/m^2K)	0.	3.6	Varies with $(T_c-T_a)^{1/4}$

7.0 DEMONSTRATION COMPONENT FABRICATION AND TESTING

The prediction methods described in Section 5.0 provide considerable insight into the adequacy of the array design but analytical models do not necessarily account for all factors which might affect performance. In particular, reflector optical quality, concentrator dimensional accuracy, and solar cell variations are all difficult to characterize and incorporate into performance prediction methods. Similarly, kinematic behavior and fabrication feasibility are difficult to assess from drawings and design analysis alone. Therefore, component and subelement testing are required to demonstrate the optical, thermal and electrical performance of a full-scale concentrator under terrestrial conditions and provide more insight into the mechanical behavior of the design. Terrestrial performance can be compared to an analytical model of the terrestrial behavior in order to validate performance prediction methods.

7.1 TEST PLAN SUMMARY

All experimental activities performed under the contract are grouped under Task 2 and have been coordinated by means of a general test plan. There are three principal objectives: (1) to demonstrate the feasibility of the design concept; (2) to verify the methods used to predict array performance; and (3) to provide information for u late of the design. The way in which individual tests are related to each other and to the non-experimental tasks of the program is shown in the Test Plan Logic Chart (Figure 7-1). The plan is organized into seven sections as shown in Table 7-1. This breakdown covers all the topics originally discussed at the contract orientation briefing in August 1981 but is grouped somewhat differently to reflect a better understanding of the relationships among the experimental tasks. Individual tests are described in more detail in the following sections. The fabrication and test schedule is shown in Figure 7-2.

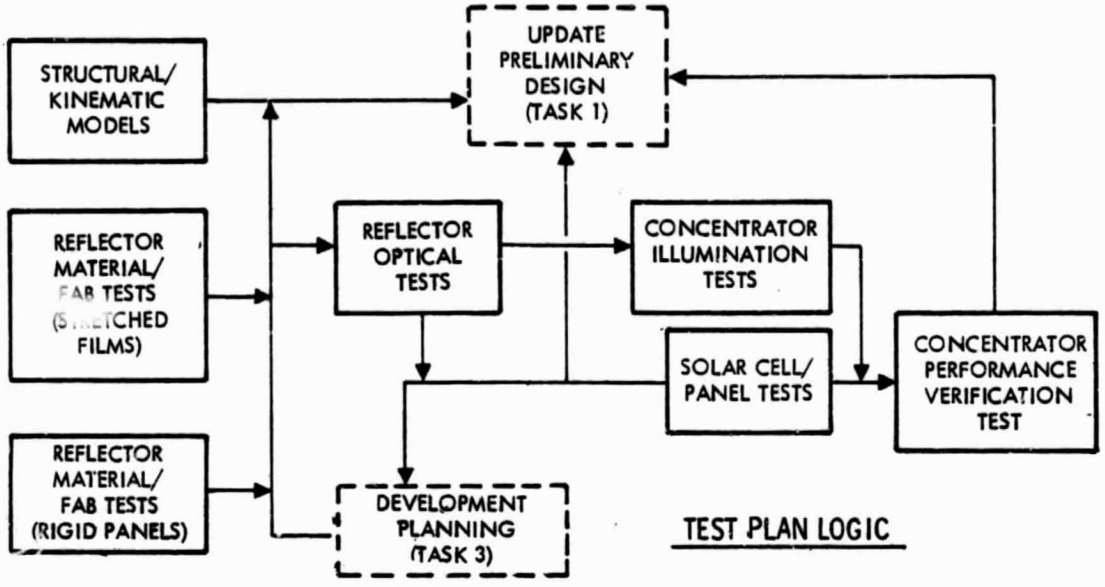

Figure 7-1. Test Plan Logic Chart

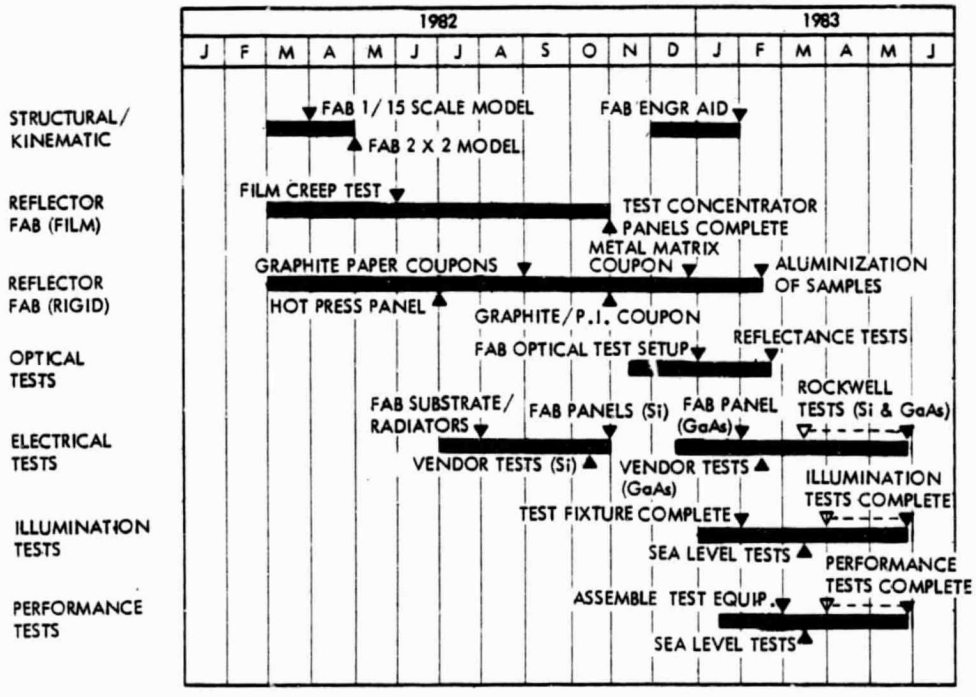

Figure 7-2. Fabrication and Test Schedule

Table 7-1. Sections of the General Test Plan

Section	Objectives	Principal Results
1. Structural/Kinematic Models	To visualize geometry; to demonstrate kinematics	Fabricated 1/15 scale simulator, 2x2 simulator and engineering aid.
2. Reflector Material/ Fabrication Tests (stretched films)	To evaluate materials and fabrication procedures; to produce demonstration panels	Fabricated functioning reflector panels successfully.
3. Reflector Material/ Fabrication Tests (rigid)	To evaluate materials and fabrication procedures	Fabricated test coupons; full scale panels not yet satisfactory.
4. Reflector Optical Tests	To provide data on panel reflectivity and specularity	Experimental determination of specular and diffuse reflectance.
5. Solar Cell/Panel Tests	To determine basic electrical, mechanical and thermal characteristics of cells and panels.	Measured panel and cell I-V characteristics; effects of CR and temperature.
6. Concentrator Illumination Tests	To determine illumination patterns during ground test operations	Measured CR distributions for range of pointing angles and geometrical distortions.
7. Concentrator Performance Verification Test	To verify overall concentrator performance under ground test conditions	Measured string and panel power outputs for range of pointing angles and distortions.

7.2 EXPERIMENTAL HARDWARE

The experimental hardware required to carry out the tests represented in Table 7-1 is a significant design effort by itself. The drawings which have been prepared are listed in the drawing tree depicted in Figure 3-2 and provided in Volume 2.

The drawings listed are of several types. Some, like those for the model simulators and the solar panels, provide guides and instructions for subcontractors. Others represent Rockwell-fabricated components and test assemblies. In general every effort was made to preserve a close similarity between test hardware and the flight hardware design. In some cases, the requirements of immediate availability necessitated substitutions but in no case do these result in significant discrepancies. Table 7-2 summarizes the differences between the full-scale test concentrator and the flight design.

Table 7-2. Flight Design Characteristics Compared with Test Concentrator Element

Item	Flight Design	Test Concentrator
Substrate/ Radiator	0.5/0.6 mm aluminum No connector bracket	0.8 mm aluminum Connector bracket
Hinges	Molded plastic, fixed and removable brackets	Bonded steel pins, removable brackets
Silicon Half-Panel	50 mm x 50 mm x 0.25 mm cell (14%)	20 mm x 20 mm x 0.25 mm x 0.3 mm cell (12.5%)
GaAs Half-Panel	20 mm x 20 mm x 0.3 mm cell (18%)	20 mm x 20 mm x 0.3 mm cell (16.1%)
Interconnects	Welded silvermesh	Soldered silvermesh (Si) Soldered Kovar Solaflex (GaAs)
Diodes	Series parallel redundant	Parallel redundant

7.3 STRUCTURAL AND DYNAMIC MODELS

A series of models were designed and fabricated as aids to understanding the geometric and kinematic features of the array design.

7.3.1 1/15 Scale Deployment Simulator

The 1/15 scale deployment simulator model demonstrates the deployment scenario, namely single-axis deployment, with dual extension. Figure 7-3 shows the simulator photographed in conjunction with a scale model of the Shuttle orbiter. The model consists of six container sections and provides a means of visualizing the relative positions of module components such as canisters, attachments, and hinge lines during various stages of deployment. It will also be useful in the design of integration hardware components for attaching the module to the Shuttle payload bay or a user spacecraft.

The 1/15 Scale Deployment Simulator was fabricated from drawing No. D416-340020 (Volume 2) by subcontractor (Penwall Industries).

7.3.2 2x2 Dynamic (Functional) Simulator

The 2x2 dynamic model is designed to illustrate the motion of complex interfaces and to help identify potential problem areas. The model also suggests realistic volumetric ratios and aids in the demonstration of the full-scale extension-retraction scenario.

Figure 7-4 shows intermediate stages in the dynamic simulator, which represents a two-element by two-element segment of the full scale array. Only the cable support system, end cap attachment and folding concentrator reflector panels are simulated in this model. The surface representing solar panels are non-functional and end cap extension is activated by means of a hand-driven screw instead of an astromast.

The simulator is designed to demonstrate the kinematics of extension and retraction for side-by-side concentrator elements under the action of end cap motion. The end caps and masts are made from expanded polyvinyl chloride (PVC) sheets 3.2 mm (1/8 inch) thick. Reflector frames are also 3.2 mm PVC covered with aluminized mylar to make reflector surfaces. The substrate/radiators are made from 0.63 mm (25 mil) aluminum sheet on which are bonded 0.76 mm (30-mil) aluminum panels to simulate the thickness of the

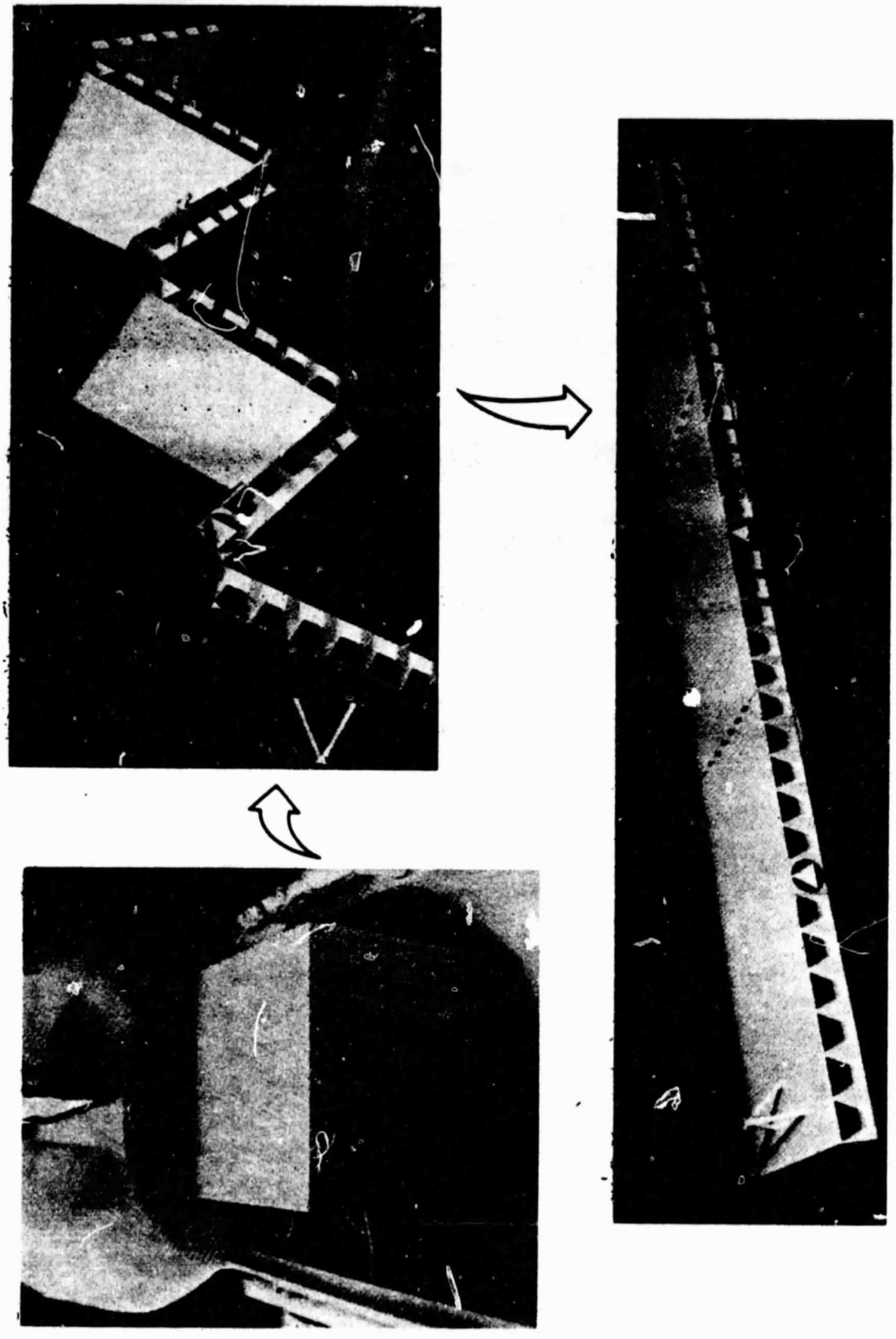

Figure 7-3. Articulated Model Deploying from Stowed Position

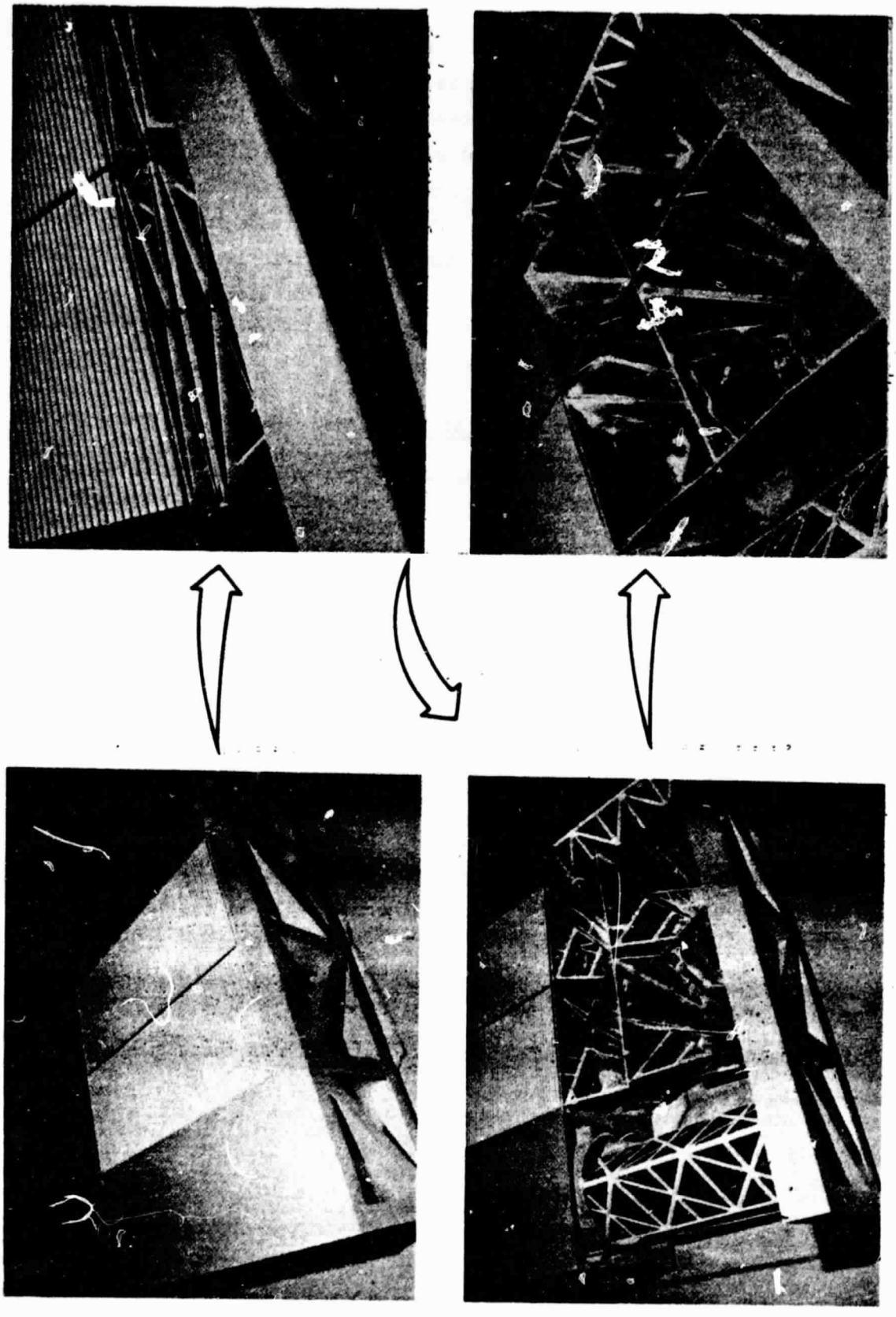

Figure 7-4. Four Element Model Undergoing Extension

the solar cell stack. The model housing is made from 9.5 mm (3/8 inch) plywood with PVC sheets representing stacked concentrator elements. There are three support cables made of (3.2 mm) plastic-coated stainless steel attached to negators within the housing. Mast extension is simulated by means of a 25.4 mm (one-inch) diameter screw jack (8 threads to the inch) which extends and retracts the end cap. Monofiliment trip lines actuated by dead weights are used to retract individual concentrator elements.

The functional 4 element simulator was fabricated from drawing No. D416-3[illegible]0010 (Volume 2) by subcontractor (Penwall).

7.3.3 Concentrator Element Engineering Aid

The concentrator element engineering aid (Figure 7-5) uses flight-weight materials and flight-type hinges throughout. Its primary purpose is to demonstrate the kinematics of an individual concentrator element as it moves from folded to open position. The engineering aid was also used for a zero-g torsion spring test to identify the force required to open the radiator half-panels and the force required to restore the panels using the radiator trip wire mechanism. The Concentrator Element Engineering Aid was assembled at Rockwell per drawing No. D416-450001 (Volume 2).

The spring tests of the Concentrator Element Engineering Aid employ a calibrated spring scale attached to the radiator half-panel hinge in order to measure the force required to over-center the hinge and stow the radiator panel. A rectangular frame fixture supports and contains the concentrator under test. The Engineering Aid was mounted horizontally in the test fixture and one full reflector panel was clamped while the other allowed to slide. The spring scale attached to the half-panels first measured the force required to fold the panel without torsion springs. The torsion springs were then installed into the concentrator elements to test the spring operation.

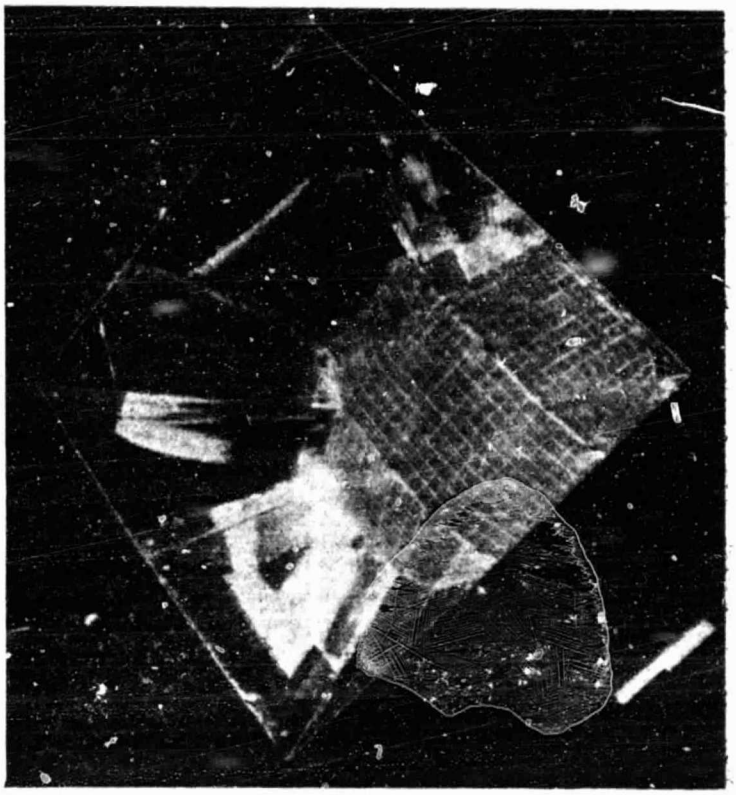

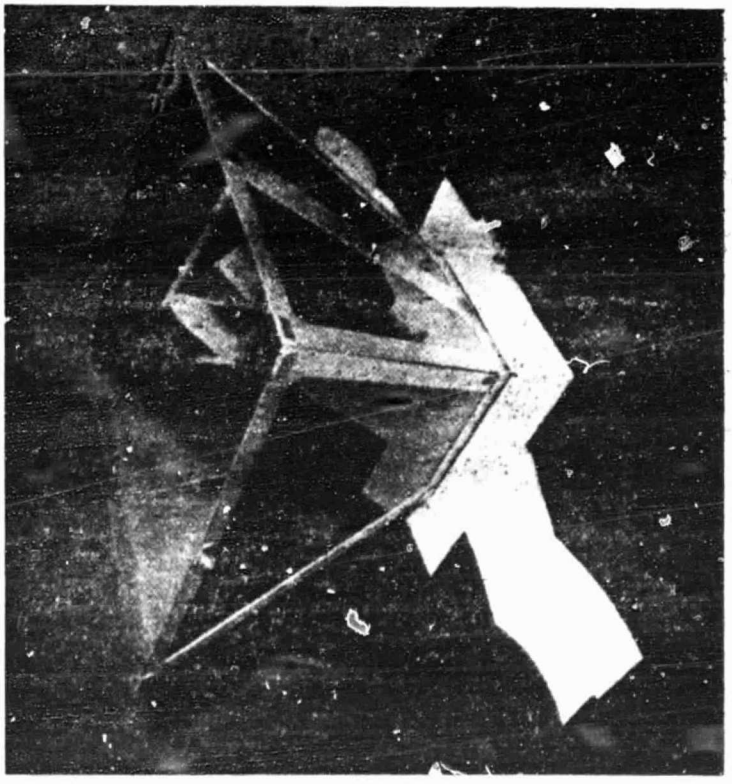

Figure 7-5. Engineering Aid

7.4 REFLECTOR MATERIAL AND FABRICATION TESTS

This series of tests consisted of shop and laboratory investigations of candidate materials and processes which could be used for reflector panels. In general, the tests sought answers where there was insufficient design information to insure trouble-free fabrication. It was not expected that all technology questions could be answered within the scope of the present program. For a particular application, some issues require further development or test verification prior to application in a full-scale array. These issues are identified and discussed below and in Section 8.2. The overall objectives of this series were:

- To demonstrate the feasibility of reflector panel designs.
- To test several material/fabrication options for suitability.
- To fabricate a set of reflector panels for use in the illumination and concentrator performance tests.

Two basic approaches were adopted, namely the stretched-film approach in which aluminized Kapton film was stretched and bonded to a rigid frame and the rigid-panel approach in which an aluminum coating was vapor-deposited onto the smooth surface of a solid sheet.

The test plan originally formulated for this portion of the work called for parallel experimental operations on both types of reflectors, starting with the fabrication of small samples (coupons) and proceeding through the construction of full-scale panels to a complete concentrator element. At each stage optical and structural evaluation was to be performed in order to select the best candidates for succeeding operations. This procedure was carried out successfully for the stretched-film candidates and has resulted in a satisfactory set of reflector panels which have been incorporated into the full-scale demonstration concentrator element. No completely satisfactory rigid panel was produced, however. Candidate configurations and experimental results are summarized in the following subsections.

7.4.1 Stretched Film Panel Development

Three panel configurations using the stretched-film approach were fabricated and evaluated in the Advanced Manufacturing Laboratory located in the Rockwell Downey Complex, where the necessary molds, ovens and machine tools were available. Table 7-3 summarizes the experimental operations performed.

Table 7-3. Stretched Film Panel Configurations and Test Approach

Configuration	Approach
Aluminized Kapton film on a polysulfone-graphite frame 0.05 mm film 3.2 mm frame	Mold polysulfone-graphite sheet, machine into frames, epoxy bond film to frame, cure at room temperature
Aluminized Kapton film on an aluminum frame 0.05 mm film 1.5 mm frame	Machine aluminum sheet stock into frames, bond film as above
Aluminized Kapton film on a graphite-polyimide frame 0.05 mm film 1.5 mm frame	Layup and cure a balanced sheet of graphite-polyimide, machine into frame, bond film as above

The stretched-film concept produced favorable results. All stretched-film configurations produced acceptable reflector panels from a mechanical standpoint. The panels survived temperature excursions up to 150°C and remained taut at room temperature for times in excess of 12 months. Selected panels and coupons were optically tested as described in Section 7.5.

7.4.2 Kapton Film Creep Test

Because of the relatively high service temperatures reached by reflector panels, a creep test was carried out on specimens of uncoated Kapton film, 25.4 mm (one inch) wide, 0.013 mm thick with a 254 mm (10 inch) free length.

The test consisted of month-long exposures of strip specimens at constant load, carried out both at room temperature and at 150°C. Specimens were supported vertically on test racks by horizontal clamps at the upper end. The specimens were loaded by dead weights clamped horizontally to their lower ends. Sample test conditions are listed in Table 7-4.

Elongation was obtained by determining the difference in height of scribe marks placed on upper (fixed) and lower specimen clamps, measured at the time specimens are first loaded and periodically during the month-long test period. For specimens exposed to elevated temperature, racks were removed from the oven and allowed to cool to room temperature prior to each elongation measurement.

Table 7-4. Film Creep Test Conditions

Temperature (°C)	Specimen Thickness		Specimen Load		Stress	
	(μm)	(in.)	(n)	(lb)	Pa x 10^{-6}	psi
23	13	0.0005	0.44	0.1	1.38	200
			1.33	0.3	4.14	600
			2.22	0.5	6.90	1000
	51	0.0020	0.44	0.1	0.34	50
			1.33	0.3	1.03	150
			2.22	0.5	1.72	250
150	13	0.0005	0.44	0.1	1.38	200
			1.33	0.3	4.14	600
			2.22	0.5	6.90	1000
	51	0.0020	0.44	0.1	0.34	50
			1.33	0.3	1.03	150
			2.22	0.5	1.72	250

The results of the film creep test were not conclusive. A number (but not all) of the samples failed at stress levels between 4.1 and 6.9 x 10^6 Pa (600 to 1000 psi). These failures were not preceded by significant elongation, however, and are thought to be due to notches or imperfections in the hand-trimmed edges of the samples rather than to creep. Although elongations of the order of one percent or less were observed in the surviving samples, any clearcut progression with time was obscured by small, apparently random changes. This is believed to be due to the necessity for making all measurements at room temperature.

One fact is clear. Large amounts of film creep were not observed over the one-month test period at stress levels up to 6.9 x 10^6 Pa (1000 psi) for temperatures up to 150°C. This, together with the fact that all stretched film panels which have been fabricated have remained taut for a period in excess of 12 months indicates that film creep will not be a problem.

7.4.3 Rigid Panel Development

A total of six rigid-panel concepts were evaluated as possible reflector candidates. Table 7-5 summarizes the configurations. It was recognized that all these rigid panel concepts would require significant development of both

Table 7-5. Rigid Panel Configurations and Test Approach

Configuration	Approach
Graphite paper/epoxy coupon*	Layup and cure graphite paper/epoxy on a glass plate. Vapor deposit aluminum onto smooth surface (∿ 500 Å coating)
Molded polysulfone-graphite panel	Hot press polysulfone-graphite pellets in a mold, trim blank
Aluminized Kapton-graphite paper/epoxy laminate panel	Laminate aluminized Kapton film to each side of graphite paper/epoxy, press and cure
Graphite/polyimide laminate coupon	Balanced ply layup on a glass plate, autoclave cure
Metal matrix (silicon carbide in aluminum) coupon*	Trim sheet and vapor deposit aluminum on one side (∿ 500 Å coating)
Mirrored (aluminized) polycarbonate coupon*	Trim off-the-shelf sheets

* These samples used for optical tests.

tooling and processing before any of these could be considered for production This program was intended only to establish feasibility of solid reflector fabrication and to identify the technology development activities necessary for proof of concept.

In an effort to obtain a general understanding of the potential of the candidates for the solid reflector concepts and obtain an estimate of possible performances, it was decided to produce sample hardware at minimum cost. Coupon-sized materials were either obtained as coarse finished samples intended for some other function or were produced with less than adequate tooling and minimal to no process development. The unpolished metal matrix configuration and the epoxy/graphite paper samples, both promising candidates for economical high production manufacture, were sent to an outside vendor for the application of a aluminum mirrored surface with an overcoat of silicon monoxide both put on by vapor deposition. The results of this one trial coating, because of the above discussed processing and tooling deficiencies, resulted in a non optimum mirror surface. Since development improvements

were not part of the contract effort, no further development attempts were made. The samples were optically tested and could not compare with the results obtained from the stretched film specimens. However, with proper surface preparation and additional tooling development, these two concepts are certainly viable and can be made to rival the stretched film concepts in terms of performance and be far superior in terms of economics for large scale manufacturer and durability.

As a result, it is recommended that technology programs be separately funded to exploit these candidate solid reflector developments in the comprehensive manner these require.

7.5 REFLECTOR OPTICAL TESTS

Optical tests were carried out on reflector panels and coupons in the Optical Laboratory at the Seal Beach facility to evaluate the diffuse and specular reflectances of coupons and complete reflector panel surfaces and to demonstrate the adequacy of surface finishes. A low-powered (2 mW) helium-neon laser (λ = 0.6328 μm) was used as a light source. Reflectance measurements were made using a 178 mm (seven inch) diameter integrating sphere with an internally mounted silicon photodiode detector. The experimental set-up is shown in Figure 7-6.

Panels and coupons were reflectance-tested in representative areas over the whole sample. In each test area both total reflectance (ρ_t) and non-specular (ρ_{ns}) reflectance were measured. Specular reflectance (ρ_s) values were obtained from measurements of total and non-specular reflectance:

$$\rho_s = \rho_t - \rho_{ns} \qquad (7\text{-}1)$$

Non-specular (diffuse) reflectance measurements were made with the laser beam passing through the integrating sphere and incident normal to the test surface at the exit aperture of the sphere (see Figure 7-7). Under these conditions, the specularly reflected compponent will exit the sphere along the path of the incident beam, and the non-specular component is collected by the sphere and measured by the sensor. The total reflectance measurement is made by tilting the test surface slightly to collect both the specular and the non-specular reflectance components within the sphere.

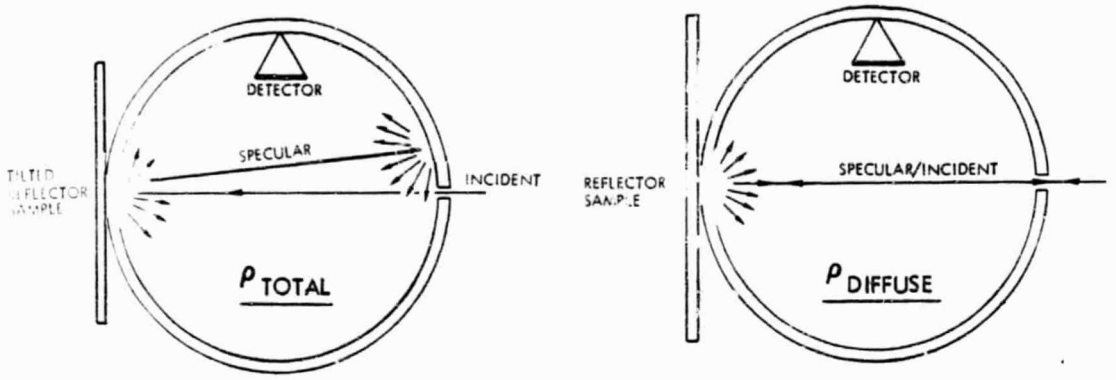

Figure 7-7. Optical Test Geometry

Optical test results are summarized in Figure 7-8. All of the full-scale, stretched-film panels had high specular reflectance (∿ 90%) and very low diffuse reflectance. The same was true of the aluminized Kapton coupon. Of the rigid-panel test coupons only the aluminized epoxy graphite paper had high specular reflectance and it was slightly lower than that for the aluminized films.

7.6 SOLAR CELL AND PANEL TESTS

7.6.1 Test Objectives

The primary objective of these tests is to establish the photovoltaic characteristics of the demonstration solar panels under controlled laboratory conditions. These conditions include elevated temperature and concentrated illumination which more nearly approximates the operating parameters during full-scale demonstration testing.

A second important objective is to measure cell parameters (short circuit current, open circuit voltage and I-V curve shape) as a function of temperature and illumination in order to update the cell models used for performance prediction.

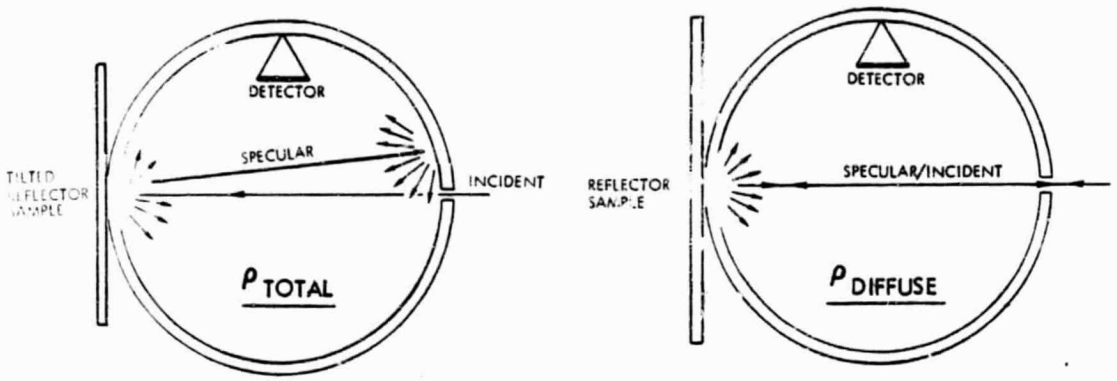

Figure 7-7. Optical Test Geometry

Optical test results are summarized in Figure 7-8. All of the full-scale, stretched-film panels had high specular reflectance (~ 90%) and very low diffuse reflectance. The same was true of the aluminized Kapton coupon. Of the rigid-panel test coupons only the aluminized epoxy graphite paper had high specular reflectance and it was slightly lower than that for the aluminized films.

7.6 SOLAR CELL AND PANEL TESTS

7.6.1 Test Objectives

The primary objective of these tests is to establish the photovoltaic characteristics of the demonstration solar panels under controlled laboratory conditions. These conditions include elevated temperature and concentrated illumination which more nearly approximates the operating parameters during full-scale demonstration testing.

A second important objective is to measure cell parameters (short circuit current, open circuit voltage and I-V curve shape) as a function of temperature and illumination in order to update the cell models used for performance prediction.

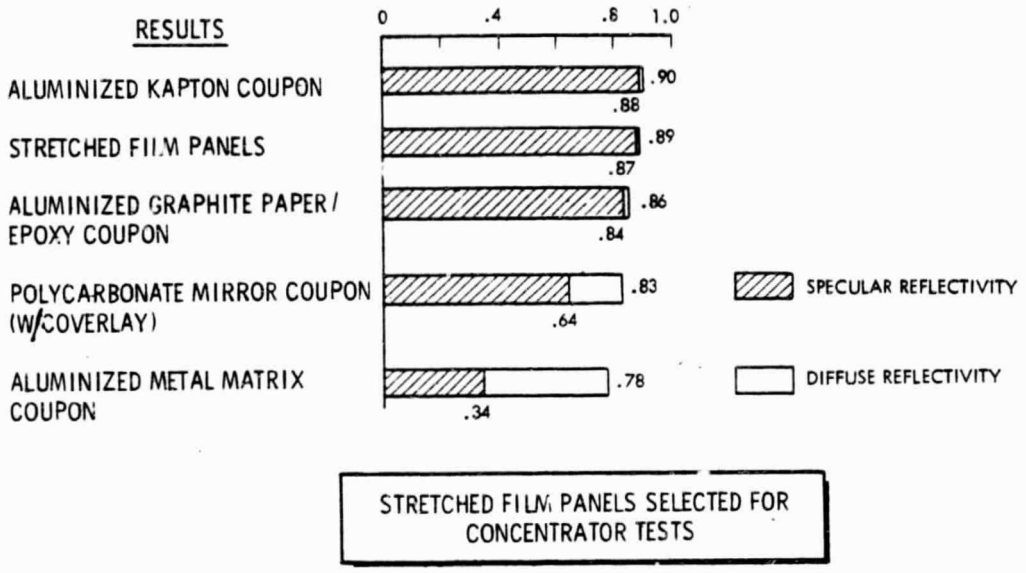

Figure 7-8. Optical Test Results

A third objective of the tests is to identify areas requiring design update or which indicate a technology deficiency.

7.6.2 Cell and Panel Fabrication

All solar cell panels used in this program were fabricated by subcontractors on Rockwell-supplied aluminum substrate-radiators. Applied Solar Energy Corporation (ASEC) fabricated and delivered two mechanically interchangeable silicon half-panels consisting of 50 cells each. In addition ASEC supplied 10 individual cells, each provided with electrical contacts. Spectrolab, Inc. fabricated one gallium-arsenide half-panel from cells produced at Hughes Research Labs. In addition, they supplied 10 individual cells with contacts. 20 mm x 20 mm cell sizes for both Si and GaAs were used to provide comparative performance data.

Both types of half-panel have the same electrical configuration, shown in Figure 7-9. Each half-panel contains one electrical string of 20 and one of 30 cells, as shown. Each string has redundant input terminals including isolation diodes. Each string is provided with a bypass diode. The silicon half-panels are configured differently in that one has a 20-cell string next to the hinge line whereas the other has the 20-cell string along the outer edge. Figure 7-10 contains pictures of the actual test panels. Tables 7-6 and 7-7 provide further information about the individual cells and the half-panels, respectively.

Every effort was made to procure solar cells and panels which matched, as closely as possible, the flight design. However some compromises were necessary. In some cases, cell properties which could be confidently expected within 1984 technology were not obtainable in time for use in the present program and substitutes with nearly similar characteristics were employed. Another basis for compromise was the practical constraints associated with fabricating only a single unit. Materials and processes suitable for production runs of thousands of units were sometimes replaced by their

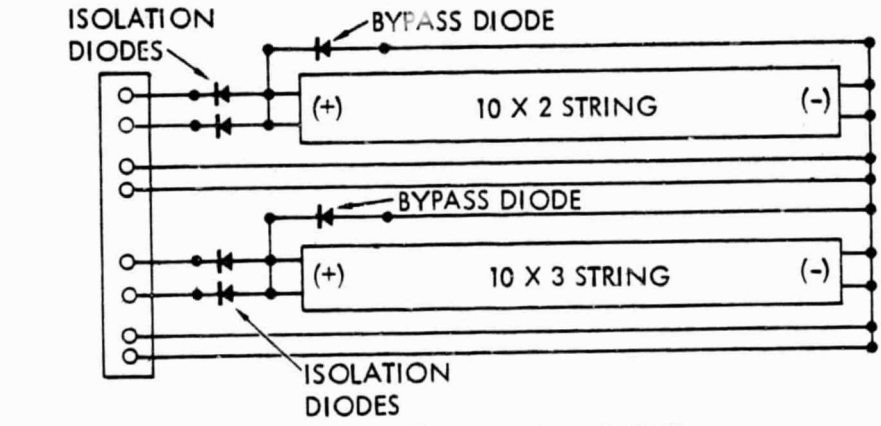

TYPICAL HALF-PANEL

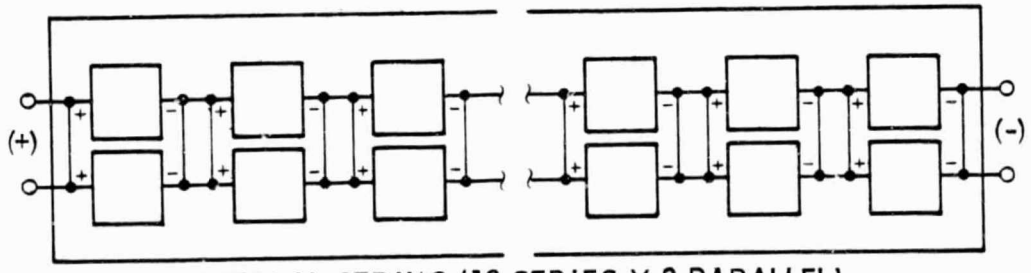

TYPICAL STRING (10 SERIES X 2 PARALLEL)

Figure 7-9. Solar Cell Panel Electrical Configuration

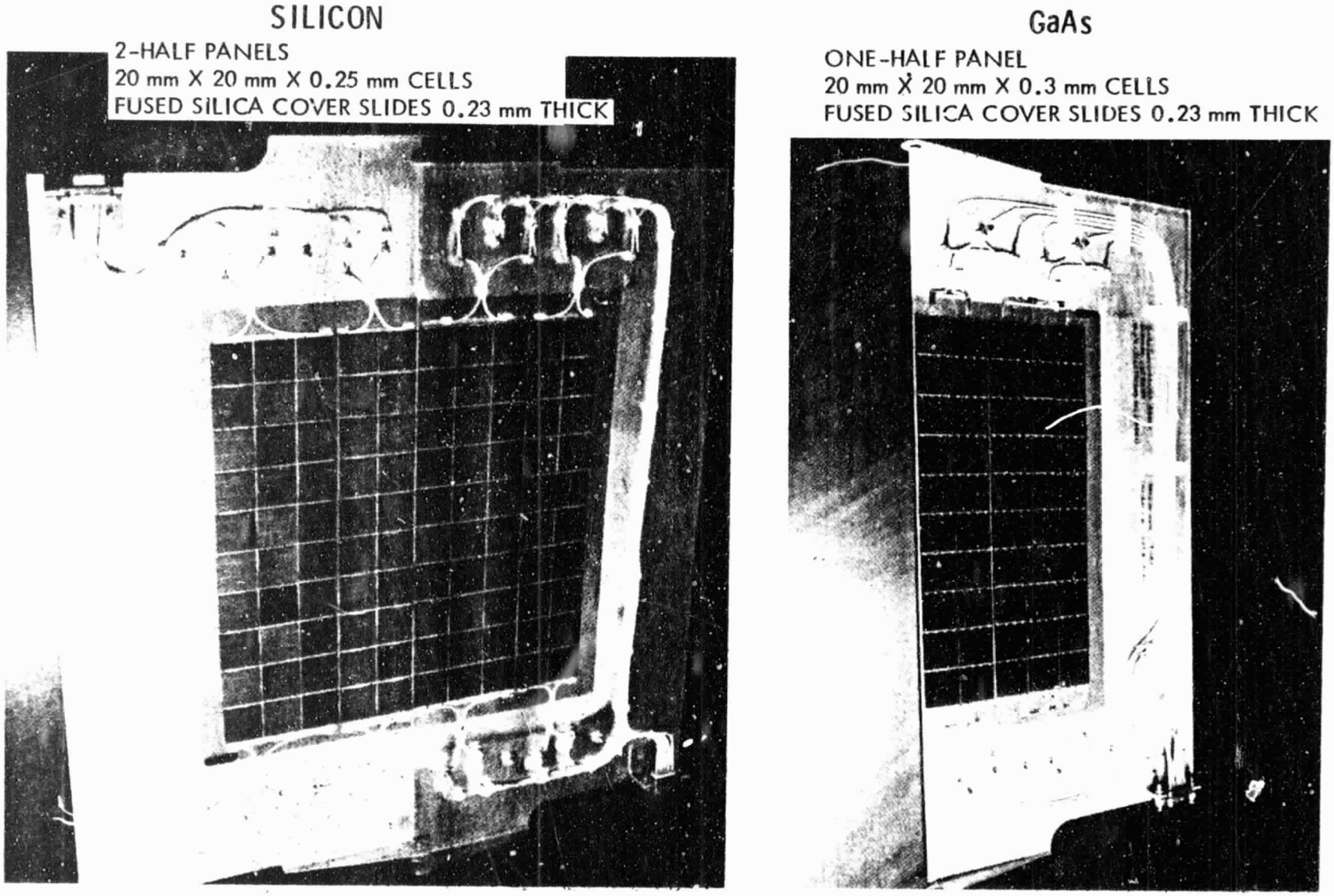

Figure 7-10. Solar Cell Panels - Test Hardware

Table 7-6. Characteristics of Individual Solar Cells

Characteristic	Cell Type	
	Silicon	Gallium Arsenide
Junction depth (μm)	0.1-0.2	0.5
AR Coating	SiO_x/Al_2O_3	Ta_2O_5
Front grid optimization (suns)	10	1
Contacts	TiPdAg	AuZnAg (upper surface) AuGeNiAg (lower surface)
Miscellaneous	Back surface reflector; 2 Ω-cm	

Table 7-7. Characteristics of Solar Half-Panels

Characteristics	Cell Type	
	Silicon	Gallium Arsenide
Bonding agent	RTV 577	DC93-500
Interconnects	Soldered, Ag mesh (0.05 mm thick)	Soldered Solaflex (0.03 mm thick)
Cover	0.23 mm fused SiO_2; MgF AR coating; 0.35 μm cutoff	0.23 mm fused SiO_2 MgF AR coating; 0.35 μm cutoff
Cover adhesive	DC93-500	DC93-500
Conductors	#24AWG stranded Cu; Teflon insulated	#24AWG stranded Cu; Teflon/Kapton insulated

nearest available equivalents. Finally some differences were introduced for diagnostic purposes in order to allow measurement of electrical phenomenon below the half-panel level. Table 7-8 compares the electrical difference between the test hardware and the flight design.

Table 7-8. Differences Between Flight Design and Test Hardware

Component	Flight Design	Test Hardware
Wire Harness	Flat cable Welded assembly Hard wired	Round wires Soldered assembly Connector output
Silicon Half-Panel Array	50 mm x 50 mm x 0.25 mm cell N_s x N_p = 4x2 FEP cover adhesive Frosted cover (0.20 mm) 14% efficiency (panel)	20 mm x 20 mm x 0.25 mm cell N_s x N_p = 10x3, 10x2 DC93-500 cover adhesive MgF AR coat (0.23 mm) 12.5% efficiency (cell)
GaAs Half-Panel Array	20 mm x 20 mm x 0.25 mm cell N_s x N_p = 10x5 18% efficiency Cover (0.20 mm)	20 mm x 20 mm x 0.3 mm cell N_s x N_p = 10x3, 10x2 16.1% efficiency Cover (0.23 mm)
Interconnect	Welded Silver mesh	Soldered Kovar "Solaflex" (GaAs only)
Bypass Diodes	One per half-panel (Si)	One per electrical string
Isolation Diodes	Series/parallel redundant	Parallel redundant

7.6.3 Tests of Individual Solar Cells

Prior to delivery, both cell manufacturers made certain measurements on representative cells. These included output current (at a specified voltage) and spectral response curves. The output current measurements (also performed on the solar cell panels) served as the primary buy-off criterion and were repeated in Rockwell's Power Electronics Lab at Seal Beach. Table 7-9 compares subcontractor and Rockwell measurements with the requirements set forth in the subcontract procurements. The Rockwell measurements agree with those of the subcontractor and both exceed the specified requirements. The test solar cells and panels delivered under the subcontracts were therefore acceptable.

Figure 7-11 presents subcontractor data on spectral response of representative solar cells of both types. The gallium-arsenide data shows the expected characteristics of shorter peak and cut-off wavelengths as compared with silicon.

Table 7-9. Buy-Off Comparisons of Output Current*

Component	Subcontractor Measurements (mA)	Rockwell Measurements (mA)	Specified Requirements (mA)
Silicon cells	140	142	135
GaAs cells	103	106	98
Silicon panel P1	710	715	675
Silicon panel P2	720	715	675
GaAs panel P3	513	525	490

* Test Conditions — 28°C, AMO corrected, output currents measured at 0.454V per series cell for silicon and 0.830V per series cell for GaAs.

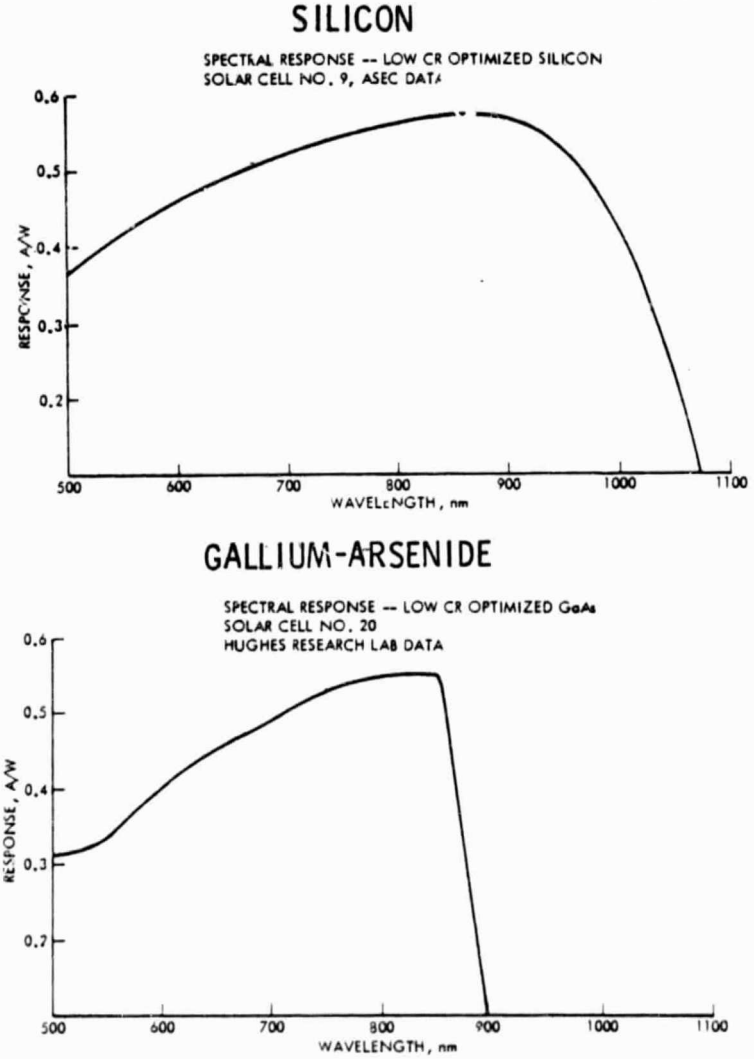

Figure 7-11. Solar Cell Spectral Response

The primary purpose of individual cell testing at Rockwell was to determine cell characteristics at elevated temperatures and at concentration ratios similar to those expected in ground and flight testing. Testing on the glazed individual cells was carried out in the Large Area Pulsed Solar Simulator (LAPSS) facility at Seal Beach. The same facility was used to carry out tests of solar panels. The light source is a pulsed-Xenon flash unit which illuminates a large area uniformly for a few milliseconds.

Figure 7-12 presents the test matrix carried out in the LAPSS facility. Solar cell temperatures were controlled by means of a circulating water bath, which also maintained the temperature of a reference standard cell. Illumination intensity (concentration ratio) was controlled by placement of the test cells according to the inverse square law. This was corroborated by checking the reference standard output. This technique proved to be accurate and repeatable. Auxiliary equipment associated with the LAPSS facility provides the ability to produce a complete current-voltage (I-V) characteristic for the device under test, corrected automatically for variations in illumination during the pulse by referencing the standard cell output. Figures 7-13 and 7-14 show the results of temperature and illumination variation for both cell types. An examination of the cell I-V curves shows that current output varied linearly with light intensity (within $\pm$ 2%) and that the shape of the curve was nearly constant over the range tested. Fill factors varied from 0.76 to 0.79.

Two of the delivered cells of each type were reserved as secondary standards and were used during panel tests in the laboratory and during full scale concentrator tests. The secondary standards were calibrated by the subcontractors to balloon-flight primary standard cells of the same type.

Reverse bias characteristics were also measured for both cell types. This information is of particular interest in designing the required bypass diode protection. Figure 7-15 presents measured results. The results show that one diode per half panel will provide adequate protection for both the Si and GaAs designs. The earlier conservative GaAs baseline design, which employed 5 diodes per half-panel (one every two sets of parallel cells), is not required.

OBJECTIVES -- EVALUATE INDIVIDUAL CELLS & PANELS UNDER KNOWN & CONTROLLED CONDITIONS

- BUYOFF
- MODELING
- BENCHMARKING

SOLAR CELLS

- TEN GALLIUM-ARSENIDE CELLS
- TEN SILICON CELLS

CR	TEMP (°C)
1	28, 50, 70
4	28, 70
6	28, 70

SOLAR PANELS

- ONE GALLIUM-ARSENIDE HALF-PANEL
- TWO SILICON HALF-PANELS

CR	TEMP (°C)
1	AMBIENT

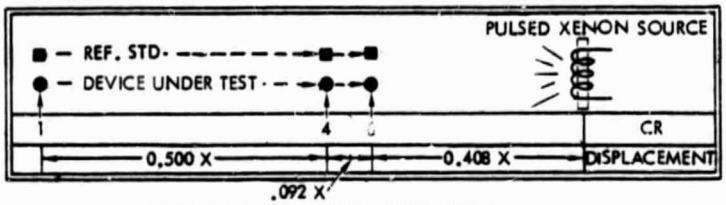

MULTIPLE SUN SIMULATION TECHNIQUE
X = 7.20 m (Si), 6.74 m (GaAs)

Figure 7-12. Test Matrix and Experimental Setup (Schematic)

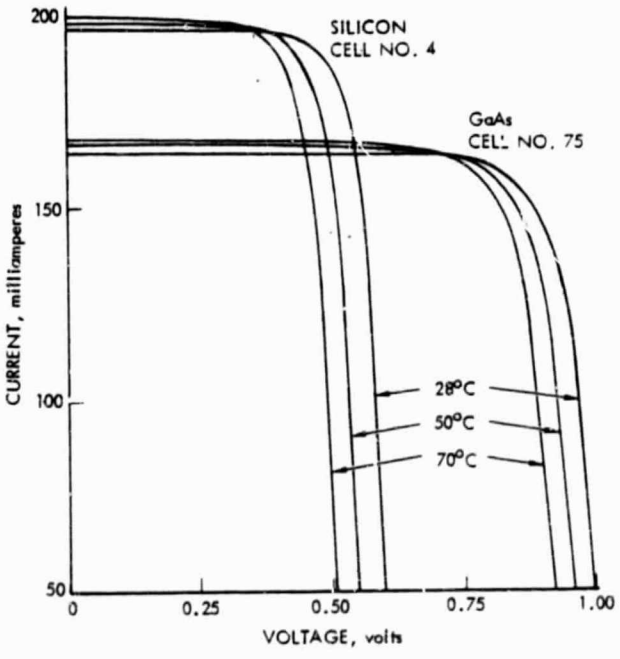

	Si	GaAs
$\frac{\Delta I}{\Delta T \cdot \Delta A}$ (mA/cm² - °C)	.02	.02
$\frac{\Delta V}{\Delta T}$ (mV/°C)	-2.0	-1.6

CR = 1

Figure 7-13. Measured Performance versus Temperature Gallium-Arsenide and Silicon Solar Cells Test Conditions - CR = 1, AMO Corrected

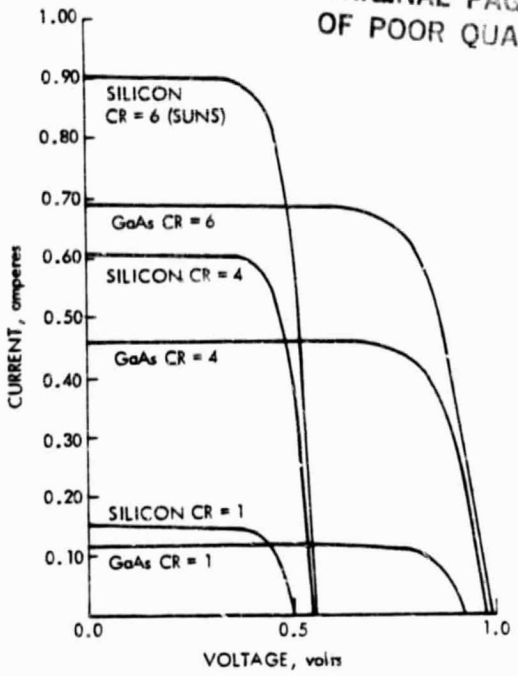

ITEM	Si	GaAs
$\frac{\Delta V}{\ln L/L_o}$ (mV)	26	32
$\frac{I}{I_o} \cdot \frac{CR_o}{CR}$	1.02	0.98
I_o / AREA (mA/cm^2)	154	110
V_o (mV)	486	927

STANDARD CONDITIONS - CR = 4, 100°C, AMO

Figure 7-14. Measured Performance versus Flux Gallium-Arsenide and Silicon Solar Cells Test Conditions - 70°C, AMO Corrected (CR = test flux - AMO flux, spectrally corrected)

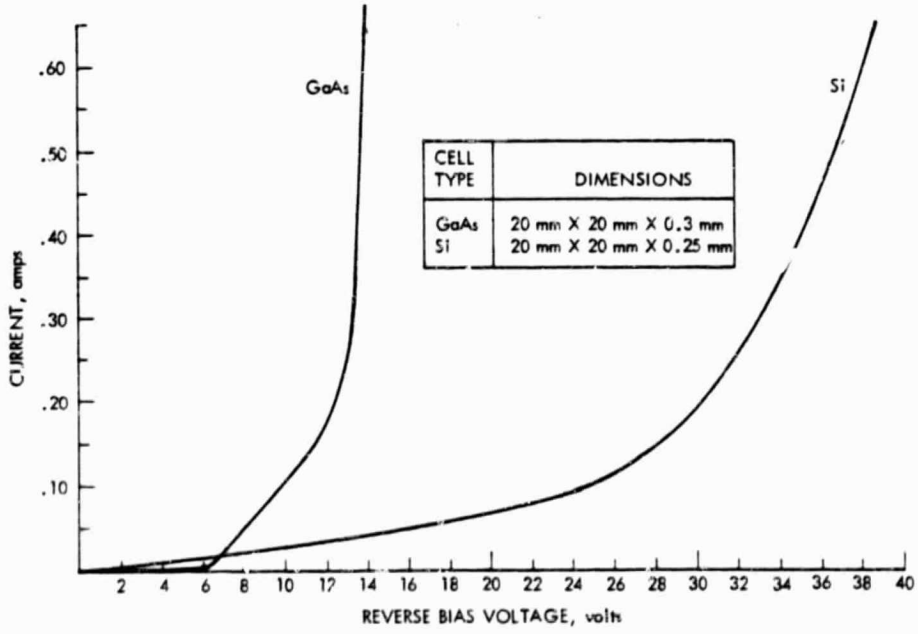

Figure 7-15. Solar Cell Reverse Bias Characteristics (28°C, not illuminated)

7.6.4 Solar Panel Tests

The photovoltaic characteristics of both the silicon and gallium arsenide half-panels were measured by the subcontractors prior to delivery. The same measurements also made at Rockwell, with results closely agreeing with the subcontractor data. Figure 7-16 shows the output of individual strings for each cell type, corrected for standard conditions of 28°C and AMO. Additional panel tests were made at Rockwell at four and six sun intensities which confirmed the linearity of output with intensity on the panel level. This also permitted estimating the concentrator element output prior to natural sunlight tests.

Prior to delivery, the subcontractors carried out limited temperature cycling tests (10 cycles between 100°C to -100°C) to assess adequacy of workmanship during panel assembly. In addition forward voltage drop and reverse leakage current were measured for all diodes prior to panel fabrication. Reverse leakage could not be measured after assembly due to the presence of the bypass diode. These measurements showed that all diodes conformed to specifications.

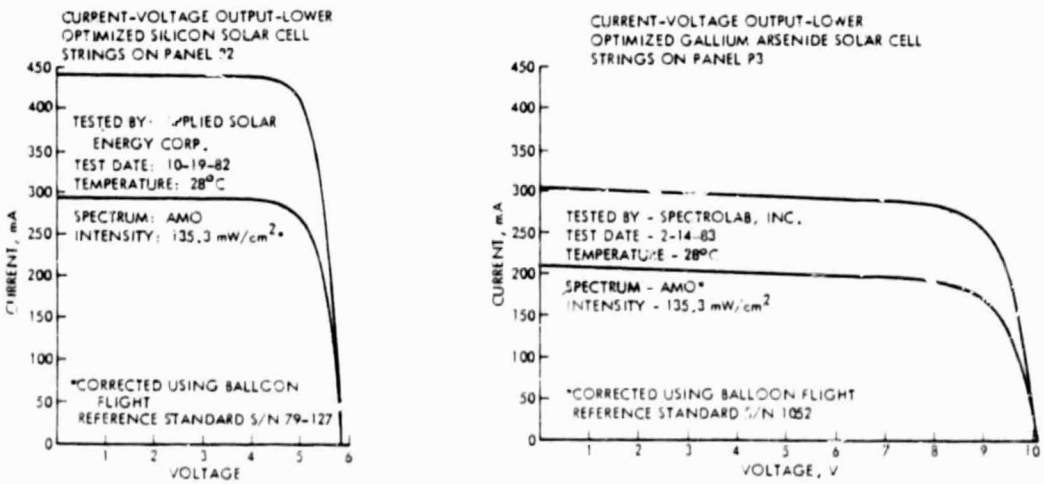

Figure 7-16. Photovoltaic Characteristics of Silicon and GaAs Solar Half-Panels (Test Hardware)

7.6.5 Update of Solar Cell Models

The solar cell model described in Section 5.5.1 was used to carry out the detailed thermal-electrical analysis of concentrator performance described in Section 5.5.3. The parameters of this model were derived from the best available cell data and used to make performance estimates of the baseline concentrator, as described in the mid-term report.[5] The results of the solar cell and panel tests described above provide the basis for an update of these parameters. Table 7-10 compares the baseline values with those derived from test data as well as those estimated for availability in 1984. The last two columns represent the best estimate for 1984 cell technology, representing only a small performance improvement from the cell parameters measured in this program.

In most cases, the updated values are close to the baseline estimates. Silicon short circuit current I_o however, is considerably higher than the earlier estimate. This is reflected in higher panel output.

Table 7-10. Solar Cell Model Parameters

Parameter Values	Units	Baseline		Test Data		1984 Design	
		Si	GaAs	Si	GaAs	Si	GaAs
I_o/area	(mA/cm^2)	129	115	154	110	159	118
V_o	(mV)	477	1003	486	927	478	938
α/area	(mA/cm^2 °C)	0.02	0.01	0.02	0.02	0.02	0.02
β	(mV/°C)	2.1	1.4	2.0	1.6	2.1	1.5
γ	(mV)	22	28	26	32	24	30

Note: Subscript zero denotes the conditions at T_o = 100°C and L_o = 4 AMO suns.

7.7 FULL SCALE CONCENTRATOR TESTS

7.7.1 Test Objectives

Full scale illumination tests in natural sunlight have been included in order to determine experimentally the amount and distribution of light concentrated on the concentrator base plane (solar panel) as a function of pointing error or controlled distortion. The experimental data provides information on the effects of the surface imperfections and geometrical errors of a realistic prototype concentrator.

A second objective is to measure solar cell and substrate-radiator temperatures. Both absolute temperatures and temperature distributions are of interest; in particular the existence of "hot spots" indicating unusually high light intensities or imperfect thermal contact between cells and substrate are of concern.

Full scale electrical performance tests are included to determine overall power output and the current-voltage characteristics of solar cell panels, half-panels and electrical strings for a variety of experimental situations. These include: direct solar pointing; off-pointing about different axes; controlled distortion of the concentrator shape; and different electrical configurations.

A final objective is to compare the results of illumination, temperature and electrical measurements with predictions carried out using the methods employed to predict concentrator performance in space, in order to assess the adequacy of the design analysis methodology.

7.7.2 Test Site Characteristics

Preliminary checkout of all equipment and procedures used in the full scale testing was accomplished at an open, black-topped parking area adjacent to the office and laboratory buildings of the Rockwell Seal Beach facility. Use of this site minimized travel time and facilitated the modifications of equipment and procedures. However, the low elevation (essentially sea level) and the proximity to the ocean results in relatively low and uncertain direct solar intensity and a fairly high amount of diffuse sunlight. For these reasons the bulk of the quantitative data taken under the present program was obtained at the high-altitude site.

The Solar Observatory at Table Mountain in California was chosen as the most suitable site for high altitude testing for several reasons. It is close to Seal Beach, (less than 100 miles by road). Its 2300 m (7500 ft) altitude results in a good percentage of clear sunlight hours with high direct solar intensity. The facility, which is presently managed by the Jet Propulsion Laboratory, provides a level, concrete surface for equipment deployment, utility electric power and locked indoor space for storage of test equipment when not in use.

Regular solar measurements have been made at the site by the Smithsonian Astrophysical Observatory during the period from 1926 to 1952. In 1977 Wilson and Butler[19] repeated these measurements and found that the mean direct solar irradiance had not changed within the small standard errors of measurement. Direct beam intensity at a zenith angle of 60° was about 990 watts/m^2.

Although conditions at Table Mountain approximate those in space to some extent, there are important differences between the ground test of a single concentrator element and the operation in space of an array of close-packed elements. Even at altitude, atmospheric attenuation reduces the intensity of direct beam radiation significantly. The atmosphere also alters the spectral quality of the light and produces diffuse radiation as well. The thermal environment is also quite different in the two cases. The ground test element can radiate heat away unhindered by blockage from adjacent concentrators. The radiator receives more reflected and emitted radiation from the surrounding terrain than it would in space. The radiator and solar panel are cooled by convection during ground tests; even in still air, free convection provides significant cooling.

7.7.3 Pretest Analysis

The optical performance of the concentrator during ground testing depends upon the amount and distribution of diffuse light entering the aperture. A ray-trace analysis was carried out using RAYPYR (see Section 5.4) under the following assumptions:

Direct beam intensity, W/m^2	1050
Diffuse intensity (isotropic), W/m^2	105
Concentrator specular reflectance	0.88
Concentrator diffuse reflectance	0.01

Figure 7-17 shows the distribution of illumination on the solar cell plane, expressed as concentration ratios in units of direct beam intensity. A comparison with the calculated distribution for operation in space (Figure 5-23) shows that the presence of 10% isotropic diffuse radiation has relatively little effect on the concentration ratio distribution (although the absolute intensities are lower because of direct beam attenuation).

The ray-trace program RAYPYR is limited to handling isotropic diffuse light. However, the isotropic assumption may be a poor one. The data presented by Weiss and Lof[20] suggest that there can be a significant amount of circumsolar diffuse radiation within the acceptance angle of the pyramidal concentrator. A precise analysis is not possible without modifying the ray-trace program. An approximate analysis which treats the percentage of circumsolar diffuse radiation as a parameter gave the following results:

% Circumsolar*	Average CR*
0	4.64
3	4.75
9	4.97
13	5.11
23	5.47
34	5.86

* Based on direct beam intensity.

The electrical performance of the concentrator during ground testing is affected by a number of environmental factors including the solar zenith angle (air mass effect), the clearness index, the air temperature, the ground reflectivity and temperature and the wind velocity. The lumped-parameter performance analysis described in Section 6.4 was used to make pretest predictions for the expected range of conditions likely to be encountered. Figure 7-18 presents peak power output, on a full-panel basis, as each parameter in turn is varied over the expected range from the set of nominal conditions given in the figure.

CR* DISTRIBUTION ON SOLAR PANEL (POINTING ANGLE ^o)

4.74	4.76	4.76	4.85	5.15	5.10	4.83	4.83	4.76	4.72
4.75	4.53	4.61	4.86	4.98	4.91	4.85	4.65	4.48	4.84
4.91	4.65	4.47	4.59	4.44	4.57	4.50	4.39	4.70	4.86
4.83	4.76	4.55	4.33	3.84	3.75	4.32	4.62	4.84	4.76
5.09	4.92	4.57	3.69	3.67	3.63	3.75	4.52	4.92	5.15
5.18	4.91	4.53	3.77	3.63	3.66	3.76	4.43	4.95	5.14
4.80	4.85	4.54	4.32	3.78	3.82	4.38	4.49	4.87	4.79
4.83	4.62	4.48	4.52	4.58	4.59	4.46	4.42	4.71	4.85
4.83	4.4	4.76	4.81	4.88	4.85	4.87	4.64	4.43	4.76
4.68	4.79	4.80	4.85	5.21	5.18	4.83	4.86	4.77	4.69

*CR AND η OPT BASED UPON DIRECT BEAM INTENSITY

- CLEAR DAY DIRECT BEAM INTENSITY ~1050 watts/m^2
- DIFFUSE COMPONENT ESTIMATED TO BE 10%

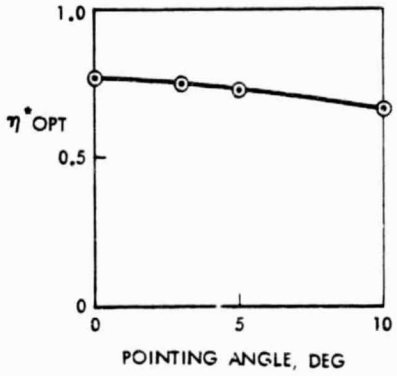

Figure 7-17. Predicted CR Distribution During Ground Testing (Isotropic Distribution)

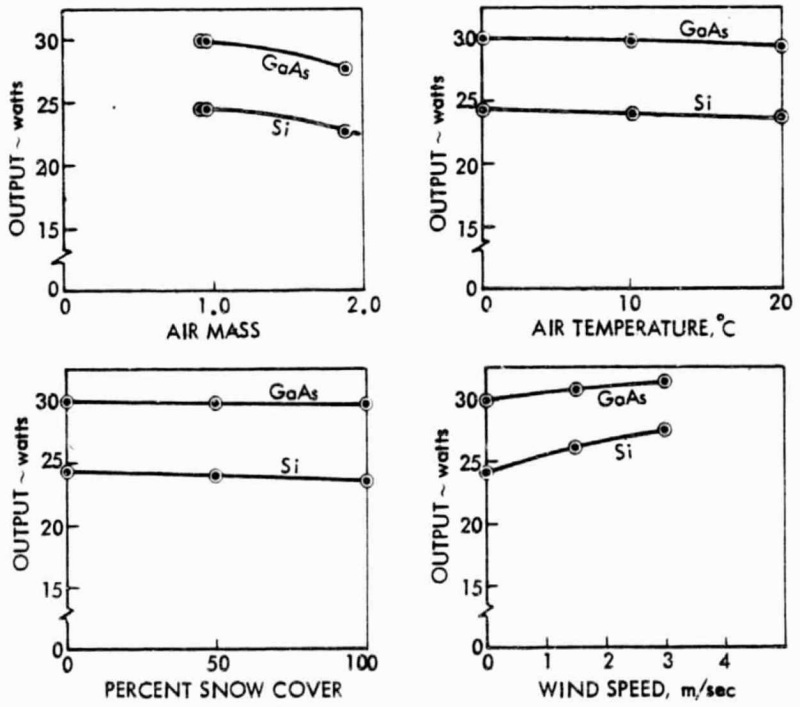

Figure 7-18. Pretest Electrical Performance Predictions (Table Mountain)

Average solar panel temperature varies noticeably with environmental conditions. In still air the variation is moderate, from 65° to 79° C with a nominal value of 74°C. Wind velocity has a larger effect. At an assumed wind speed of 1.5 m/sec (3.4 mph) average panel temperature drops to 55°C. Even the highest predicted panel temperatures are well below those expected in space.

7.7.4 Test Equipment

The test item for all full scale testing consists of an assembly of four film-frame reflector panels, two of which are hinged to permit folding. The reflector assembly (the concentrator) is closed off at the truncated base either by diffuse reflector plate (for illumination tests) or by two solar half-panels. The concentrator is supported as a unit by means of a rigid rectangular test fixture made of light angle stock. The fixture was mounted on a tracking equatorial telescope mount as shown in Figure 7-19.

The top (aperture) of the concentrator is clamped to the fixture by means of four support pins imbedded in the reflector frames. They are positioned on the fixture by means of adjustable clamps, in either the normal (fully open) configuration or in one of the distorted configurations. The reflector aperture is fitted with a removable cover made of light-weight aluminum sheet. The cover is provided with a small (6 mm diameter) central alignment hole, a rectangular opening for photographic calibration, and a circular opening large enough to admit the lens barrel of a 35 mm camera. The camera, a Nikon FM with a Nikkor 55 mm macro lens, is supported by a standard camera tripod when in use. The camera was loaded with Kodak 2415 technical pan film for illumination experiments. Film was developed at the photographic laboratory in Rockwell's Downey facility using Kodak D-19 high-contrast developer. Evaluation of film records and quantitative analysis of film exposure is accomplished at the photographic laboratory using a densitometer.

Solar intensity was not directly measured during the tests but inferred from the extensive data base for clear-sky conditions summarized by Wilson and Butler[19]. During the present test program the criterion for "clear sky" was qualitative, namely the absence of clouds in the vicinity of the sun and no visible smoke or haze. Solar intensity was monitored by means of a reference

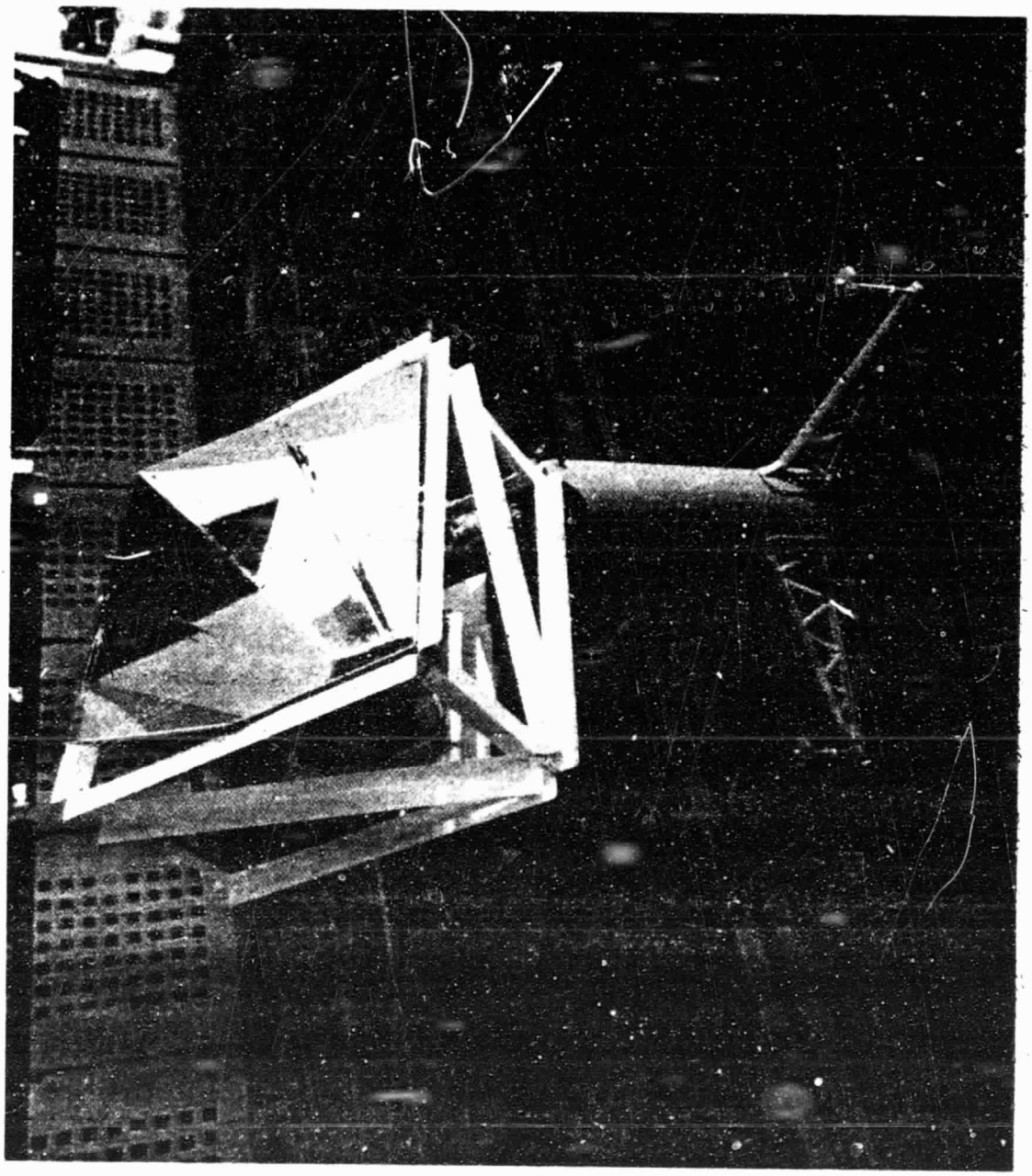

Figure 7-19. Concentrator Element Test Hardware

cell mounted on the sunward surface of the support fixture. Typically cell output varied by less than 1% during a given series of clear sky of measurements. The onset of haze or cirrus clouds however, produced dips of 10% or more in the readings, at which time testing was discontinued.

Temperatures on the under-surface of the aluminum substrate-radiators were measured by copper-constantan thermocouples bonded by means of aluminum adhesive tape. Each half-panel carries four couples; one at the center of the hinge line, one at the edge of the region occupied by solar cells, and one each at the mid-point and corner of the radiator edge. A thermocouple is also used to monitor the temperature of the reference cell. Front-surface solar cell temperatures are measured by means of a AGA Thermovision 680 infrared camera[21] system (Figure 7-20) which transforms infrared images into color-coded displays of isothermal regions. The camera is provided with its own adjustable stand which allows a view into the concentrator from a direction sufficiently off-axis so as to avoid interception of rays which would reach the solar panel. Permanent records of the color display are made with a polaroid camera.

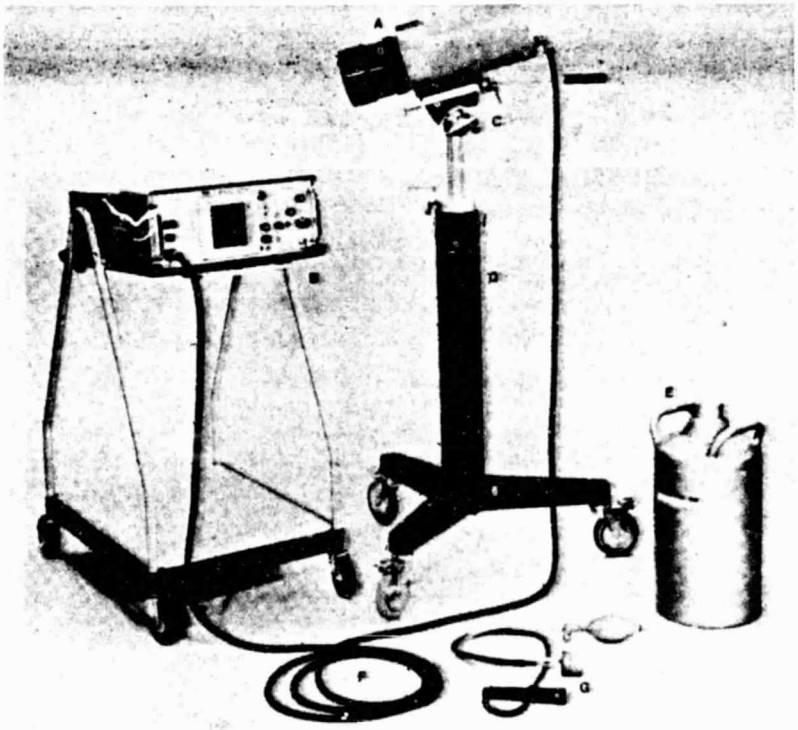

AGA Thermovision System 680 complete with the normal accessories required for routine thermographic investigations, including A: IR Camera Unit Model 680 B Display Unit Model 102 B, C Panorama (pan/tilt) Head D Mobile-column Monopod E Ster- age Container for 10 litres of liquid nitrogen content F Inter- connection Cable (5 metres long) and G Filling Accessory for liquid nitrogen

Figure 7-20. Concentrator Performance Verification Test Test Instrumentation (from Reference 21)

Current-voltage characteristics of individual electrical strings, half-panels and full panels are determined by means of a manually swept variable resistance load. Current is measured by means of an ammeter with a 0.01 ohm shunt; voltage by means of a high-impedance digital voltmeter. Current and voltage are displayed and recorded on an X-Y plotter.

7.7.5 Illumination Test Procedures and Results

Initial test plans called for the measurement of illumination distributions on the base plane by photographing the back side of a translucent diffuse screen. Preliminary tests proved this approach to be unsatisfactory, probably due to variation in screen transmission with incident angle. Front-photography of a diffuse reflecting surface (aluminum sheet painted with 3M velvet white paint) was used in all measurements described here.

Alignment of the concentrator optical axis is accomplished by moving the supporting fixture as a whole. Solar direction is determined by noting the location of the image of a small alignment hole in the aperture cover projected onto a marked template covering the base plane. Adjustments about the polar axis (East-West adjustments) were made by rotating the tracker. North-South adjustments were made by means of a set screw located on the tracker. A clock drive maintained alignment within a fraction of a degree between adjustment periods, usually 30 minutes or less.

Illumination was measured by photographic densitometry. With the aperture cover in place, a rectangular opening is exposed progressively by withdrawing an opaque slide in six equal steps. At each step the image of the opening is photographed by multiple exposure, typically at f/16 and 1/250 second through a neutral density filter. The resulting photographic image of the rectangle provides a calibration in relative units from six suns intensity for the first exposed step to one sun for the last. Several such calibration frames were photographed on each roll of film. These allowed the relating of optical densities measured in test frames (where the reflecting base plane is photographed with the aperture cover removed) to the relative illumination in suns.

Figure 7-21 is a typical test frame showing the illuminated base plane under zero pointing angle conditions. The qualitative correspondence with the theoretical pattern shown in Figure 5-23 is evident. The diagonal boundaries originating from the corners, the lower illumination in the center and the higher values around the edges are all present. There are also noticeable departures from the ideal pattern, apparently associated with imperfections of the reflector panel hinge lines and a slight bowing of the reflector frames. Densitometric measurements, with a resolution approximately equal to 1/100 the total base area, gave an illumination range from 4.3 to 5.8 suns, with an average value of 5.25 suns. The intensity range compares with the theoretical values 3.6 to 5.3 (4.6 average) taken from Figure 5-23, but is about 0.6 suns higher.

Similar illumination measurements were made for a range of pointing angles and for controlled distortions of the concentrator structure. Difficulties with exposure levels and camera view angles prevented the obtaining of useful illumination data during distortion. Figure 7-22 summarizes the measurements made during off-pointing. Measured average concentration ratios fall off gradually with pointing error in good agreement with theoretical predictions. Again, however, the indicated illumination values are about 0.6 suns too high.

The most probable explanation for these differences lies in the assumptions about the amount and distribution of diffuse sunlight. As is shown in Section 7.7.3 the pretest predictions based on the assumption of 10% isotropic diffuse light gave an average illumination of about 4.6 suns at the base plane. However a hypothetical 15% diffuse light concentrated within 15° of the solar direction could give an apparent illumination as high as 5.2 suns.

7.7.6 Solar Panel Temperature Measurements

Several series of thermocouple measurements of substrate and radiator temperatures were taken periodically, interspersed with the electrical performance measurements described in Section 7.7.7. Average substrate temperatures ranged from 44° to 71°C. When allowance is made for the approximately 2°C drop through the solar cells, the measured values are in fair agreement with pretest predictions (55° to 79°C). Generally speaking,

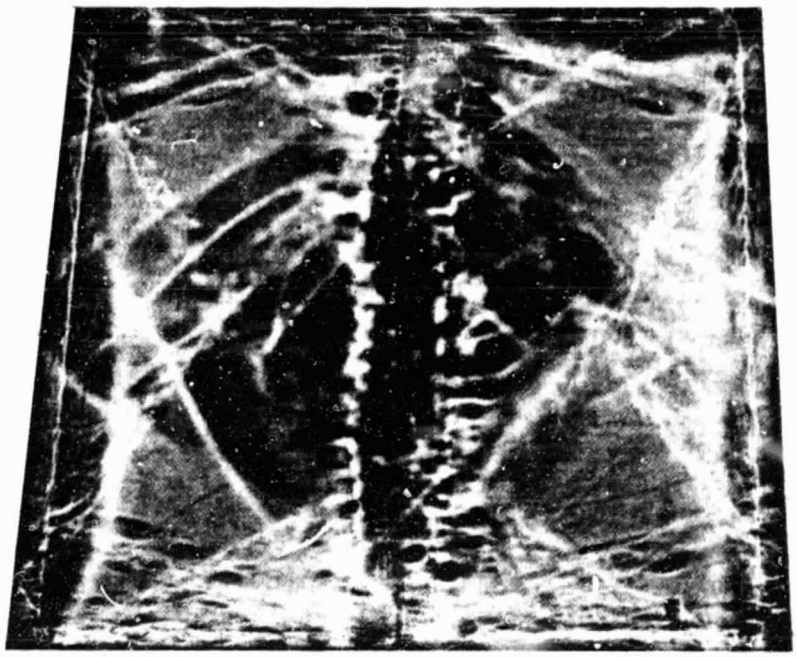

Figure 7-21. Typical Illumination Test Frame (Zero Pointing Angle)

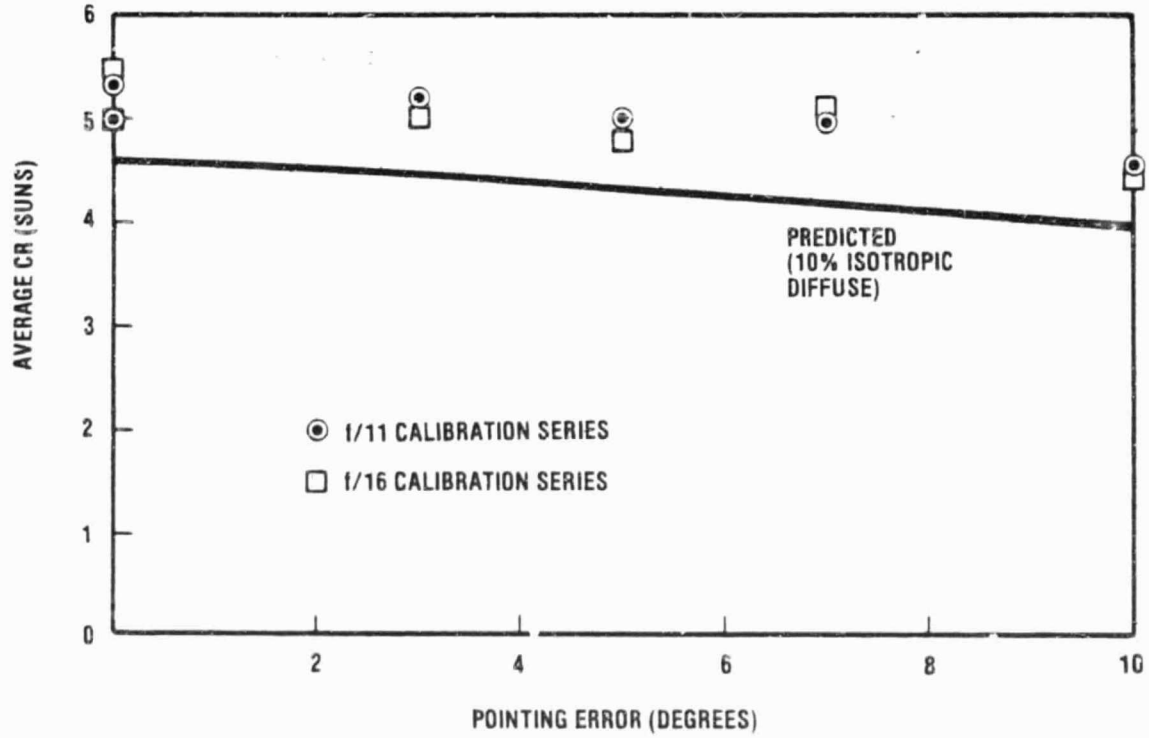

Figure 7-22. Experimental Average Concentration Ratios on Base Plane (Table Mountain)

temperatures were higher (54° to 71°C) in May than during the March test period (44° to 51°C). During the May tests a progressive increase in average temperature with time of day was observed, no doubt reflecting higher ambient temperatures. Several factors difficult to control limited attempts to compare measured and predicted temperatures more closely. Emitted and reflected radiation varied throughout the day in a manner difficult to account for. Although testing was discontinued in windy conditions, light intermittent breezes did occur. The effect of power conversion on the panel heat balance was noticeable and could change panel temperatures by 5° to 10°C.

The Thermovision infrared camera gave a detailed picture of the distribution of solar cell temperatures over the solar panel during operation. Figure 7-23 is a black and white print from a color picture of the Thermovision record for a typical run. The temperature calibration scale along the bottom of the picture (color-coded in the original record) provides a means of defining cell surface temperatures within 2°C. The Thermovision camera does not make an absolute temperature measurement, but must be calibrated for a given surface at one known temperature. In the present case, thermocouple measurements on the bottom (substrate) side of the panel were used to deduce cell temperature, assuming a 2°C drop through the stack.

The Thermovision camera was used only to obtain representative solar cell temperature patterns during the present test program. It shows the expected pattern of highest temperature in the middle, in spite of lower illumination there. The high resolution of the Thermovision camera makes it a promising development tool during later phases of concentrating array development.

7.7.7 Electrical Performance Tests

The most significant tests of the present program were those in which the electrical output of the illuminated concentrator was measured. Optical, thermal and electrical factors all contribute to the end result.

The bulk of the performance testing with silicon panels used an electrical configuration in which each half-panel had both electrical strings hooked up in parallel and the two half-panels connected in parallel. When the single gallium arsenide half-panel was tested, the opposite (silicon) half-panel was loaded near its maximum power point. Current-voltage characteristics were

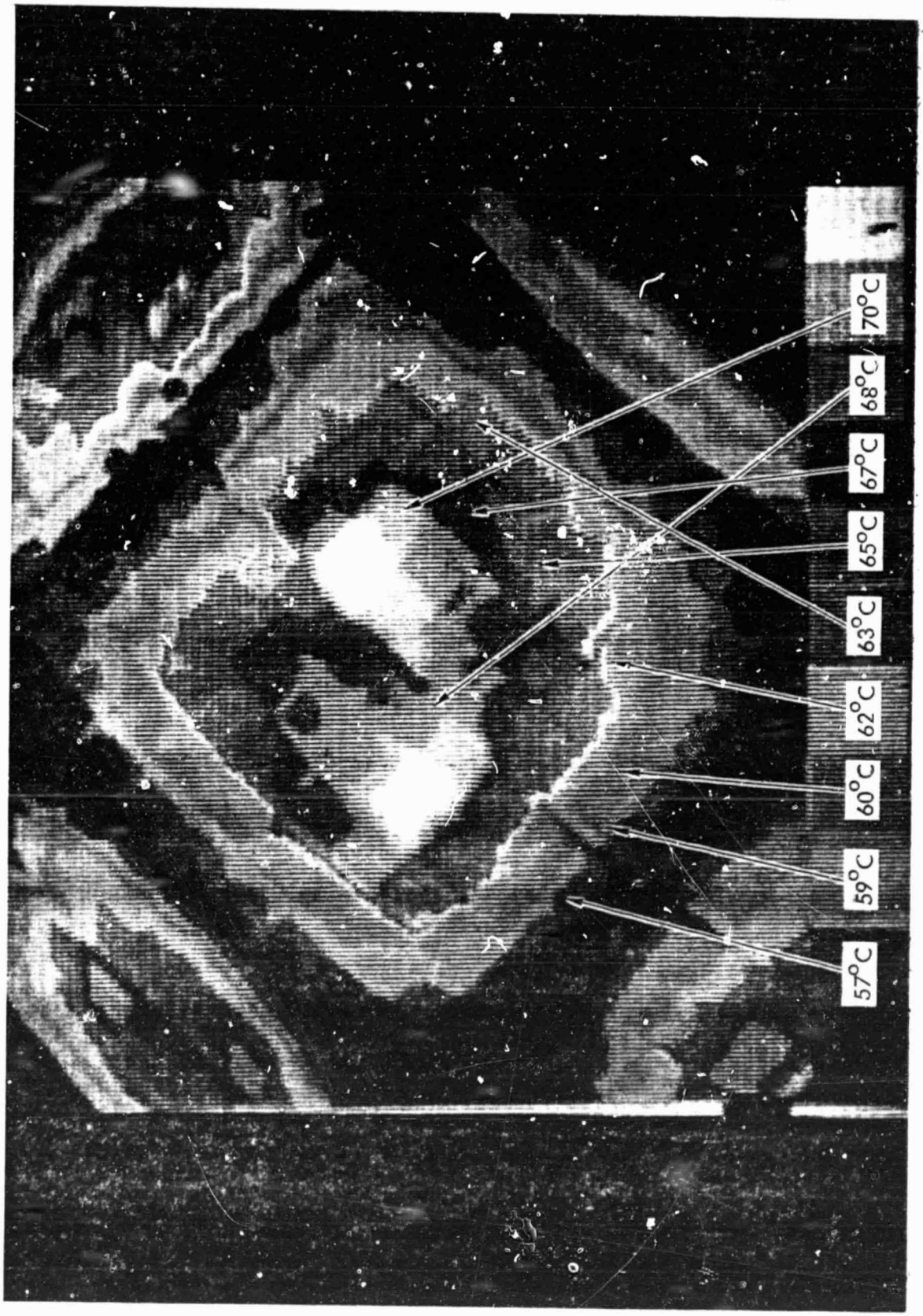

Figure 7-23. Silicon Solar Panel Temperature Distribution (Table Mountain)

determined at each experimental setting (e.g., a particular pointing angle or distortion configuration). Because the experimental maximum power point occurred at a temperature determined by factors difficult to control, a standardized procedure was adopted. Power output was computed from the measured short circuit current I (insensitive to temperature), an average fill factor derived from the experimental current-voltage curves, and a temperature-corrected open circuit voltage V, based on temperature coefficients derived from the electrical tests described in Section 7.6. The power calculations were carried out according to

$$P_{max} = (FF)\ I_{meas}\ V_{corr} \qquad (7\text{-}2)$$

Figure 7-24 presents experimental values of both silicon full-panel and GaAs half panel outputs as a function of pointing error. The normal incidence (0°) value is very close to the pretest prediction of 24 watts for silicon. The experimental values for pointing angles tilted about the North-South axis (θ) parallel to the panel hinge line follow rather closely the predicted output for a solar intensity of 1000 W/m^2, the value expected at Table Mountain. Outputs for other tilt axes fall below the values for North-South tilt, indicating greater electrical mismatch losses. Some of these losses, at least, are due to the existence of two electrical strings per half-panel rather than the single 5px10s string which would be used for a 50-cell half-panel in a flight design. Figure 7-25 shows similar results obtained for sea-level tests of a silicon panel. Output is at a lower level reflecting the lower solar intensity typically available at Seal Beach.

Figure 7-24 also shows the experimental power output obtained for the gallium arsenide half-panel. Again the normal incidence power of 15 watts (30 watts/panel) matches the pretest prediction. Falloff of power output with pointing angle is gradual and there is some effect of electrical mismatch associated with rotation about different axes.

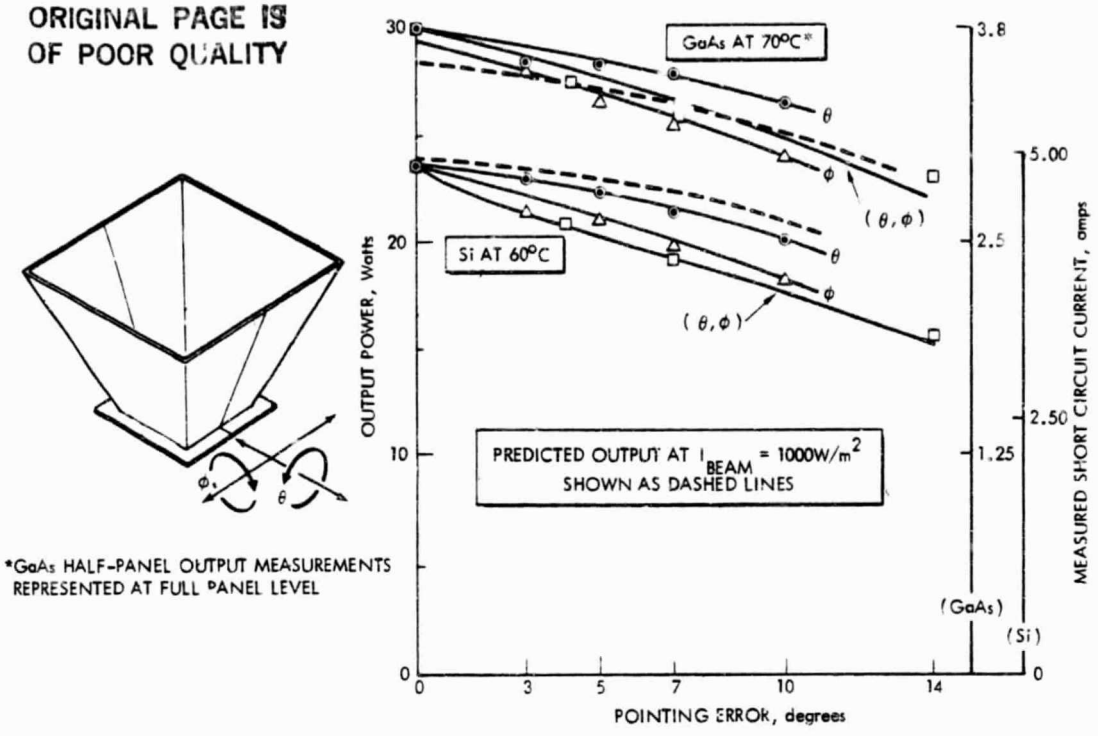

Figure 7-24. Silicon Full Panel and GaAs Half Panel Output versus Pointing Error (Table Mountain Observatory)

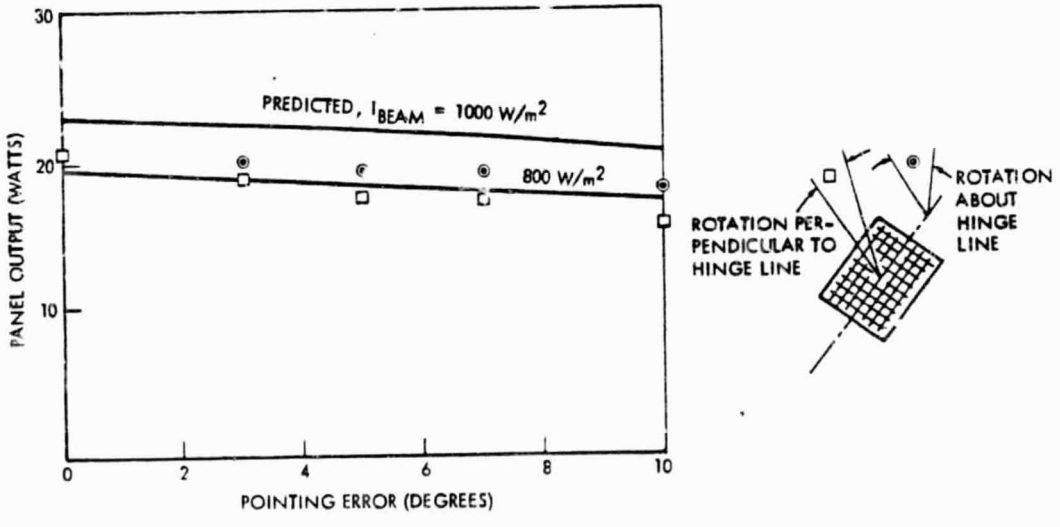

Figure 7-25. Experimental Concentrator Output (Silicon Panel at Sea Level)

The effect of geometrical distortion on concentrator output was determined primarily using the silicon panels. The pyramidal structure of the reflector panels proved to be too rigid to accept much twisting distortion without the application of undue force. No translations of the aperture corners greater than 13 mm (0.5 in.) were attempted for fear of damaging the structure and little output loss was measured at this condition. Large distortions could be produced by inward displacements of one or both reflector panel hinges, however. Figure 7-26 shows the effect on electrical output for both cases. Performance drops rapidly with hinge displacement until a plateau is reached at which optical concentration becomes ineffective and panel output corresponds to the amount of direct sunlight which gets through the partially folded reflectors.

7.7.8 Summary of Full Scale Test Results

Full scale testing of the prototype concentrator element confirms the performance expected from the design. Optical and temperature measurements showed the expected distributions and trends. Differences in absolute level are explainable on the basis of factors difficult to estimate accurately or control. Electrical performance, which is the result of optical, thermal and electrical factors, agrees very well with analytical predictions. Both output level and the insensitivity of output to pointing angle are confirmed for both silicon and gallium arsenide configurations.

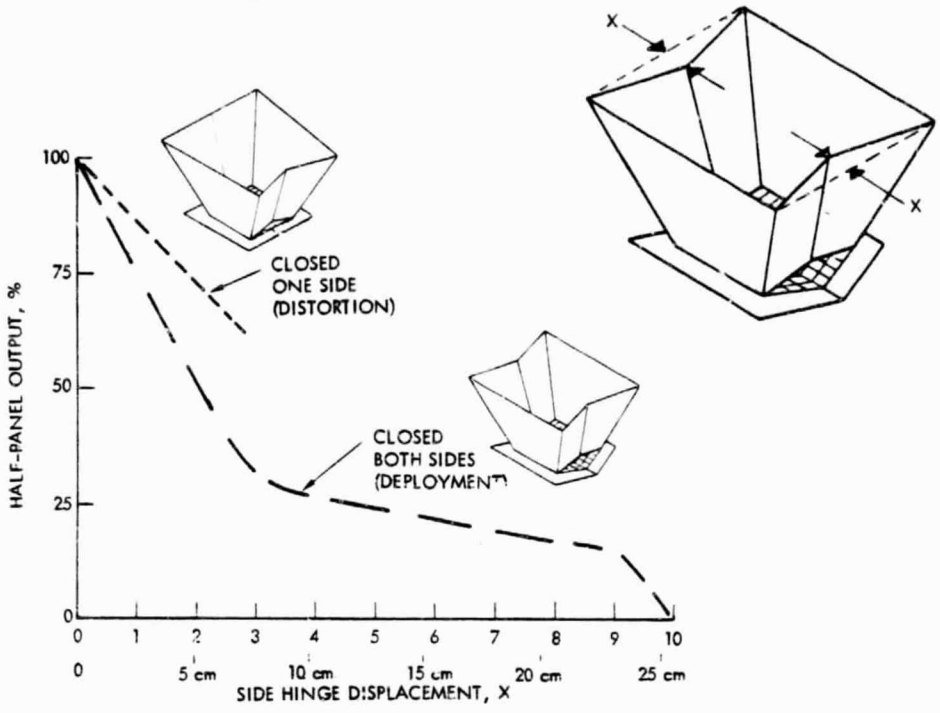

Figure 7-26. Silicon Half-Panel Output with Hinge Distortions

8.0 DEVELOPMENT PLANNING

8.1 TECHNOLOGY ASSESSMENT

The logic diagram shown in Figure 8-1 shows the approach Rockwell has taken to identify, validate, and cost the technology needs. Ten potential technology requirements were identified during the contract effort (see Table 8-2). These potential requirements were then screened by essentially asking four key questions (Table 8-1) to validate that new technology is really involved. Those requirements which passed this gate (8 passed) were then further evaluated to determine items to be recommended for supporting Research technology (SRT) items.

Each of the potential technology requirements were initially validated by asking the four questions shown in Table 8-1. This initial screening was able to identify solutions for on-going R&D activities for two of the ten items discussed. The remaining eight items which passed gate no. 1, were scrutinized further for confirming data.

Table 8-2 summarizes the ten potential technology items identified, along with the rationale used to reject eight of the items for SRT consideration.

8.2 SUPPORTING RESEARCH TECHNOLOGY (SRT) ITEMS

Table 8-3 provides a summary of the two SRT items identified. Effort in these areas are currently under investigation by NASA. The welded interconnect technology is considered essential for the concentrator array design due to its higher operating temperature. However, planar arrays will also benefit from this technology for low earth orbit mission applications where a large number of thermal cycling of the array will occur for long life (10 years). The optical stability of reflectors in space needs to be demonstrated for concentrator array applications. The thin film Kapton reflectors used in the preliminary design configuration are not expected to present a problem since both sides of the Kapton material is coated with aluminum for optical and thermal performance characteristics.

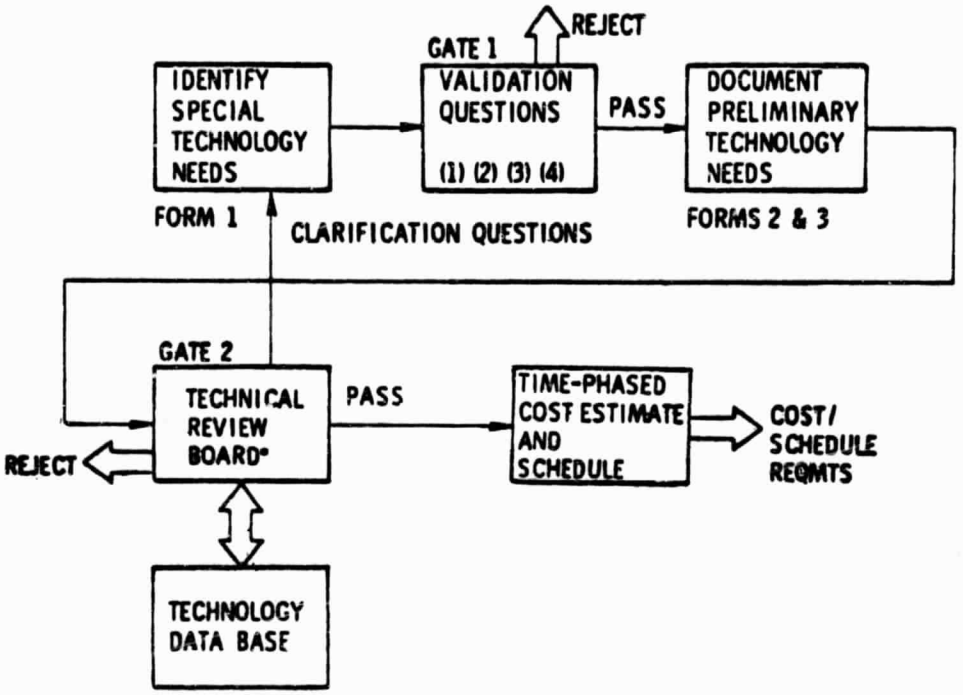

Figure 8-1. Logic Diagram - Technology Assessment

Table 8-1. Validation Questions

1.	Is comparable work being conducted now (or contemplated) by NASA, DOD, or industry?
2.	Could the required need date be satisfied by the on-going technology rate/trend line?
3.	Are there viable alternatives if the technology need is not satisfied?
4.	Is the solution to the problem primarily a short-term effort (less than one year)?

Table 8-2. Summary of Potential Technology Requirements

Potential Items	Status
•Vibration-free canister-deployed astromast	Program development item
•Silicon solar cells (large area)	Currently under development
•Solar cell cover bonding	Program development item
•Solar cell adhesive	Program development item
•GaAs solar cells	Currently under development
•GaAs solar cell cover bonding	Program development item
•Solar cell interconnect design	Program development item
•Solar cell interconnect bonding process	Recommended SRT items
•Optical stability of lightweight reflectors	
•Radiation-resistant thermal control coating	Program development item

Table 8-3. Technology Development

Supporting Research Technology (SRT) Items

- Welded interconnects -- long cycle life at elevated temperature
  - Type and schedule -- ultrasonic, laser, parallel gap
  - Performance -- temperature cycling, Si and GaAs
  - 1985 implementation — 1983 start
  - Conclusions -- not a show stopper; NASA LeRC comprehensive program

Lightweight Reflectors -- Long Term Optical and Mechanical Stability

- Configuration -- coating/substrate -- film/frame, molded panel
- Performance -- recover experiment package
- Up to one year space exposure desirable
- Conclusions — Several potential programs identified:
  LDEF, SAFE II, STEP

8.2.1 Performance Improvement Items

Table 8-4 lists six items that would enhance the performance of the array module, but are not considered necessary to demonstrate concentrator array feasibility for space mission applications. Two of these items (Astromast and solar cells) are discussed below.

Hybrid Lattice Mast Development

The double-laced mast design is a more recent development, more sophisticated and possibly a higher risk than the single-laced mast. In the interest of cost effectiveness, the critical components of the canister-deployed mast should be common to both designs since future application will determine which design is chosen.

The design of the hybrid single-laced/double-laced mast can be optimized with respect to weight by changing the configuration of the shear members, i.e., battens and diagonals. Standard-sized battens will not allow stowage of the hybrid mast in the space provided for a single-laced mast. The batten stiffness can be reduced so that under the assumed critical load conditions the longeron buckling strength would be reached simultaneously in the single- and double-laced section.

Table 8-4. Performance Improvement Items

Item	Advantage
Pyrolytic graphite radiators	-- Reduces cell operating temperature — Reduces physical movement between cell and panel during temp cycling
Spectrally selective reflectors	— Rejects IR while reflecting other wavelengths
Graphite epoxy structural shapes (extruded)	— Cost/weight reduction
Reduced weight astromast	— Weight reduction
Lightweight rigid reflector panels	— Cost/weight reduction
Improved solar cell performance	— Cost effective/area reduction (higher efficiency)

The design concept for hybrid lattice masts has been proven on about a half scale of the proposed design. The development of the L-SAT actuator and the upscaling of other mast designs indicate one major area which needs to be monitored very carefully. The fabrication of the longeron composites is highly critical. There are indications that void content may lead to interlaminar cracks at a low number of deployment/retraction cycles. The longerons experience a combination of high shear, bending, and torsion loads in the transition from fully stowed to deployed condition, and it is not yet fully understood what causes the flaws. Although tests at Astro have shown no measurable degradation of longeron bending strength, the situation is of great concern. Improvement of longeron fabrication processes, either layup or pultrusion methods, are indicated.

A technology development program to address these issues has been estimated by Astro Research Corp. (subcontractor) to require about $400,000 and would take one year or less to complete.

Solar Cell Performance/Cost Improvements

Silicon Solar Cells. There are no known technology deficiencies which would prevent the solar cell manufacturer(s) from delivering devices in support of a production program. The solar cell characteristics used in the performance modeling and analysis section would be transferred into a procurement specification. These are summarized as:

Output, min. avg.	—	473.6 mV (50 mm x 50 mm x 0.25 mm covered)
Efficiency	—	14% (AMO, CR = 1, 28°C)
Absorptance	—	0.70 max
Cell optimization	—	CR = 4
Cover thickness	—	0.2 mm (fused silica)

These devices could be delivered at a maximum rate of 5,000 per week. Lead time would be twelve weeks. A typical delivery shcedule is shown in Figure 8-2 to support a production of four modules (307,000 cells). Typical test programs needed to support production of flight half-panels would include: cell type approval testing by the cell vendor, cell space qualification and characterization by the panel manufacturer, as well as accelerated temperature cycling of a half-panel built using the flight production materials, processes and personnel.

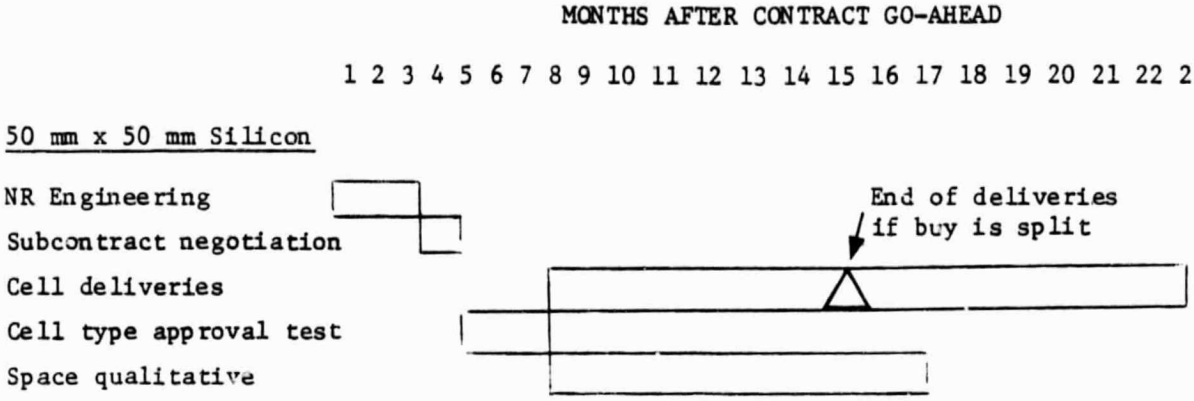

Figure 8-2. Typical Silicon Solar Cell Delivery Schedules

If improved performance were needed the following approaches could be pursued. Thin cells could be used to lower the mass without decreasing performance. In this case a Boron diffused back surface field cell (BSF) would be advantageous. The thin cell's lower absorbed radiation dose would not negate the BSF. An alternate approach to reduced cost would be to use certain terrestrial solar cells. The heavy shielding of the cells by the reflectors and radiator as well as the benign radiation environment in the low inclination-low altitude orbits may make this possible.

GaAs Solar Cells. There are no known technology deficiencies which would prevent the solar cell manufacturer(s) from delivering devices in support of a production program. Both Spectrolab and Applied Solar Energy are concerned about the contact metalizations of the devices. Both cell suppliers have occasionally experienced low contact pull strengths, but they are optimistic concerning production readiness of their systems. Contact solderability and weldability is good with most pull-tab tests yielding above the industry standard 500 g criteria. The solar cell characteristics used in the performance modeling and analysis section would be incorporated into a procurement specification as follows:

Output, min. avg.	— 97.4 mW (20 mm x 20 mm x 0.30 mm covered)
Efficiency	— 18% (AMO, CR = 1, 28°C)
Absorptance	— 0.75 max
Cell optimization	— CR = 4
Cover thickness	— 0.20 mm (fused silica)

The delivery schedule for the cells deserves some attention. Present planning calls for a maximum production rate of 100,000 20 x 20 mm cells per year (assuming 50% yield, 20% equipment down time and one production shift per day). This would be after a 26 week lead time (78 weeks if a production line has not already been established). To support production of four modules approximately two million cells would be needed. At the above delivery rate, twenty years of cell deliveries would be needed. The delivery rate could be nearly doubled by adding a second shift (180,000 cells/year). $500,000 capital equipment investment would add 50,000 cells per year per shift. If both shifts were implemented and the capital was invested 7 years would still be required. With the understanding that the 4 GaAs modules produce 50% more power than the 4 Si modules, and assuming cell quantities could be cut accordingly, only 4-1/2 years of deliveries would be required. If two suppliers were utilized a two year program would be achievable.

The same pre-production testing would be required for the GaAs program as for the silicon program (temperature cycling, etc.).

If higher performance were required thin cells could be used. These should be readily available four years after the production of thick cells begins. The utilization of GaAs solar cells results in benefits due to their inherent characteristics (low temperature coefficient, radiation resistance, etc.).

The combined effects of a high power GaAs low-CR solar array program would be to firmly establish two GaAs solar cell manufacturers in the United States and to provide the lowest cost solar panels to a flight program such as manned space station. Once the production lines are established the commercial satellite manufacturers will start using the cells. They just cannot afford to start the production lines since their individual needs don't justify the expense and risk. A large program is needed to initiate the production lines and space qualify the cells.

8.3 LOW CONCENTRATION RATIO SOLAR ARRAY (LCRSA) TECHNOLOGY READINESS DEMONSTRATION TEST PLAN

8.3.1 General

The primary objective of this program is to finalize a preliminary design of a low-concentration-ratio (CR = 2-6) solar array for service in low earth orbit to provide an output in the 300 kW to 1000 kW range. The array may consist of two or more modules. No specific missions have been defined for the array, nor have particular user satellites been identified. However, in order to arrive at a specific design, a number of test requirements have been identified.

The demonstration test program is also structured to minimize cost and to meet technical and schedule objectives:

a. Early independent/concurrent development of each unique component/assembly to provide timely de-bugging and problem solution.
b. Acceptance and certification testing to be conducted on hardware scheduled for flight.
c. Multiple use of test equipment and facilities during in-process, acceptance, certification, and pre-flight validation testing.
d. Acceptance and certification testing at the highest level of assembly to provide efficient use of test equipment, personnel, and facilities.
e. Static load testing of the primary structure, prior to subsystem hardware installation.
f. Modal testing of the primary structure, after hardware installation, in both launch and extended configurations.
g. Use of flight hardware for Orbiter physical integration.
h. Flight testing of a fractional power, protoflight test article to ensure physical and functional capability prior to initiating a point design.
i. Self-contained development test article (DTA) requires no electrical/data interface with Orbiter, except for RF activation/deactivation signal.

8.3.2 Design Requirements

A ground test and flight test demonstration of the array is recommended as the next phases of this project. While structural design will be based upon forces in orbit, the design will be made compatible with appropriate support system (rigging) as required during the one-g ground demonstration to preclude loads in excess of the design capability. Figure 8-3 provides a typical configuration that can be flight tested using the STS orbiter. Figure 8-4 depicts the flight configuration for the DTA. Section 4 discusses the manufacturing flow for fabrication of a concentrator array. A fractional power configuration is recommended that will allow evaluation of structural, kinematic and electrical performance.

The design requirements may be organized into three missions phases: (1) launch; (2) deployment; and (3) orbital operation. For each phase, the requirements may be further broken down into four categories: (1) static loads; (2) dynamic loads; (3) thermal environment; and (4) electrical environment. The following requirements are recommended.

8.3.3 Launch Phase

In its stowed configuration, a solar array DTA must be of such a size that it fits within the Shuttle cargo bay and does not penetrate beyond the bay envelope. Attachments to the orbiter shall be compatible with the location and load capability of orbiter attachments delineated in Reference 6. The attachments shall provide for the removal of the solar array DTA.

Static Loads

The critical load factors listed in Table 8-5 shall be used to determine the Shuttle launch-induced loads. The landing load factors are included to provide for the possibility of mission abort-induced return and landing. The structure will withstand a differential pressure of 3450 Pa (0.50 psi).

Dynamic Loads

The solar array DTA shall survive the Shuttle cargo bay acoustic environment (decibels versus frequency) given by Figure 8-5. This curve represents the recommended environment based on STS-1 flight data. The stowed solar array module will have a minimum modal frequency of 9.0 Hz.

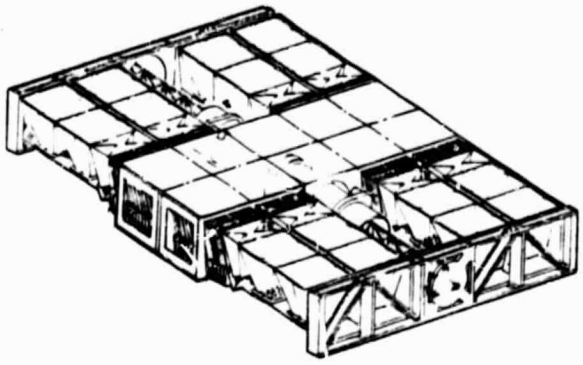

Figure 8-3. Development Phase Demonstration Model

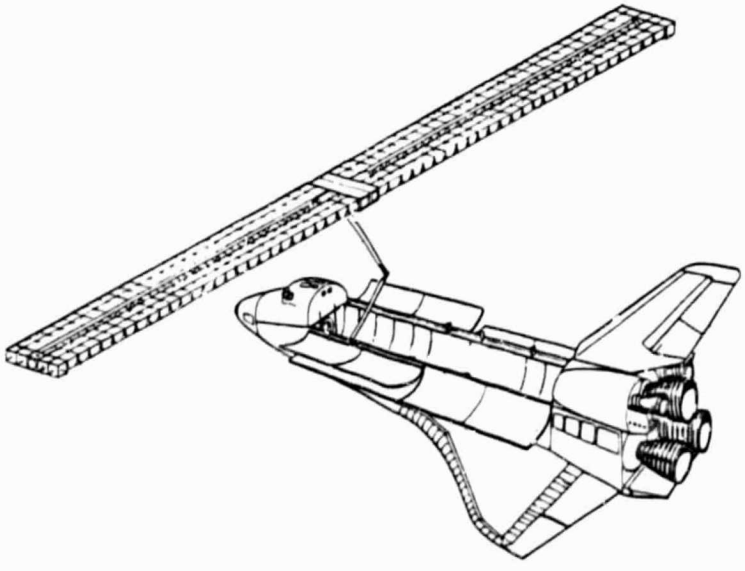

Figure 8-4. Concentrator Array Module - Shuttle Flight Test Concept

Table 8-5. Static Load Factors

Condition	N_X (g's)	N_Y (g's)	N_Z (g's)
Liftoff 1	2	3	5
Liftoff 2	-5	-3	-5
Maximum-Q	-1.9	$\pm$ 0.4	0.25 -0.50
Landing 1	5	3.5	10
Landing 2	-5	-3.5	-7
End Boost	-3.17 -3.05	0 0	-0.60 -0.80

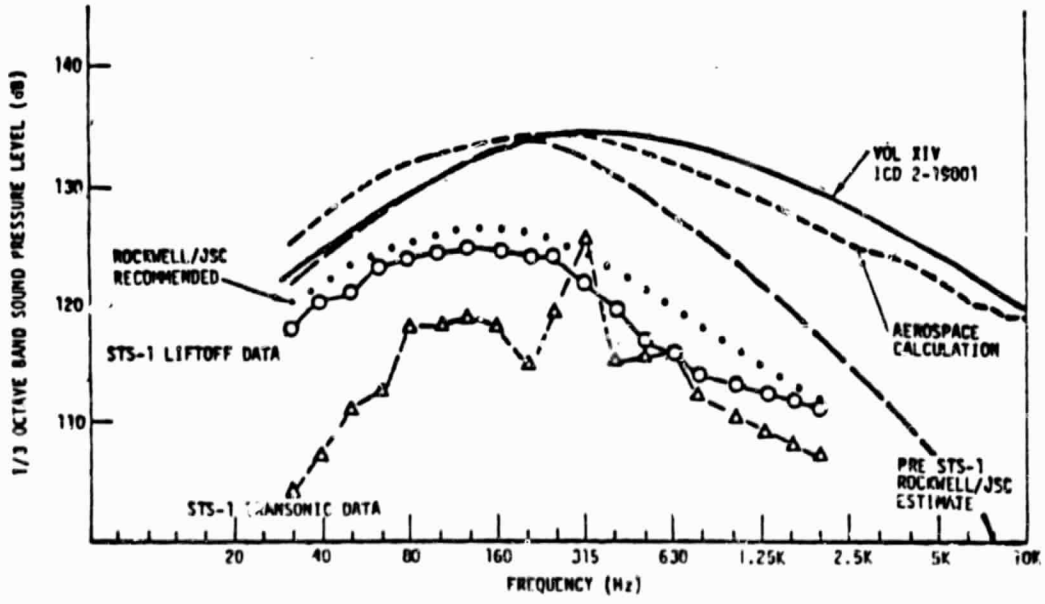

Figure 8-5. Shuttle Cargo Bay Acoustic Environment

Thermal Environment

It is assumed that the DTA will be electrically inert during the launch phase, with negligible heat dissipation. The thermal behavior will be determined by the closed-door environment of the shuttle bay, as modeled by the Simplified Payload/Orbiter Thermal Simulator (SPORTS model), Reference 8. This model provides thermal characteristics (temperatures, capacitances and conductances) for exposed payload bay surfaces and boundary temperatures for the underlaying structure.

Electrical Environment

The DTA will be electrically inert during launch (see above).

8.3.4 Deployment Phase

This phase includes release and removal of the solar array DTA from the Shuttle cargo bay and deployment of the individual concentrator elements.

The RMS interface will react all structural loads. The RMS will also provide two-axis articulation of the array to maintain pointing toward the sun to within $\pm$ 0.5 degree. Electrical power for deployment/extension of the solar array DTA and data acquisition will be provided by batteries aboard the self-contained payload.

Static Loads

Static loads during this phase are assumed to be no greater than static loads during orbital operation.

Dynamic Loads

The structural attachments to the payload bay must provide for controlled release and removal of the solar array DTA. The rate of extension of the masts and release rates for concentrator structural components shall not impose loads in excess of the launch and orbital operations capability.

Thermal Environment

The open-door environment of the Shuttle bay will be simulated by the SPORTS model during the early portion of the deployment phase.

Electrical Environment

The array will be protected from electrical transients associated with partial illumination of the elements by facing the array away from the sun during deployment.

8.3.5 Orbital Phase

The solar array is designed for low earth operation. However, it is recognized that similar requirements for high power solar arrays may arise at higher orbits. Therefore, insofar as possible, the present design will be compatible with high orbit operation, although not necessarily with optimum performance.

The key on-orbit test requirements are:

- Verify ability to successfully withstand repeated temperature cycling.
- Verify on-orbit dynamic characteristics.
- Verify ability of astromast to extend 66 concentrators smoothly.
- Verify on-orbit power output.
- Verify ability of astromast to retract 66 concentrators.
- Determine response of solar array to changes in sun angle.

Static Load

The solar array masts, end cap assemblies, and concentrating element stack assemblies shall sustain the loads associated with atmospheric drag, gravity gradients and solar pressure within acceptable deformation tolerances. The altitude range for orbital operation is assumed to be 500 to 600 km. Acceptable deformation is defined as that which maintains all concentrator optical axes within three degrees of the solar direction under the combined influence of mechanical loads, thermal stresses, and pointing errors for the array as a whole.

Dynamic Loads

The attachment of the array to the orbiter will result in the transfer of dynamic perturbations, namely pointing and stationkeeping maneuvers. To provide adequate frequency separation between the array and the orbiters control system, a minimum modal frequency (attached through the RMS interface) of 0.037 Hz shall be provided.

Thermal Environment

In addition to direct solar load, the array is exposed to Earth Emission and albedo. Global annual average values of 237 watts/m^2 and 0.3, respectively, will be used to evaluate Earth radiation effects on the design. An orbit inclination of 28.5 degrees will be assumed to evaluate eclipse duration, irradiation fluence levels, and array-Earth configuration factors. Thermal interaction between array and the orbiter is assumed to be very minor and will be ignored.

Electrical Environment

It is assumed that the solar array delivers power to a self-contained electrical load bank at a voltage between 150 and 300 volts.

8.3.6 Component Acceptance/Certification Requirements

Classically, complete acceptance testing precedes certification testing, and the certification article is not flown. However, as tailored for the Low Concentration Ratio Solar Array Program, and where it is considered cost-effective and is approved by the NASA, a combined acceptance/certification test program would be implemented and the certified part flown. The test levels for acceptance, certification, and combined acceptance/certification are defined in Table 8-6. These requirements would be subsequently reflected in procurement specifications or contractor test specifications.

The acceptance and qualification tests would be conducted sequentially in the same test setup. First the acceptance levels are established and the component verified for correct performance. The certification levels are then established and component performance verified.

Pin Retention Test

All "push-home" electrical connector contacts (including wire harnesses as well as components) should be subjected to this test (with a calibrated tool) at least twice, once at component or wire harness acceptance and one after installation, but before functional integration of the system. The push force must be 22.2 + (2.2)N [80 (+8)] ounces per pin, and the socket retraction (pull) force must be 1.4N (5.0) ounces (minimum) per pin.

Table 8-6. Low Concentration Ratio Solar Array Component Test Requirements

Environments	Component Certification	Component Acceptance
Thermal vacuum	Pressure: 1×10^{-5} torr (or lower) Min. temp: -84°C (-120°F) Max. temp: +71°C (+160°F) Temp rate of change: 3°C/min (5°F/min) average Dwell: 2 hours (min) Cycles: 8 (min) Test description: Component operating and all critical parameters monitored. Perform cold and hot start after 30-minute soak. Perform complete functional after each cold and hot start. Monitor for corona discharge and arc-over during pump down..	Pressure: 1×10^{-5} torr (or lower) Min. temp: -74°C (-102°F) Max. temp: +61°C (+142°F) Temp rate of change: 3°C/min (5°F/min) average Dwell: 2 hours (min) Cycles: 8 (min) Test description: Component operating and all critical parameters monitored. Perform cold and hot starts after 30-minute soak. Perform complete functional after each cold and hot start after return to ambient. Monitor for corona discharge and arc-over during pump down.
Thermal cycling	Min. temp: -84°C (-120°F) Max. temp: +71°C (+160°F) Temp rate of change: 3°C/min (5°F/min) average Dwell: 2 hours (min) Cycles: 8 (min) Test description: Demonstrate operation at high, low, ambient, and transition temp and after hot and cold starts after being off for 30 min. Complete functional tests during first and last cycle and abbreviated functional during all other cycles.	Min. temp: -74°C (-102°F) Max. temp: +61°C (+142°F) Temp rate of change: 3°C/min (5°F/min) average Dwell: 2 hours (min) Cycles: 8 (min) Test description: Demonstrate operation at high, low, ambient, and transition temp and after hot and cold starts after being off for 30 min. Complete functional tests during first and last cycle and abbreviated functional during all other cycles.
Burn-In (thermal cycling)	NR	Min. temp: -74°C (-102°F) Max. temp: +61°C (+142°F) Temp rate of change: greater than 1°C/min (2°F/min) Dwell: 2 hours (min) Cycles: 18 (including thermal cycling and thermal vacuum) Test description: Component operating and all critical parameters monitored. Perform cold and hot starts after 30-minute soak, Complete functional after each 50 hours of operation and abbreviated functional during all other cycles. Total operating time 100 hours including thermal cycling and thermal vacuum. Last 25 hours to be free of failures.
Random vibration	0.40 g^2/Hz, three minutes each orthogonal axis	0.10 g^2/Hz, one minute each orthogonal axis
Transient/pyro shock	1200 g's (if sensitive to this environment)	300 g's (if sensitive to this environment)
Acceleration	+20 g's, five minutes each axis (if sensitive to this environment) unless orientation in orbiter is specified. Accounts for emergency landing loads.	NR

Electrical Bonding

Proof of compliance with the electrical bonding requirements of MIL-B-5087 will be by test. A bonding meter, Shallcross Model 673 or equivalent, should be used to measure the bonding resistance of each mechanical interface on the component case. The maximum resistance will be 2.5 milliohms. Use of an ohmmeter such as a Simpson Model 760, or equivalent, is specifically prohibited.

Function Test

A functional test (and any alignment verification) should be conducted before and immediately after each environmental test. These tests establish correct performance before the environmental test and prove that no degradation was suffered as a result of the test environment. Abbreviated functional tests would be conducted during environmental exposure to find intermittent failures or performance excursions. Continuous monitoring of all performance parameters (including all on-orbit recorded measurements) will be required during every portion of the environmental exposure.

Thermal Vacuum Test

The test specimen will be mounted on a test fixture and placed in a test chamber in which the specimen temperature can be controlled and maintained between the maximum and minimum temperatures shown in Table 8-6. Temperature sensors will be placed at representative locations on the component mounting flange. The test fixture and test specimen will be placed in the test chamber at atmospheric conditions. The chamber pressure will be reduced to simulate ascent from sea level to space vacuum in approximately 90 seconds. During this period, the maximum pressure reduction rate will be 15 torr/sec for a maximum of 30 seconds, or at reasonable rates for the test facility used. Predicted rate of temperature change is 3°C/minute.

Temperature stabilization is defined as being attained when all temperature readings taken five minutes apart are within 3°C of the specified temperature. The total number of cycles will be eight for acceptance and eight for certification. Functional performance checks shall be performed at the high and low temperature levels. After the last functional performance test, the chamber condition will be returned to ambient. Complete functional tests will be performed on the test specimen at ambient pressure and temperature prior to the next test phase.

Thermal Cycling Test

The test specimen will be subjected to the thermal profile (at ambient pressure) and to the maximum and minimum temperatures shown in Table 8-6. Predicted rate of temperature change is 3°C/minute. Monitoring of critical circuits and parameters will be required during the entire test sequence. Monitoring equipment will be capable of detecting intermittent performance variations as well as long-term drifts in critical parameters.

Operating Burn-In Test

An operating burn-in test will be performed on all electronic components. The test will be conducted at maximum operating temperature and ambient pressure. The minimum total operating time will be 100 hours for the flight units, including the operating time during all prior checkout and acceptance tests, with no failures during the last 25 hours.

Random Vibration Test

The test specimen will be subjected to the anticipated vibration levels for three minutes in each of three orthogonal axes. A functional test will be conducted before the vibration test and after the completion of each axis of the random vibration test. During the test, components will be powered and functionally sequenced through various operational modes to the maximum extent possible.

Explosive Atmosphere Test

This test shall be required of all electrical or electronic components mounted in the cargo bay. The component shall be placed in an explosion-proof chamber capable of having an ambient explosive atmosphere introduced into it. The test item shall be cabled up to its GSE unit outside the chamber. After the chamber is closed and the explosive atmosphere has been introduced, the test unit shall be powered up and operated through a functional test which shall cause the actuation of all internal switches, powering up of any sub-units, or any function which might cause an electrical transient. The component shall not cause ignition of the explosive atmosphere while operating or while being powered down at the completion of the test.

Run-In (Limited)

A run-in test will be performed on each moving mechanical assembly before it is delivered to inventory. The run-in test will be performed in lieu of the burn-in requirement for electrical components. The primary purpose of the run-in test is to detect material and workmanship defects which occur early in the component life. Another purpose of the run-in test is to wear-in parts of the moving mechanical assembly so that they perform in a consistent and controlled manner. Satisfactory wear-in may be manifested by a reduction in running friction to a constant low level.

The run-in test will be conducted for a minimum of 10 hours except for those items where the number of cycles of operation, rather than hours of operation, is a more appropriate measure of the ability to perform in a consistent and controlled manner. For these units, the run-in test will be for at least 5 cycles. The run-in test conditions should be representative of the operational loads, speed, and environment; however, operation of the assembly at ambient conditions may be conducted if the test objectives can be met and the ambient environment will not degrade reliability or cause unacceptable changes to occur within the equipment. During the run-in test, sufficient periodic measurements will be made to indicate what conditions may be changing with time and what wear rate characteristics exist.

8.3.7 System Acceptance/Certification Requirements

The basic housing assembly (no concentrators or components installed) will be subjected to a proof and influence coefficient test. Test objectives will be (1) confirmation of the structural analysis and (2) verification of the integrity of the basic structure to withstand launch and re-entry loads.

The test will be conducted by loading the basic structure to 1.25 times the maximum launch/re-entry loading conditions and measuring stresses and deflections at critical locations.

The basic end cap assembly will be subjected to a proof and influence coefficient test as described above.

A cradle influence coefficient test will be performed to verify the stiffness of the cradle. Results of this test will be combined with the results of the DTA modal survey tests to provide a test-verified dynamic math model for the launch configuration.

Prior to the test, and immediately after the test, all components will be functionally tested during the System Performance Test at Air Mass One (AM1).

System Performance Test (AM1)

Electrical output of the complete system will be verified to establish baseline system electrical performance at air mass one. This same test will be conducted immediately before and after each major system test/demonstration to verify that no degradation has occurred due to the test environment.

Electrical output at AM1 will be measured by recording current-voltage (I-V), diode performance, and conductor isolation.

Acoustic Test

The test objectives are: (1) verification of the structural integrity of the DTA for the dynamic launch environment; (2) absence of reflector/solar panel damage caused by the dynamic environment acting on the stacked concentrators under simulated acceleration loading; and (3) verification of specific component random vibration input spectra. Certain components that have not been subjected to the complete random vibration spectra may be verified by successful participation in this test series, if approved by the NASA.

The DTA will be installed in an acoustic test facility with its longitudinal axes vertical (launch configuration). Instrumentation (accelerometers) will be added to measure the vibration input of components and critical areas of the structure. Microphones will be installed near and within the DTA to monitor the sound pressure levels. A thin plastic bag will encase but not touch the DTA during each acoustic test to prevent contamination.

The DTA will be positioned in the chamber by supporting the transportation dolly on low frequency air bags (20 Hz or below).

Acoustic testing of the DTA will consist of three levels:

a. Low level test at 6 dB below maximum predicted lift-off level.

b. Medium level at 3 dB below maximum predicted lift-off level.

c. Full level test at maximum predicted lift-off level.

The test frequency range will be from 31 to 10 kHz with a spectral distribution as shown in Figure 8-5 which is representative of the maximum predicted flight levels at lift-off. In addition to the sound field requirements, the ambient temperature inside the reverberation chamber will remain relatively constant ($\pm$ 2.8°C from the starting temperature) during the test runs. The allowable tolerance on acoustic test levels will be $\pm$ 2 dB.

The number and placement of acoustic transducers will be specified in the DOP and coordinated with the responsible test conductor.

An empty chamber checkout verification will be performed prior to installation of the DTA in order to verify that the combined chambers, the modulators, and the noise source are functioning in the required manner. At the completion of all calibration procedures, an acoustical test which is 6 dB below the levels in Figure 8-5 and representative of the transonic and maximum-q environment, will be performed. The specimen will be exposed to this sound pressure level for a time required to establish steady-state conditions and record all data, or 40 seconds, whichever is greater.

Upon verification of data at the -6 dB level, the sound pressure will be increased to medium level for 20 seconds to verify equalization, and data will be taken.

Evidence from the medium level acoustic tests will be used to demonstrate that the flight level acoustic enviornment, shown in Figure 8-5, can be achieved in shape and amplitude. The test specimen will then be subjected to the acoustic environment of Figure 8-5 , which is representative of the lift-off environment. The exposure time will be 1 minute (minimum).

Modal Survey

A modal survey of the DTA will be conducted to verify the dynamic math model which supports analysis of the predicted launch loads. Verification of the dynamic math model will provide higher confidence of the analytical predictions.

The objective of the modal survey is to determine the dynamic characteristics of the system with respect to mass, stiffness, and damping by applying sinusoidal excitation to the system at specific stations determined from the dynamic math model of the launch configuration.

The DTA will be the complete system, stowed and latched as for launch. The test article will be mounted to a rigid fixture which will be mounted to the fixed seismic base of the facility. The dynamic math model of the test article will be used to specify excitation input stations and strategic accelerometer locations. Significant lateral and longitudinal characteristic vibration modes will be considered. Excitation of each selected station will be sequentially applied by sweeping sinusoidally from 5 to 50 Hz with all forces and accelerations continuously recorded. After completion of the sine sweeps, the data will be used to determine all natural frequencies and to identify the major structural modes.

The cradle is dominated by structural behavior and for this reason, a static influence coefficient test will be used to verify stiffness. This will be done during the static load testing.

Extension/Retraction Demonstrations

Ability of the DTA to successfully extend to its full length, and retract to its launch configuration, can be demonstrated, if considered necessary, at a facility which has a precision level surface. Other considerations are:

Precision level surface area = (67m x 6m) (220 ft x 20 ft)
Cleanliness level: 100,000
Lighting: sufficient for motion picture coverage
Wind velocity = essentially zero

The test article will be fully extended in each direction, supported over its length and width. Three complete cycles of extension/retraction will be performed while monitoring motor currents, temperatures, time for each half-cycle, and discretes indicating end of movement.

Mass Properties Determination

For the static weight and center-of-gravity test, the DTA will be in the launch configuration. The test objective is to determine the test article static weight and center of gravity. The test will be performed with the DTA horizontal and attached to a three-point support.

Measurements will be taken with the DTA Z-Z and X-X axes levels. Then the test article will be rotated 90 degrees about the Z-Z axis until the Y-Y axis is level, and measurements will be taken again. Measurements will verify that the center of gravity is within X = 0 $\pm$ 1.3 mm, Y = 0 $\pm$ 1.3 mm, and the Z tolerance specified by the experiment integration contractor. The resultant weight and reaction point measurements will then be used to establish the actual weight of the test article and its center of gravity. Test documentation will include the weight and balance report. Weight and center of gravity data will also become the initial entry of the weight and balance log, which will be maintained from the time of test completion until test article launch.

8.3.8 Pre-Launch Operations

After the DTA/cradle integration tests have been completed, the LCRSA cargo element, and all required support equipment, will be transported to the launch site. After the cargo element receiving inspection, pre-launch operations will be implemented to prepare the cargo element for integration with the Orbiter and subsequent launch. The following sections describe the tests required.

Pre-Launch Functional Test

After the LCRSA cargo element and all support equipment arrives at KSC, receiving inspection will verify that no damage has occurred during transit. All support equipment will be reverified before connecting to the cargo element. Each DTA component will be functionally tested to verify that its performance is consistent with factory tests. Critical alignments will be optically verified for "no significant change" from the factory alignment measurements.

The DTA will be commanded to perform an extension/retraction test, including RF commands and data collection. This test will be the same or as near as possible to the factory demonstration test. It will sequence the cargo element as near to a planned mission demonstration sequence as possible to demonstrate DTA component flight readiness.

Test objectives to be accomplished include the following:

- Verify compatibility and integrity of the DTA components, simulating all mission operation.
- Demonstrate RF communications/component performance to ensure proper operation for both extension and retraction modes.
- Verify alternate and redundant modes of operation.

Flight-type batteries will be used. The cargo element will be controlled and visually monitored through the extension and retraction modes. All RF commands will be executed through the LCRSA support equipment, which represents the Orbiter functional interface.

8.3.9 Cite Compatibility Test

As soon as the cargo element is transported to the Operations and Checkout Building (OCB), it will be installed horizontally in the cargo interface test equipment (CITE). The CITE has the same physical interface as the Orbiter bridge and keel fittings. The installation of the cargo element into this fixture will verify form and fit of the Orbiter interfaces. Interface verification with the caution and warning wire harness (which is unique to the LCRSA cargo element) will also be accomplished. In the installed position, the cargo element is then ready for transfer to the canister which will transport the cargo element to the Orbiter Processing Facility (OPF).

8.3.10 Orbiter Installation

The LCRSA cargo element will be transported to the OPF by the canister. After the exterior of the canister has been cleaned, the canister will be opened and the cargo element removed by the Payload Handling Fixture (PHF). The cargo element will be lowered into the cargo bay for transfer of the load to the Orbiter payload retention fittings.

After the retention fittings are aligned and closed, the PHF will release the cargo element. Final closeout of the cargo element will be completed at this time.

The task of installing the LCRSA cargo element-unique cabling in the Orbiter cargo bay wire trays, and the RF equipment installed in the Orbiter's aft flight deck, will be accomplished during the Orbiter's mission-unique payload accommodation equipment modification period, accomplished previously in the OPF.

8.3.11 Orbiter In-Bay Readiness Test

No in-bay readiness tests are planned for the LCRSA cargo element.

8.3.12 On-Orbit System Test Requirements

Instrumentation

Instrumentation installed on the DTA must be flight certified. The following basic measurements will be recorded during the flight demonstration test:

1. Sun orientation (± 20 degrees, in one degree increments).
2. Total power output (current, 0-100 amps; voltage, 0-200 VDC).
3. Temperatures (representative solar panels, structural components, electrical load bank, load bank radiator, data recorder, RF switch, representative motors, negators, latches, and the Astromast).
4. Accelerometers at representative locations.

Data Recording Motion Picture Requirements

Data recording will be accomplished by the data recorder installed in the support structure.

Motion picture coverage of the entire extension movement, and the entire retraction movement, will be provided from a vantage point on the RMS, as well as an Orbiter window.

Orbital Operations

The RMS will be used to unlock the DTA, remove it from the cargo bay, and extend the test article away from the Orbiter (pointing it away from the sun).

The RF switch will be commanded to the "on" position by the mission specialist on the aft flight deck. After the test article is fully extended, orient the assembly toward the sun.

Basic electrical performance characteristics at AMO will be obtained during the first 15 minutes of operation. The next 30 minutes will be spent altering the sun orientation angle slowly, from zero to minus 20 degrees and back through zero to plus 20 degrees. At this point in time, the Orbiter will enter the first eclipse period. The test objective now is to determine the system impact as the test article enters the eclipse (cooldown rate) and then emerges into the sunlight (the rise-time and the overshoot of current and voltage). Ten complete eclipse cycles (minimum) are required, with a total test time (including extension and retraction) of approximately five hours, thirty minutes.

The RF switch will be commanded "off" by the mission specialist. The data recorder will automatically shut down and the battery will be automatically isolated when the test article is fully retracted (as it was during the launch operations).

The RMS will install the DTA into its special cradle and secure it for the return trip.

8.3.13 Data Reduction and Reporting

Data reduction will be performed in a suitably equipped laboratory where computerized data processing will permit evaluation of system performance. The key parameters will be charted and presented in the final system test report. This report will be submitted 90 days after completion of the flight test program.

8.3.14 Test Article Disposition

The DTA will be off-loaded from the Orbiter, the data tape removed for processing, and the test article immediately inspected for signs of damage/degradation. Any signs of damage/degradation will be photographed and the test article prepared for any diagnostic testing/detailed examination.

9.0 SPACE MISSION APPLICATIONS

9.1 SPACE STATION — AN EXAMPLE

The low concentration ratio solar array module preliminary design configuration requires some minor design modifications for the Space Station application. The Space Station baseline design would preferably use gallium arsenide solar cells in two array modules (wings) and would have a single-direction extension design so the array module (wing) swept volume would not interfere with the Shuttle berthing operations. The array design calls for a set of symmetrical wings attached to the power module by 0.9 m (3 ft) dia. booms, 15.2 m (50 ft) long (Figure 9-1). The arrays are swept through two degrees-of freedom each. At the spacecraft and power module interface there would be the boom deployer/continuous (orientation drive) 360° rotation assembly (Figure 9-2). The power is transferred through the assembly by a large diameter slip ring assembly. At the boom/array module interface there is a second degree-of-freedom drive assembly. This drive assembly rotates the array through ± 52° using a dual drive assembly as shown in Figure 9-3.

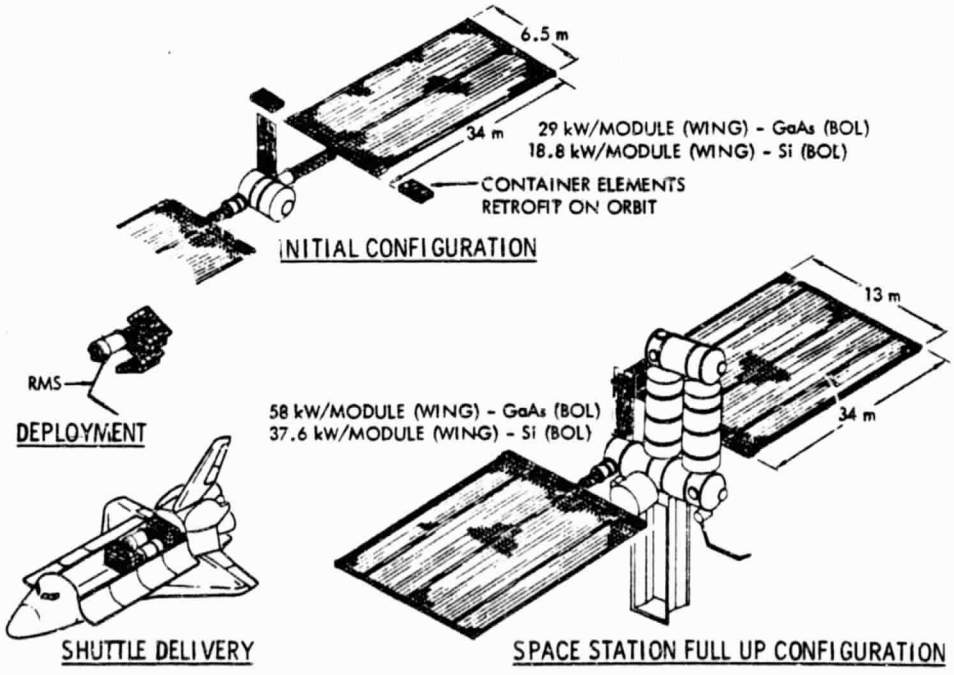

Figure 9-1. Array Module and Space Station Interface Example

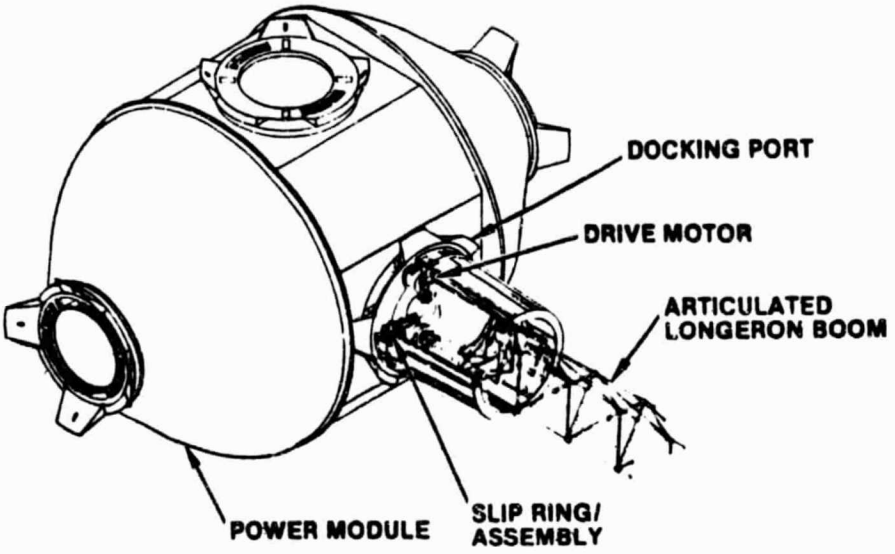

Figure 9-2. Power Module Attachment

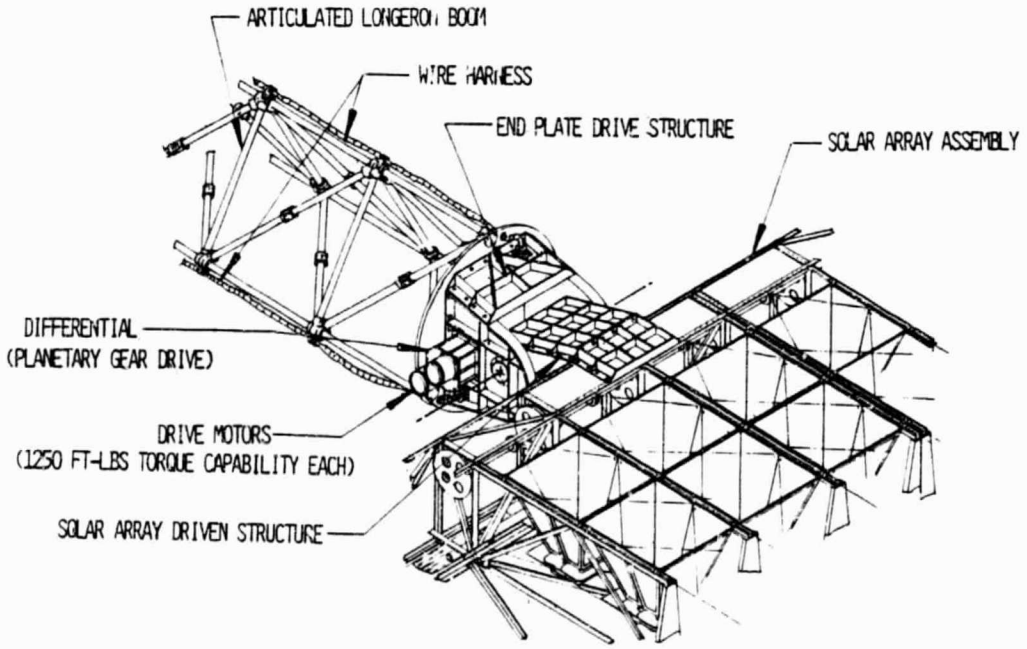

Figure 9-3. ± 52 Degree Excursion Joint

Modifications to the array module preliminary design would be very minimal. The concentrator elements, stacks, housing and mechanical assemblies remained virtually the same. The housing design is split down the centerline with closeout structure added and the CEM's rotated 90°. All other design features remain the same. For a power requirement, for example, requiring 29 kW per wing (BOL) initially and 58 kW in a fullup configuration would be provided by GaAs cells shown in Figure 9-1. Using Si cells, the power would be 18.8 kW and 37.6 kW, respectively. The initial design provides for rearranging the mast/housing assembly to allow for retrofitting containers on-orbit to the initial configuration in order to bring them to their fullup configuration.

The beginning of life mission configuration consists of two container elements with a mast assembly each and five rows of sixty-six concentrator elements in each stack. Using the preliminary design array module mast, the assembly would be capable of withstanding an ultimate load of 0.023 g's. Two additional containers can be retrofitted to each wing at the end of the housing assemblies. Each of these containers has six rows of sixty-six concentrators. This fullup configuration is capable of 0.012 g's ultimate.

9.2 BENEFITS OF SMALLER SCALE CONCENTRATOR ELEMENT

A N = 12 concept was studied for thermal, electrical and mechanical feasibility (refer to Figure 5-4).

The N = 12 concentrator element is half the size of the N = 6 design. The aperture is 0.25 m (9.84 in.) x 0.25 m. 40.5 kW (BOL) was chosen as an example for the power requirement for a module (wing). The array is a single extension type with two masts. For a GaAs design wing, a single-laced mast (N = 6 type) array will withstand an acceleration of about 0.0085 g ultimate load, and the hybrid will withstand a 0.027 g load. The Si design calls for the same mast (N = 6 type), and will withstand a 0.004 g ultimate load in a single-laced configuration and a 0.013 g ultimate load using the hybrid mast configuration. The performance estimates using GaAs cells for the module are shown in Figure 9-4. The N = 12 design reduces the solar cell temperature without significant impact upon array module recurring cost compared to the preliminary design configuration using GaAs cells.

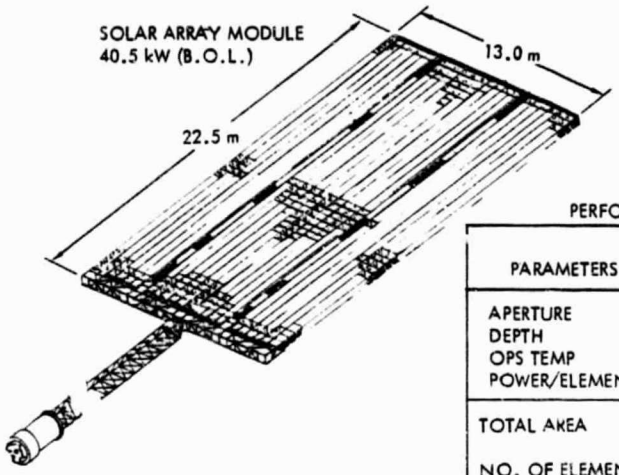

- SMALLER ELEMENT SIZE ~ 1/4
- REMAINS DEPLOYABLE & RETRACTABLE
- SINGLE DIRECTION EXTENSION
- SIMPLER FOLD & SAME COMPACT STOWAGE

PERFORMANCE OF GaAs SOLAR ARRAY

PARAMETERS	MULTI 100 kW (B.O.L.) 175 kW MODULE	75 kW (10 yrs) (TWO MODULES)
APERTURE	.5 m X .5 m	.25 m X .25 m
DEPTH	.37 m	.185 m
OPS TEMP	116°C	90°C
POWER/ELEMENT	40.5 W	11 W
TOTAL AREA	1320 m^2	585 m^2
NO. OF ELEMENTS	4356 (.5 m X .5 m APERTURE)	7392 (.25 m X .25 m APERTURE)
W/kg (BOL)	41	40
W/m^2 (BOL)	133	135
$/W (BOL)	166	168

- DD&T REQUIREMENTS SIMILAR TO PLANAR

Figure 9-4. Modification for Space Station Application (Example)

9.3 TECHNOLOGY APPLICATION RECOMMENDATIONS

Figure 9-5 illustrates the technology development steps required to provide confidence for application of technology to space missions. The current contract effort has resulted in a preliminary design for a generic concentrator solar array module definition. The next phase(s) of continuing effort recommended would be to complete the SRT items discussed in Section 8.2 and in parallel perform the ground/flight demonstration of an array module for space station mission applications for the near term. Section 8.3 discusses a recommended configuration for a development test article. Figure 9-6 illustrates a recommended schedule for implementation for the space station program.

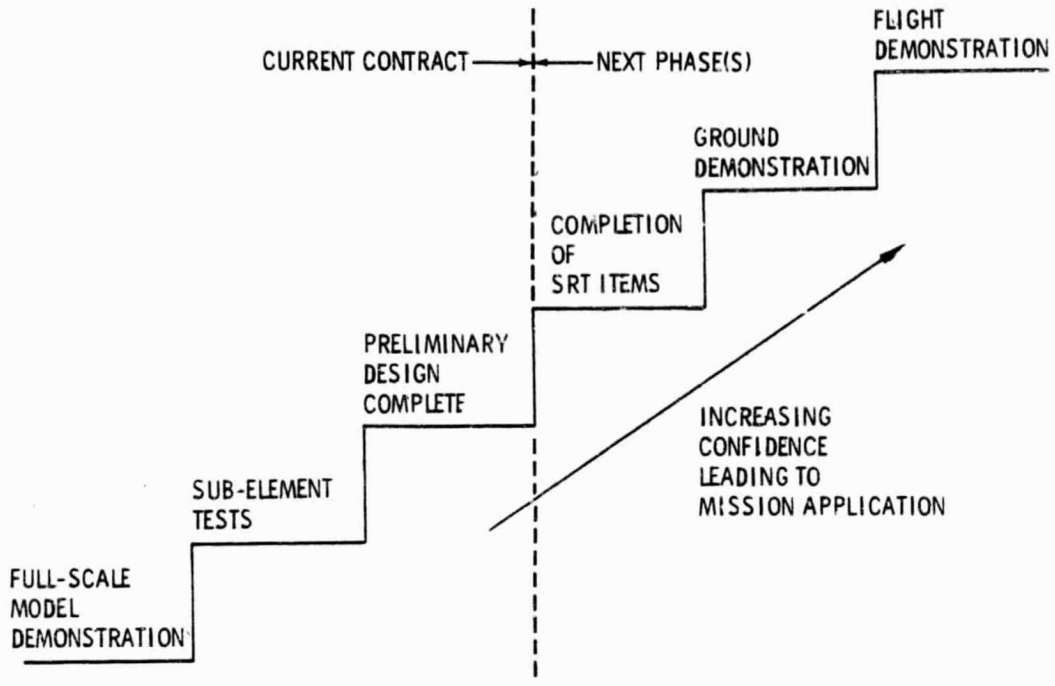

Figure 9-5. Test Philosophy Summary

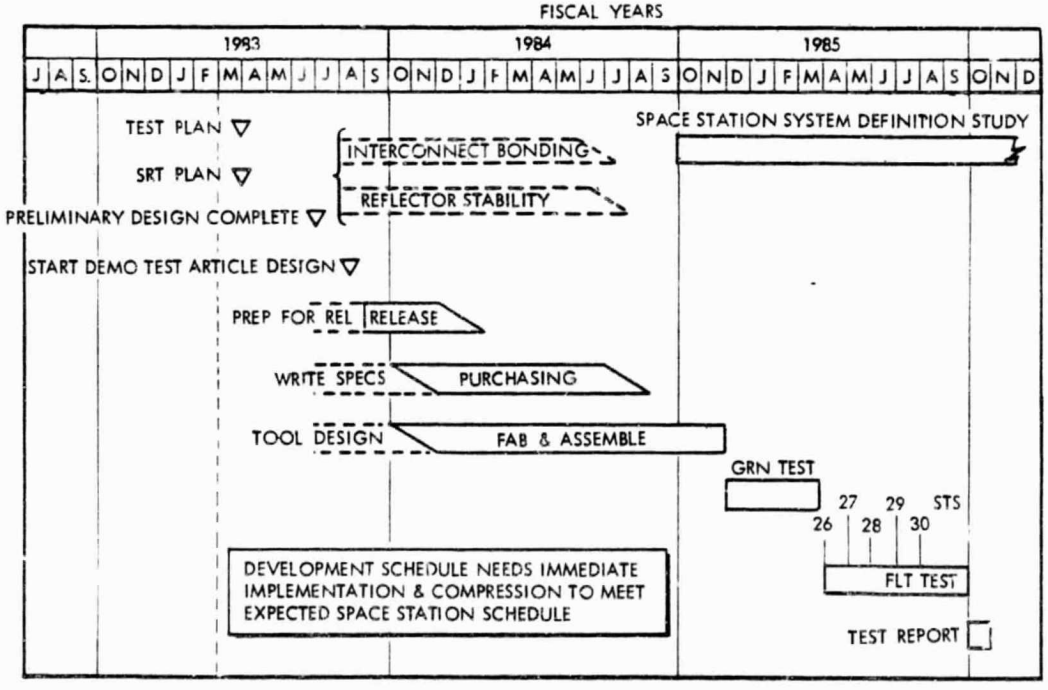

Figure 9-6. Application to Space Station Program

10.0 REFERENCES

1. Study of Multi-kW Solar Arrays for Earth Orbit Applications, Final Report (NASA-MSFC NAS8-32988) Rockwell International Corporation, SSD 80-0064; May 15, 1980.

2. NASA-MSFC Study of Multi-kW Solar Arrays for Earth Orbit Application, Final Report, Lockheed Missiles and Space Company, LMSC-D715841; April 1980.

3. Study of Multikilowatt Solar Arrays for Earth Orbit Applications, Final Report, TRW, 33295-6001-UT-00; September 19, 1980.

4. French, E. P., et al. Gallium Arsenide Solar Concentrator Hardness Study, AFAPL-TR-78-30, Rockwell International Final Report, Contract F33615-77-C-3130, SD 78-AP-0037 (May 1978).

5. Low Concentration Ratio Solar Array for Low Earth Orbit Multi-100 kW Application, Mid-Term Report, Rockwell International Corporation, SSD 82-0172 (November 1982).

6. Space Shuttle Program, Level II Program Definition and Requirements, Space Shuttle System Payload Accommodations, NASA, JSC 07700, Volume XIV, Revision G; September 26, 1980.

7. Hill, Robert E. and Coody, M. C., "Vibration and Acoustic Environments for Payload Cargo Integration," AIAA 21st Aerospace Sciences Meeting, Reno, Nevada, January 1983.

8. Simplified Payload Orbiter Thermal Simulator (Sports Model), Rockwell Report STS 81-0333, dated February 1981.

9. "Report on Phase I of AF Contract F33615-81-C-5150, Manufacturing Technology for GaAs Solar Cells," Applied Solar Energy Corporation and UTL Corporation Report (1983).

10. "Low Concentration Ratio Solar Array Deployment Actuator Mid-Term Report," Peter R. Preiswerk, Astro Research Corporation (August 1982).

11. "Low Concentration Ratio Solar Array Deployment Actuator Final Report," Peter R. Preiswerk, Astro Research Corporation (26 May 1983).

12. Frederick, D. H., Haugen, E. A., and Hamilton, D. A., "Loads Environment for Payload/Cargo Integration," Paper No. STS 82-0816 presented at the 21st AIAA Aerospace Sciences Meeting, Reno, Nevada (January 1983).

13. MSC/NASTRAN User's Manual Version 60. Caleb W. McCormick, ed. The MacNeal-Schwendler Corp., Los Angeles (May 1976, Rev. May 1980).

14. Pipes, Louis A., PhD. Applied Mathematics for Engineers and Scientists, 2nd ed. McGraw-Hill, New York (1958), p.116.

15. French, Edward P., "Heat-Rejection Design for Large Concentrating Solar Arrays," prepared for and contained in the Proceedings of the 15th IECEC, Seattle, Washington; August 18-22, 1980, pp. 394-399.

16. Buckhard, Donald G , et al, "Solar Concentrating Properties of Hexagonal, Pyramidal and Circular Cones," Applied Optics, Volume 17, No. 15, p. 2431; August 1, 1978.

17. Patterson, R. E. and Yesui, R. K., "Parametric Performance Characteristics and Treatment of Temperature Coefficients of Silicon Solar Cells for Space Application," JPL Technical Report 32-1582, May 15, 1973.

18. "Space Transportation System Reimbursement Guide," NASA JSC, JSC-11802; May 1980.

19. Wilson, R. C. and Butler, C. P., "Total Solar Irradiation at Table Mountain, California, 1926-1977," Solar Energy, Vol. 21, pp. 351-352 (1978).

20. Weiss, Thomas A., and George O. Lof, "The Estimation of Daily, Clear Sky Solar Radiation Intercepted by a Tilted Surface," Solar Energy, Vol. 24, pp. 287-294.

21. AGA Thermovision 680 Operating Manual, AGA Infrared Systems Publication 556 104 557 (1975).